Temporal Assessment of Hybrid Flood Defenses

A Dynamic Bayesian Network

Tim de Kok

Witteveen+Bos

April 26, 2021

TU Delft

Temporal Assessment of Hybrid Flood Defenses

A Dynamic Bayesian Network

by

Tim de Kok

student number: 4363841

to obtain the degree of Master of Science
at the Delft University of Technology,
to be defended publicly on April 16, 2021 at 10:30 AM.

Delft University of Technology:	Dr. ir. O.M. Nápoles
	Dr. ir. B.C. van Prooijen
	Ir. G.A. Torres Alves
	Ir. M.H.K. Niazi
Witteveen en Bos:	Ir. B. van Es
	Ir. G.R. Spaargaren

Acknowledgments

This thesis is the final step to achieve my Master's degree in Hydraulic Engineering at the TU Delft. In my thesis, which I conducted at Witteveen en Bos, I propose a conceptual framework to design and assess hybrid flood defense systems within the context of current Dutch design guidelines.

Many people have contributed to this thesis, whom I would like to thank personally. To start with my thesis committee, who have helped and supported me during the writing of this thesis. First, I would like to thank Ir. Bart van Es, my daily supervisor at Witteveen en Bos, for all of his support and time throughout the development of this thesis. Bart, every meeting we had helped me stay on track towards the completion of this work. Your insights, support and advice shaped the thesis to what it is today. I want to thank you for everything you have taught me and for all of the feedback you continued to provide for every draft, presentation and MATLAB model. It would not be at this level without your help.

I would like to thank Dr. ir. Oswaldo Morales Nápoles, the chair of the thesis committee for everything that I have learned from you and for all your wonderful anecdotes during our meetings. Oswaldo, I want to thank you for your enthusiasm during our talks. You have taught me everything I know about probabilistic and Bayesian networks in particular. Thanks to your help, BANSHEE was used, greatly improving the probabilistic modelling applied in this thesis. Taking your advice, I will now take my time to enjoy this moment as everything I have done for the past 7 years has led up to this moment.

I would like to thank Ir. Hassan Niazi, the architect of this topic together with Bart. Hassan, your help during the first months helped me shape the foundation of this thesis. Thanks to your thesis, many of the elements of this thesis were made possible. Your clear understanding on this topic helped form the MATLAB models. I really enjoyed all of our talks, you have a great way of explaining complex topics and this provided me with the clarity to start this journey. Your continued support, from different time zones, is highly appreciated. It really was a pleasure working with you.

I would like to thank Ir. Gina Torres Alves, your understanding of copulas and dynamic probabilistic modelling has had a great influence on this work. Gina, you are the quickest to respond to email of everyone at the TU Delft. Your, quick clear answers to all of my questions were super helpful in developing the probabilistic elements of this thesis. Your final advice on the structure of this paper has really made the work to what it is today.

I would like to thank Dr. ir. Bram van Prooijen, for all your support and great feedback. Bram, you have helped me scope this research, which provided me with the focus I required when starting this work. Your advice helped me think about the critical elements that need to be included in academic writing. Thanks to your advice, the thesis has the "clear and to the point" structure it has now.

I would like to thank Ir. Gerben Spaargaren, for the opportunity to graduate in cooperation with Witteveen en Bos. Gerben, your input helped structure what should be included in the main body of this thesis. I enjoyed the coffee moments at Witteveen en Bos and want to thank you for making me feel part of the W+B team despite the pandemic.

Last but not least, I would like to thank my friends, my parents, brother and sister and most of all Bibi. Thank you for all of your support and love. I would not have been able to do it without all of you.

Tim de Kok
Utrecht, April 2021

Abstract

Implementation of nature-based solutions (NBS) in flood defenses is hindered by a lack of probabilistic tools and design guidelines that can be used to assess spatial and temporal variability in these biophysical systems. It is well established that nature-based elements, such as vegetation, attenuate waves, capture sediment, strengthen the subsoil and invoke numerous ecological benefits. This thesis proposes a conceptual framework to design and assess hybrid flood defense (HFD) systems within the context of current Dutch design guidelines: '*wettelijk beoordelings instrumentarium*' (WBI). The framework builds a dynamic probabilistic tool (DPT) to assess the effect of temporal variability of NBS elements on wave loading. The framework was applied in a case study at Hellegatpolder to investigate temporal effects of nature-based elements on nearshore wave heights during storm conditions.

Data was collected specifically for the idealized HFD system at Hellegatpolder. Vegetation and nearshore wave height data was unavailable and therefore, an autocorrelation function was developed to sample temporal vegetation data. A numerical XBeach model was constructed to model nearshore wave heights for a bare and vegetated foreshore, resulting in a uniform database. Development of a static and dynamic Bayesian network allowed dynamic probabilistic modelling of nearshore wave heights. Application-specific model settings combine normative hydraulic storm data with the database and probabilistic models. The developed DPT was applied to model nearshore wave heights for a bare and vegetated transect for each vegetative season.

Numerical modelling using XBeach was applied to model 7 years of data with a temporal resolution of 30 minutes for both bare and vegetated foreshore scenarios. The numerical results conclude that vegetation at Hellegatpolder attenuates waves with an average of 54%, where wave attenuation was 1.7 times greater in July compared to December. The effect of bathymetry morphology on nearshore wave height was found insignificant for short time scales.

A static Bayesian network (SBN) was built to model nearshore wave heights in a fixed point in time. The validated SBN was able to model nearshore wave heights with 90% accuracy. A dynamic Bayesian network (DBN), was created to model offshore hydraulic parameters time series. DBN achieved an accuracy of >85% for short time scales (<25 hours). Utilizing the DBN for long term modelling resulted in progression towards the mean value of the marginal distributions. Statistical validation of both models rejected the representation of the dependence structure using only a Gaussian copula.

Application settings were defined in MATLAB to manipulate the database, probabilistic models and normative hydraulic storm conditions. The configured DPT was run to model nearshore wave heights for a bare and vegetated foreshore specifically at Hellegatpolder. During storm conditions average wave attenuation due to vegetation was 45%. Average wave attenuation results were thus lower than those available in the numerical dataset (54%). Moreover, wave attenuation was 3 times greater in summer compared to winter months. Furthermore, the DPT resulted in dynamic wave loading (i.e. varying through time) compared to the static WBI loading conditions. Resulting DPT wave heights were 82% lower during winter months than the normative loading defined by the WBI.

These results show the effect of variability on wave attenuation. The percentages and factors are expected to differ for other locations. Nevertheless, the obtained results clearly illustrate the significance of temporal modelling of HFD systems. The method presents a novel conceptual framework to include the effects of NBS elements in the design and assessment of flood defenses. The conceptual framework, numerical and probabilistic models can be applied for other HFD systems, enabling engineers to assess flood defenses more realistically – a critical step in the implementation of NBS in design guidelines.

Contents

Nomenclature

AIC	Akaike information criterion
BN	Bayesian network
cdf	Cumulative density function
CVM	Cramér von Mises
DAG	Directed acylic graph
DBN	Dynamic Bayesian network
DPT	Dynamic probabilistic tool
ERC	Empirical rank correlation
HFD	Hybrid flood defenses
IRT	Iteration run time
NAP	"*Normaal Amsterdams peil*'
NBS	Nature based solutions
NRC	Normal rank correlation
pdf	Probability density function
RC	Rank correlation
RCM	Rank correlation matrix
RTI	Relative temporal improvement
SBN	Static Bayesian network
SSD	Sum of squared differences
TSST	Two sides sampling test
WBI	"*Wettelijk beoordeelings instrumentarium*'

List of Figures

List of Tables

1

Introduction

Floods between 1980 and 2009 confiscated more than 500.000 lives, injured more than 350.000 and directly affected more than 2.800.000.000 people worldwide (Doocy et al., 2013). Climate scenarios for the next 100 years predict even more intense storms (IPCC, 2014). On top of that, sea-level rise is expected to contribute significantly to average water level increase (Muis et al., 2020). Furthermore, roughly 10% of the world's current population lives in low-lying coastal areas and that number is only expected to increase (FitzGerald et al., 2008). Combined, these developments will exponentially increase the annual damage due to floods over the following years (Fig. 1.1). Harnessing all flood defense possibilities is therefore crucial to battle this global natural threat.

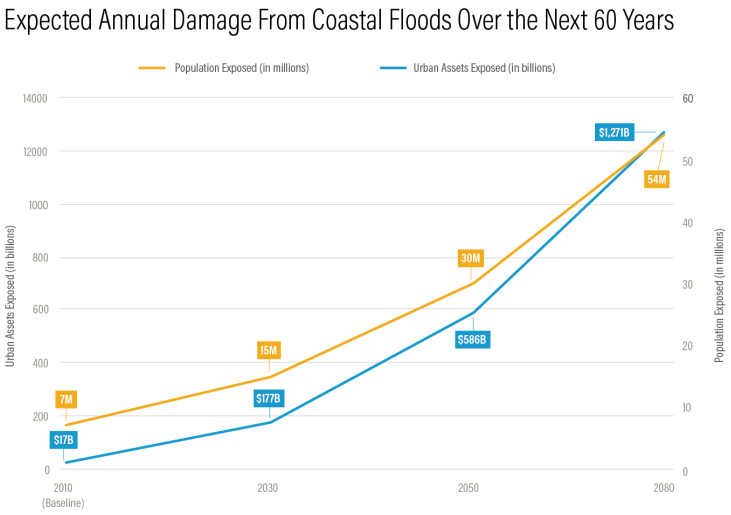

Figure 1.1: Expected population and urban assets exposed to flooding (Courtesy of World Resource Institute).

1.1. Opportunity

Nature based solutions (NBS) such as vegetated foreshores have the ability to improve protection against flooding, while simultaneously improving the functioning of an ecosystem (Borsje et al., 2018). Exploiting the potential of NBS to complement conventional flood defenses results in hybrid flood defense (HFD) systems, as shown in Figure 1.2.

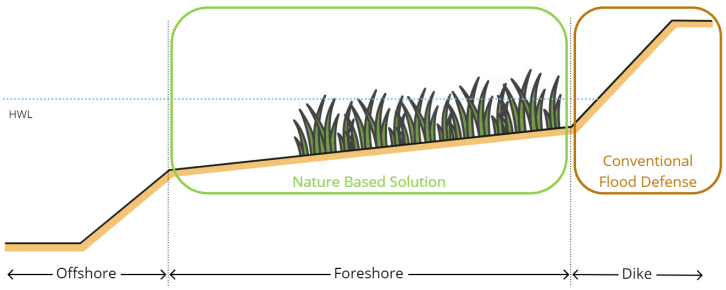

Figure 1.2: Hybrid flood defense system; a conventional flood defense and a nature based solution.

Myriad of studies have illustrated the positive effects of NBS elements in HFD systems (Kobayashi, 1993; Möller et al., 1999; Gedan et al., 2011; Borsje et al., 2018; Vuik et al., 2019). The most promising effects

induced by vegetation include dampening of waves, capturing of sediment and cohesion of the subsoil. Their combination has significantly reduced the consequences of large storm events (Gedan et al., 2011), as the probability of foreshore failure and wave overtopping decreases considerably.

Besides the improvements in terms of flood risk reduction, there are numerous ecological benefits as well. For example, conservation or restoration of natural ecosystems, improvement of water quality by cycling through wetlands, carbon capture (Temmerman et al., 2013), etc. Combining the benefits of both flood reduction potential and the external ecological advantages, the cost benefit appraisal of HFD systems in comparison with conventional methods improves significantly (Menéndez et al., 2018; Vuik et al., 2019).

1.2. Problem Statement

Hybrid flood defenses combine dynamic ecosystems (i.e. vegetation varies through time) with a static sea defense (i.e. strength constant through time). The strength is constant as maintenance of the soil, rock structure is maintained at a constant level. Moreover, rocks and soil are, unlike vegetation, inherently not variable throughout the design lifetime of a flood defense. The flood reduction properties of both the dynamic ecosystem and the static sea defense determine the strength of the system. In order to guarantee flood safety, the combined strength should exceed the dynamic hydraulic load. Static sea defenses have been studied extensively and guidelines have been standardized in the Netherlands (De Waal, 2016). Wave reducing effects of dynamic ecosystems have been studied in both global case studies (Menéndez et al., 2020) and numerical models (Willemsen et al., 2020). The dynamic character of nature based ecosystems results in physical uncertainty regarding the strength of the system.

Due to the dynamic nature of ecosystems, static assessment (i.e. non varying value for all parameters) of HFDs does not provide sufficient information to define actual system response. Vegetation breaking during a storm will, for instance, reduce the wave attenuating character of the system as a whole (Vuik et al., 2018a), thus reducing the system strength. This significantly influences how HFD systems are assessed, as the uncertainty is mitigated through overdimensioning or exclusion of the NBS elements from the system as a whole (Mink and Sansoglou, 2020).

The vicious circle instigated by physical uncertainties in HFD systems is illustrated in Figure 1.3. A lack of probabilistic tools in current design guidelines restrict the assessment of the physical uncertainty in HFD systems. The uncertainty is subsequently mitigated by either overdimensioning or implementation of conventional flood defenses (Mink and Sansoglou, 2020). Naturally, little can be learned if implementations are scarce. In turn, the lack of learning maintains the physical uncertainty surrounding the system.

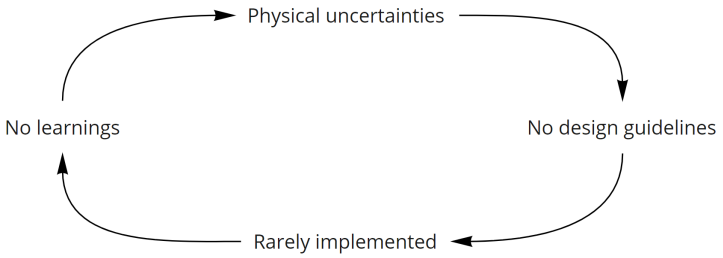

Figure 1.3: Vicious circle hindering HFD implementation.

Numerical models have the ability to model HFD systems and solve complex problems in the system, yet they are computationally exhaustive and complex in their application. Probabilistic models have the advantage of being more computationally efficient. The models can be implemented in data scarce environments and provide a system-level probabilistic description of the system (Niazi et al., 2021). Unfortunately, these probabilistic models have not yet been developed nor implemented within current guidelines, hindering the implementation of HFD systems in general.

Problem Statement

Implementation of nature-based solutions in flood defenses is hindered by a lack of probabilistic tools and design guidelines used to assess spatial and temporal variability in the biophysical systems.

1.3. Objective

There is an urgent need for harnessing the power of probabilistic models to quantify the uncertainty of wave dampening effects by NBS elements in HFD systems. Therefore, enabling wave attenuation by vegetated foreshores to be included in the assessment of the flood defense is crucial. To do so, a conceptual framework is conceived, acting as design guidelines for the development of a dynamic probabilistic tool (DPT). The DPT can be applied for varying spatial locations and is placed within the 'wettelijk beoordeelings instrumentarium' (WBI); current dutch design guidelines.

The objective for the DPT is to model a time series of wave heights at the dike toe. The physical processes that influence wave progression, and thus wave attenuation, are related to each other in the DPT. The dynamic nature of the system is included in the model by utilizing dynamic probabilistic models. In doing so the loading and duration are included in the tool, thereby capturing short and long term temporal system response. To support the feasibility of the DPT, the conceptual framework is applied for a case study location to assess the HFD system including the NBS elements.

Thesis Objective

Development of a probabilistic tool that includes temporal effects of NBS in determination of nearshore wave loads used in design guidelines.

Research Questions

Guiding this research towards fulfillment of the objective, two main research directions are segmented. Each containing a number of research questions. The first focuses on the expansion of current design guidelines to include temporal assessment of NBS elements in HFD systems. The second targets temporal assessment of wave attenuation due to vegetation, which is examined through application of the DPT. The symbiosis of the two questions structures the development of a method to create a dynamic probabilistic tool used for modelling nearshore wave heights in HFD systems.

Temporal assessment of wave attenuation

1. What are the fundamental elements of a HFD system that are required for temporal modelling of nearshore wave heights?
2. What is the monthly variation of numerically obtained wave attenuation on vegetated foreshores?
3. Are Bayesian network structures suitable for periodic modelling of HFD system parameters?
4. What is the influence of temporal variability on wave height transformation in HFD systems?

Design guidelines for HFD systems

1. How can temporal assessment be included in the current WBI 2017 guidelines?
2. What are the added benefits of using the DPT to include temporal assessment of HFD systems in the current design and assessment guidelines?

1.4. Significance

In the paper by Van Wesenbeeck et al. (2014) the call for 'mainstreaming ecosystem-based flood defense solutions' is made, as too often traditional and 'proven' solutions are applied instead of HFD solutions. Natural variability in vegetated foreshores make the determination of flood risk challenging, creating hesitant implementation of HFD by decision makers. Thereby neglecting positive and negative effects induced by the NBS elements. It is therefore crucial to create a dynamic probabilistic tool that fills the current knowledge gaps related to temporal evolution of wave attenuation by vegetation, leading to more ease in implementing HFD systems.

This thesis builds on the work by Niazi et al. (2021); Niazi (2019), Vuik et al. (2018b) and Van Zelst (2018), who conducted in-depth research concerning the application of probabilistic methods in the assessment

of HFD systems. This thesis assesses the temporally varying aspect of these systems and connects the probabilistic method as a whole to current flood defense assessment guidelines.

Temporal Modelling
Current assessment methods are static in time (i.e. fixed normative loading). There are however, developments within the current WBI 2017 guidelines to include dynamic loading in the assessment of flood defenses (Mourik, 2020). Currently, dynamic loading of grass covers is used to determine the residual strength as failure is dependent on the load and the duration. The residual strength technique is expected to be applied more generally in the future. Thereby, underlining including temporal aspects in the assessment.

Modelling dynamic wave loads will thus allow the application of contemporary design and assessment methods. The dynamic probabilistic tool integrates the probabilistic temporal response of HFD system elements into the output produced by the DPT. In doing so, the residual strength of both NBS and conventional flood defense elements can be determined. Furthermore, this enables the assessment of complex system processes such as strengthening and weakening of the system through bathymetry and vegetation morphology throughout its design lifetime.

Implementation in Guidelines
Studies by Niazi et al. (2021) and Vuik et al. (2018b) propose probabilistic approaches to assess HFD systems. Yet their work does not present connections to design guidelines. This thesis aims to lay this foundation as an initial step towards design guidelines. Through development of a general method, the guidelines to develop the tool can be implemented for various spatial locations (i.e. also for systems that are not included within the scope in this thesis).

1.5. Scope
Narrowing the scope of this research is necessary as both flood protections and nature based solutions are diverse topics that can differ significantly on a global scale. Furthermore, the assessment of flood defenses are extensive and so the area of assessment is also limited.

Hybrid flood defense system with marsh vegetation in coastal areas will be the main focus in this thesis. The conventional flood defenses considered are dikes as schematized in Figure 1.2. The failure mechanisms examined are limited to hydraulic failure mechanisms. Therefore, the main system elements in the probabilistic model will be restricted to influential parameters regarding hydraulic transformation over the foreshore. Dike elements will only be applied for numerical modelling purposes and are left out of the main probabilistic parameter set.

1.6. Outline
Chapter 1 introduces the importance of flood defenses and the current opportunities of HFD systems. The problem surrounding these systems and the objective are presented. Chapter 2 explains the theoretical background concerning the methods applied throughout the thesis. Chapter 3 proposes the conceptual framework for the development of a DPT. Chapter 4 presents the application of the framework to a case study location in the Netherlands and highlights the application of the framework within the context of the WBI. Chapter 5 shows the results obtained in the case study. All relevant results are presented and discussed in this chapter. Finally, chapter 6 describes the general and specific conclusions and recommendations.

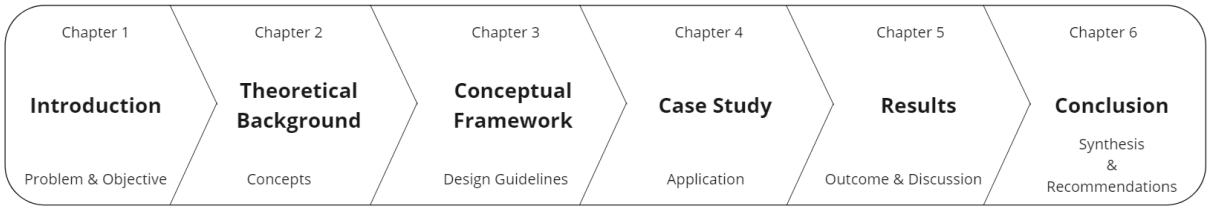

Figure 1.4: Outline of the thesis structure.

2

Theoretical Background

This chapter presents the literature used in the development and execution of this thesis. In this chapter, the current design guidelines are described. Moreover, HFD systems and the inherent variability of the nature based elements are presented. The numerical model XBeach is discussed, whereafter the basic statistical methods used in this thesis are disclosed. Finally, Bayesian networks (BN) are examined in the final section. Throughout this chapter, text boxes present theory regarding HFD systems which falls outside of the scope of this thesis. The objective for this chapter is to present the reader with the theoretical knowledge required to understand the concepts and methods applied throughout this work.

2.1. Hybrid Flood Defense System

A HFD system is a combination of a traditional flood defense (i.e. dike) and a NBS. Both elements reduce the risk of flooding by respectively forming a barrier between water and hinterland and attenuating waves. The conventional flood defense and NBS both provide strength for the system. Hydraulic forces act as loads on the system. The following sections show the fundamental parameters in relation to vegetation wave interaction within coastal HFD systems.

2.1.1. Conventional Flood Defense

Conventional flood defenses encompass a set of man made structures that act as a barrier between the water and hinterland. Dikes and seawalls are both acknowledged as conventional coastal flood defenses. These structures are designed to be able to resist extreme hydraulic conditions and are fully integrated into design guidelines. In these systems, a balance of strength and loads govern the design of the system (section 2.2). The main parameters used in the determination of the strength are the height, slope, form and friction parameters of the flood defense (Table 2.1).

Table 2.1: Main conventional flood defense parameters in HFD systems.

Parameter	Notation	Note
Crest height	h_c	Influences the water level that can be resisted
Offshore slope	α	Influences reflection, wave run-up and impact

2.1.2. Nature Based Solution

The term NBS is rather broad and is narrowed down to a vegetated foreshore in this thesis. The foreshore acts as an inter tidal area containing vegetation which emerges during low water and is submerged during high water as shown in Figure 2.1. Both vegetation and foreshore influence the hydraulic conditions present in the system due to depth induced wave breaking on the foreshore and wave dampening due to vegetation drag. Additional positive effects for the system are sediment capture and geotechnical strengthening of the foreshore due to vegetation (Gedan et al., 2011).

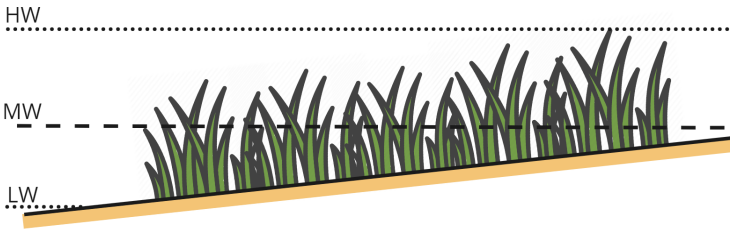

Figure 2.1: Idealized profile highlighting the importance of the water level in relation to vegetation and foreshore emergence.

Foreshores
Depth-induced wave breaking was found to significantly contribute to wave attenuation in HFD systems (Borsje et al., 2018; Vuik et al., 2018b). Here the foreshore effects are included in the wave action balance through depth-induced wave breaking (S_b) and bottom friction (S_f) as shown in Equation 2.1.

$$\frac{\delta(E \cdot c_g)}{\delta x} = -S_f - S_b \tag{2.1}$$

Table 2.2: Main foreshore parameters in HFD systems.

Parameter	Notation	Note
Bathymetry	x, y	Defines the physical boundary of the system
Bottom roughness	c_f	Influences wave dissipation due to bottom friction

Vegetation
Studies regarding the effect of vegetation on hydrodynamics provide evidence of a causal relationship between vegetation presence and wave attenuation (Kobayashi, 1993; Vuik et al., 2016). In these studies, various vegetation parameters were examined to assess the individual relation to wave attenuation. Dalrymple et al. (1984) defined the bulk drag coefficient ($\widetilde{C_D}$) to quantify the dissipation of wave energy over a vegetated field. In that approach, linear wave theory was assumed valid and the vegetation was simplified as rigid cylinders. The wave energy reduction due to vegetation (S_v) was included in the wave action balance as shown in Equation 2.2.

$$\frac{\delta(E \cdot c_g)}{\delta x} = -S_v \tag{2.2}$$

Appendix A dives further into the derivation of the drag coefficient and its relation to vegetation parameters. Summarizing the information from the appendix results in a number of vegetation parameters that are of importance for determining wave attenuation. Complying with the predefined scope, the vegetation parameters were translated to their respective marsh parameters (Table 2.3).

Table 2.3: Main vegetation parameters in HFD systems.

Parameter	Notation	Note
Height	h_v	Required to determine the vegetation area
Width	b_v	Used to determine the vegetation area and the Reynolds number
Density	N_v	Necessary for calculating the total drag force
Drag coefficient	C_D	Applied for determining the total drag force

2.1.3. Hydraulic Forces
The main purpose of flood defenses is to prevent water from reaching the hinterland. The fundamental hydraulic parameters that influence this process are instinctively the water level and wave parameters. High water levels provide larger probabilities of water overtopping the height of the flood defense. Similarly, larger waves can undermine the stability of the flood defense or lead to run-up and overtopping

over the structure as shown in Figure 2.3. Other hydraulic parameters, such as currents and velocities, ultimately influence the fundamental wave and water level parameters. Thus, the main hydraulic parameters in HFD systems were defined as the water level (Wl), wave period (T_p) and offshore and nearshore wave height (H & H_{ns}).

Table 2.4: Fundamental hydraulic parameters in HFD system assessment.

Parameter	Notation	Note
Water level	Wl	Influences submergence of foreshore and dike (Fig. 2.1)
Offshore wave height	H	Influences the hydraulic conditions on the foreshore
Offshore wave period	T	Influences the hydraulic conditions on the foreshore
Nearshore wave height	H_{ns}	Required for flood defense assessment (Fig. 2.3)

Fluvial Flood Defense

Apart from coastal flood defenses there are also fluvial flood defenses which can be found alongside rivers. In contrast to coastal flood defenses, the main threat of over-topping is due to high water discharge in the river instead of over-topping due to waves. While waves still influence this process, the water level in the river is dominant in the determination of flood risk.

Including NBS for fluvial dikes requires additional caution as different processes are present. By altering the bathymetry of the river for instance, the water level in the river would change. Thus, affecting flood risk at the corresponding river dike section. Moreover, reducing the flow velocity in the river by placing vegetation would lead to an increase in water level due to continuity. Therefore, implementing NBS in combination with fluvial dikes would require another approach.

A different approach is necessary as the parameters that are of influence to the system are not the same as those used in coastal areas. For instance, the causes of flooding vary significantly as flow conditions dominate the water levels in fluvial environments. Additionally, the bathymetry variability is also different. Therefore, different processes and inter-dependencies are present in these systems.

The parameters of influence on the bathymetry would depend on upstream conditions and surrounding hydraulic structures (i.e. dams, dikes and sluices). An increase in flow conditions would lower the water level due to continuity and can simultaneously influence the sediment fluxes by either more being imported from upstream or more being eroded at the section of interest. All these parameters should be included in a fluvial analysis to provide a set of parameters that correctly represent the physics of a HFD analysis in fluvial conditions.

2.2. Design Guidelines - WBI

In the Netherlands, a country prone to flooding, design codes were developed to support assessment and design of flood defenses. The WBI was created by Rijkswaterstaat, a government agency responsible for infrastructure and water management, as a standardized set of guidelines used to assess flood defenses (Rijkswaterstaat, 2017).

2.2.1. Flood Defense Assessment

The WBI describes a standardized approach to flood defense assessment, shown in Figure 2.2. Combining a schematized version of the dike with normative failure probabilities for the dike segment and the corresponding normative hydraulic loads, enables assessment of the dike (Ministerie van Infrastructuur en Milieu, 2017a). In turn, the assessment enables reporting of the current safety of the flood defense. Schematizing the flood defense system is not included in the WBI guidelines, yet necessary for assessment of the system. Normative flood risk probabilities are defined for different dike segments in the Netherlands and can be obtained from Hydra NL; a tool developed by RWS and used in the WBI (Duits, 2019).

Subsequently, Hydra NL can be used to determine the corresponding normative hydraulic loads for the flood defense system. Given the schematized system and normative hydraulic loads, all failure mechanisms can be assessed and reported.

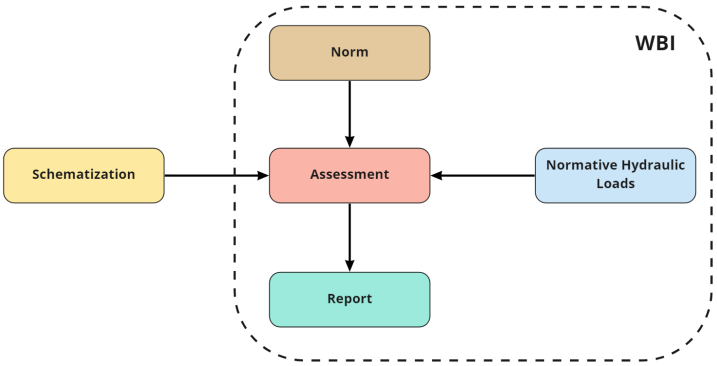

Figure 2.2: Visual representation of the current technical WBI assessment approach (Ministerie van Infrastructuur en Milieu, 2017a)

The WBI defines many failure mechanisms and proposes methods to test each failure mechanism for a given system (Ministerie van Infrastructuur en Milieu, 2017a). Both geo-technical (i.e. stability of the dike) and hydraulic (i.e. wave impact and overtopping) failure mechanisms are included. Each test method includes a set of calculations that can be applied to assess the probability of failure. As defined in the scope, this research focuses on hydraulic failure mechanisms, for which the most important assessment formula are the overtopping discharge and wave impact.

Overtopping

In the determination of wave overtopping, the principal formula used in the design of the flood defense is defined in the Eurotop manual (van der Meer et al., 2018) as defined in Equations 2.3 and 2.4.

$$\frac{q}{\sqrt{g \cdot H_{m0}^3}} = \frac{0.023}{\sqrt{\tan\alpha}} \cdot \gamma_b \cdot \xi_{m-1,0} \cdot \exp\left[-\left(2.7 \frac{R_c}{\xi_{m-1,0} \cdot H_{m0} \cdot \gamma_b \cdot \gamma_f \cdot \gamma_\beta \cdot \gamma_v}\right)^{1.3}\right] \tag{2.3}$$

with a maximum of:

$$\frac{q}{\sqrt{g \cdot H_{m0}^3}} = 0.09 \cdot \gamma_b \cdot \exp\left[-\left(1.5 \frac{R_c}{H_{m0} \cdot \gamma_f \cdot \gamma_\beta \cdot \gamma_v}\right)^{1.3}\right] \tag{2.4}$$

where:

q	=	Mean overtopping discharge
H_{m0}	=	Wave height
g	=	Gravitational pull
α	=	Slope
γ_b	=	Berm factor
γ_f	=	Friction factor
γ_β	=	Oblique wave factor
γ_v	=	Wall influence factor
R_c	=	Freeboard
$\xi_{m-1,0}$	=	Surf similarity parameter

Wave Impact

Wave breaking on the dike slope leads to significant forces that require absorption by the dike cover. Depending on the cover layer of the dike, various methods can be applied to assess the strength of the

dike (CETMEF, 2007). The main parameters vary per equation due to the many variables included in the types of rock covers. The essential parameters include the wave height and period in the determination of failure as those define the load and recurrence of the loading.

Overview
Figure 2.3 illustrates the relevant parameters in hydraulic failure formulas. There are a number of parameters that are mostly related to the dike and are not discussed in more depth throughout this thesis as it is not within the scope (i.e. γ, R_c etc.). As can be seen, the wave height and water level at the toe of the dike are the main hydraulic parameters in the assessment of dike stability. These parameters are used in WBI tools used for standardized assessment such as *Riskeer*, and *BM-Gras Buitentalud*.

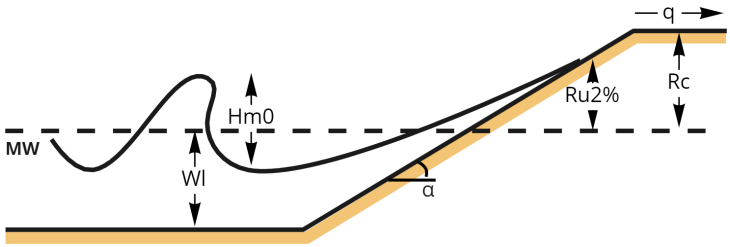

Figure 2.3: Main parameters used in the determination of hydraulic failure.

2.2.2. Hybrid Flood Defenses
Vegetated foreshores are not included in the standard assessment of HFD systems. To include their effects on hydraulic propagation, reference is made to the WBI appendix II documentation (Ministerie van Infrastructuur en Milieu, 2017b). It is stated that the effects of foreshores are not included in standard assessments and that a tailored assessment needs to be applied. This can be done using WBI software (i.e. *Ringtoets/Riskeer*, *Hydra-NL*). The effects of vegetation are not included in the WBI.

2.3. Variability in HFD Systems
A recurring challenge in attempting to model hybrid flood defenses, is to capture the natural variability of the parameters in the system. Currently, ecosystems are modelled as linear systems (i.e. not changing through time), while they are inherently non-linear (Gedan et al., 2011). More specifically, variation in biophysical, hydraulic and bathymetry parameters complicate the modelling of waves over vegetated foreshores, making it difficult to describe them with a simple rule of thumb. The inability to accurately account for dynamic variability in nature, is also one of the main knowledge gaps preventing the implementation of hybrid flood defenses (Bouma et al., 2014).

Variability can be subdivided into both spatial and temporal variability. Furthermore, the scales of the variability are specified in terms of micro (i.e. cm's or minutes), meso (i.e. meters or days) and macro (i.e. km or years) scale. In regard to the scope of this research, spatial variability is not explored in more depth. All processes smaller than micro scales are neglected, as the variability of the physical processes at these scales are believed to be of less impact to the entire system compared to the other scales. Thus, focusing on temporal variability in the order of hours to months.

Hydraulic
The fundamental hydraulic parameter, water level and wave height, are inherently variable through time. Focusing on coastal waters, the water level is influenced by the tidal forcing. Moreover, the wave parameters are influenced by both ocean swell and the combination of wind speed and fetch (i.e. the distance over which the wind can create waves). Therefore, the temporal variability of these parameters is directly related to the temporal variability of the forcing variables.

The water level is forced by the tides which in turn are excited by solar-lunar forces. As the orbital motions are predicted with consistent accuracy, the mean water level can be determined with significant accuracy. However, the mean water level also depends on other conditions such as storm surge. This can lead to coastal water levels being larger due to water level set up. Thus, over the course of a year,

the mean water level does not vary significantly. In contrast, on hourly scales, the water level varies significantly.

Similarly, wave parameters are dependent on ocean swell and meteorologic forcing (combined: metocean conditions). These forces vary on hourly, daily and monthly timescales. The combination of these forces will influence the hydraulic parameters. While hourly metocean conditions vary slightly, seasonal metocean conditions can have a great impact on the mean hydraulic conditions throughout the year.

Vegetation

The variability of vegetation parameters is expected to depend on the seasons (Koch et al., 2009). Naturally, the production of biomass depends on the climate, which differs per geophysical location. This study focuses on salt marsh systems. A study in Louisiana (US) presented results where the biomass in March was five times larger than the biomass in September of that same year (Darby and Turner, 2008). Another study analysed two marsh types in England and found the biomass to vary between 0.5 kg/m^2 in May to 1.8 kg/m^2 in October (Fig. 2.4). The significant seasonal variations in parameters, influence the strength of the system as a whole.

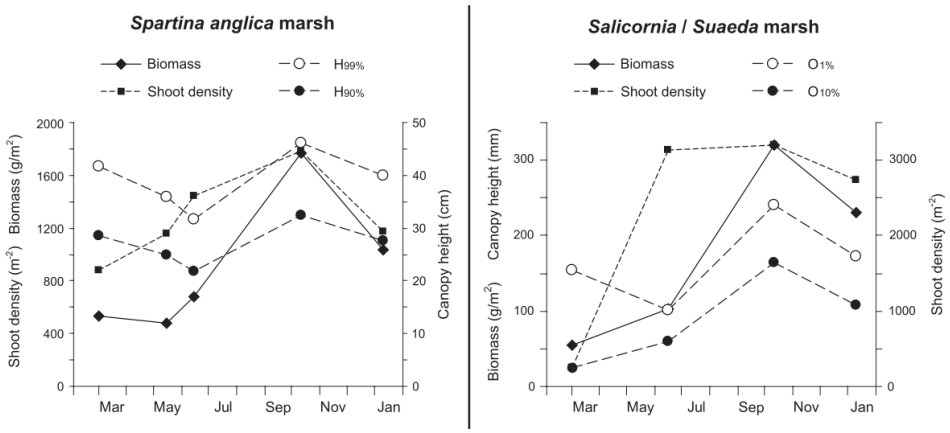

Figure 2.4: Seasonal variability of marsh grasses (Neumeier, 2005).

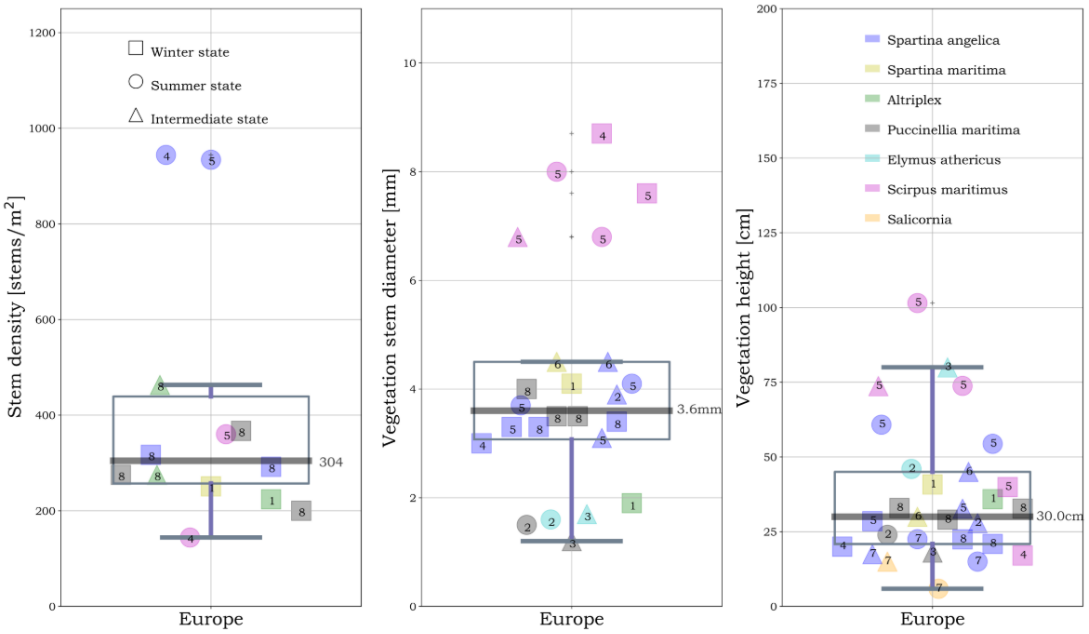

Figure 2.5: Physical variability in salt marsh properties (Van Zelst, 2018).

Van Zelst (2018) combined data from multiple studies where salt marsh parameters were measured. Figure 2.5 illustrates the mean values found in these studies (i.e. each value is based on numerous measurements). Furthermore, the variability between winter, summer and intermediate (i.e. autumn and spring) states and species type was shown to influence the vegetation parameters.

Seasonality is clearly the main factor influencing vegetation variability in HFD systems. Therefore, changes in the system will remain relatively constant and vary in the order of months. It should be noted that stem breakage can lead to quick decrease of system strength (Vuik et al., 2018a). Thus, the composition of the vegetated system is mostly dependent on the species, seasons and external forcing.

Mangroves

Salt marshes are mostly present at higher latitudes, mangroves are also a common vegetation to be found along a given coastline. According to Van Zelst (2018), 31% of the global coastlines is vegetated and of the coastlines that are vegetated, roughly 55% is covered with mangroves. Figure 2.6 depicts the vegetated locations and the vegetation type.

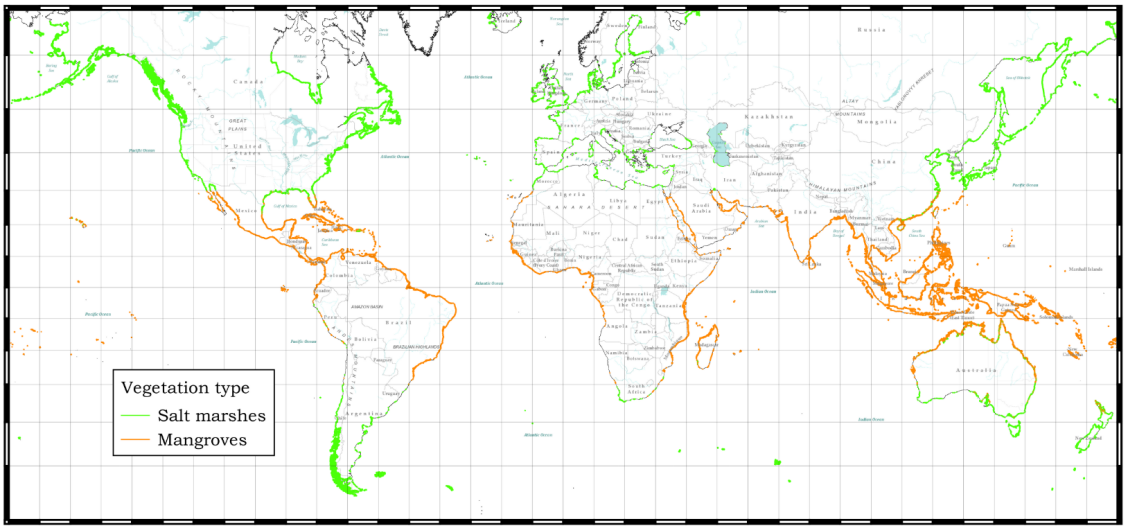

Figure 2.6: Indication of the vegetation that is present on a global level (Van Zelst, 2018)

While salt marshes are defined as a single layer system, mangroves are more complex and are more accurately defined as a three layer system of: submerged roots, a canopy and a trunk which connects the two. Each layer naturally has its own properties as shown in Figure 2.7. This will add more complexity in regard to the drag coefficient as a different drag coefficient is specified at each height.

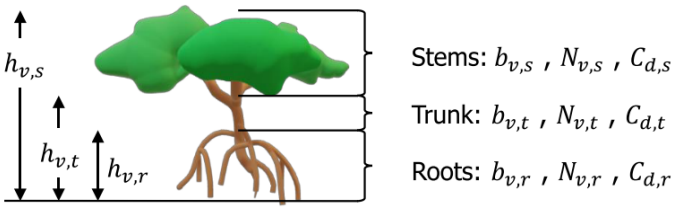

Figure 2.7: Mangroves represented as a three layer system (Niazi, 2019).

Bathymetry

The bathymetry variation of coastal HFD systems depends on the fluctuations in sediment transport rates, as shown by Equation 2.5. Representing a bathymetric profile as a 3-D space, the bed level (z_b)

through time (t) depends on the alongshore (S_y) and cross shore (S_x) fluxes combined with a sink or source term (V). Without sinks or sources in the system, the bed level depends on the fluxes. Waves, currents and winds influence these fluxes and thus manipulate the bed level.

$$\frac{\delta z_b}{\delta t} + \frac{\delta S_x}{\delta x} + \frac{\delta S_y}{\delta y} = V \tag{2.5}$$

Where:

z_b	=	Bed level
S	=	Sediment transport rates per width of flow in horizontal x- and y-directions
V	=	Sink or source term

2.4. Numerical Modelling - XBeach

XBeach is an open-source numerical model developed to model hydrodynamic and morphological processes near the shoreline. Although it was initially developed to assess sandy coastlines, over the years the application of processes such as bed-updating and vegetation have been included.

There are three main hydrodynamic modes in which XBeach can numerically solve wave progression within the domain. The first is a stationary mode, in which wave-averaged equations are solved, thereby neglecting infragravity waves and reducing run time. The second is the surfbeat or instationary mode, where short and long wave variations are resolved using the wave action balance equations. The third and final mode, is the non-hydrostatic mode which resolves waves using the non-linear shallow water equations in combination with a non-linear hydrostatic pressure term.

Of the three models, the non-hydrostatic mode most accurately solves hydraulic processes the cost of which is an increase in computational time as a larger spatial grid resolution and smaller time steps are required. Moreover, this mode is applicable to both steep and mild slopes and can thus be implemented for a wide range of scenarios.

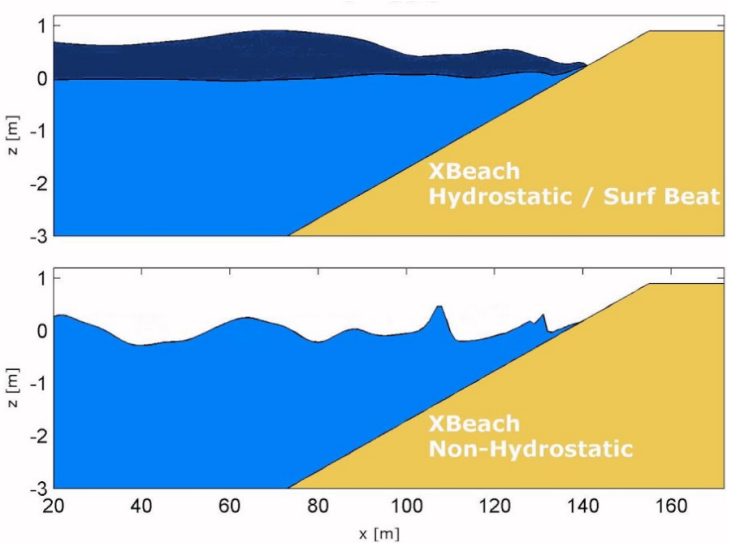

Figure 2.8: Illustration of the XBeach hydrodynamic modes (courtesy of Deltares).

Numerical Domain

XBeach uses a three dimensional grid (i.e. x, y, z) to define the computational domain. The grid size determines the amount of cells within the model. Moreover, the model solves coupled two dimensional horizontal equations for hydrodynamics, sediment transportation and bottom updating within every cell.

A two dimensional numerical grid is created if no y-coordinates are specified. Thereby creating a grid where the x-direction is positive towards the coastline and the z-direction is used to specify bed levels and wave heights, with positive values being upward.

Boundary Conditions

There are multiple boundary conditions required for an XBeach model to function properly. On top of which a set of additional conditions can be specified to include in the numerical calculations.

The numerical model can be seen as a two dimensional space with four boundaries (i.e. left, right, top, bottom). The first boundary (left) is the seaside or offshore boundary which represents the location from which waves and the tide are forced artificially into the numerical domain. The second boundary (bottom) is the bathymetry profile starting from the offshore boundary and ending at the opposite boundary where the flood defense (i.e. dike) is situated. The third boundary (right) will not be defined in this thesis, the hydrodynamics should not reach this location. Finally, the fourth boundary (top) is also undefined as the free surface does not reach this location, thus providing space for the waves to propagate through the numerical domain.

At the seaward boundary, wave boundary conditions can be set as either a spectral or non-spectral wave boundary condition. The non-spectral type is applied in this thesis and requires a set of significant wave heights (H_{rms}) and wave periods (T_{m01}). Moreover, the wave groups can be defined as a single sea state (i.e. only one set of H_{rms} and T_{m01}) or as a time series of sea states. Tide can be modelled as a uniform water level or as a time varying water level. Finally, the offshore boundary characteristics are defined in terms of reflecting waves.

The bathymetry is defined in terms of composition of the bed and the actual bathymetric profile.

Numerical Processes
XBeach itself is built on a library of formulas which contains all necessary equations for solving the physical processes that occur. There are many libraries available within the XBeach documentation, the most important of which are discussed below and elaborated on in detail in Appendix B.

1. Non-linear shallow water equations to ensure optimal wave resolution;
2. Wave action balance;
3. Dissipation to include vegetation-hydraulic interaction;
4. Sediment transportation to enable morphological processes; and
5. Bottom updating to assess the effects of morphology throughout model run time.

As the shore parallel y direction is neglected, Coriolis effects are also left out of the equations. Moreover, all wave processes are assumed shore normal therefore, all angle of incidence formulas are also removed for wave related equations.

2.5. Statistical Background

This section presents the statistical methods that are applied throughout this thesis. Furthermore, the theoretical basis required to grasp the concepts of dynamic multivariate modelling are presented.

2.5.1. Probability Distribution

The probability distribution of a random variable X is a function that defines the probability p_i for each value x_i (Nápoles et al., 2013):

$$p_i = P(X = x_i); 0 \leq p_i \leq 1; \sum p_i = 1 \tag{2.6}$$

Parametric distributions can be fitted to continuous variable (X) to represent the variable using a probability distribution. A probability density function (pdf) can be used to compute the probability over an interval for a random variable (Eq. 2.7).

$$P(a \leq X \leq b) = \int_a^b f(x)dx \tag{2.7}$$

The cumulative distribution function (cdf) defines the probability that the variable X is smaller or equal to x (Eq. 2.8). The original dataset can be represented by the theoretical probability distributions (pdf or cdf).

$$F(x) = \int_{-\infty}^{x} f(x)dx \tag{2.8}$$

2.5.2. Correlation

The relation or dependence between variables is summarized through their correlation. The measure of dependence is known as the covariance of a pair of variables X, Y where covariance is measured using Equation 2.9, where $E(X)$ and $E(Y)$ represent the expectation of X and Y respectively. A positive covariance implies that large values for X coincide with large values for Y and vice versa. A negative covariance indicates that large values for X coexist with small values for Y and vice versa.

$$Cov(X, Y) = E([X - E(X)][Y - E(Y)]) \tag{2.9}$$

The measure of dependence or correlation can be expressed using the covariance and the standard deviation, which is generally known as Pearson's correlation coefficient ρ. Again, using two variables X, Y the correlation can be determined as

$$\rho(X, Y) = \frac{Cov(X, Y)}{\sigma_X \sigma_Y} \tag{2.10}$$

where σ_X and σ_Y represent the standard deviation of X and Y. Aside from Pearson's correlation coefficient, Spearman's rank correlation coefficient can also be used to describe the relation between two variables. While Pearson's coefficient can be used to describe the amount of linear dependence in the data, Spearman's coefficient (Eq. 2.11), is used to assess how monotone the data is. Spearman's rank correlation coefficient is similar to that of Pearson, yet the variables X, Y are replaced with their corresponding ranks R and S, where n defines the number of observations.

$$r = \frac{Cov(Rank(X), Rank(Y))}{\sigma_{Rank(X)} \sigma_{Rank(Y)}} = 1 - \frac{6 \sum R_i - S_i}{n(n^2 - 1)} \tag{2.11}$$

Furthermore, the confidence bounds corresponding with Spearman's rank coefficient are determined using the Fischer transformation (Eq. 2.12). In which the confidence bounds are denoted by $p\%$ and (1 - p)%.

$$r_{conf} = tanh\left(atanh(r) \pm \frac{\Phi(1 - \frac{p}{2}, 0, 1)}{\sqrt{n - 3}}\right) \tag{2.12}$$

Autocorrelation

The autocorrelation is the correlation of a variable with a delayed version of itself. The autocorrelation function defines the correlation per time-shift. The autocorrelation for 0 time-shift is equal to 1 as the exact same data is used. Using Pearson's correlation coefficient (Eq. 2.10), and applying the variables $X_{t=0}$ and $X_{t=1}$, will provide the autocorrelation of the data with a time shift equal to $t = 1$.

2.5.3. Copula

Dependence modelling by copulas has its roots in the representation theorem by Sklar (1959). A copula defines the joint cumulative distribution function (cdf) $H(X, Y)$ of two continuous variables (X, Y) and combines their uniform marginal distributions into a multivariate distribution on the unit square $[0, 1]^2$ (Genest and Favre, 2007). Thereby representing the dependence between the two variables. The corresponding cdf can be written as:

$$H(X, Y) = C(F(x), G(y)), \qquad x, y \in \mathbb{R} \tag{2.13}$$

where $F(x)$ and $G(y)$ represent marginal distributions of X and Y respectively, while C represents the copula on the unit square. Depending on the multivariate data, several copula families can be fitted to determine which is most accurate in representing the dataset.

Sampling

Using copulas, sampling can be applied to obtain pseudo-data that is correlated. Sampling implies that

a random value is selected from a probability distribution. As the selected variable is related to other variables through copulas, their values follow from the initial sample. With multiple variables connected through copulas, a single sample can result in a set of values which can be substantiated by correlations that are based on empirical data. Thus resulting in a pseudo-dataset.

2.5.4. Goodness of Fit

Multiple statistical tests were applied to test the goodness of fit of the statistical application. Statistical tests are discussed for use in the application of one dimensional probability distributions, copulas and Bayesian Networks. Appendix C presents the following tests that were used in this thesis:

- Sum of squared differences (SSD);
- Akaike information criterion (AIC);
- Semi correlations;
- Cramér von Mises (CVM);
- d-calibration statistic.

2.6. Bayesian Network

Bayesian networks are probabilistic models that have been applied in different fields to model dependence structures between variables through inference, an estimate of an outcome based on given information, to determine an output sample. They are based on Bayes's theorem (Eq. 2.14) which states that the probability of an event changes once more information becomes available for that event. In this section, the difference between static and dynamic Bayesian networks will be discussed. Moreover, the MATLAB toolbox used to develop and utilize BNs is explained.

$$P(A|B) = \frac{P(B|A) \cdot P(A)}{P(B)} \tag{2.14}$$

2.6.1. Static Bayesian Network

Bayesian Networks (BN) describe a joint distribution through conditional independence relationships. BNs are directed acylic graphs (DAG). DAGs consists of nodes (N1 - N3 in Figure 2.9) and arcs (A1 & A2 in Figure 2.9). Nodes represent the variables that are modelled within the BN, while arcs represent the dependence structure between the nodes. The dependence structure between the nodes can be represented by a rank correlation matrix (RCM) which is used to build a single copula that defines the entire structure. Subsequently, inference in the BN can be applied to sample variables through conditioning of other parameters in the network.

Inference can be conducted in BNs through conditionalizing, updating and sampling. For example, conditionalizing node ($N1$) affects the dependent variable ($N3$) through the dependence arc. Updating the network adjusts the marginal distribution for ($N3$) through the copula representing the BN. Subsequent sampling from the updated node ($N3$) is called conditional sampling. This results in conditional samples for node 3 $P(N3|N1)$.

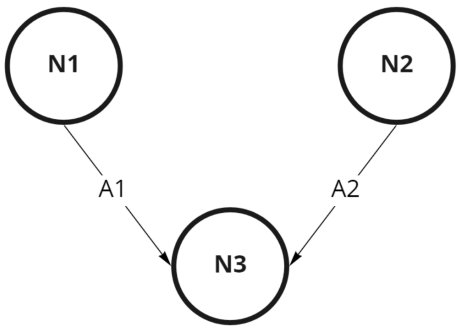

Figure 2.9: An example of a BN structure with the circles representing the nodes and the arrows representing the arcs.

2.6.2. Dynamic Bayesian Network

A dynamic Bayesian network (DBN) can be defined as a series of BNs that are interconnected by temporal relationships (Kjærulff, 1993). Enabling the description of multivariate dynamic systems. Different applications of DBN have been used in literature. DBNs have been applied as a decision tool for tunnel construction (Wu et al., 2015), modelling ecosystems over time (Uusitalo et al., 2018) and assessing the effects of climate change on ecosystem components (Trifonova et al., 2019).

The mathematical formulation of a DBN can be defined as $G = (V^t, E^t, E^t_{\rightarrow})$, where G represents a graph of variables $V^t = \{x_1^t, x_2^t, ...x_n^t\}$, where x_n^t represents the node n at time t (Abebe, 2020). Moreover, E^t represents the set of links in a given time slice while $E^t_{\rightarrow}$ represents the set of links between time slices. A schematic example is shown in Figure 2.10.

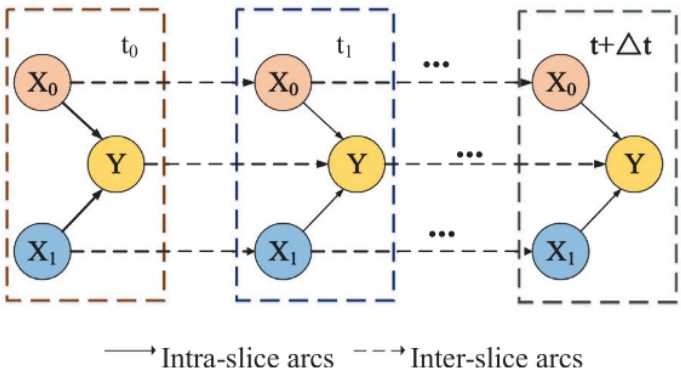

Figure 2.10: A DBN structure in which variable Y^t is dependent on X_0^t and X_1^t, as well as all variables from the previous time slice $t-1$ (Chang et al., 2019).

2.6.3. BANSHEE Toolbox

BANSHEE is a MATLAB toolbox used for development, validation, visualizing and making inference with BNs (Paprotny et al., 2020). BNs can be constructed through defining parent child relations in MATLAB code and running *bn_rankcorr* to obtain the rank correlation matrix for the BN. The rank correlation can be used to conduct inference, compute the Gaussian distance and assess the CVM statistic. All functions available in the toolbox were utilized in the development of Bayesian networks, for additional information regarding the toolbox the reader is referred to Paprotny et al. (2020).

3

Conceptual Framework

The current thesis proposes a conceptual framework to design and assess HFD systems. This framework develops a dynamic probabilistic tool (DPT) that is used for temporal assessment of the effects of NBS elements on wave loads. The tool and corresponding approach are placed within current Dutch design and assessment guidelines. This chapter presents the overview of the framework, whereafter the specific steps in the guidelines are discerned in more detail.

3.1. Overview

The dynamic probabilistic tool developed in this thesis finds its place within the current WBI guidelines (section 2.2) as illustrated in Figure 3.1. The normative offshore hydraulic loads used to assess or design a flood defense are transformed to hydraulic loads that include the processes induced by the NBS element in the HFD system. Thus, enabling the assessment of HFD systems in accordance with WBI guidelines.

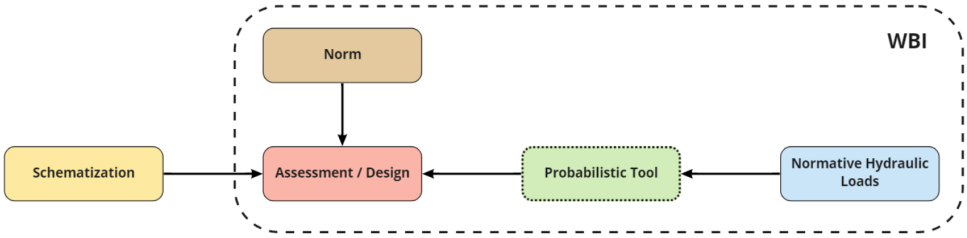

Figure 3.1: Location of the dynamic probabilistic tool within the WBI guidelines.

A database, probabilistic model and application settings form the fundamental elements of the DPT (Fig. 3.2). The probabilistic model requires a set of parameters to represent the system statistically. The database stores datasets representing the system parameters and is connected to the probabilistic model through application settings. Additionally, the application settings are used to manipulate the database and probabilistic models for specific applications (i.e. short or long term; extreme or day to day values). Each element can be adjusted or improved to facilitate another application purpose.

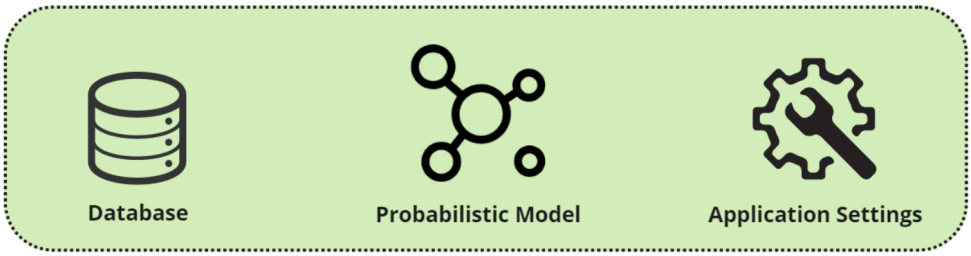

Figure 3.2: Illustration of the three main elements in the dynamic probabilistic tool.

3.2. Guidelines

Three main processes form the foundation of the guidelines used to develop a location specific DPT(Fig. 3.3). The first concerns development of a database (yellow boxes), for which the overall database completeness is ensured through statistical and numerical expansion (purple boxes). Second, the creation of probabilistic models (green boxes) provide the probabilistic backbone of the tool, enabling the computationally efficient predictive modelling properties of Bayesian networks. Finally, construction of application settings (red boxes) facilitate the implementation of the DPT for site and application specific assessment of the HFD system.

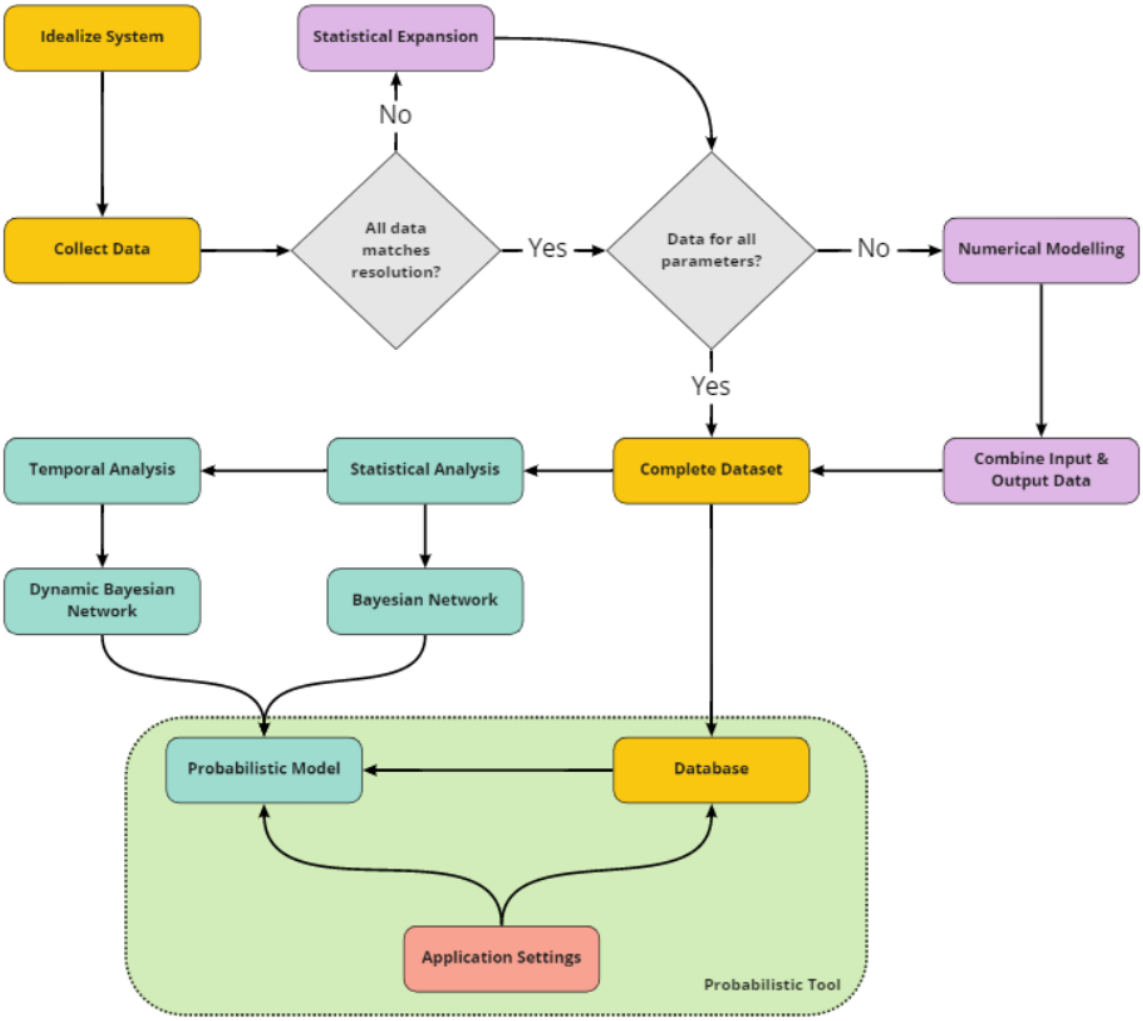

Figure 3.3: General process for development of a dynamic probabilistic tool that can be used to asses HFD systems.

3.2.1. Database

Three main parameter classes were defined to represent the HFD system: Hydraulic, vegetation and bathymetry (Fig. 3.4). Each parameter class contains the fundamental variables that effect wave propagation over the foreshore (section 2.1). Complying with the variable requirements for numerical and probabilistic modelling (section 2.4 and 2.6).

Data must be collected for each variable. As highlighted in the problem statement, the inherent temporal variability in nature based elements results in physical uncertainty regarding the strength of the system through time (section 2.3). To capture and model this uncertainty in the final tool, the temporal resolution of the variability should be included in the dataset. If required, statistical expansion (i.e. copula sampling,

linear interpolation, etc.) must be applied to match the temporal resolution of the database.

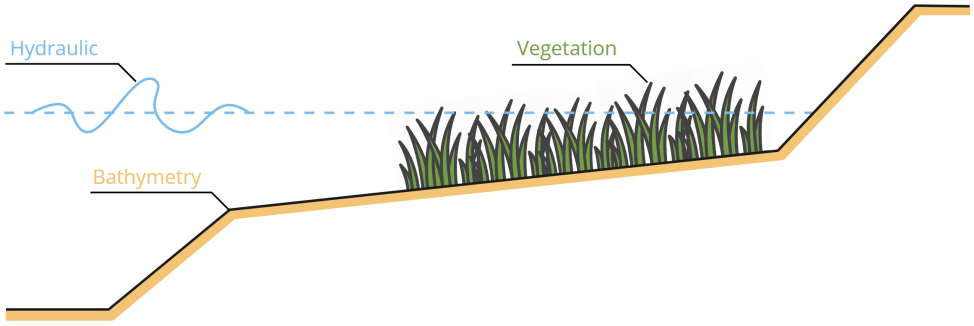

Figure 3.4: Main HFD system parameter categories: Hydraulic, bathymetry and vegetation.

If fundamental data is lacking (i.e. nearshore wave height, morphology, etc.) numerical modelling shall be applied to expand the database. The XBeach toolbox in MATLAB should be applied to mode wave propagation through the system (section 2.4). Numerical settings should be tuned to comply with the processes included in the specific application of the model (i.e. including morphology or vegetation dampening). Calibration and validation of the numerical model ensure computational efficiency and physically accurate outcomes. Lacking data can be extracted from the numerical results and merged with the incomplete database. Ultimately resulting in a complete temporally uniform database.

3.2.2. Probabilistic Models

Dynamic and static BNs (section 2.6) must be developed to model nearshore wave height in HFD systems. A statistical analysis of the database is required to assess the database dependence structures and marginal distributions. Rank correlation matrices (RCM) are used to depict the probabilistic dependence between the variables. Theoretical marginal distributions represent the observations of the variables and are used to transform samples within uniform range or domain [0,1] back to their original units. A static Bayesian network (SBN) represents the system within a temporal slice, while a dynamic Bayesian network (DBN) relates temporal slices with one another. Through calibration and validation, multiple DAG structures (i.e. dependence structures) must be developed using the BANSHEE toolbox in MATLAB. The most suitable variant is chosen based on physical and statistical accuracy. Conditionalized sampling from both Bayesian Networks enables predictive modelling of HFD system parameters.

3.2.3. Application

Application settings connect the database and the probabilistic model. Depending on the application, the settings should include filtering of the system, input conditions, model run time and other application specific settings. Furthermore, the settings should define the conditionalization process of the BNs. Ultimately, the model settings form the algorithm used to run the DPT to completion, resulting in model output.

Flood Defense Assessment: Storm Conditions

WBI guidelines can be followed for the assessment of a flood defense during storm conditions (section 2.2). The guidelines combine normative hydraulic parameters with a schematized flood defense to determine the probability of failure. Model application settings must be developed to include the effects of vegetated foreshores on wave heights at the dike toe (i.e. used to design and assess the dike, Fig. 2.3). To do so the following steps are executed consecutively:

1. Read normative input data for hydraulic and vegetation parameters;
2. Filter database for extreme values;
3. Setup the probabilistic model, conditionalizing the network using specified data;
4. Sampling wave heights at the dike toe from the BN.

In turn, the nearshore wave heights are used to assess the probability of failure in accordance with the hydraulic failure mechanisms defined in the WBI (section 2.2). This results in a hybrid flood defense assessment in accordance with WBI standards.

3.3. Summary

This chapter presented a conceptual framework used to develop a DPT for design and assessment of HFD systems within the context of the WBI (Fig. 2.2). A database, probabilistic models and application settings form the fundamental DPT elements (Fig. 3.2). As HFD systems vary on a global scale, design guidelines provide the set of steps that must be followed to develop a DPT that can be used for design assessment (Fig. 3.3).

4

Case Study

This chapter presents the method for the development of a DPT at Hellegatpolder. This is achieved through application of the conceptual framework discerned in chapter 3. One can assess all methodological steps required for the development of the DPT, as well as the application method for assessment of the HFD system using both the DPT and the WBI guidelines.

After defining the location and corresponding site specific information in section 4.1, an overview of the applied methodology is presented in section 4.2. Thereafter, each element in the method is discerned, starting with the creation of a database in section 4.3. The database is used to build probabilistic models in section 4.4. Finally, application settings for storm analysis are defined in section 4.5, completing the DPT and enabling assessment of the dike at Hellegatpolder with and without NBS elements included in the design.

4.1. Location

The location chosen for the case study is the Hellegatpolder salt marsh, situated in the Western Scheldt, an estuary in the Netherlands. Data availability, presence of salt marsh and availability of literature concerning wave attenuation field studies are the most important reasons for selecting this location. Figure 4.1 presents the location of Hellegatpolder (dashed box), the dike segment 32-4 (grey line) bordering the marsh and the salt marsh (green area) which contains the transect (brown line) analysed in this thesis.

Figure 4.1: Location of Hellegatpolder in the Western Scheldt, the Netherlands. Depicting dike section 32-4 (grey line), the salt marsh (green area) and the transect (brown line).

Hellegatpolder is in direct contact with the ocean, as the estuary that connects to the port of Antwerp is not closed off from the North sea. The dike bordering the salt marsh is part of dike section 32-4, which has a normative signal probability of flooding of 1/3000 per year (Duits, 2019). The wind directions that

lead to high loads are between 240-330°, which does not correspond with the dominant south west (225°) wind direction present in the Netherlands. Aside from the meteorologic influence on the waves, shipping in the Western Scheldt also causes wave formation. *Spartina angelica* marsh grasses are present on the foreshore. Additional external influences in the system include dredging of the channels to ensure access to the port of Antwerp. Finally, water levels in the estuary are influenced both by river discharge and tidal forcing from the north sea, which is known to be semi-diurnal. This results in ebb and flood flows in the channels with each tidal cycle.

4.2. Method Case Study

The objective of the case study is the modelling of nearshore wave heights (main hydraulic failure parameter shown in Figure 2.3) during storm conditions, through application of the DPT within the WBI approach. In this assessment, the NBS process included in the DPT comprise of wave dampening due to vegetation. No data nor numerical models were available to obtain spatial vegetation morphology and was thus excluded from the analysis. Furthermore, bathymetry evolution was excluded from the main processes as it was found insignificant for the timescales assessed in this thesis (section 5.1.2). Application of the DPT results in the comparison of wave heights for the scenarios:

1. WBI normative nearshore wave heights (no DPT modelling);
2. Modelling nearshore wave heights over a bare foreshore using the DPT;
3. Modelling nearshore wave heights over a vegetated foreshore for each season using the DPT.

The conceptual framework defined in Figure 3.3 was followed in the development of a DPT for Hellegatpolder. The main elements: database development, creating probabilistic models and application of the DPT are discussed separately below:

Database

Starting with system idealization at the location. Subsequently, data was collected for the main parameter categories and matched for the aimed temporal resolution of 30 minutes (i.e. sufficient for capturing storm response). As vegetation data was unavailable, discerned further in section 4.3, field measurement data was statistically expanded to obtain vegetation data that matched the temporal resolution. Moreover, data at the toe of the dike was not available in literature data, thus the numerical model was applied to expand the dataset to include these parameters. The combination of data collection, statistical and numerical expansion resulted in a complete dataset ready for the development of the probabilistic model.

Probabilistic Model

The database was used to develop two Bayesian networks that form the probabilistic models in the dynamic probabilistic tool. A static Bayesian network (SBN) relates offshore hydraulic and vegetation variables to nearshore wave heights. Thereby, enabling the modelling of the system within a single time step. Additionally, a dynamic Bayesian network (DBN) was conceived to model offshore hydraulic variables through time. Together, the DBN can create a time series of offshore hydraulic conditions while the SBN can be used to relate the offshore variables to the nearshore wave loads as shown in Figure 4.2.

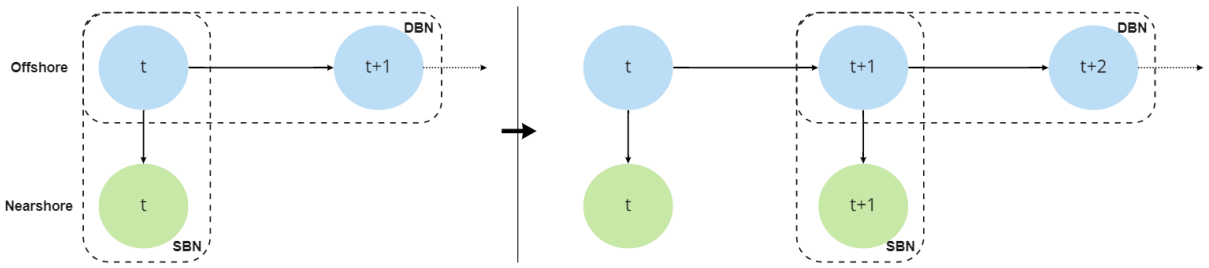

Figure 4.2: Illustrating the symbiosis of the static and dynamic Bayesian networks (SBN & DBN). Provided the initial condition (blue t) enables modelling of the DBN into the future (blue t+1) and transformation to nearshore conditions using the SBN (green t). Subsequently, shifting the network allows for dynamic modelling (right).

Application
Finally, assessment of the dike segment 32-4 at Hellegatpolder was conducted in accordance with the WBI approach. To determine hydraulic failure, wave heights at the dike toe were modelled during storm conditions. First, model application settings were developed to manipulate the probabilistic model to create a RCM using only storm conditions from the database. The addition of application settings completed the DPT. Through utilizing the DPT, nearshore wave heights were obtained and compared for the three main scenarios.

4.3. Database

The method for developing a temporally uniform database containing the fundamental HFD system parameters is disclosed in this section. The system at Hellegatpolder is idealized in section 4.3.1. This resulted in a set of fundamental parameters required for numerical and probabilistic modelling of the system. Data collection for all parameters is described in section 4.3.2. The statistical expansion of vegetation and hydraulic data to ensure temporal uniformity is depicted in section 4.3.3. As nearshore wave heights were unknown, the development of a numerical model is discussed in section 4.3.4. Ultimately, the result of this section is a complete database ready for developing a probabilistic model and can be applied as the underlying database in the DPT.

4.3.1. System Idealization

Fundamental system parameters were determined for all general parameter categories depicted in Figure 3.4. Based on the theory regarding HFD systems, section 2.1, the main parameters required for the assessment of wave attenuation due to vegetation were included. Moreover, the requirements for both probabilistic modelling and numerical modeling were taken into account. The resulting fundamental parameters are illustrated in Figure 4.3. The main parameters included for each parameter category were segmented per modelling type, and presented in Table 4.1.

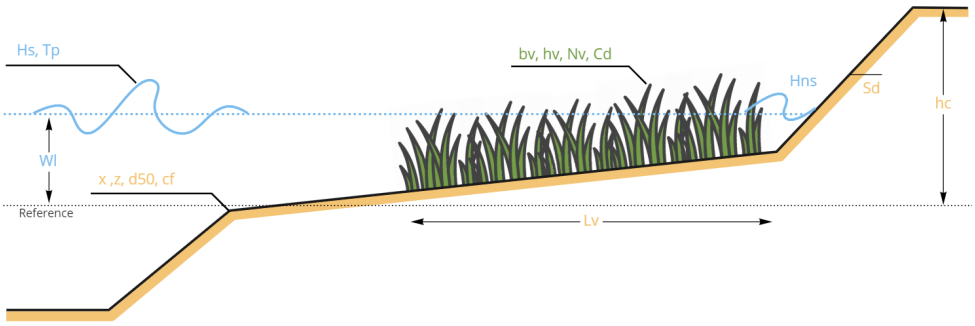

Figure 4.3: Idealized HFD system at Hellegatpolder.

Table 4.1: Parameters required for numerical and probabilistic modelling of HFD systems.

Parameter Category	Numerical Modelling	Probabilistic Modelling
Bathymetry	x-, z-coordinates, S_d, h_c, d_{50}, c_f, L_v	-
Hydraulic	H_{m0}, T_p, Wl	H_s, T_p, Wl, H_{ns}
Vegetation	C_d, b_v, h_v, N_v	C_d, b_v, h_v, N_v

Bathymetry
The bathymetric profile defines the transect as a whole and is represented by a set of horizontal and vertical coordinates (x,z). Bathymetry evolution is visible on longer timescales yet the effect on nearshore wave heights during storms was found to be negligible (section 5.1.2.3). For applications where the bathymetry is to be included in the probabilistic model, the reader is referred to Appendix K.

Furthermore, the vegetation edge depends on the site specific vegetation edge height, thus determining the vegetation length (L_v). Additional parameters required for numerical model purposes include an onshore

boundary (i.e. dike parameters; h_c, S_d), median grain diameter (d_{50}) and bottom roughness (c_f). As bathymetry evolution is not assessed in the current case study, these variables were kept constant and are thus not included as parameters in the probabilistic model.

Hydraulic
Three hydraulic variables are deemed dominant in relation to nearshore wave height prediction. Instinctively, the water level (Wl) was included as it defines the mean height at which waves reach the dike. For the sake of simplicity, water level setup was not included in this thesis, instead the offshore water level was assumed constant. Furthermore, offshore wave related parameters, such as the significant wave height (H_{m0}) and peak period (T_p), were included. These define the initial wave heights before interaction with the foreshore and vegetation. Transformation of these variables over the foreshore results in nearshore wave heights at the dike toe (H_{ns}), required for the determination of hydraulic failure mechanisms.

Vegetation
As waves traverse the foreshore of a HFD system, they encounter vegetation that exerts a force on the flow. This force, known as the drag force (C_d), was represented empirically by both hydraulic and vegetative parameters. More specifically, the horizontal shape of the vegetation is important in determining the drag coefficient.

This thesis studies only marsh grasses, the vegetation shape can be represented by a cylinder with a diameter (b_v). The drag coefficient is related to the total drag force through integration over the frontal area of the vegetation A_v, the density of the vegetation (N_v) and the horizontal vegetation length (L_v). Here the frontal vegetation area was defined using the average width and height (h_v) of the marsh stem (4.4).

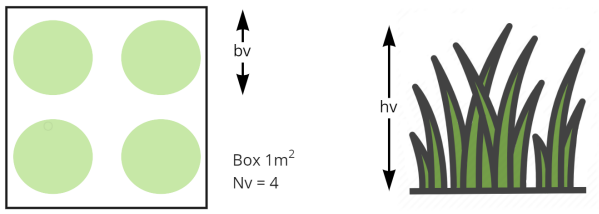

Figure 4.4: Salt marsh parameters.

4.3.2. Data Collection
Uniform temporal data was obtained for all parameters defined in Figure 4.3. Vegetation parameters were retrieved from literature and statistically expanded to obtain a finer resolution dataset (section 4.3.3). Nearshore wave heights were not available and thus not included in the data collection for Hellegatpolder, instead these values were obtained through numerical expansion (section 4.3.3). For the purpose of numerical modelling bathymetric data was collected. The main data sources, are highlighted in Table 4.2.

Table 4.2: Overview of collected data for Hellegatpolder

Parameter	Data source	Time span	Temporal resolution
Hydraulic	Rijkswaterstaat (2020)	2008-2020	30 min
Vegetation	Overview in Van Zelst (2018)	-	Monthly
Bathymetry	"Vaklodingen"	1955-2015	Yearly

Bathymetry
For the case study, the bathymetry profile is used only to enable numerical modelling. Data was collected from the "*Vaklodingen*" database which is publicly available and was retrieved from *Open Earth* (Deltares, 2020) using the *netCDF* toolbox in MATLAB. Each monitoring campaign segments the coast into grids known as "*Kaart bladen*" (KB) in which various profiles are stored. Hellegatpolder transects are stored in KB 116_4948 containing six transects traversing the salt marsh. For each transect yearly data was available going back as far as 1955. Out of the six transects, transect one was selected, as it had the least amount of missing data. Figure 4.5 shows the transect in January 2011.

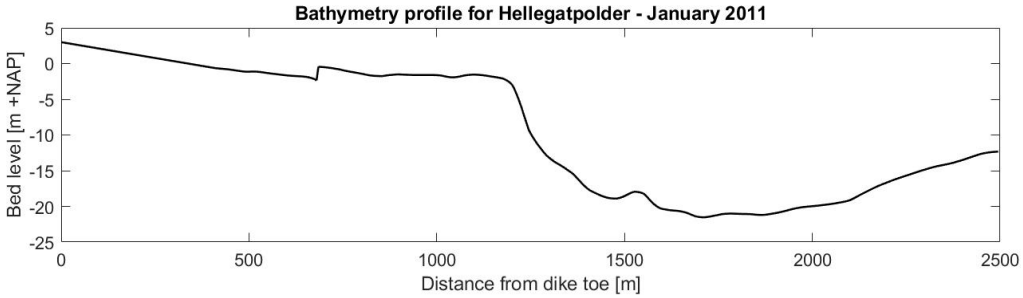

Figure 4.5: Bathymetry profile for transect one at Hellegatpolder in January 2011

The profile contains x-, z-coordinates spaced 5 meters apart along the entire transect. The transect profile was at an angle with the shore line, as to represent the direction for which the most frequent and severe wave conditions occur. Aside from profile information, the transect bed friction was provided as a constant value equal to 0.2. In the study by Hu et al. (2021), marsh analyses in the Western Scheldt were conducted, in which the mean grain size at Hellegatpolder was found to be 122.6 μm. Furthermore, the vegetation edge at Hellegatpolder was found at +1 meter NAP (Vuik et al., 2016), thus enabling determination of the horizontal vegetation length.

Dike coordinates were not available in the transect. As an onshore boundary was required in XBeach, two general values for the dike slope and crest height were chosen. Based on the research by Niazi (2019), the mean crest height (h_c), assumed 12 meters, and dike slope (S_d), assumed 0.3 mm^{-1}, were applied as the constant values used to represent the dike for numerical modelling purposes.

Hydraulic

Offshore hydraulic data was collected from Rijkswaterstaat (Rijkswaterstaat, 2020) at the location "*Overloop van Hansweert*" (X coordinate = 56002.00 Y coordinate = 380549.00; using RD coordinates (EPSG: 28992)). Extensive datasets for wave height (H_s), wave period (T_p) and water level relative to NAP (Wl) were collected between January 2000 and September 2020 with a temporal resolution of 30 minutes.

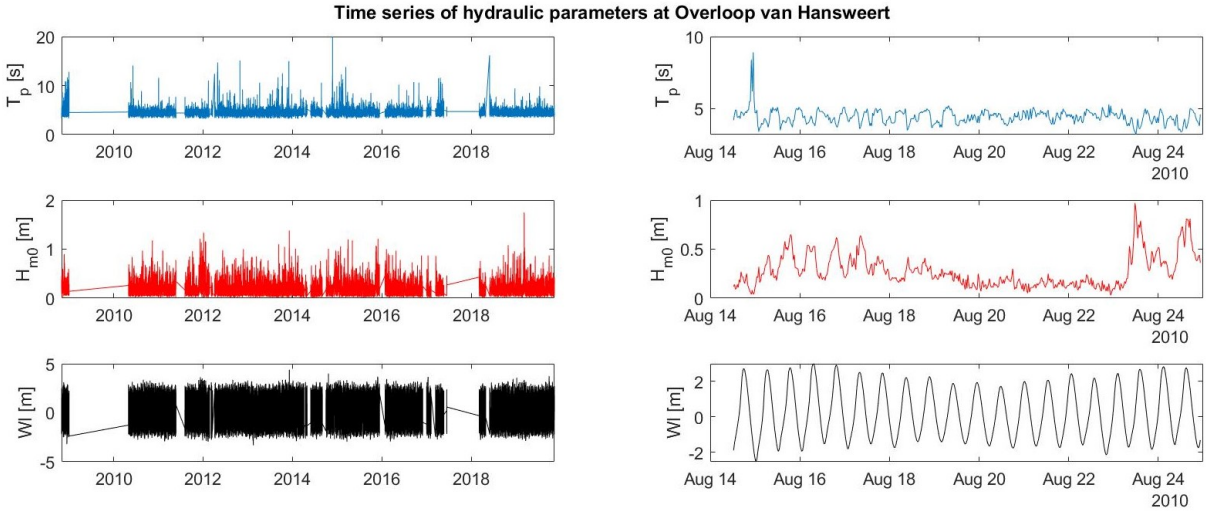

Figure 4.6: Time series of wave period (T_p), wave height (H_{m0}) and water level (Wl) at Overloop van Hansweert.

The datasets time series contain gaps during which no measurements were recorded. Joining the three time series and only showing the homogeneous data (i.e. points in time for which data is available for all three parameters) results in the time series plots shown in Figure 4.6.

Vegetation
Vegetation data was obtained through statistical expansion as the required temporal resolution of 30 minutes was unavailable for the case study location. Field measurement data was collected from literature (Van Zelst, 2018), for the species *Spartina angelica*. The field data, each representing the mean of numerous field measurements, are shown in Table D.1. The drag coefficient was not synthetically expanded as it is calculated using Equation A.2.

4.3.3. Statistical Expansion
Vegetation parameters field data (Table D.1) was used to develop a synthetic vegetation dataset. The objective was to obtain monthly data that represents vegetation evolution for multiple years. To do so, statistical expansion was completed. Sufficient data was available for statistical expansion of vegetation parameters using copula sampling. A coefficient of variation and a sine function were applied to model the vegetation density and width. Gaps in the hydraulic dataset were filled through interpolation for improved temporal modelling.

Vegetation Height
An autocorrelation copula function was developed to sample correlated synthetic monthly vegetation height for multiple months (N). Monthly mean vegetation height were distinguished from Table D.1 and used to determine the autocorrelation value for monthly time-shifts (ρ_s). Subsequently, an autocorrelation copula function was built to generate a time series of uniform data samples (u_N) through execution of the following steps:

1. Create an array of 10 random uniform samples (X_t);
2. Use X_t and ρ_s to create an array X_{t+1} containing 10 samples $\in$ [0 1] that are correlated to X_t;
3. Continue 2^{nd} step for all time steps (N);
4. Average every array containing 10 values to obtain a single value $u_t \in$ [0 1] per time step (t).

Three approaches were taken to convert the uniform data samples (u_N) back to their marginal values using a yearly, quarterly and monthly probability distribution. For a more in depth analysis of the autocorrelation sampling approach and the marginal conversion method, the reader is referred to Appendix D. Marginal values were assumed constant throughout the month and reproduced for multiple years to fit within the original dataset for a temporal resolution of 30 minutes.

Vegetation Width & Density
Similarly, vegetation width and density time series were synthetically developed. However, as fewer data was available for these parameters, a mean and coefficient of variation (Neumeier, 2005) was determined and applied to obtain representative data throughout the year.

Mean values were distinguished from Table D.1, accompanied by a coefficient of variation (i.e. the maximum deviation from the mean). Combination of the mean and coefficient of variation in a sine function, and shifting the period to match the minima and maxima of the original data from literature, resulted in monthly synthetic time series. Expanding the sine function for multiple years and assuming the monthly values to be representative throughout each month resulted in time series with a 30 minute temporal resolution for multiple years.

Hydraulic Expansion
The raw hydraulic dataset was analysed to find gaps in each time series. Gaps smaller than 24 hours were filled through linear interpolation between the two edges of the data gap.

4.3.4. Numerical Modelling
Nearshore wave heights at the dike toe were obtained through numerical modelling of the collected data in XBeach. The data in section 4.3.2 was used to set up a 2D XBeach model in MATLAB using the XBeach toolbox. The transect was defined using the bathymetry parameters. The effects of vegetation dampening and bathymetry morphology on wave dampening were included in the XBeach settings. Using the offshore hydraulic data collected in section 4.3.2, the model was run for 7 years to model wave progression every 30 minutes. Morphology was not found to be of influence on wave heights for the time scales assessed in this thesis (section 5.1.2). Thus, the effects of a foreshore with and without vegetation were modelled to include synthetic nearshore wave heights in the dataset.

4.3.4.1 Numerical Architecture

The main objective in the development of an XBeach model was including the processes induced by vegetation and bathymetry morphology into the model as to efficiently run multiple years of input data. Multiple XBeach runs were developed and run separately to include various vegetation states in the numerical settings. Each run was executed sequentially to include bathymetry evolution in the assessment. This resulted in an iterative numerical model outline that sequentially runs a segment of data, and then uses the output to initialize the subsequent run.

More specifically, the input dataset was sliced into N chunks of input data and then consecutively executed in XBeach. The process was initiated for each run n in which data preparation, setup of the XBeach model settings, running XBeach and processing the output were iteratively executed for all runs N. Figure 4.7 provides the general outline of this approach. Each element represents a MATLAB subscript containing numerical processes (Appendix E). After completion of the iterative process the output was compressed to create a single database containing wave height at the toe of the dike.

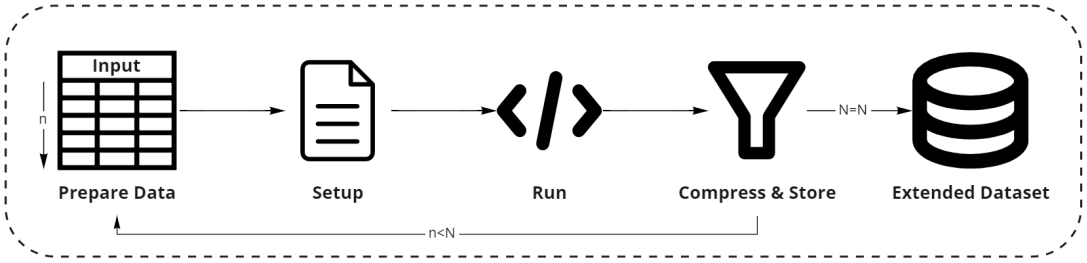

Figure 4.7: Outline of the five main steps in XBeach modelling, where n represents the current run number and N is the total number of runs.

4.3.4.2 Numerical Settings

XBeach model settings were tuned to include the effects of vegetation dampening and morphology on wave attenuation. As elaborated in the theoretical knowledge (section 2.4), the choice for a non-hydrostatic model was made to ensure all relevant wave processes were included in the output. A one dimensional grid with only x and y coordinates was selected. The default settings of XBeach were selected to ensure stable simulations. The following parameters were however modified for this specific case study (disclosed in more detail in Appendix F):

1. XBeach grid size optimization;
2. Morphology settings including the morphological acceleration factor;
3. Wave settings that neglect currents, wind and incidence angle;
4. Model run time that includes spin-up time;
5. An output write interval of 30 seconds for all output types;
6. Vegetation grid that defines the location of vegetation in the model; and
7. Generation of a time-varying tide throughout the run.

The XBeach transect shown in Figure 4.8 depicts the bathymetry profile defined using bathymetry data and model settings. The vegetated section runs from +1m NAP (observation point 3) until the start of the dike toe at +3m NAP (observation point 5). At the offshore boundary (observation point 1) varying dynamic hydraulic conditions (i.e. tides and waves) were defined using johnswap spectra tables and tide time series. This resulted in a model ready for calibration and validation.

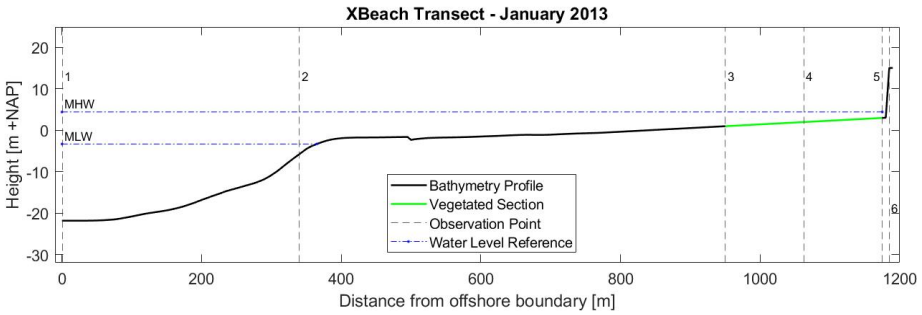

Figure 4.8: Two dimensional XBeach transect illustrating the bathymetric profile for January 2013. The vegetated section starting at +1m NAP is depicted in green. The dashed black lines indicate observation points used for referencing.

It should be noted that stem breakage was not included in the model settings as these settings were not available in XBeach at the time of writing. This is mainly due to their relation to hydraulic forcing not yet being fully understood. Nonetheless, the phenomenon greatly affects wave attenuation (Vuik et al., 2018a). In general little data was available on this subject and therefore these processes are not included in the XBeach model settings.

4.3.4.3 Calibration

Combining a computationally heavy numerical model with an extensive dataset required optimization of model settings to ensure its accuracy and computational efficiency. Therefore, the model calibration objective was to maintain nearshore wave height accuracy while reducing model run time, to allow numerical modelling of 7 years of data with a temporal resolution of 30 minutes.

Four settings were believed to significantly impact model accuracy and computational time: Grid resolution, XBeach run time, morphological settings and the output write interval. Inclusion of morphology requires additional processes to be solved within the numerical grid, thus demanding more computational time. Likewise, the grid size influences the amount of grid cells and thus the total amount of calculations required within a run. Moreover, the grid size influences model accuracy in regard to wave resolving. In addition, writing data to output files is computationally intensive. Therefore, reducing the global output interval decreases the computation time as well. All settings were tuned to achieve an efficient and accurate numerical model.

Each calibration scenario resulted in a set of run settings that were used to subsequently run the XBeach model for the month of January 2013. Model accuracy and run time results were compared to the reference scenario (i.e. default settings) for each variant to obtain a calibrated XBeach model. Extensive results are disclosed in Appendix G and discussed in detail in the results. Ultimately, the calibrated model slightly underestimated the nearshore wave heights in the order of 5% while running 35 times faster than the reference scenario.

4.3.4.4 Validation

The calibrated numerical model was validated to assess the physical accuracy of wave dampening processes due to bed friction, depth induced breaking and vegetation drag. Field measurement data collected by Vuik et al. (2016) at Hellegatpolder provides physical data which can be compared to the results of the numerical model. The validation approach considered the comparison of wave heights measured before and after the marsh edge.

In the numerical settings, the vegetation and hydraulic settings were adjusted to match the conditions in the paper by Vuik et al. (2016). Hydraulic conditions were presented as a combination of water levels and wave heights at point 1 and point 2. Therefore, the numerical model was run to reproduce the hydraulic conditions at point 1, to then compare the resulting numerical values at point 2 with those presented in the paper.

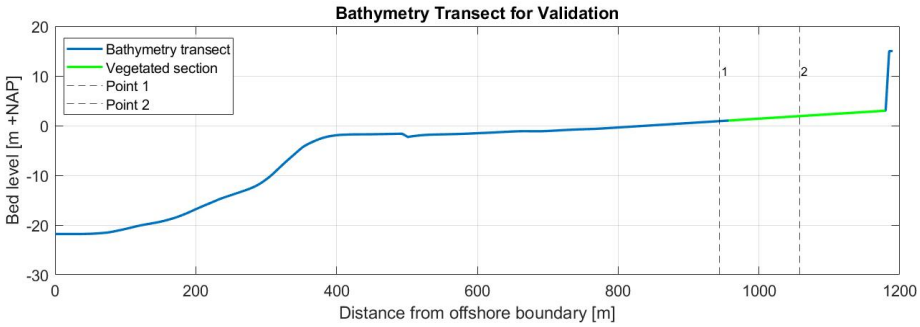

Figure 4.9: Bathymetry transect used in the validation of the numerical model. Points 1 and 2 represent the locations for which wave heights were compared.

The validation runs, discussed in section 5.1.2.2, confirmed the ability of the numerical model to produce physically accurate results within a maximum 13% margin of error.

4.3.4.5 Numerical Run Scenarios

Three XBeach run scenarios were developed using the validated numerical model (Table 4.3). The first assesses the effects of a bare static (i.e. without morphology) foreshore in relation to wave attenuation. The second builds on the first model and includes vegetation parameters on the foreshore, enabling the assessment of wave attenuation due to vegetation. The third and final model, builds on the second and includes morphology in the run settings to assess the effects of foreshore morphology on wave attenuation. Each scenario results in a different nearshore wave height dataset. Only the first and second were included in the final dataset used in probabilistic modelling, discussed further in section 5.1.2.

Table 4.3: Three run scenarios applied to obtain a synthetic numerical dataset.

Scenario	Processes Included		Effect on wave attenuation
	Vegetation	Morphology	
Bare Static Transect	No	No	Bare foreshore
Vegetated Static Transect	Yes	No	Vegetation
Vegetated Dynamic Transect	Yes	Yes	Morphology & Vegetation

4.3.5. Summary

The previous section presented the fundamental system parameters for the idealized system (section 4.3.1). For each parameter category, data was collected from public and literature sources (section 4.3.2). To overcome the limitation in vegetation data, a statistical method was defined to create a synthetic vegetation dataset (section 4.3.3). A numerical model was developed to allow 2D modelling in XBeach to obtain nearshore wave heights (section 4.3.4). Run scenarios were defined to model nearshore wave heights, with (H_{ns_v}) and without (H_{ns}) vegetation present on the foreshore. All parameters included in the database containing 7 years of data with a temporal resolution of 30 minutes are illustrated in Figure 4.10.

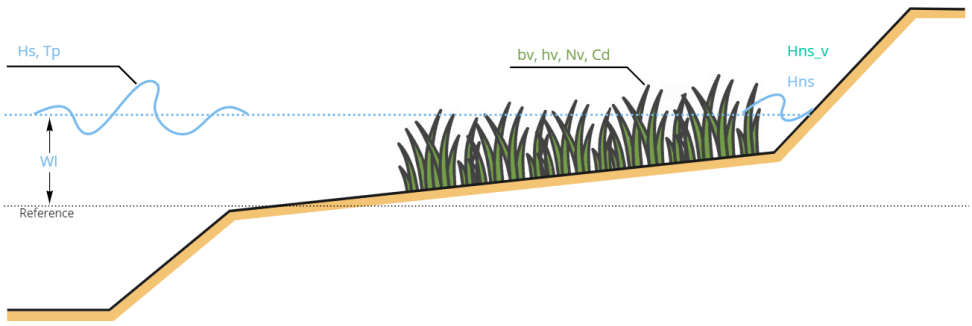

Figure 4.10: HFD parameters included in the database used in probabilistic modelling.

4.4. Probabilistic Models

A dynamic and static Bayesian network (DBN & SBN) were developed to enable probabilistic modelling of nearshore wave heights in HFD systems. Four steps were completed in the development of these models (Fig. 4.11). The statistical analysis in section 4.4.1 created the foundation for the development of Bayesian networks. Multiple networks were developed for each variant. The network variants and calibration process for both SBN and DBN are disclosed in section 4.4.2. Finally, to ensure statistical and physical accuracy, validation of the calibrated networks is described in section 4.4.3.

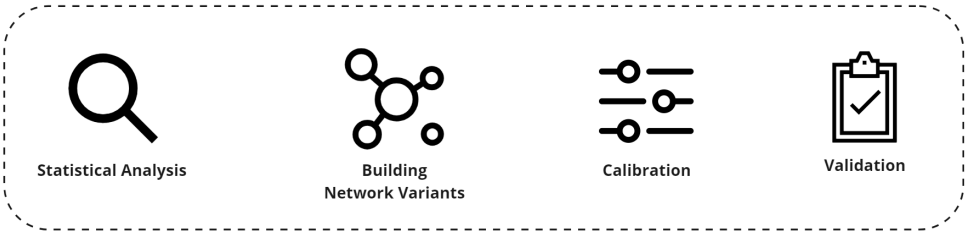

Figure 4.11: Four main steps in the development of both a static and dynamic-Bayesian network.

4.4.1. Statistical Analysis

A statistical foundation provides required information for development of Bayesian network structures. A one dimensional marginal analysis for the HFD system database results in definition of all nodes within the network. Through assessing the autocorrelation structure, the parameter category best fit for temporal modelling in the DBN was selected. The (autocorrelation) copula analysis provided the initial assessment of the application of a Gaussian Bayesian network. The extended statistical analysis is presented in Appendix H, while the main conclusions used for decisions in the case study method are discerned below.

4.4.1.1 Temporal Analysis

An autocorrelation analysis was conducted to assess the parameter category best suitable for temporal modelling. Appendix H.2.2 presents the assessment of both vegetation and hydraulic parameters. Hydraulic parameters were chosen for temporal modelling mainly due to the reliability of the data and short term temporal variability. Figure 4.12 presents the autocorrelation plot for the offshore water levels used for development of DBN network variants.

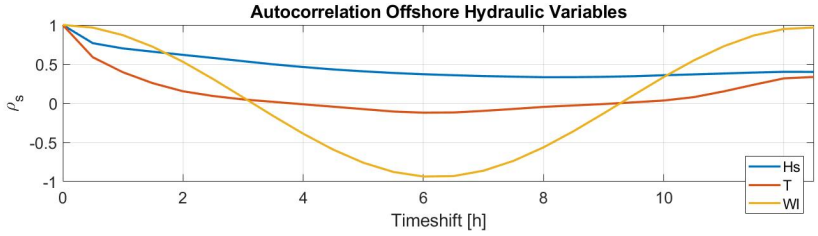

Figure 4.12: Autocorrelation plot for all offshore and vegetation parameters shifted through time and assessed in terms of Spearmans correlation coefficient. Note the difference in time scale between the two plots.

4.4.1.2 Copula Analysis

A static (i.e. standard correlations) and dynamic (i.e. autocorrelation) copula analysis support the application of Gaussian Bayesian networks. Full assessment of all copula types is disclosed in Appendix H.3. For the static analysis, 6 out of 13 pairs were best modelled by a Gaussian copula. In the dynamic assessment, Gaussian copulas were found to best model water level variables which are represented most in the networks. Thus, both copula analyses comply with the application of a Gaussian Bayesian network.

4.4.2. Calibration

The objective in BN calibration was to maximize the 'knowledge' in the model, while minimizing the amount of influence (i.e. arcs). Multiple DAGs were created and analysed for each BN. Starting with

a saturated DAG to represents a network including arcs between all physically related variables (i.e. same parameter class or related through physical processes). By removing arcs based on either physical assumptions or by applying a minimum absolute correlation coefficient, numerous DAG variants were developed. Each variant was scored in terms of its ability to model the underlying dataset (i.e. accuracy) and the number of arcs and nodes (i.e. simplicity). Development of variants and the calibration process is discussed separately per BN.

4.4.2.1 Static Bayesian Network

The SBN was developed to model nearshore wave height with and without vegetation by representing all system parameters within a single point in time. The parameters in the system are represented by nodes in the Bayesian network (Fig. 4.13). Five DAG variants were developed to represent the system as disclosed in Table 4.4.

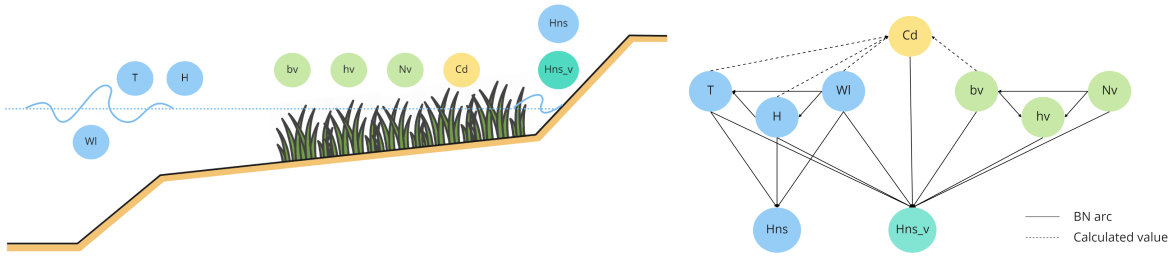

Figure 4.13: All SBN parameters nodes presented in their physical location(left). DAG variant representing a physical substantiated network saturation (right).

Table 4.4: Static Bayesian network variants assessed in network calibration.

Index	Variant	Description
i	Physical saturation	Vegetation $\perp$ Offshore Hydraulic $\perp$ Drag coefficient
ii	Vegetation independence	i + $b_v \perp h_v \perp N_v$
iii	Hydraulic independence	i + $T \perp H \perp Wl$
iv	Hydraulic simplification	i + $Wl \perp T$
v	Hydraulic & vegetation simplification	ii + $Wl \perp T$

Variant *i* was built based on the physical relation between the variables. As vegetation parameters and offshore hydraulic parameters were assumed independent, no dependence arcs were drawn between these nodes. Moreover, the drag coefficient was assumed independent from the offshore hydraulic and vegetation parameters as it is a calculated value (Eq. A.2). It is therefore related to the parameters used in the equation through calculation arcs (i.e. dashed line in Figure 4.13 right). This variant forms the basis for all others, the other variants are simplifications of this variant through the reduction of arcs.

Variant *ii* and *iii* both explored the independence between all vegetation and offshore hydraulic parameters respectively. Variant *iv* reduced the hydraulic arcs in the system to correlation coefficients (ρ_s) exceeding 0.4. This results in the water level (Wl) being independent from the wave period (T). Variant *v* combines both *iv* and *ii*, resulting in vegetation independence and simplification in the hydraulic dependence structure.

Calibration Process

The five DAG variants were built using the BANSHEE toolbox in MATLAB and assessed in terms of accuracy and model simplicity. Model accuracy was examined through completion of the following steps:

1. Loading the synthetic dataset;
2. Defining the network structure in terms of parents and children;
3. Using the network structure and dataset to determine the rank correlation matrix for the network using *bn_rankcorr* (BANSHEE);

4. Conditionalizing all nodes except nearshore wave heights using data from record i in the database;
5. Drawing 'full' 10.000 samples, 'next' interpolated for $Hns_v(i)$ & $Hns(i)$ using *inference* (BANSHEE);
6. Comparing the 90% confidence bounds for the samples with the actual empirical data from the single record;
7. Repeat steps 4-6 until $i = 250$.

Calibration results presented variant v as the option resulting in highest accuracy while having the least amount of arcs in the system (Appendix I.1). The corresponding BN structure is depicted in Figure 4.14 (left) complemented by the corresponding rank correlation matrix (right).

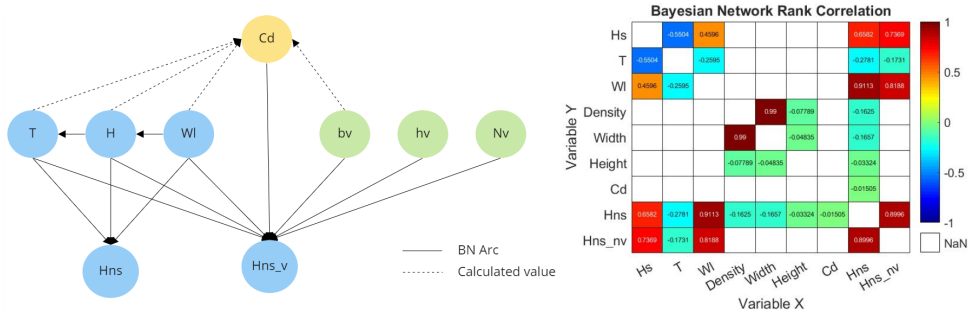

Figure 4.14: Calibrated static BN structure (left) and corresponding rank correlation matrix (right).

4.4.2.2 Dynamic Bayesian Network

The DBN enables modelling of offshore hydraulics through time by relating inter-time slices within a Bayesian network. Building on the autocorrelation and copula analysis in section 4.4.1.1, the offshore hydraulic variables were found suitable for temporal modelling. Multiple DAG variants were developed for the DBN by differentiating the number of previous 0.5 hour time steps the main variables are related to (Fig. 4.15). A total of 7 variants were developed as shown in Table 4.5.

Table 4.5: Dynamic Bayesian network variants assessed in network calibration.

#	Variant	Description
i	Uniform 0.5 hour time shift	T dependent on H, H dependent on Wl, (t) dependent on $(t-1)$
ii	Uniform 1 hour time shift, low saturation	***i*** + (t) dependent on $(t-2)$
iii	Uniform 1 hour time shift, full saturation	***ii*** + $(t-1)$ dependent on $(t-2)$
iv	Uniform 1.5 hour time shift, low saturation	***ii*** + (t) dependent on $(t-3)$
v	Uniform 1.5 hour time shift, full saturation	***iii*** + (t) - $(t-2)$ dependent on $(t-3)$
vi	Wave (H, T) 1.5 hour time shift, Water level 3 hour time shift, full saturation	***v*** + $Wl(t)$ - $Wl(t-3)$ dependent on $Wl(t-6)$
vii	Wave (H, T) 0.5 hour time shift, Water level 6 hour time shift, full saturation	H dependence as in ***i*** Wl dependence as in ***vi*** $Wl(t)$ - $Wl(t-6)$ dependent on $Wl(t-11)$, $Wl(t)$ - $Wl(t-11)$ dependent on $Wl(t-12)$

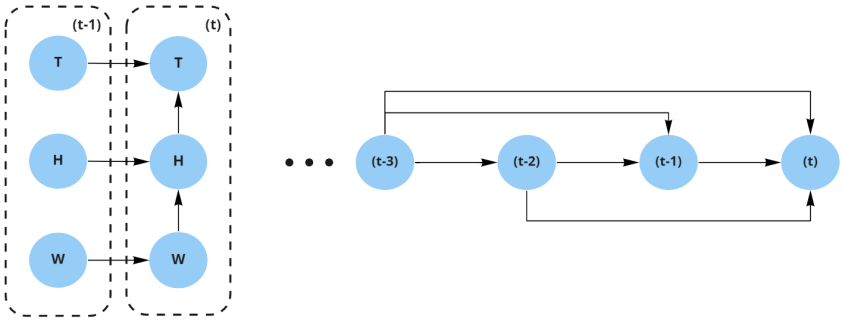

Figure 4.15: Outline of the dynamic Bayesian network for offshore hydraulic variables (left), accompanied by an example temporal network structure spanning multiple time steps (right).

Variant i builds on the hydraulic variable structure determined in the SBN analysis (section 4.4.2.1). This results in the wave period (T) depending on wave height (Hs) and wave height (Hs) depending on the water level (Wl) within the current time step (t). Furthermore, each variable in the current time step (t) depends on the previous time step ($t-1$). Variant ii and iii explore the effect of including dependence to the second previous time step ($t-2$). Variant ii assumes dependence between the current time step (t) to all previous time steps ($t-n$), while variant iii induces dependence between each time step ($t-n$) and all its previous time steps ($t-(n-1)$).

Variant iv and v are similar to variant ii and iii, whilst including the 3^{rd} previous time steps ($t-3$) or 1.5 hours. In doing so, exploring the effect of additional autocorrelation dependence (all time steps with autocorrelation (ρ_s) larger than 0 Figure 4.12) within the DBN to improve accuracy. Variant vi builds on variant v yet it includes the 6^{th} previous time step for only the water level, as the autocorrelation for the water level had full negative dependence at that point (Fig. 4.12). Finally, variant vii expanded and simplified variant vi. Simplification was achieved by modelling dependence for wave parameters (H, T) as in variant i. Expansion was conducted for water level parameters based on variant vi and including the dependence for the 11^{th} and 12^{th} time steps as these resembled the second maximum peak in the autocorrelation plot (Fig. 4.12).

Calibration Process

All seven DAG variants were developed using the BANSHEE toolbox in MATLAB and assessed in terms of accuracy and simplicity. Model accuracy was determined in regard to the variant being able to model the underlying empirical data. Determining the accuracy in the calibration process was completed through execution of the following steps:

1. Loading a continuous section from the synthetic dataset;
2. Defining the network structure in terms of parents and children;
3. Using the network structure and dataset to determine the rank correlation matrix for the network using *bn_rankcorr* (BANSHEE);
4. Conditionalizing all nodes representing previous time steps ($t-1$) until ($t-n$) for record ($i-1$) until ($i-n$) in the database;
5. Drawing 'full' 10.000 samples, 'next' interpolated for $H(t)$ & $T(t)$ & $Wl(t)$ using *inference* (BANSHEE);
6. Comparing the 90% confidence bounds for the samples in t with the empirical data from record i;
7. Store the mean of the samples in t in the database for $H(i)$ & $T(i)$ & $Wl(i)$ (enabling continuous sampling);
8. Repeat steps 4-7 until $i = 90$.

Furthermore, the DBN was calibrated to model the inherent periodic motion of offshore water levels (Wl). The modelling resuts were visually assessed for each variant and scored on their ability to well (++) or poorly (–) model the periodic motion (Appendix I.2). Based mostly on periodic and overall accuracy, variant 7 was deemed best for modelling offshore hydraulic conditions. The DBN structure and corresponding rank correlation matrix are depicted in Figure 4.16.

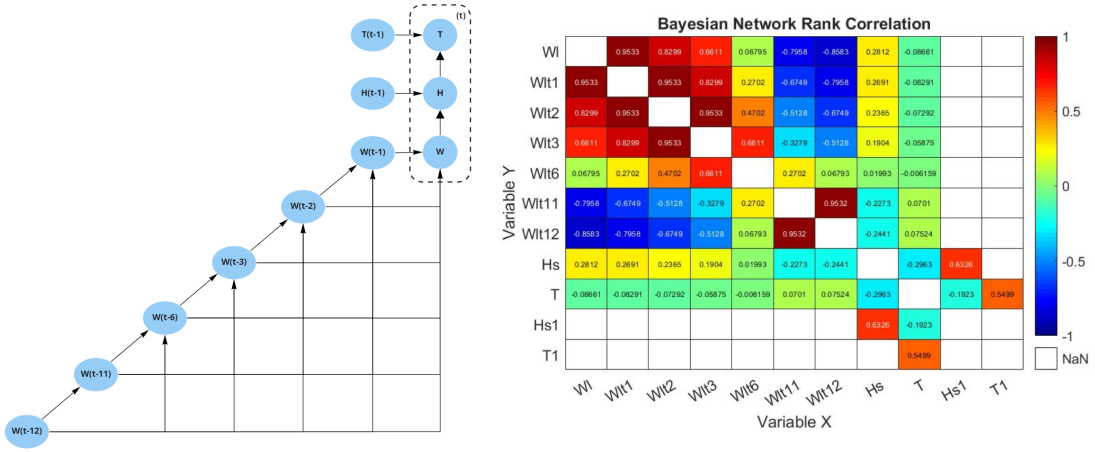

Figure 4.16: Calibrated dynamic BN structure (left) and corresponding rank correlation matrix (right).

4.4.3. Validation

Both calibrated Bayesian networks were validated to assess statistical and physical accuracy of the models using the BANSHEE toolbox in MATLAB (Paprotny et al., 2020). Statistical validation encompassed assessing the dependence structure using the semi-correlation and Cramer von Mises (CVM) goodness of fit statistics (with function: *cvm_statistic*). These were accompanied by statistical validation of the normal copula by testing the d-calibration hypothesis (with function: *gaussian_distance*). The methods for these goodness of fit statistics can be found in section 2.5.4.

Physical accuracy was ensured through a two sided sampling test (TSST). In the TSST, the database was split into two sections. Subsequently, the physical accuracy of the model was assessed. The first section of the database was used to build rank correlation matrices (with function: *bn_rankcorr*). The second section of the database was used to conditionalize the model. After conditionalization, the BN sample confidence bounds were compared with the empirical data in the second section of the database (similar to the calibration process). In doing so, the building and conditionalizing databases are independent from one another. Therefore, the TSST allows for physical validity of the output to be assessed using the independent dataset. Finally, the DBN was run for longer time periods to assess the long term modelling capacity of the model.

4.4.4. Summary

The past section presented development of a dynamic and a static Bayesian network, forming the probabilistic models in the DPT. Statistical analysis of the database formed the foundation for development of the networks (section 4.4.1). Hydraulic variables were found to be represented through time in the DBN, and application of a Gaussian Bayesian network was supported by copula analysis. Network variants were developed to calibrate the SBN and DBN in its ability to accurately model the underlying database (section 4.4.2). The calibrated BNs were validated to assure statistical and physical accuracy (section 4.4.3). The two main elements required in the DPT, a database (section 4.3) and probabilistic models (section 4.4), were now complete and ready for application.

4.5. Application

Assessment of the dike segment at Hellegatpolder during storm conditions was completed by developing application specific settings combining the database and probabilistic models. The WBI approach was applied in dike assessment. Additionally, model settings were developed to tune the DPT to transform the normative hydraulic conditions specified by the WBI to nearshore wave heights. This analysis was completed with and without vegetation on the foreshore for all four seasons.

4.5.1. Normative Conditions

Normative hydraulic and vegetative values were collected for the Hellegatpolder dike segment. Standard WBI procedures were followed to obtain normative hydraulic conditions. Moreover, vegetation parameters

were collected from the database developed in section 4.3. Normative conditions form the input for the DPT to be transformed to nearshore wave heights, including foreshore and vegetation effects.

Hydraulic
The dike section (Dijktraject 32-4) at Hellegatpolder has a signal value (normative value allocated to each dike section in the Netherlands) of 1:3000, meaning that it is allowed to have a probability of failure equal to 1 in 3000. The water level and wave height corresponding with this probability was obtained from Hydra-NL (Duits, 2019), another tool developed by Rijkswaterstaat and HKV, and presented in Table 4.6.

Table 4.6: Frequency table for water level and wave height for dike section 32-4.

Frequency	Water Level [m +NAP]	Wave Height [m]
1:1000	5.281	1.574
1:3000	5.584	1.723
1:10000	5.925	1.889

The static normative water levels were transformed to time series using the 'Waterstandsverloop' tool developed by Rijkswaterstaat (Botterhuis et al., 2017). The tool calculates the water level gradient during a storm using a trapezium method (i.e. combining the tidal signal with a peak signal to mimic storm surge). The resulting normative water level time series are depicted in Figure 4.17.

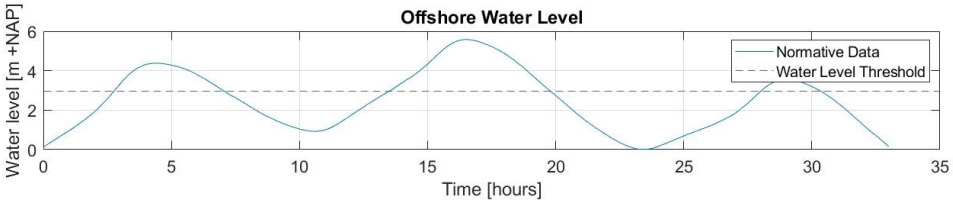

Figure 4.17: Normative offshore water levels during storm conditions at Hellegatpolder.

Vegetation
The DPT was applied to assess nearshore wave heights during each season. Normative values were obtained for all vegetation parameters, for each season as presented in Table 4.7. As one would expect, in the Northern hemisphere, vegetative states were observed to be denser, wider and taller in the summer period compared to the winter period.

Table 4.7: Vegetation parameters used to assess the various seasons.

Season	Nv [N/m^2]	bv [mm]	hv [cm]
Winter	765	2.7	33
Spring	1200	3.05	35
Summer	1650	3.3	75
Autumn	1400	3.1	5

4.5.2. Settings
Based on the specific application approach, a set of model settings were developed. Here the vegetation and hydraulic databases were combined with the static module. An overview of the model settings used to initialize the DPM is depicted in Figure 4.18. Initially, the input data was read, whereafter the setup of the static Bayesian network (SBN) was completed by filtering the database for extreme values. Then, each normative water level input was compared to the provided water level threshold. If the threshold was exceeded, the SBN was conditionalized using the corresponding water level, normative wave parameters and provided vegetative parameters. Finally, the SBN was sampled to obtain probabilities for nearshore

wave heights. Once all water levels were examined, the corresponding time series and attenuation statistics were stored for further analysis.

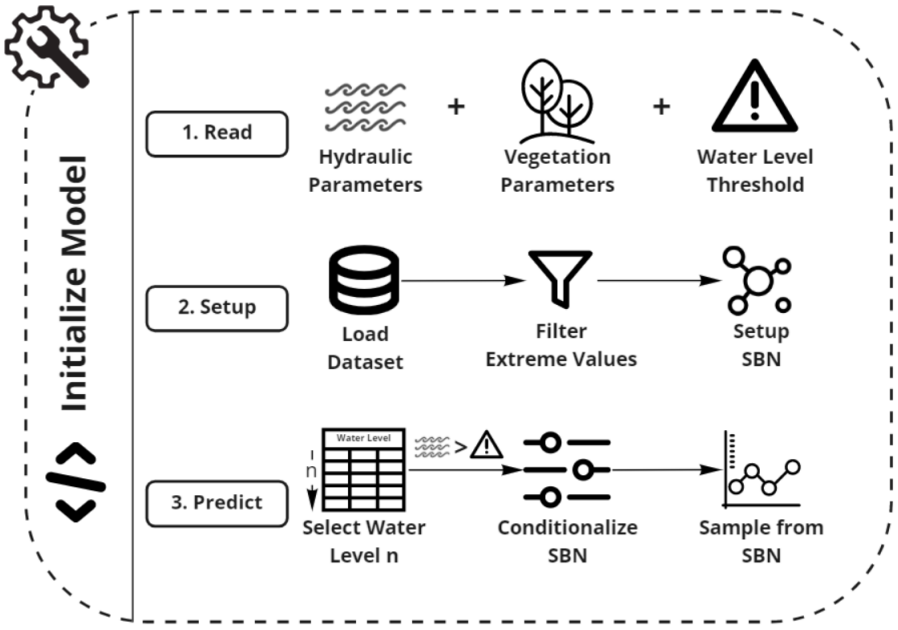

Figure 4.18: Model settings used to initialize the DPM for flood defense assessment application.

4.5.3. Run Scenarios

The DPT was applied to assess two design scenarios which was compared with the reference WBI scenario. The WBI scenario assumes the constant hydraulic forcing obtained from the Hydra-NL database as the normative condition at the dike toe. The first DPT scenario was applied to transform the normative offshore conditions to nearshore conditions for a bare transect. The second scenario includes four runs to assess the effects of seasonal vegetation states on wave height transformation.

4.6. Summary

This chapter presented the development of the DPT for HFD assessment during storm conditions at Hellegatpolder, chosen for the abundance of available data (section 4.1). The conceptual framework defined in chapter 3 was applied to case study location (section 4.2), highlighting the main steps taken.

A uniform, synthetic temporal database was obtained for fundamental system parameters through system idealization, data collection, statistical sampling and numerical modelling (section 4.3). Bathymetry parameters were removed from the database. Thereby, leaving offshore hydraulic parameters, vegetation parameters and nearshore wave heights including and excluding vegetation on the foreshore (Fig. 4.10).

A static and dynamic Bayesian network were developed using the remaining parameters (section 4.4). Statistical analysis of the database supported the application of Gaussian Bayesian networks and presented hydraulic parameters as the best option for temporal modelling. Methods for calibration and validation were discerned, allowing the accuracy and simplicity of the networks to be determined.

Finally, application specific settings were discerned to assess the dike segment at Hellegatpolder in accordance with the WBI guidelines (section 4.5). Normative water level time series, wave heights and seasonal vegetation parameters were obtained as input for the DPT. Model settings were developed to enable modelling of nearshore wave heights in the HFD system without a foreshore, with a bare foreshore and with varying vegetative states on the foreshore.

5 Results

This chapter presents and discusses the results obtained through application of the case study. Statistical and numerical expansion results are presented in section 5.1, highlighting the seasonal variability in wave attenuation and resulting in the development of a uniform temporal database. The results concerning the development of the static and dynamic Bayesian networks are presented in section 5.2. Finally, section 5.3 describes the importance of the inclusion of NBS elements in the assessment of the HFD system at Hellegatpolder during storm conditions.

5.1. Database

The final database contained hydraulic and vegetation parameters for a total of 7 years with a temporal resolution of 30 minutes. Hydraulic parameters included offshore hydraulic parameters obtained from Rijkswaterstaat as described in section 4.3.2. Vegetation parameters were expanded through statistical expansion, for which the results are presented and discussed in section 5.1.1. Moreover, nearshore wave heights with and without vegetation on the foreshore were modelled in accordance with the method defined in section 4.3.4. The numerical results are discussed in section 5.1.2.

5.1.1. Vegetation: Statistical Expansion

Vegetation data was lacking during data collection and expanded statistically to obtain temporally varying data for vegetation height, width and density. Results are presented and discussed in the sections below.

5.1.1.1 Vegetation Height

The autocorrelation copula function was applied to obtain synthetic correlated vegetation height time series (section 4.3.3). Three marginal distribution conversions were applied to convert the correlated normal samples to their marginal values. Appendix D.1 discloses the full set of results (Table 5.1).

Table 5.1: Resulting SSD values per synthetic vegetation transformation variant.

Index	Transformation method	SSD
i	Yearly Probability Distribution	2.203
ii	Quarterly Probability Distribution	0.675
iii	Monthly Probability Distribution	0.157

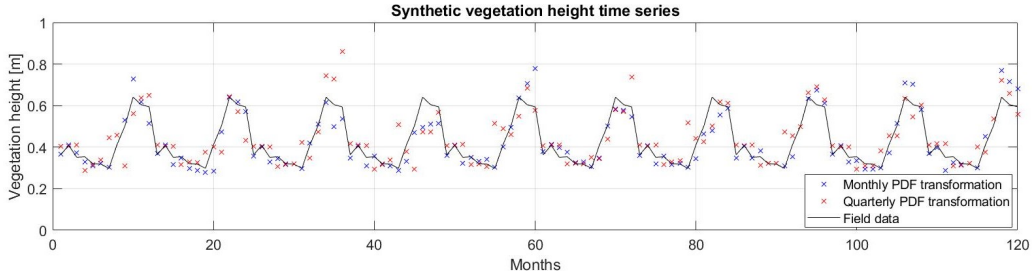

Figure 5.1: Synthetic vegetation height time series for quarterly and monthly pdf transformations.

The difference in transformation method is highlighted in Figure 5.1. Quarterly transformation was achieved through development of a probability density function (pdf) for each quarter. Monthly transformation was obtained through development of 12 pdfs. The pdfs for monthly data were specific due to the lack of data available for each month. This is visible in Figure 5.1, where the monthly samples (blue crosses) closely follow the field data (black line). The quarterly transformation resulted in more spread out pdfs (Fig. D.5) and thus allowed for more "randomness" in the samples. This is underlined by the sum of squared difference (SSD) results in Table 5.1, where the quarterly deviates more from the mean than the monthly transformations. In conclusion, the quarterly marginal distribution was chosen to model vegetation height, as it well represented the original data structure while leaving room for randomness.

5.1.1.2 Vegetation Width & Density

Both the vegetation width and density were synthetically developed using a sine function with a mean and coefficient of variation to model temporal variability. The mean and coefficient of variation were determined using the field data in Table D.1 and are presented in Table 5.2. Shifting the sine function to match minimum values in January, similar to the field measurements, resulted in synthetic time series.

Table 5.2: The mean and coefficient of variation for the vegetation width and density.

Variable	Mean	Coefficient of Variation
Width	3 mm	0.285 mm
Density	1200 n/m^2	433.33 n/m^2

5.1.1.3 Vegetation Time Series

The matching of all synthetic vegetation data based on record date times resulted in temporally uniform vegetation time series (Fig. 5.2). Naturally the statistical methods for obtaining vegetation data was accompanied by uncertainties, as a number of assumptions were made. Starting with the lack of available data in Table D.1. This resulted in uncertainty in the pdfs, creating results that could differ significantly with reality. Moreover, the coefficient of variation method simplified the variation and was based on little data available in literature, again leading to uncertainty. As the drag coefficient depends on these parameters, the uncertainty is transferred to the drag coefficient during numerical- and probabilistic modelling. Nevertheless, as application of the framework was deemed more important than synthetic accuracy of the vegetation dataset, the obtained data was applied during numerical modelling and stored in the final database.

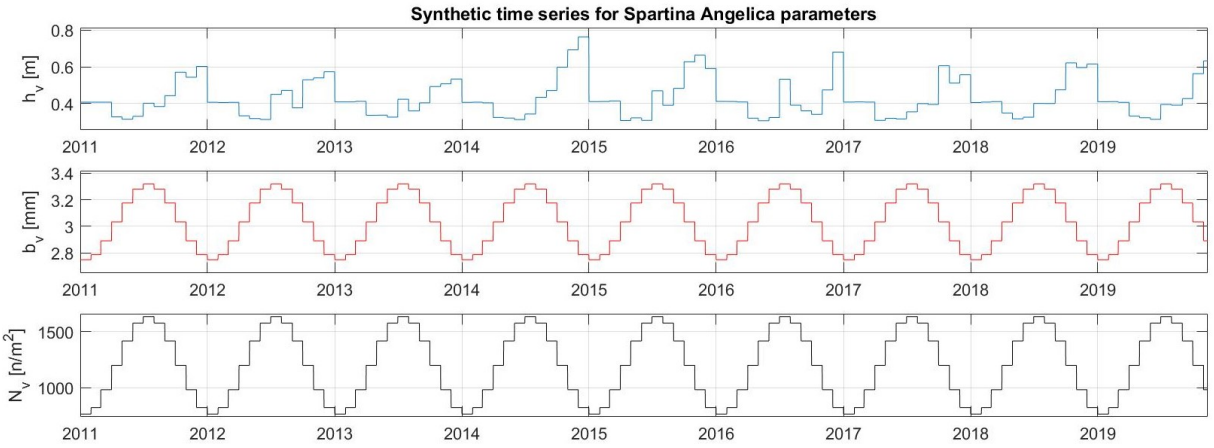

Figure 5.2: Synthetic time series for *Spartina Angelica* stem width b_v, height h_v and density N_v) for Hellegatpolder.

5.1.2. Nearshore Wave Heights: Numerical Modelling

Numerical modelling was conducted to obtain nearshore wave height data. Applying the collected data, a 2D XBeach system was created (Fig. 5.3). Combining numerical settings and numerical architecture, the model was calibrated, validated and run to transform waves over the foreshore. Three numerical run scenarios were explored to retrieve nearshore wave heights:

1. Modelling wave transformation over a bare static foreshore;
2. Modelling wave transformation over a static vegetated foreshore;
3. Modelling wave transformation over a dynamic (i.e. bathymetry morphology included) vegetated foreshore.

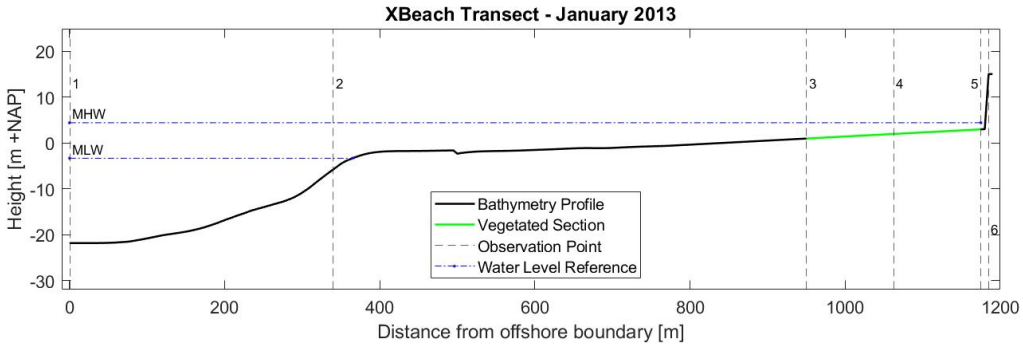

Figure 5.3: XBeach bathymetry transect used as the initial bathymetry in the calibration models. The dashed lines represent observation points while the green line defines the vegetated section in the transect.

5.1.2.1 Calibration

The developed XBeach model was calibrated to allow accurate yet efficient modelling of the extensive dataset. Four setting adjustments were assessed during calibration. Each scenario applied collected data for January 2013, allowing the comparison of each scenario. The iteration run time (30 minutes), relative temporal improvement (RTI) and scenario accuracy are presented in Table 5.3. In depth assessment of each calibration scenario is provided in Appendix G.

Table 5.3: Calibration scenario results for iteration run time (IRT), relative temporal improvement (RTI) in comparison to the reference scenario and accuracy of each scenario compared to the reference scenario through relative correlation (RC) and wave height comparison.

Variant	Scenario	IRT [min]	RTI [X]	RC	Accuracy [%]
i	Reference	20	-	1	100
ii	Optimized grid resolution	3	6.7	0.99	98
ii	Previous + Decreased run time	0.68	29.4	0.98	95
iv	Previous + Excluding morphology	0.63	31.7	0.98	95
v	Previous + Reduced output interval	0.57	35	0.98	95

In general, reducing model run time to 25% of the original had the most significant impact (computational run time reduction: 90%). Optimizing the grid to 25% of the original amount of grid points did not have the same effect in reducing run time (computational run time reduction: 66%). While reducing model time was computationally more efficient it came at the cost of accuracy (2% decrease versus 3% decrease). Furthermore, excluding morphology settings and reducing output interval slightly improved run time while having no effect on nearshore wave height accuracy. The negligible effect of morphology on model run time was unexpected as morphology processes were believed to be of significant impact on the numerical formulas that required solving during modelling. The negligible effect of morphology on short time scales is further discussed in section 5.1.2.3. Calibration effects concerning the output interval were expected, as this merely influenced output files.

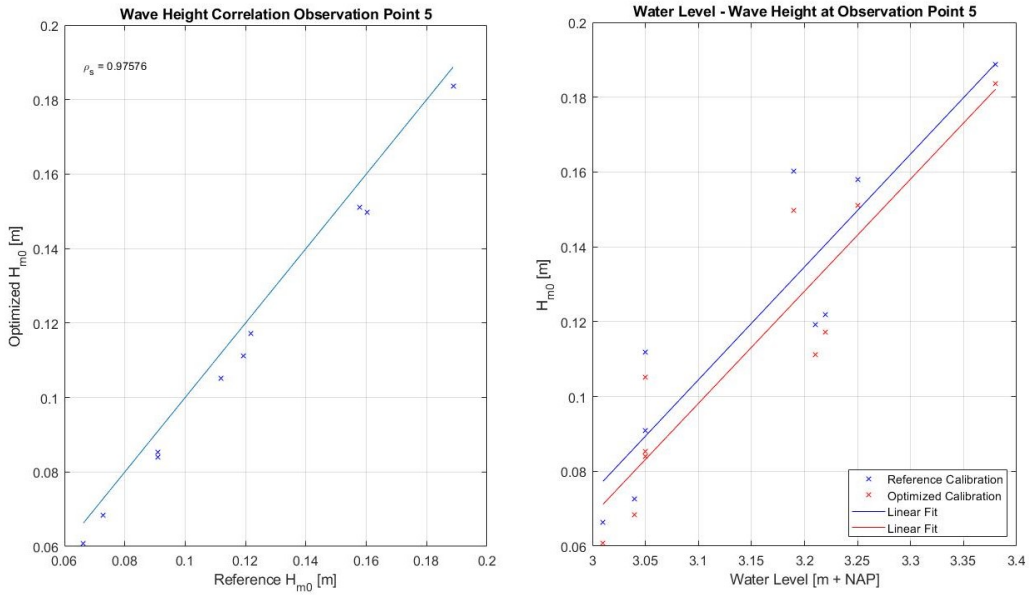

Figure 5.4: Scatter plot comparing reference nearshore wave height and optimized wave height at observation point 5 (left). Water level wave height plot for the reference (variant i) and optimized wave height simulations (variant v) at observation point 5 (right).

Figure 5.4 presents the comparison of modelled nearshore wave heights (observation point 5, Figure 5.3) for variant i (reference) and the final calibrated model, variant v. The plot on the right clearly illustrates the decrease in wave height accuracy, as the calibrated model slightly underestimated the nearshore wave heights in the order of 5%. As the model run time was effectively reduced by a factor 35 (i.e. RTI), the nearshore wave height error of 5% was deemed acceptable and thus the calibrated model settings (deviating from those defined in Appendix F) are highlighted in Table 5.4.

Table 5.4: Numerical settings for the optimized output interval scenario

XBeach Setting	**Value**
Number of grid points	560
Model run time percentage	25 %
Morphology settings	Off
Output interval	5 s^{-1}

5.1.2.2 Validation

Validation of the calibrated XBeach model was conducted using field measurement results obtained by Vuik et al. (2016) to assess physical accuracy of the numerical output. During the field measurement campaign at Hellegatpolder, Vuik et al. (2016) recorded wave height and water levels before and after the marsh edge (points 1 and 2 in Figure 4.9). The XBeach model was run to produce wave height - water level combinations equal to those obtained by Vuik et al. (2016) before the marsh edge (point 1). The resulting numerical wave height - water level combinations after the marsh edge (point 2) were compared with the field measurement results, as shown in Figure 5.5.

The blue markers in Figure 5.5 represent the field study data and the red markers represent the numerical model data. Although there is a larger spread in the numerical model data, the trend lines show that larger water levels lead to less wave attenuation. This was expected as wave motion interacts less with the bottom and thus depth induced wave breaking occurs later on the transect. Moreover, larger water depths lead to greater vegetation submergence, which leads to waves propagating over the vegetation, thereby reducing the effect of vegetation induced wave attenuation.

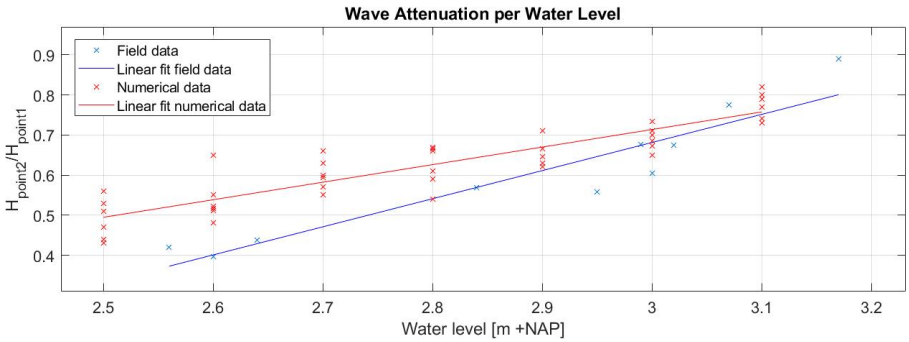

Figure 5.5: Field study and numerical wave height reduction between points 1 and 2 per water level.

For lower water levels the numerical model consistently results in larger wave heights, in the order of 13%, than those obtained by Vuik et al. (2016). These discrepancies are believed to be due to the significant difference in bathymetry profile. The numerical model has a more gradual bathymetry profile compared to the field model study, where the marsh edge was determined as a 0.5 meter 'cliff' in the bathymetry profile. This was believed to affect wave breaking at the marsh edge, resulting in a discrepancy between wave height results, as the difference between numeric and field study decreases with an increase in water level. In theory, this should reduce the effect of wave breaking due to the marsh edge. Neglecting the angle of incidence in the numerical model was believed to result in larger wave heights, as wave spreading was not included. This would also explain the larger wave heights observed. In relation to the area of application of this thesis, water levels of interest start at 2.9 m +NAP (i.e. water levels and thus waves reach the dike toe). At these water levels the margin of error was determined to lie within 8% and less, a margin of error deemed acceptable.

As disclosed in section 4.3.4.2, stem breakage was not available in the XBeach settings. Their effects are thus not included in the validated XBeach model. In future research their effects should be included, as their influence during storm conditions was found to be of importance (Vuik et al., 2018a).

5.1.2.3 Scenario Results

Numerical results were generated for three subsets of numeric settings, in turn creating the three databases presented in Table 5.5. The first model excluded morphology and vegetation processes, to develop a reference dataset (i). A second numerical model included only vegetation parameters, creating a dataset that included the influence of vegetation dampening (ii). Finally, the third model included both vegetation and bathymetry processes. This resulted in a dataset used to assess the effect of bathymetry (iii), while not being used for probabilistic modelling. The first two (i & ii) scenarios were merged with the input dataset to form the final database for probabilistic modelling.

Table 5.5: Extended HFD databases created using the numerical model.

Index	Database	Processes Included
i	Reference	No Vegetation & No Morphology
ii	Vegetation	Vegetation & No Morphology
iii	Morphology	Vegetation & Morphology

Reference & Vegetation

Studying nearshore wave heights for the reference and vegetation database, featured the effect of wave attenuation due to vegetation. The lower plot in Figure 5.6 highlights the transformation from offshore wave heights (blue) to nearshore wave heights for the reference (red) and vegetation (yellow) scenarios. Naturally there are large gaps in the nearshore wave height time series as waves are not able to traverse the foreshore during lower tides. This is supported by the intersections between the water level and reference line of 2.9m +NAP in the upper plot in Figure 5.6. The lower plot features the effect of vegetation on wave attenuation, as the reference scenario results in higher wave heights compared to the vegetation scenario.

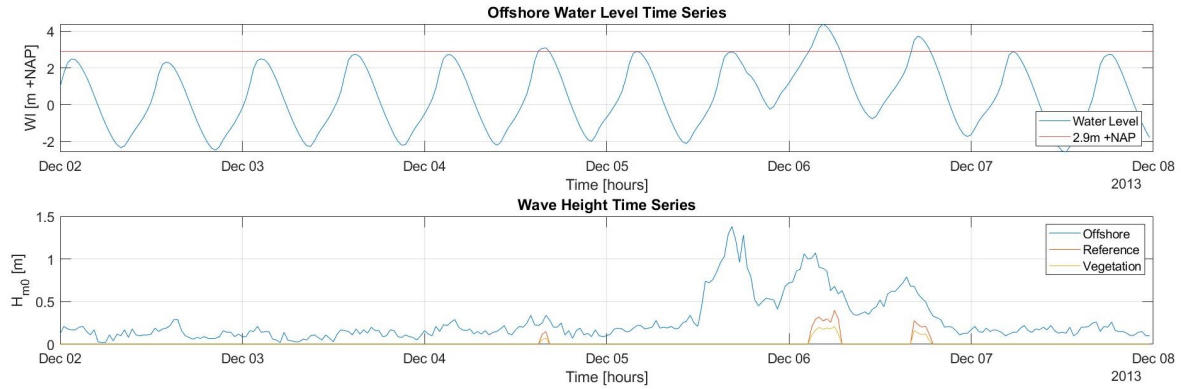

Figure 5.6: Offshore water level time series (upper plot) with a reference water level of 2.9 meters + NAP (red line). Wave heights (lower plot); Transformation from offshore wave height (blue line) to reference scenario (red line) and vegetation scenario (yellow line) nearshore wave heights.

Figure 5.6 merely highlights a segment of the dataset. A total 7 years (Jan 2013 - Dec 2019) of data were numerically processed to include nearshore wave heights. Comparing nearshore wave heights for the bare and vegetated transect allowed the assessment of wave attenuation due to vegetation per month (Fig. 5.7). The numerical results underline the theory regarding wave attenuation due to vegetation. Namely, that waves are dampened more by dense and larger vegetative states. Moreover, the uncertainty in June is not present as only a few numerical measurements were obtained in this month. This is explained by the mild storm conditions present in this month. These results emphasize the importance of including temporal modelling within design guidelines.

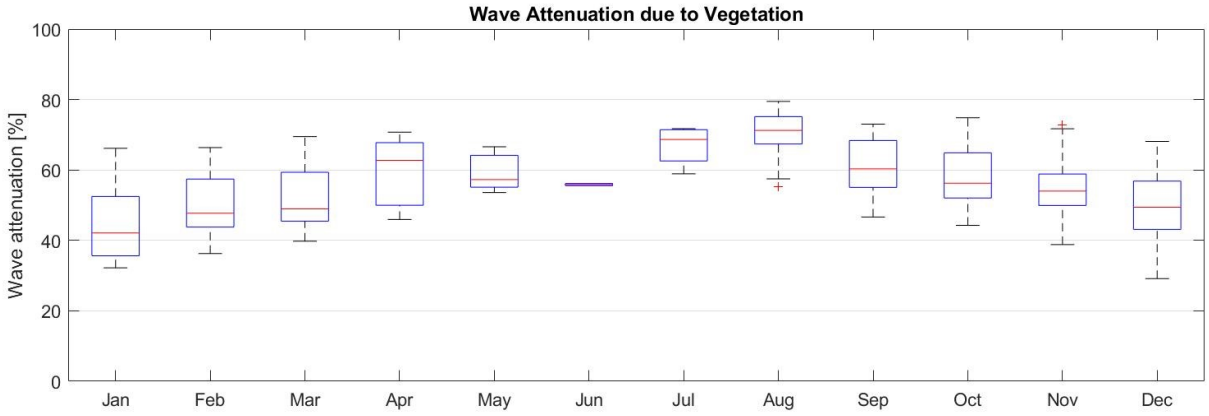

Figure 5.7: Box plots presenting wave attenuation due to vegetation for each month at Hellegatpolder.

Morphology

Comparing the bathymetry and nearshore wave heights for the vegetation scenario (*ii*) with the morphology scenario (*iii*) illustrated the negligible short term effects of morphology. Figure 5.8 depicts the numerical bathymetry evolution (initial - Jan 2013 & Numerical - Jan 2014) compared to one year of 'Vaklodingen' data (initial - Jan 2013 & Vaklodingen - Jan 2014). Evidently, the initial profile contains steep slopes which XBeach naturally smooths to a profile containing fewer gradients in the bathymetry profile. Furthermore, the numerical progression of the foreshore edge extends further offshore, similar to the measured evolution of the bathymetry profile. Regarding the simplicity of the numerical model in terms of efficient run settings, the long term response provides promising results in terms of foreshore evolution.

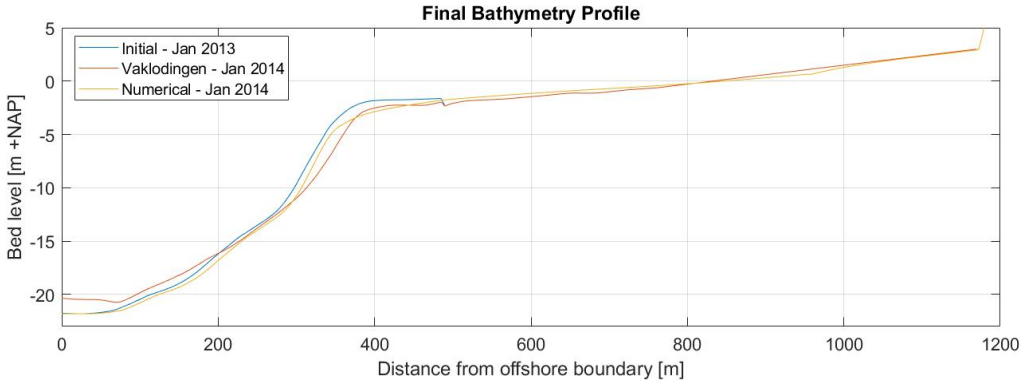

Figure 5.8: Comparison of the numerical evolution of the bathymetry profile with the measured bathymetry evolution in the Vaklodingen database.

Overall, model validity in terms of morphology was difficult to acknowledge, as external effects such as channel dredging and foreshore suppletion processes were not taken into account. These effects could be present in the Vaklodingen dataset, hindering secure assessment of model processes. Furthermore, no data was available for short term (hours-days) processes, as the Vaklodingen dataset has a yearly temporal resolution. As short term bathymetry processes are important for HFD analysis during storm conditions, accuracy of such responses cannot be guaranteed.

Comparison of nearshore wave heights for the vegetation and morphology dataset indicates the negligible importance of morphology on nearshore wave heights. Nearshore wave heights were compared for the same input data period at observation point 5 (Fig. 5.9). The results clearly indicates the similarity of nearshore wave heights with and without vegetation present on the foreshore. Instinctively, small scale bathymetry changes should not affect hydraulic propagation, underlining these results. Therefore, due to the lack of influence of morphology on nearshore wave height, bathymetry data was excluded from the extended dataset used for probabilistic modelling.

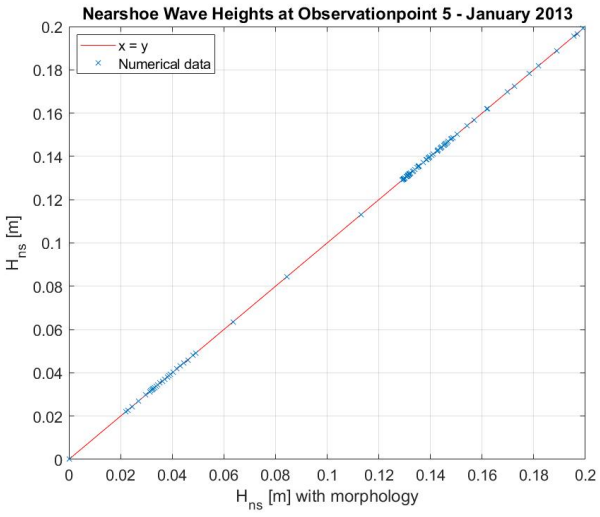

Figure 5.9: Scatter plot comparing the nearshore wave heights obtained with(out) morphology.

Probabilistic Modelling of Bathymetry Parameters

In future applications of the model, including morphology in the probabilistic database could be possible through transformation of the (x,z)-coordinates to a set of representative parameters. As (x,z)-coordinates are difficult to apply in probabilistic modelling, an algorithm was developed to convert the coordinates to parameters, alternatively random fields could be applied (Hristopulos, 2020). Appendix K presents the algorithm usable in future studies to include morphological parameters in the probabilistic modelling dataset.

5.1.3. Summary

In conclusion, the collected incomplete datasets were expanded to a complete, uniform and temporal database for the parameters illustrated in Figure 5.10. Statistical expansion facilitated the development of a temporal vegetation dataset which expanded vegetation data containing 4-13 points of data, to a monthly uniform dataset spanning 7 years (84 data points per variable). The numerical model settings were calibrated to run 35 times more efficiently while only deviating from the default settings accuracy with a margin of 5%. Furthermore, the numerical model was validated with field data to produce nearshore wave height data within a maximum margin of error of 13%. Numerical results for three separate scenarios described the negligible effect of morphology for shorter time scales. Ultimately allowing accurate modelling of nearshore wave heights with and without vegetation on the foreshore, building a complete database used in probabilistic modelling (Table 5.6).

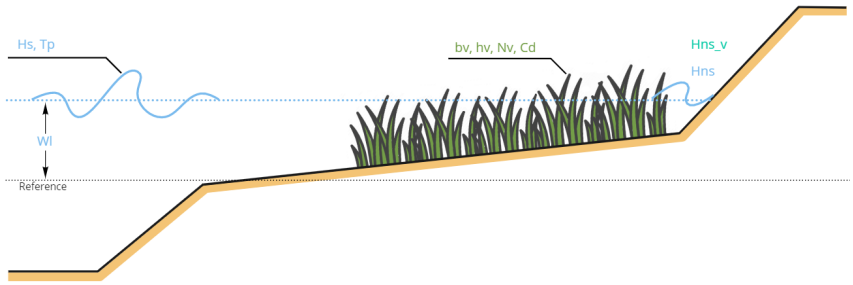

Figure 5.10: Overview of the HFD system parameters at Hellegatpolder included in the final dataset.

Table 5.6: Segment of the final temporally uniform database applied for probabilistic modelling.

Date	H_s [m]	T_p [s]	Wl [m]	N_v [n/m^2]	b_v [mm]	h_v [m]	C_d [-]	H_{ns_v} [m]	H_{ns} [m]
1-1-2013 00:30	0.41	4.7	2.94	766.7	2.7	0.409	0.215	0	0
1-1-2013 01:00	0.28	4.6	3.07	766.7	2.7	0.409	0.273	0.063	0.125
1-1-2013 01:30	0.22	4.3	2.96	766.7	2.7	0.409	0.321	0	0
⋮	⋮	⋮	⋮	⋮	⋮	⋮	⋮	⋮	⋮
28-10-2019 02:00	0.08	4.7	3.03	1200	3	0.563	0.866	0.016	0.056
28-10-2019 02:30	0.17	4.1	3.1	1200	3	0.563	0.397	0.044	0.092
28-10-2019 03:00	0.16	4.4	3.06	1200	3	0.563	0.403	0.032	0.082

5.2. Probabilistic Models

A static and dynamic Bayesian network (SBN & DBN) form the probabilistic models in the DPT. The symbiosis of the two allows dynamic modelling of HFD systems. Results concerning statistical analysis and the foundation of both models, is disclosed in section 5.2.1. Calibration and validation results for the static and dynamic Bayesian network are presented in sections 5.2.2 and 5.2.3 respectively.

5.2.1. Statistical Analysis

The statistical analysis provided the foundation required to define nodes and arcs in the Bayesian networks, whilst allowing the assessment of the Gaussian copula assumption. Marginal analysis resulted in the best fit marginal distributions. Moreover, the correlation analysis enabled assessment of dependence structures. Finally, the copula analysis allowed inherent bi-variate copula structures to be assessed.

5.2.1.1 Marginal Distribution Analysis

Each variable in the database was analysed to determine the best fit theoretical marginal distribution using the Akaike information criterion (AIC). The complete analysis can be found in Appendix H, where all distribution graphs are presented separately. An overview of the best fit marginal distributions, obtained using the *ALLFITDIST* function in MATLAB developed by Sadegh et al. (1969), for the synthetic dataset are provided in Table 5.7.

Table 5.7: Theoretical distributions for all hydraulic (H) and vegetation (V) variables included in the synthetic dataset, determined using the AIC.

H-Variable	Theoretical Distribution	V-Variable	Theoretical Distribution
H	Generalized extreme value	N_v	Weibull
T	t Location-scale	b_v	Normal
W	Gaussian mixture	h_v	Generalized Pareto
H_{ns}	Gamma	Cd	Generalized Pareto

5.2.1.2 Correlation Analysis

For the variable groups: offshore hydraulics and foreshore vegetation, the (auto-) correlation structures were assessed. Correlations between variable pairs define their mutual dependence and were required for modelling bivariate copulas. Auto-correlation arrays were used to examine the temporal character of each variable.

Correlation

The hydraulic parameter correlation analysis in Table 5.8 illustrates the dependence between offshore hydraulic variables. Wave height and wave period were, unexpectedly, found to be negatively correlated. Normally, larger waves are expected to have larger wave periods, otherwise larger waves would always break due to the limitation in wave steepness. This unexpected result is assessed in Appendix L. It was concluded that the combination of tidal flow, shipping in the Western Scheldt and wind waves could lead to unexpected water level - wave height correlations. Especially, shipping waves could affect the signal as the measurement location "*Overloop van Hansweert*" is situated in the shipping channel.

Table 5.8: Spearman's Correlation coefficients for each offshore hydraulic variable pair.

	Wave Height	Wave Period	Water Level
Wave Height	1	-0.25	0.30
Wave Period	-0.25	1	-0.10
Water Level	0.30	-0.10	1

The vegetation parameter correlation analysis in Table 5.9 highlights the strong correlation between vegetation width and density. This was expected as both parameters were developed synthetically using a sine function that was matched in time. Therefore, periodic motions were similar for both variables. It was somewhat unexpected that negative correlations were present between vegetation width and height as longer stems were expected to require a wider stem diameter. Moreover, the negative density and width was also unexpected, as longer stems were expected to correlate with extensive biological production (i.e. more stem growth in general).

Table 5.9: Spearman's Correlation coefficients for each vegetation variable pair.

	Density	Width	Height
Density	1	0.99	-0.33
Width	0.99	1	-0.39
Height	-0.33	-0.39	1

Auto-correlation

The degree to which each variable is related to its prior values was determined through an autocorrelation analysis. As one would expect, the degree of autocorrelation was related to physical forcing of the variable. Biological forcing is much more gradual (i.e. variation in the order of months), while metocean forcing acts on shorter time scales (i.e. hours). It was therefore no surprise that the variations in autocorrelation time scales differ for the hydraulic and vegetation dataset (Fig. 4.12).

Note that hydraulic parameters are related only to the last couple of hours. The autocorrelation of the water level (Wl) highlights constant forcing by the tides. Periodic tidal movement can be observed as the tidal period of 12.5 hours resembles almost full correlation after this time shift.

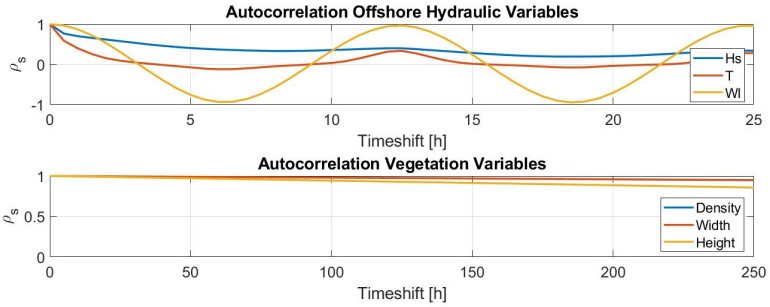

Figure 5.11: Autocorrelation plot for all offshore and vegetation parameters shifted through time and assessed in terms of Spearmans correlation coefficient. Note the difference in time scale.

Short term variations are of interest for the storm assessment application in this thesis. Vegetation parameters were assumed to vary less during the duration of a storm (i.e. neglecting stem breakage), an assumption supported by the autocorrelation analysis. Therefore, hydraulic variables were chosen to be modelled as time series in the DBN.

5.2.1.3 Copula Analysis

The bi-variate copula analysis presents joint dependence structures used as an initial dependence analysis of the synthetic dataset. The copula fits were determined using semi-correlation analyses, for which resulting normalized scatter plots, pdf- and cdf-copulas were obtained (Appendix H). Bayesian networks model the underlying dependence structure using a single multivariate copula. Therefore, the copula analysis allows the discussion of the single copula simplification.

Bi-variate Copula Analysis

Table 5.10 presents an overview of the fitted copulas for all parameters within the same time step. Most bi-variate copula structures were found to be Gaussian. Supporting the application of a Gaussian Bayesian network.

Table 5.10: Best copula fits using a semi-correlation analysis for hydraulic and vegetation variable pairs.

	Variable Pairs	
Copula Family	**Hydraulic**	**Vegetation**
Gaussian	(Wl & T), (H & H_{ns}), (H & Wl)	(b_v & h_v), (C_d & H_{ns}) , (h_v & H_{ns})
Clayton	(T & H_{ns})	-
Gumbel	-	(N_v & b_v), (N_v & h_v)
Frank	(Wl & H_{ns})	-
t (3 degrees of freedom)	-	(N_v & H_{ns}), (b_v & H_{ns})
t (6 degrees of freedom)	(H & T)	-

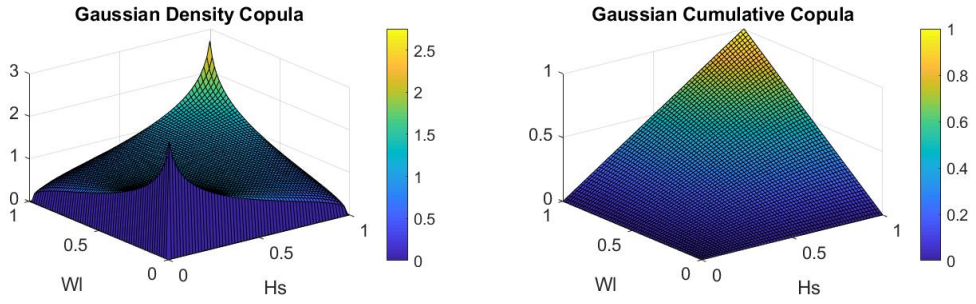

Figure 5.12: Bi-variate pdf- and cdf-copulas, depicting the Gaussian copula modelling the joint dependence of wave height (H_s) and wave period (T_p).

Autocorrelation Copula Analysis
Temporal dependence structures were assessed for the hydraulic parameters using autocorrelation copulas. Comparison of the copula structures for various time shifts enabled the best copula fit to be determined through a semi-correlation analysis (Appendix H). Resulting copula families are presented in Table 5.11.

Table 5.11: Best fit autocorrelation copula per time shift, determined using semi correlations.

	Time Shift						
Variable	**.5 hour**	**1 hour**	**1.5 hours**	**2 hours**	**2.5 hours**	**3 hours**	**6 hours**
Water Level	Gaussian	Gaussian	Gaussian	Gaussian	Gaussian	Gaussian	t (4° freedom)
Wave Height	Clayton	Clayton	Clayton	-	-	-	-
Wave Period	Gumbel	Gumbel	Gumbel	-	-	-	-

Normalized scatter plots for a 30 minute and 6 hour time shift are presented in Figure 5.13. The left plot highlights the positive correlation between water levels 30 minutes apart. The positive correlation is expected as the transition from high water to low water within a 30 minute time span is physically not possible. In contrast, the plot on the right highlights the negative correlation between water levels six hours apart. This was expected as a 6 hour time shift is equal to half a tidal period.

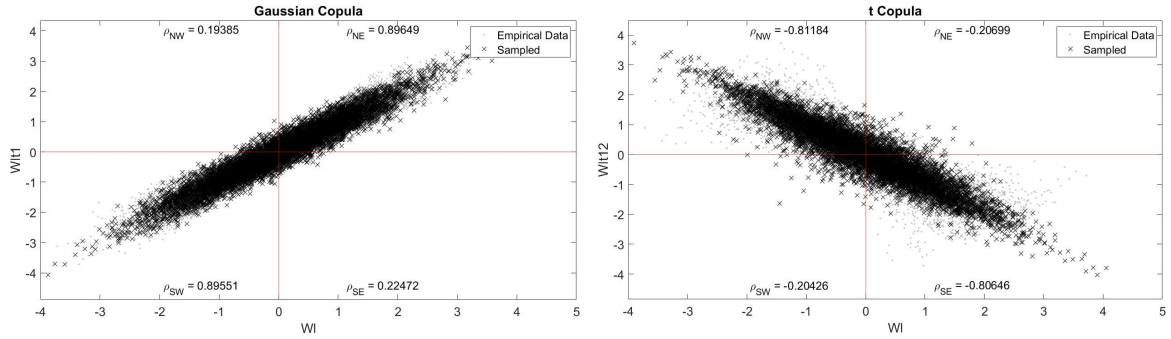

Figure 5.13: Normalized scatter plots comparing water level copula samples with empirical data for a single time shift (left) and 12 time shifts (right).

5.2.2. Static Bayesian Network

The representation of a HFD system in a single time-step was conducted using a static Bayesian Network (SBN). Calibration results for the SBN are presented in section 5.2.2.1 and validation results in section 5.2.2.2. The SBN results present a BN that was validated to sample nearshore wave heights with roughly 90% accuracy.

5.2.2.1 Calibration

Five DAG variants were assessed in terms of accuracy and simplicity to determine the best SBN structure. Model accuracy was examined through conditionalizing all parameters except nearshore wave heights, sampling nearshore wave heights and comparing the 90% confidence bounds of the samples with the corresponding empirical data (i.e. corresponding with the conditionalized values). Simplicity was assessed through the number of arc structures present in the BN.

The saturated network (variant *i*) includes full dependence structures between offshore hydraulic and nearshore wave heights as well as full dependence between vegetation and nearshore wave height. The drag coefficient is calculated using the dependent variables and has only one child node; nearshore wave height. For vegetation (variant *ii*) and hydraulic (variant *iii*) independence, the arcs between the parameter groups were removed, leaving only nearshore wave height dependence arcs. Hydraulic simplification (variant *iv*) removed the low dependence arc (i.e. ρ_s <0.4) between wave period (T) and water level (Wl). The final DAG (variant *v)* assessed a combination of vegetation independence and hydraulic simplicity. The complete analysis can be found in Appendix I, the results were summarized in Table 5.12.

Table 5.12: Accuracy and simplicity results for all SBN variants.

		Accuracy [%]		Simplicity	
Variant	**DAG Description**	$\mathbf{H}_{ns}$	$\mathbf{H}_{ns\_v}$	**Arcs**	**Nodes**
i	Saturation	84	92	16	9
ii	Vegetation Independence	84	93	13	9
iii	Hydraulic Independence	83	76	13	9
iv	Hydraulic Simplification	85	91	15	9
v	Hydraulic & Vegetation Simplification	85	93	12	9

Interestingly, hydraulic independence (variant *iii*) was found to have a large impact on the nearshore wave height (H_{ns_v}) accuracy. In contrast, the decrease in accuracy for nearshore wave heights (H_{ns}) was barely affected. This underlines the importance of the dependence structure for hydraulic parameters in regard to wave attenuation. It is hypothesized that the relation of the variables affects the drag coefficient, which in turn affects wave attenuation due to vegetation. Thereby supporting the importance of offshore hydraulic variables in regard to wave attenuation due to vegetation.

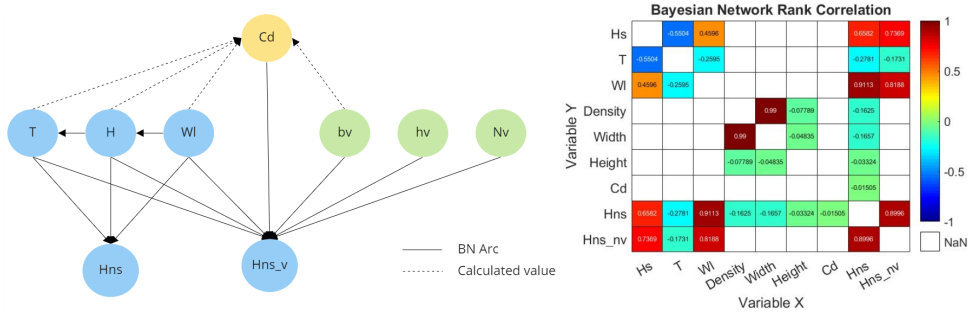

Figure 5.14: Calibrated static BN structure (left) and corresponding rank correlation matrix (right).

Variant v was determined to be the favorable DAG variant in terms of accuracy and simplicity. Vegetation parameters were independent and hydraulic parameter dependence structure was simplified. The calibrated SBN structure and rank correlation matrix are illustrated in Figure 5.14. Rank correlations for nearshore wave heights including (H_{ns_v}) and excluding (H_{ns}) vegetation on the foreshore in relation to other HFD system parameters are presented in Table 5.13. Based on these results it is evident that an increase in wave height and water level would lead to an increase in nearshore wave heights. An expected outcome, as greater initial wave height and more submerged foreshore would result in less wave attenuation due to vegetation and depth limitations. Furthermore, reduced vegetation parameters were shown to negatively impact nearshore wave height. A result explained by the vegetation drag parameter which is greater for denser, wider and taller vegetative states.

Table 5.13: Rank correlation between nearshore wave height including (H_{ns_v}) and excluding (H_{ns}) vegetation on the foreshore in relation to the other parameters in the system.

	H_s	T	Wl	N_v	b_v	h_v	C_d
H_{ns_v}	0.66	-0.28	0.91	-0.16	-0.16	-0.03	-0.02
H_{ns}	0.74	-0.17	0.82	-	-	-	-

Regarding the calibrated SBN, it was unexpected that the rank correlation between the drag coefficient and nearshore wave height was so low (ρ_s = -0.02). As there is a direct physical relation, the dependence was expected to be greater as the current dependence is almost negligible. In general the dependence strength between vegetation parameters and nearshore wave height was low. The largest rank correlation was determined to be -0.16 for vegetation density (N_v) and nearshore wave height (H_{ns_v}). Further research into the dependence structures, with actual vegetation data could provide solace into the actual dependence structures. This could even provide higher sampling accuracy of the SBN. As expected,

the general importance of offshore wave height and water level were found to be of great importance in the final dependence structure (RC: 0.73 and 0.82 respectively). Water levels define both the level of submergence of the vegetation and water depth over the foreshore. Greater water levels should physically result in larger waves reaching the dike toe.

5.2.2.2 Validation

The calibrated SBN was validated to assess statistical and physical accuracy of the model. Numerous statistical methods were applied to assess the underlying dependence structure, while a two sided sampling test was conducted to assess compare the results produced by the SBN with independent empirical data.

Representing the dependence structure of the HFD using a Gaussian Bayesian network leads to simplification of the actual dependence structure. This is mostly induced by the fact that a multivariate Gaussian copula is forced upon the underlying parameters, which were found to be a mixture of copula families (Table 5.10). This was clearly highlighted by the semi-correlation analysis (Appendix H), and the assessment of CVM statistics (Fig. 5.15). These goodness of fit tests respectively showed 46% and 17% of the underlying variable pairs being well represented by a Gaussian copula. The statistical tests thus support the statement that a Gaussian BN simplifies the actual dependence structure.

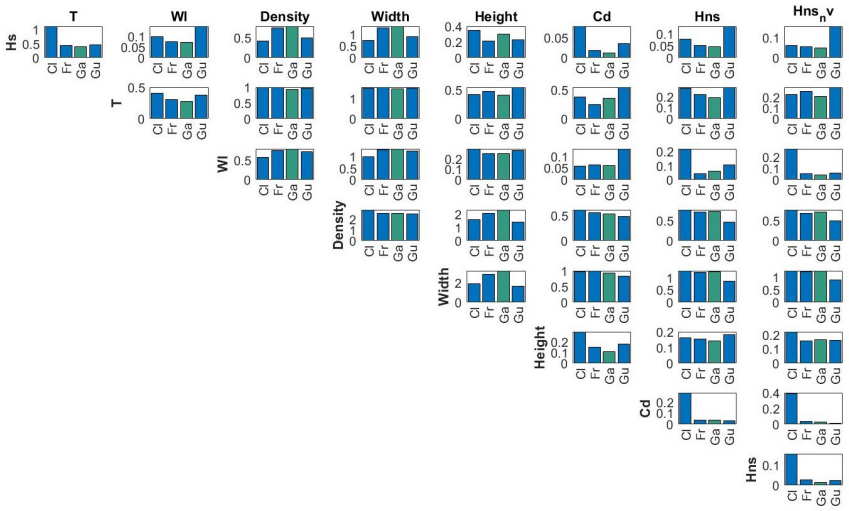

Figure 5.15: Resulting Cramer von Mises statistics (function: *cvm_statistic* in BANSHEE) for all variable pairs included in the static Bayesian network. Gaussian CVM statistic is highlighted in green.

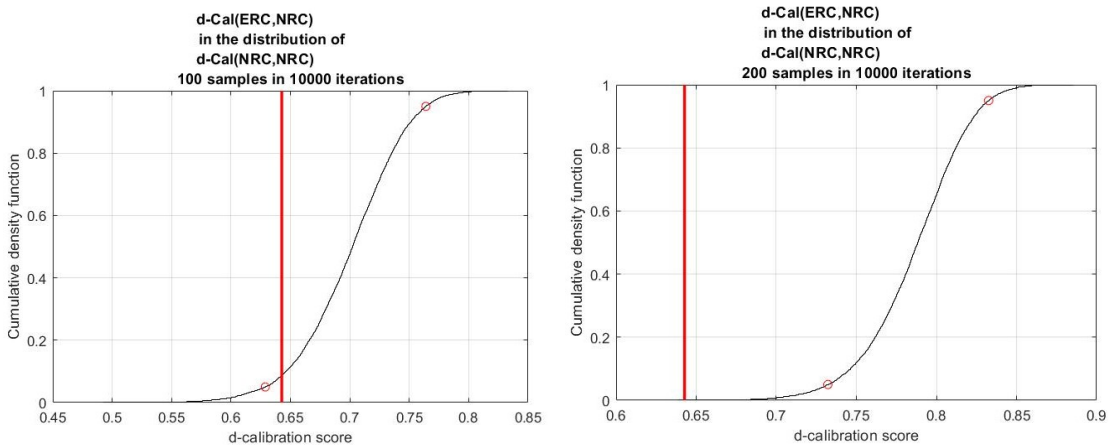

Figure 5.16: d-Calibration statistic comparing the empirical rank correlation (ERC) with the normal rank correlation (NRC) for 100 samples (left) and 200 (right).

Testing the d-calibration hypothesis for various sample sizes, resulted in a range between roughly 1 and 100 for which the hypothesis was accepted (Fig. 5.16). This underlines the previous statement regarding the statistical simplification of the Bayesian network.

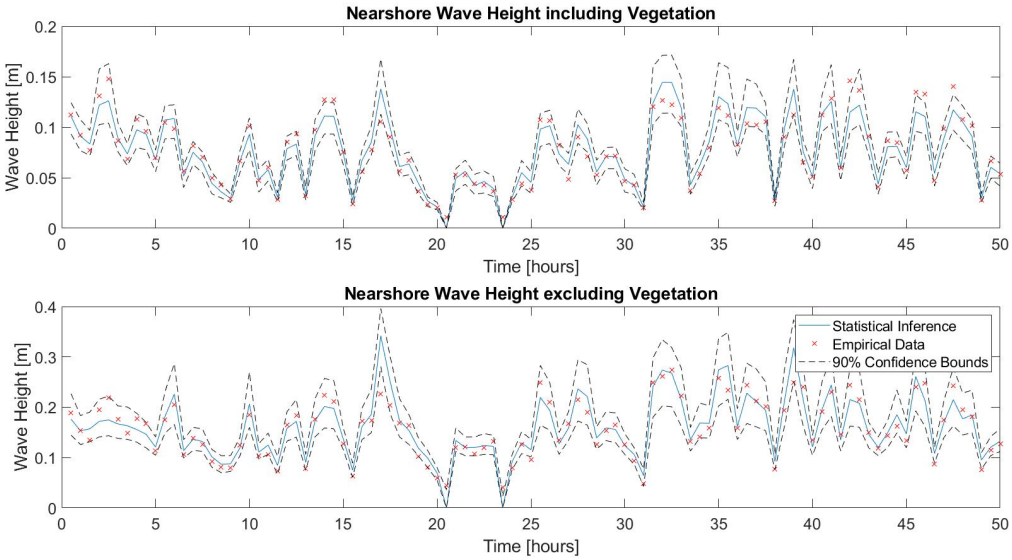

Figure 5.17: Validation results for the two sided sampling test for nearshore wave heights including vegetation on the foreshore (top) and excluding vegetation on the foreshore (bottom) for 50 samples.

A two sided sampling for the SBN was conducted and applied to assess the accuracy of the model in regard to inferring nearshore wave heights. The total dataset contained roughly 400 data points, resulting in 200 data points in each separate database. Accuracy for nearshore wave height including and excluding vegetation on the foreshore were found to be 89% and 91% respectively (Fig. 5.17).

In regard to physical accuracy, the model was well able to predict nearshore wave heights for day to day conditions. However, due to the lack of extreme data, it was not possible to validate extreme behaviour using the SBN. Nevertheless, the statistical simplification provides room for improvement in terms of model accuracy. The resulting decrease in accuracy could be overcome using vine-copulas to model the dependence structure. In such a model, multiple copulas can be selected to define the network, resulting in improvement of sampling accuracy, as the Frank copula (Wl & H_{ns}) would not be simplified to a Gaussian. This is expected to have a large effect as the water level (Wl) greatly influences nearshore wave height (H_{ns}).

Ultimately, the validated SBN was able to sample nearshore wave heights within a 11% margin of error for nearshore wave heights excluding vegetation on the foreshore (H_{ns}) and within a 9% margin of error for nearshore wave heights including vegetation on the foreshore (H_{ns_v}). Both wave heights are consistently modelled with narrow confidence bounds (Fig. 5.17). In general, the sampled wave heights are larger than the empirical values, leading to a slight overestimation of the model. In conclusion, empirical nearshore wave heights are accurately modelled by the SBN, despite the Gaussian copula simplifying some dependence structures.

5.2.3. Dynamic Bayesian Network

Offshore hydraulic time series were modelled using a dynamic Bayesian network (DBN). The calibration and validation of the offshore hydraulic parameters included in the DBN resulted in a probabilistic model able to accurately model offshore variables for short time scales.

5.2.3.1 Calibration

Seven DAG variants were examined to determine the best DBN structure. The objective was to obtain accurate samples for the current time step by conditionalizing on values for the previous time steps.

Moreover, the ability to model the periodic movement of the parameters was assessed, combined with the simplicity of the BN. A complete assessment of the DBN calibration can be found in Appendix I. Table 5.14 presents the results in terms of accuracy of the samples within the confidence bounds and the ability to sample the period structure of water level time series and simplicity of the network defined in the number of arcs and nodes.

Table 5.14: Summary of all DAG variant results assessed in Appendix I. Accuracy of the offshore parameter predictions within the confidence bounds was determined, as well as accuracy of the periodic motion on a scale from able (++) to unable (–). Finally, simplicity of the model was depicted by the number of arcs and nodes.

	Accuracy [%]				**Simplicity**	
Variant	**Wl**	**Hs**	**Tp**	**Period**	**Arcs**	**Nodes**
1	23	65	53	- -	5	6
2	16	63	44	- -	8	9
3	13	67	64	+	11	9
4	16	16	36	- -	11	12
5	17	66	57	-	20	12
6	11	66	66	+	24	13
7	28	70	71	++	25	11

Furthermore, the DBN was calibrated to model the inherent periodic motion of the offshore water level (Wl). As highlighted in the autocorrelation analysis (Fig. 4.12), the water level follows a sinusoidal forcing within the order of a day (i.e. secondary effects due to spring and neap tide were neglected). The samples obtained from each variant were visually assessed in their ability to well (++) or poorly (–) model the periodic motion. Figure 5.18 highlights the ability of variant 7 (++) with numerous previous time steps included in the model to better represent the periodic motion compared to variant 1 (–) for instance, which only contains a single previous time step in the network. This result highlights the importance of including previous time steps in the network structure to model periodic motion.

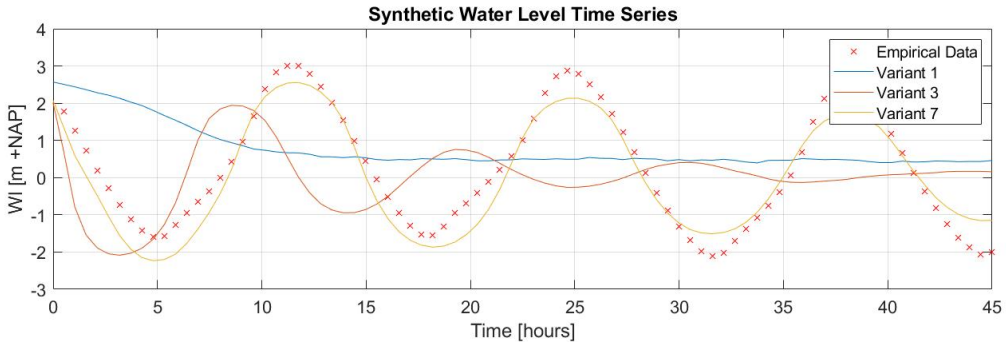

Figure 5.18: Variance in periodic motion of the sampled water level (Wl) results per DAG variant through time, compared to empirical values.

The extended calibration analysis can be referenced in Appendix I.2. Determining the best choice of DBN depends partially on the area of application for the DBN. For long term (i.e. days) inference, variant 7 would be able to model periodic water level and corresponding wave parameters accurately. For short term (i.e. hours) inference, variant 1 could suffice. Furthermore, there are still many DAG combinations to be examined. Yet, for this thesis, a balance was chosen between:

1. Number of time shifts (no time shifts greater than 6 hours were included in the model);
2. The ability to model periodic motion such as the water level;
3. The determination of sample accuracy (the 90% confidence bounds);
4. The simplicity of the model.

Assessing each criteria separately and combined provides the reasoning behind choosing the calibrated best variant for the DBN. If only criteria 1 would be taken into account, the simplest model in terms of time shifts is variant 1. Similarly, only assessing criteria 2 would result in choosing variant 7 (Fig. 5.18). Only referencing criteria 3 would result in variant 7 as it achieved the highest accuracy for all variables. Assessing criteria 4 in isolation would result in variant 1, as it has the least amount of nodes and arcs. As accuracy was chosen to weigh more than simplicity, variant 7 was chosen. The corresponding DBN structure and rank correlation matrix are depicted in Figure 4.16.

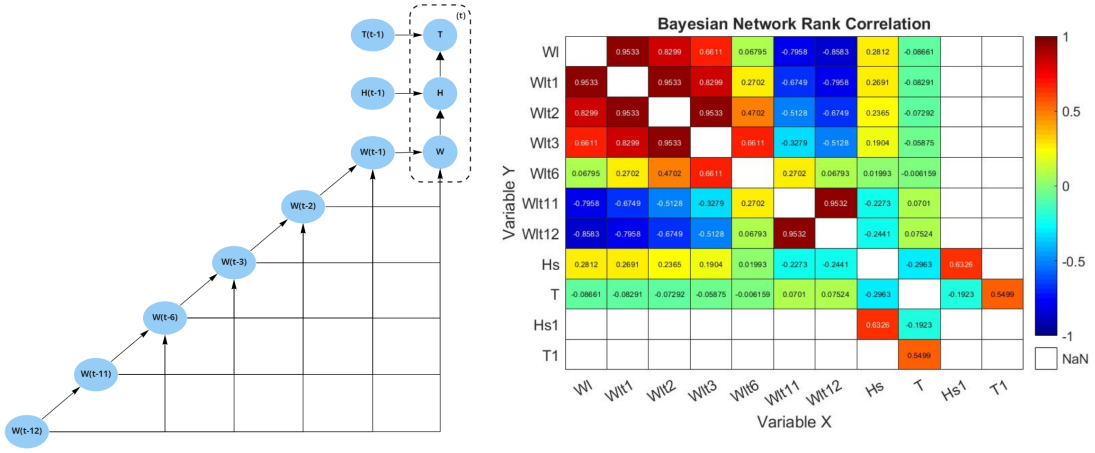

Figure 5.19: Calibrated DBN structure (left) and corresponding rank correlation matrix (right).

5.2.3.2 Validation

Similar to the validation of the SBN, the DBN was also statistically and physically validated. Assessment of the underlying dependence structure was achieved using semi-correlations and the CVM statistic. The semi-correlation analysis showed that Gaussian, Clayton, Gumbel and t copulas well represent the underlying dependence structure (Table 5.11). In contrast, the CVM analysis found Clayton copulas to best represent the underlying pairs as illustrated in Figure 5.20 (Appendix J).

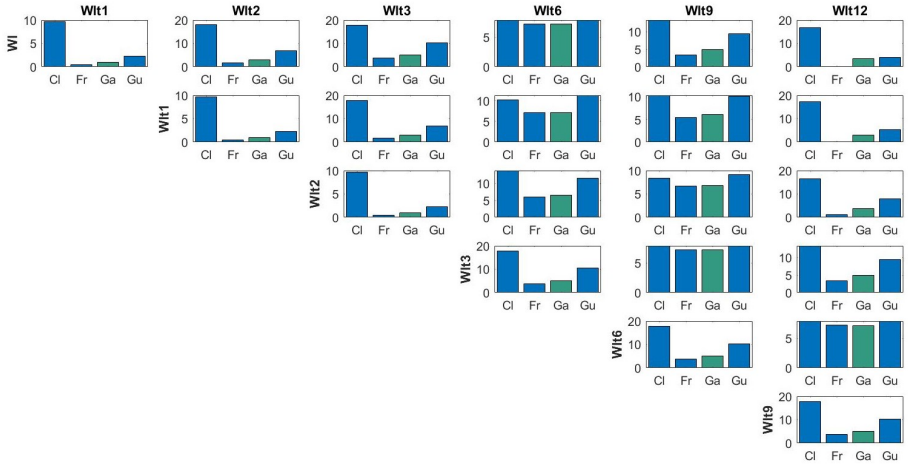

Figure 5.20: Resulting Cramer von Mises statistics for all variable pairs included in the dynamic Bayesian network. Gaussian CVM statistic is highlighted in green.

The simplification of a Gaussian copula was accentuated by the d-calibration hypothesis. The hypothesis was only accepted for 10 samples as shown in Figure 5.21. A sample size this small will almost always pass the d-calibration hypothesis and therefore the normal rank correlation is concluded to be unsuitable for modelling the dependence structure of the variables in the DBN.

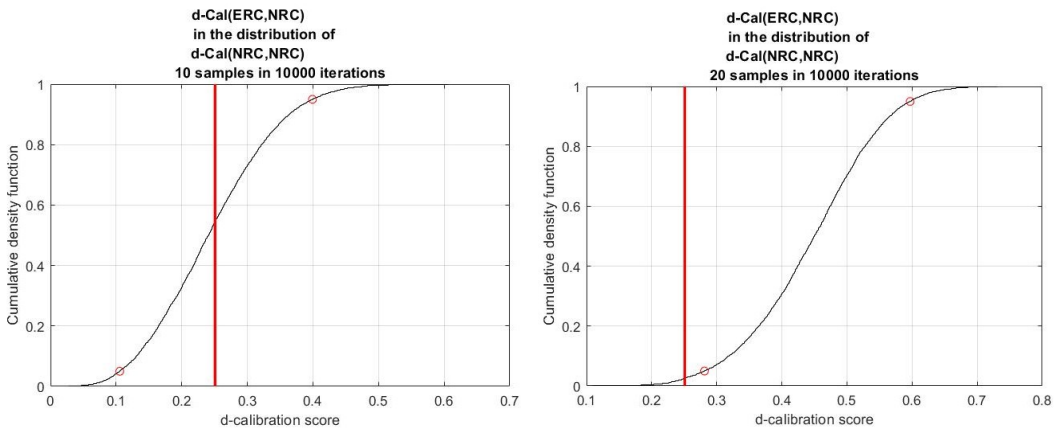

Figure 5.21: d-calibration score (red line) for the empirical rank correlation (ERC) matrix in the distribution of the normal rank correlation (NRC) matrix for 10 samples (left) and 20 samples (right).

Physical accuracy of the DBN was conducted for a segment of the validation dataset (50 hours), as the data tends towards the mean value after a while, reducing accuracy. The DBN was able to capture periodic movement of the water level while slowly dampening through time. Corresponding wave heights and wave periods were modelled with an accuracy of 88% and 85% respectively. The corresponding run is presented in Figure 5.22.

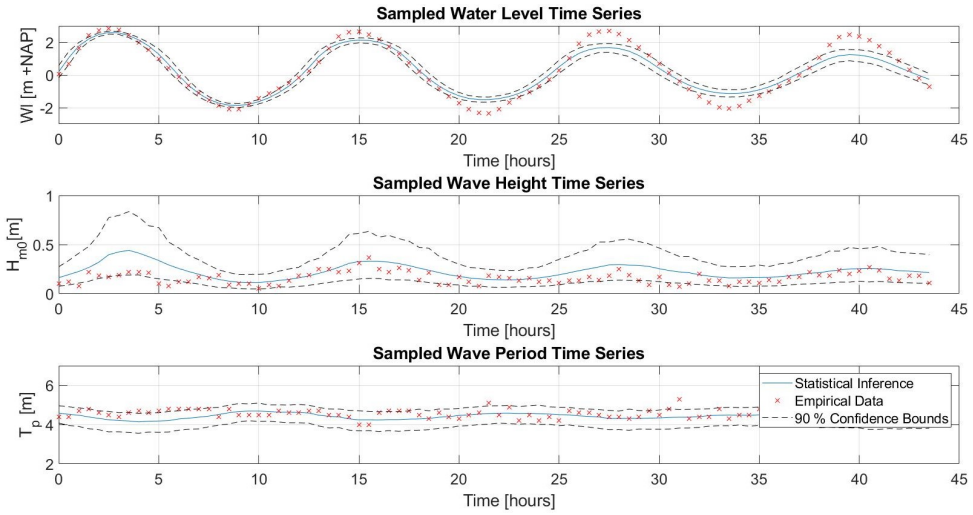

Figure 5.22: Comparison of the sampled results of the split test with the validation dataset for offshore water level (top), offshore wave height (middle) and offshore wave period (bottom).

The positive correlation between water level and wave period can be observed clearly, as both periodic motions exhibit synchronous evolution through time. Interestingly, the wave height confidence bounds expand for increasing water levels. Moreover, the confidence bounds decrease over time, similar to the amplitude of the sampled water level time series. The prior could be explained by the physical boundary at 0 for wave heights, resulting in more narrow samples being drawn from the marginal distribution. The former is discussed in the following paragraph. The confidence bounds for water levels are clearly very narrow, this was found to be related to the number of previous time steps included in the model. Figure I.17 illustrates this statement, as less previous time steps were included in that variant. Therefore, less variables were conditionalized, leading to less dependence with the current time step, providing a wider sampling range and thus confidence bounds.

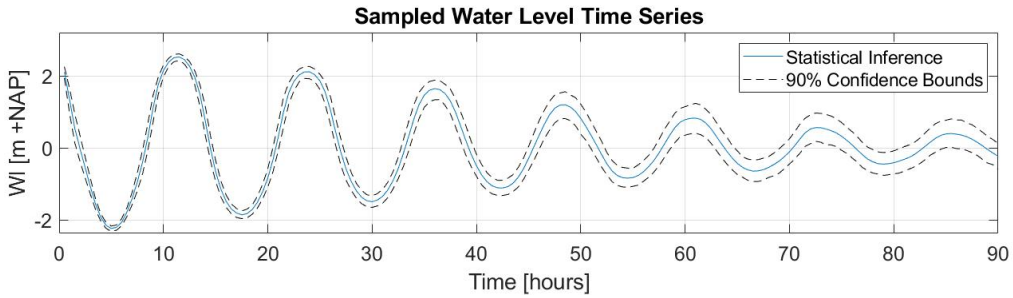

Figure 5.23: Long term water level modelling using the DBN, showing progression towards the mean over time.

The current DBN setup has limitations and cannot yet be applied for longer time periods, as illustrated in Figure 5.23. It is evident that long term sampling of the DBN leads to progression towards the mean parameter values. Improvements of the current model could, similar to the SBN, would be the implementation of a vine-copula model to improve the dependence structure. Furthermore, other methods could be assessed to overcome the inability to model long term time series without averaging out towards the mean. Hidden variables and Markov processes could be assessed for these purposes as done in the research by Uusitalo et al. (2018) and Trifonova et al. (2019). Nevertheless, the DBN is able to accurately model short term offshore hydraulic time series within a margin of error of 15%.

5.2.4. Summary

This section provided the statistical, calibration and validation results for the static and dynamic Bayesian networks. The statistical analysis (section 5.2.1) underlined the simplification induced through using Gaussian Bayesian networks. Moreover, the marginal and (auto)correlation analyses provided the fundamental building blocks for both BN structures. The static (section 5.2.2) and dynamic- (section 5.2.3) Bayesian network calibration and validation results presented model accuracy in the order of 90% and 85% respectively.

The results clearly highlights the ability of the SBN for modelling nearshore wave heights within narrow confidence bounds at an accuracy of 90%. Underlining the physical accuracy of the model and supporting the application of the model in regard to flood defense assessment in the subsequent section. The DBN results provide narrow bounded results for water level time series. The periodic motion was not sustainable as longer sampling processes resulted in a progression towards the mean. The DBN was thus found most accurate in the first 25 hours of sampling. In summary, the DPT now contains a temporally uniform database and accurate probabilistic models that are ready for application.

5.3. Application

The DPT was applied to model nearshore wave heights with and without vegetation on the foreshore during normative storm conditions. The results obtained through DPT modeling were compared to the reference WBI approach. This was completed through implementing the model settings defined in section 4.5 to utilize the database and probabilistic model for application.

5.3.1. WBI Approach - Reference

In accordance with the current WBI guidelines, the normative hydraulic conditions defined in section 4.5.1 were used to assess the dike segment at Hellegatpolder. This entails 1.723 meter wave heights at the toe of the dike. Moreover, the wave loading is constant through time as highlighted by the red line in Figure 5.24.

5.3.2. DPT Application

The DPT was applied to model nearshore wave heights with and without vegetation. The results were segmented per season, illustrating the effect of seasonality on wave attenuation. Table 5.15, presents the maximum wave heights modelled using the DPT with and without vegetation. Moreover, the average reduction due to vegetation is presented per season.

Table 5.15: DPT results for modelling storm conditions over the HFD. Presenting the nearshore wave heights and the reduction coefficient for vegetation included and excluded on the foreshore.

	Max Wave Height [m]		Average Reduction
Season	**No Vegetation**	**Vegetation**	**Due to Vegetation [%]**
Spring	0.9	0.29	35.8
Summer	0.9	0.17	81.9
Autumn	0.9	0.27	40.3
Winter	0.9	0.31	25.7

It is evident from these results that both a foreshore and vegetation reduce wave height compared to the WBI reference. Maximum nearshore wave heights for foreshore and vegetation scenarios were found to be 0.9 meters and 0.31 meters respectively. Clearly, summer vegetation results in greater wave attenuation. This is expected as larger vegetation height, -width and -density result in a greater frontal area and drag coefficient. Which, according to Equation 2.2, results in more reduction in wave energy and thus increased wave attenuation. In accordance with this statement, winter vegetation results in the least amount of wave attenuation. The occurrence of winter storms is more common than summer storms, therefore the average wave reduction is expected to shift towards a lower average reduction. The reduction due to vegetation for all seasons is in the order of 25 - 80%, clearly underlining the importance of including vegetation in the design and assessment of HFD systems.

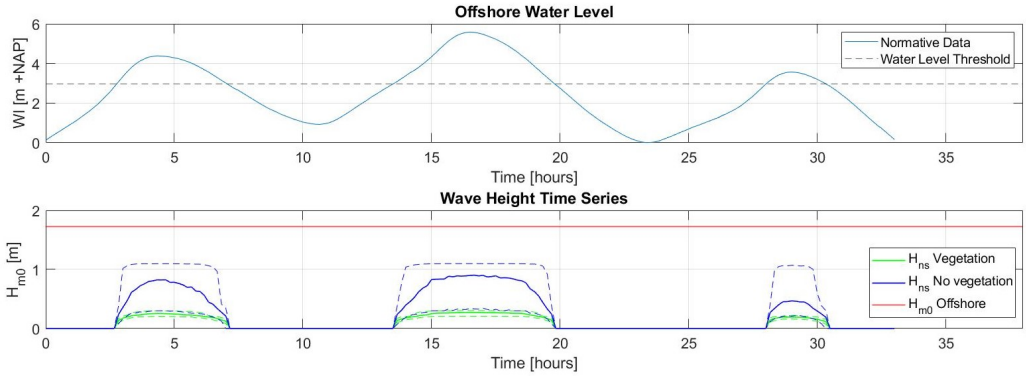

Figure 5.24: Normative hydraulic loading during storm conditions using the DPT (top), and the corresponding sampled values obtained using the DBN including and excluding vegetation (bottom). Note that the dashed lines represent 90% confidence bounds.

Figure 5.24 highlights nearshore wave heights obtained as output from a DPT run. Nearshore wave heights excluding vegetation on the foreshore (red line) and including summer state vegetation on the foreshore (green line) are depicted for the mean of the sample (solid line) and 90% confidence bounds (dashed line). It should be noted that modelled wave heights have a larger margin of error than the depicted 90% confidence bounds. This is mainly due to the lack of extreme values in the current underlying dataset. Furthermore, dynamic nearshore wave loading during storms is clearly illustrated in Figure 5.24. The bottom plot shows gaps in all wave heights except offshore waves. The reasoning is that waves are not able to traverse the foreshore for water levels below a 2.9 m +NAP threshold (upper plot).

In the future, the DPT can be applied to include dynamic loading in a probabilistic manner. The probabilistic loading can be used to assess vegetation response (i.e. stem breakage) during loading conditions. Naturally, additional research into the relation between hydraulic loading and vegetation is needed. However, once additional data has been collected and researched, their effects can easily be included in the current DPT. Expansion of the database and alteration of the BNs to include the physical relation would allow their effects to be included in the model. This ability underlines the applicability and modular flexibility of the tool.

Within the Dutch design guidelines, the WBI proves tools such as *Riskeer* and *BM-Gras Buitentalud* to assess and design flood defenses. The assessments were related to failure mechanisms for which normative probabilities were determined. Relevant failure mechanisms within the scope of this thesis were related to wave impact and wave overtopping. For these, the associated failure mechanisms are:

1. Failure due to grass erosion outer slope (e.g. due to wave impact);
2. Failure due to grass erosion crest- and inner slope (e.g. due to wave overtopping);
3. Failure due to stone stability on outer slope (e.g. due to wave impact or erosion);
4. Failure due to asphalt breakage (e.g. due to wave impact).

Analysis of these mechanisms required two main elements: hydraulic loads and flood defense parameters (i.e. crest height, slope angles, friction factor etc.). Provided that the latter are either available to the engineer assessing a dike, or set as variables in the design process, these are neglected. Therefore, only hydraulic loads are of interest. Hydraulic loads obtained from the DPT are compatible with the WBI tools to assess the failure mechanisms. Illustrating the feasibility of implementing the DPT within the WBI.

In conclusion the DPT is able to model nearshore wave heights for HFD systems using only the database, probabilistic models and the application settings. Computational run time was in the order of 10-20 seconds to model 25 hours of data. As a comparison, the numerical model developed in this thesis required 25 minutes to model the same amount of data. Thus, the DPT only requires 1% of the computational time required by the numerical model to assess the system, highlighting the efficiency of the DPT.

5.4. Summary

In summary, this chapter discloses the results obtained during the execution of the case study method (chapter 4). During development of the database, statistical expansion techniques allowed a vegetation dataset to be developed synthetically that includes temporal variability. Nearshore wave heights were included in the database through numerical modelling. Furthermore, two additional datasets were modelled: one including vegetation on the foreshore, the other one excluding vegetation (i.e. bare foreshore). This resulted in a temporally uniform dataset containing 7 years of data with a temporal resolution of 30 minutes.

A static and dynamic Bayesian network were calibrated and validated to model nearshore wave heights in and through time. Although statistical validation did not support the modelling of a multivariate Gaussian copula in both BNs, the physical sampling accuracy for both SBN and DBN was in the order of 90% and 85%. Long term modelling using the DBN illustrated that short term (i.e. 25 hours) accuracy was attainable. Long term modelling interestingly showed progression towards the mean.

The results obtained through application of the DPT highlighted the importance of including vegetated foreshore in the assessment of HFD systems. Normative hydraulic conditions obtained from the WBI approach resulted in constant loading of the flood defense. Applying the DPT to include the NBS elements in the HFD resulted in wave reduction in the order of 47% and 82% for a bare and vegetated foreshore respectively (Fig. 5.25). As expected, summer vegetative states resulted in roughly 3 times more wave attenuation. Furthermore, the DPT not only highlighted the average wave attenuation induced by the NBS elements, it also highlighted the inherent dynamic hydraulic loading obtained through DPT utilization. Finally, computational efficiency was highlighted in application of the DPT, and was found to run 100 times faster than numerical models.

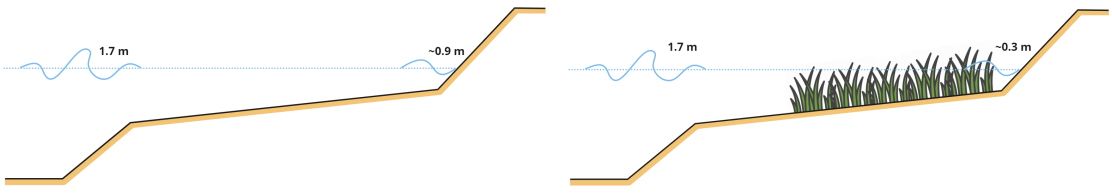

Figure 5.25: DPT nearshore wave height results for a bare foreshore (left) and vegetated foreshore (right).

6

Conclusions & Recommendations

This chapter finalizes the thesis by summarizing the most important aspects of this work. To start, the research questions are answered in section 6.1. Subsequently, conclusions concerning design guidelines and temporal assessment of wave attenuation are disclosed in section 6.2. These conclusions accentuate the applicability and importance of including temporal assessment of HFD systems within current design guidelines. Finally, section 6.3 presents alternative application possibilities for the DPT within design and assessment to open the door for future research.

6.1. Research Questions

This thesis comprises two main research areas. The first aimed to assess the importance of temporal assessment of HFD systems. Whereas the second concerned the implementation of the DPT within guidelines to facilitate design and assessment of HFD systems.

6.1.1. Temporal Assessment of Wave Attenuation in HFD Systems

Research questions concerning the temporal assessment of wave attenuation in HFD systems are discussed below.

What are the fundamental elements of a HFD system that are required for temporal modelling of nearshore wave heights?

The three main parameter categories for the numerical and probabilistic modelling of nearshore wave heights are: bathymetry, hydraulic and vegetation. In regard to numerical modelling, parameters are required to define the initial state and boundary conditions in the system, allowing for wave transformation processes to be simulated numerically. In contrast, a probabilistic model does not have requirements. Instead, system parameters with a physical relation to wave attenuation due to vegetation are included in the model through dependence structures.

Numerical modelling required the definition of a bathymetry profile, offshore hydraulic boundary conditions and vegetation and friction parameters in the system. An x-, z-coordinate system represented the bathymetry profile in the numerical model, combined with the dike slope (S_d) and crest height (h_c). The bathymetry was set constant in the probabilistic model and thus required no parameters. Wave heights (H_s), wave periods (T_p) and water levels (Wl) represented the offshore conditions in both models. Vegetation parameters included the height (h_v), width (b_v), density (N_v) and drag coefficient (C_d) in both models. Furthermore, the numerical model required definition of the friction coefficient (c_f), the grain size (d_50) and the vegetation length (L_v) to model the system. These parameters were kept constant during probabilistic modelling and were thus not included. The difference in parameter requirements for the modelling purposes are highlighted in Table 4.1.

What is the monthly variation of numerically obtained wave attenuation on vegetated foreshores?

Numerical modelling of nearshore wave heights for both a bare and vegetated foreshore allowed the determination of wave attenuation due to vegetation specifically for Hellegatpolder. Monthly wave attenuation due to vegetation is presented in Figure 5.7. It is evident that during summer months (July - August)

wave heights are reduced the most. This is supported by the fact that summer vegetative states, being more dense, wide and tall, induce more drag on the flow. Interestingly, the mean wave attenuation in August is roughly 1.7 times greater than in January. Generally, the extreme offshore wave heights were found mostly in winter and spring months, thus coinciding with the milder vegetative states, the combination of which results in higher waves during winter and spring seasons.

Are Bayesian network structures suitable for periodic modelling of HFD system parameters?

Dynamic Bayesian networks (DBN) were found suitable for short term periodic modelling of HFD system parameters. The DBN was not able to model longer time series as the sampled values progress towards the mean over longer periods of time (>25 hours). The BN sampling process was believed to induce this effect because 1.000+ samples were drawn from a conditionalized distribution. As the mean value of the array of samples was used to conditionalize the next time step in the DBN, extreme values occurred less frequently. Over time, this results in samples progressing more towards the mean.

Modelling longer time spans using the DBN requires further research. Markov chains or hidden variables could be assessed to utilize their dynamic modelling properties. Furthermore, numerical models can be used to generate hydraulic loading scenarios. Subsequently, BNs can be conditionalized to probabilistically model nearshore wave heights.

What is the influence of temporal variability on wave height transformation in HFD systems?

Including temporal variability of vegetation and offshore hydraulic parameters allowed different system states to be related to corresponding wave attenuation. In doing so, seasonal variation of vegetation was related to wave dampening. Moreover, different hydraulic loading states (i.e. wave height and water level) were related to wave attenuation. The combination was included in the probabilistic model to determine the relative importance of each element in regard to nearshore wave height with (H_{ns_v}) and without (H_{ns}) vegetation on the foreshore. Rank correlations for both wave heights in the final BN are highlighted in Table 5.13.

Based on these results for Hellegatpolder, it was shown that a combination of large waves, high water levels and reduced vegetation density, width and height result in the greatest nearshore wave heights. Moreover, the relative importance of the water level (Wl) was shown to be of greater influence on nearshore wave heights compared to offshore wave heights (H_s). In addition, water levels were found to be of more influence on nearshore wave height for vegetated scenarios (i.e. ρ_s: 0.91 vs 0.82). This result is explained by the relation of water level to vegetation submergence and drag force. In contrast, the dependence of offshore wave height on nearshore wave heights decreases for the vegetated foreshore. In non vegetated scenarios the sole effect of wave height is more dominant as it is only affected by depth induced wave breaking. In general, the hydraulic parameters have the greatest effect and thus temporal variation of these variables will induce a dynamic nearshore wave loading on the system.

6.1.2. Design Guidelines for HFD Systems

Research questions concerning the design guidelines for HFD systems are discussed below.

How can temporal assessment be included in the current WBI 2017 guidelines?

The current WBI 2017 guidelines suggest normative hydraulic conditions to design and assess flood defense systems. The DPT finds its place after determination of the hydraulic conditions as it transforms these conditions to nearshore wave heights. Figure 3.1 highlights the placement of the DPT within the WBI. The resulting hydraulic conditions comply with the input required in *Riskeer* and *BM-Gras Buitentalud*. Tools developed by Rijkswaterstaat to asses failure mechanisms during the design and assessment of flood defenses.

What are the added benefits of using the DPT to include temporal assessment of HFD systems in the current design and assessment guidelines?

Including temporal assessment of HFD systems in the current design guidelines has two main benefits. First of all, more realistic wave heights are obtained by including depth induced wave breaking and

vegetation dampening as a result of using vegetation. As the wave heights are used to design and assess flood defenses, resulting flood probabilities will change towards more realistic values by using the DPT. This is supported by the location specific results obtained for Hellegatpolder in section 5.3, where wave heights were found to be dampened between 25 - 83% over vegetated foreshores.

Second, temporal assessment of HFD systems allows wave loading and its duration to be modelled. Combined, these are used to determine the residual strength of the vegetation and the flood defense. Again, the results in section 5.3 highlight the difference in loading conditions between the current guidelines and the results obtained using the DPT. The WBI guidelines specify a single normative wave loading, resulting in constant wave loading. Application of the DPT resulted in dynamic wave loading. Dynamic loads were obtained as vegetation dampening and submergence levels of the foreshore vary due to the tides. Standardizing dynamic loading in the assessment of HFD systems is currently being researched by Rijkswaterstaat, the design guidelines are ready and compatible.

6.2. Conclusion

This thesis presents a conceptual framework for temporal assessment of hybrid flood defense (HFD) systems, which is placed within the current WBI 2017 guidelines. The conceptual framework results in the development of a dynamic probabilistic tool (DPT) in MATLAB. The DPT includes the effects of depth- and vegetation induced wave attenuation in the modelling of nearshore wave heights. This framework was applied in a case study to develop a DPT which was able to model nearshore wave heights at the Hellegatpolder salt marsh during storm conditions. This section discloses the most important conclusions, segmented into the conclusions for the temporal assessment of wave attenuation for the HFD system at Hellegatpolder and the conclusions regarding the implementation of the conceptual framework in the current design guidelines.

6.2.1. Temporal Assessment of Wave Attenuation in HFD Systems

Data was collected for fundamental idealized system parameters at Hellegatpolder. Nearshore wave height data was unavailable. Therefore, a 2D numerical XBeach model was developed to model 7 years of data with a temporal resolution of 30 minutes. Results were obtained with and without vegetation on the transect. Comparing wave heights showed an average wave attenuation of 54% due to vegetation. Moreover, the importance of including temporal variability was emphasized by the fact that wave attenuation was found to be 1.7 times greater in the months July and August compared to December and January. Temporal variability of vegetation parameters is thus an influential factor on wave attenuation. Furthermore, the short term effect of morphology on nearshore wave height was found insignificant and thus neglected in probabilistic modelling. The resulting numerical datasets were matched with the collected data to form a temporally uniform database.

A static and dynamic Bayesian network (SBN & DBN) were developed to respectively model nearshore wave heights in a point in time and offshore hydraulics time series. Due to the inherent Gaussian dependence structure of Bayesian networks, simplification of the actual dependence structure was inevitable. Nonetheless, two sided sampling validation of the SBN resulted in 90% of the sampled nearshore wave heights modeled within the 90% confidence bounds of the predicted samples. The DBN was able to reproduce the short term (i.e. $<$25 hours) periodic motion of the tides. Moreover, the DBN accurately sampled hydraulic variables with an accuracy of at least 85% within the 90% confidence bounds. Long term modelling of the DBN consistently progressed towards the mean marginal values, which was found to be inevitable due to the current sampling process. Both BNs were easily integrated in the DPT as they were developed in MATLAB using the BANSHEE toolbox.

Nearshore wave heights were modelled using the DPT for a bare and vegetated foreshore. Normative water level time series and a constant wave height of 1.7 meters were obtained from Hydra-NL and used to model nearshore wave heights for a duration of 25 hours. Application of the DPT resulted in dynamic wave loading time series with a maximum of 0.9 and 0.3 meters respectively for a bare and vegetated foreshore. The average wave attenuation due to vegetation was 45% (Table 5.24). This is less than the average wave attenuation obtained in numerical modelling (i.e. 54%), which was expected as the application considers extreme water levels of 5 m +NAP. This leads to complete vegetation submergence and increased water depth over the foreshore. Both result in less wave attenuation.

Another important finding in the application of the DPT was the importance of temporal modelling. Nearshore wave heights were modelled for different vegetative seasons. Wave attenuation due to vegetation was found to lie between 25 - 82%, with wave attenuation in the summer being 3 times greater than in the winter. As the hydraulic forcing was kept constant, the effect of vegetation variability is evident.

6.2.2. Design Guidelines for HFD Systems

Currently, the effects of vegetated foreshores on wave heights are neglected during design and assessment of HFD systems. This thesis provides a method and corresponding MATLAB models for the development of a DPT that allows modelling of dynamic wave loads at the toe of the dike. Thereby, enabling the design and assessment to include the effects of nature based elements. The methods were shown to be compatible with the WBI 2017 guidelines, as normative conditions obtained from the WBI were used to run the model, and the output is similar to that required for subsequent assessment modules used by Rijkswaterstaat.

Both the numerical and probabilistic model were developed in MATLAB, providing the user with additional freedom in application as the code can be altered for the application scenario. During the development of both models, the advantages of probabilistic modelling were evident. Numerical modelling required cumbersome development of settings and boundary conditions. On top of that, running the calibrated numerical model for a month required hours to run. In contrast, the development of the BNs required minutes to set up and run. The efficiency of the model is useful during design and assessment as engineers can assess multiple scenarios within a shorter time frame. Moreover, probabilistic modelling includes uncertainty in the results, which is not included in numerical modelling.

Ultimately, the utilization of this approach results in more realistic design and assessment scenarios, as the proven wave attenuating elements (i.e. foreshore and vegetation) are included in the modelling of nearshore wave heights. Moreover, dynamic loads enable determination of the residual strength for all elements in the system as load and duration are known. Including these effects is a significant step into the ability to design and assess HFD systems.

6.3. Recommendations

Throughout the development of the conceptual framework and application thereof, additional ideas, improvements and implementation methods were collected to steer future development of this work. The recommendations are categorized for topics concerning the method and those regarding the design guidelines.

6.3.1. Method

Application of the conceptual framework resulted in the development of a database, numerical- and probabilistic models. These elements form the main models that were examined and utilized to accurately model nearshore wave heights. Recommendations are presented below to further explore the development of the model to achieve a more complete and accurate DPT.

Data Collection

Temporally uniform data is currently lacking for vegetation and nearshore wave heights. This is a limitation of the method as data availability would allow for direct development of probabilistic models and application settings. It is therefore crucial that field studies are conducted to measure the temporal variability of HFD system parameters. Field measurement campaigns for various HFD systems should consistently measure the bathymetry variation, vegetation parameters and nearshore wave heights. The study by Hu et al. (2021) provides initial steps in the right direction. Furthermore, as field measurement campaigns are difficult to scale due to the labour intensity, remote sensing techniques (Van Zelst, 2018), drones and radar could be applied to obtain datasets more efficiently.

Numerical Modelling

To improve the numerical model, additional effects such as 3D response, dynamic vegetation input and stem breaking processes should be included in the numerical processes. The current model was 2D, neglecting many processes that occur in 3D environments such as wave refraction, shore-parallel flows and variability. Expanding the current numerical model will allow spatial variability to be assessed.

This is interesting for various reasons; determination of the weakest points in the system and assessment of spatial variability of vegetation on HFD response. Current 3D vegetation research conducted by Thompson et al. (2016) underlines the inherent spatial variability and can be applied in further research to expand current guidelines.

The current XBeach vegetation settings lack functionality. All vegetation parameters are static and cannot be set as time series, unlike all other parameters. For example, the drag coefficient is a constant value that cannot be set dynamically to follow the parameters that define the value such as wave period and vegetation parameters. Moreover, stem breakage and stem flexibility are not included in the XBeach settings. Once these modules are available in XBeach, the physical accuracy of the model will undoubtedly improve.

Probabilistic Models
Both probabilistic models were built using Gaussian BNs. Not all underlying bivariate copula structures were well represented using Gaussian copulas, resulting in loss of accuracy of the model. Using more sophisticated methods such as vine copula models could improve the network representation as each bivariate copula pair can be represented using a specific copula family. Before implementing vines, possible negative effects such as model run time require an in depth analysis.

Initial dynamic modelling using BNs provided promising results for short time analyses. However, long term assessment will require improvement in the current method as they progress toward the mean values of the marginal distributions. Furthermore, hidden variables and Markov processes could be assessed to overcome these limitations as done in the research by Uusitalo et al. (2018) and Trifonova et al. (2019). Development of a probabilistic model that can well predict long term time-series will facilitate development of the DPT in more sophisticated application, such as assessing sea level rise effects in regard to the response of the HFD.

6.3.2. Design Guidelines
It is crucial that HFD systems are included in design guidelines. The conceptual framework can realize this, yet more proof is required to support implementation. To achieve this, a number of recommendations are presented concerning future applications and research required to progress implementation of the design guidelines within the WBI.

Future Applications
The current DPT and its modules provide preliminary insights into the use of probabilistic methods to design and assess HFD systems. However, there are additional processes that can be researched and included in the DPT. Long term processes such as bathymetry morphology and vegetation evolution impact wave attenuation over longer time spans. Moreover, their effects influence evolution of system strength. The expanded DPT could hypothetically be used to assess SLR scenarios and be applied for monitoring and forecasting HFD system response. These alternative applications are discussed extensively in Appendix M.

Further research into these applications will lead to improvement or creation of new modules in the DPT. Assessing the effects of foreshore morphology and including the corresponding parameters in the model will enable secondary assessment of foreshore strengthening or weakening through time. This naturally has implications for the nearshore wave heights due to depth induced wave breaking. Once bathymetric evolution is included in the DPT, data and models concerning vegetation morphology can be used to further expand the realm of applications, whilst improving nearshore wave height prediction. Secondary effects such as soil strengthening and sediment capture, could be included for long term analyses of HFD systems using the DPT. Furthermore, the expansion or decrease of the marsh could be predicted through time, which instinctively influences wave attenuation.

With the additional processes included in the datasets, probabilistic modules and run settings, more complex analyses could be conducted such as the assessment of sea level rise (SLR). Water level time series for different SLR scenarios can be assessed using the DPT to predict corresponding hydraulic offshore conditions. Subsequently, the effect in regard to the morphology of both bathymetry and vegetation can

be modelled. The combined effect can then be used to predict nearshore wave heights for the various scenarios. Presenting a much more complete picture to both engineers assessing system response, and decision makers interested in the long term scenarios.

Monitoring and forecasting could be achieved with the expanded DPT. Continuous monitoring of an HFD system is possible by connecting the DPT model to online hydraulic databases (e.g. to the Rijkswaterstaat database). The connection provides data to be continuously read by the model and used to predict future scenarios. These monitoring results can be used by engineers for maintenance assessments for dike sections. The forecasting scenarios and their probabilities, provide the engineer with the information required for assessment and maintenance decisions.

All together the DPT can be further developed in terms of usability and adaptability to dataset coupling and numerical modelling programs. A general user interface (GUI) will improve the ease of use for engineers with no MATLAB experience. This will result in a more advanced tool that can effortlessly be used by engineers to efficiently assess HFD systems during extreme conditions and during their design lifetime.

Future Research
The overarching objective of the conceptual framework is to progress the application of NBS elements in the design and assessment of HFD systems. To achieve this, additional case studies should be conducted to provide Rijkswaterstaat and engineering companies with proof that the methodology is a valid option for the design and assessment of HFD systems. The MATLAB models developed in this thesis are provided in the supplementary files to be used and tuned to assess additional HFD systems. Additional research should concern the application of the conceptual framework for:

1. A coastal mangrove system to examine the application for all vegetation types;
2. A fluvial system to assess the effects of fluvial loading conditions;
3. A HFD system with mixed vegetation on the foreshore.

In general, the conceptual framework should be applied parallel to the assessment of a HFD system. In doing so, the data collected for these systems can be compared to that produced by the DPT. This will provide additional proof for the accuracy and ease of use of the conceptual framework.

Bibliography

Y. Abebe. *Development of a Spatiotemporal Decision Support Framework for Managing Urban Stormwater Infrastructures and Climate Change Adaptation.* PhD thesis, University of British Columbia, 2020.

B. W. Borsje, S. de Vries, S. K. Janssen, A. P. Luijendijk, and V. Vuik. Building with Nature as Coastal Protection Strategy in the Netherlands. In *Living Shorelines*, chapter 8, pages 137–156. Marine and Fluvial Systems, 2018. ISBN 9781498740029. doi: 10.1201/9781315151465-10.

T. Botterhuis, R. Waterman, and C. Geerse. Gebruikershandleiding Waterstandsverloop: versie 3.0. *Software Manual*, 2017.

T. J. Bouma, J. van Belzen, T. Balke, Z. Zhu, L. Airoldi, A. J. Blight, A. J. Davies, C. Galvan, S. J. Hawkins, S. P. Hoggart, J. L. Lara, I. J. Losada, M. Maza, B. Ondiviela, M. W. Skov, E. M. Strain, R. C. Thompson, S. Yang, B. Zanuttigh, L. Zhang, and P. M. Herman. Identifying knowledge gaps hampering application of intertidal habitats in coastal protection: Opportunities & steps to take. *Coastal Engineering*, 87:147–157, 2014. ISSN 03783839. doi: 10.1016/j.coastaleng.2013.11.014. URL `http://dx.doi.org/10.1016/j.coastaleng.2013.11.014`.

C. C. CETMEF. The rock manual. the use of rock in hydraulic engineering (2nd edition). `https://www.kennisbank-waterbouw.nl/DesignCodes/rockmanual/`, 2007.

Y. Chang, X. Wu, C. Zhang, G. Chen, X. Liu, J. Li, B. Cai, and L. Xu. Dynamic Bayesian networks based approach for risk analysis of subsea wellhead fatigue failure during service life. *Reliability Engineering and System Safety*, 188(June 2018):454–462, 2019. ISSN 09518320. doi: 10.1016/j.ress.2019.03.040.

B. R. a. Dalrymple, J. T. Kirby, and P. A. Hwang. Wave diffraction due to areas of energy dissipation. *Journal of Waterway, Port, Coastal, and Ocean Engineering*, 110(1):67–79, 1984.

F. A. Darby and R. E. Turner. Below- and aboveground Spartina alterniflora production in a Louisiana salt marsh. *Estuaries and Coasts*, 31(1):223–231, 2008. ISSN 15592723. doi: 10.1007/s12237-007-9014-7.

J. P. De Waal. Basisrapport WBI 2017. Technical report, Deltares, Utrecht, 2016.

Deltares. Dataset documentation vaklodingen, 2020. URL `https://publicwiki.deltares.nl/display/OET/Dataset+documentation+Vaklodingen`.

S. Doocy, A. Daniels, C. Packer, A. Dick, and T. D. Kirsch. The human impact of earthquakes: a historical review of events 1980-2009 and systematic literature review. *PLoS currents*, 5, 2013.

M. Duits. Hydra-NL Gebruikershandleiding versie 2.7. Technical report, HKV, 2019.

D. FitzGerald, M. Fenster, B. Argow, and I. Buynevich. Coastal Impacts Due to Sea-Level Rise. *Annual Review of Earth and Planetary Sciences*, 36(1):601–647, 2008. ISSN 0084-6597. doi: 10.1146/annurev.earth.35.031306.140139.

K. B. Gedan, M. L. Kirwan, E. Wolanski, E. B. Barbier, and B. R. Silliman. The present and future role of coastal wetland vegetation in protecting shorelines: Answering recent challenges to the paradigm. *Climatic Change*, 106(1):7–29, 2011. ISSN 01650009. doi: 10.1007/s10584-010-0003-7.

C. Genest and A. C. Favre. Everything you always wanted to know about copula modeling but were afraid to ask. *Journal of Hydrologic Engineering*, 12(4):347–368, 2007. ISSN 10840699. doi: 10.1061/(ASCE)1084-0699(2007)12:4(347).

A. Hanea, O. Morales Napoles, and D. Ababei. Non-parametric Bayesian networks: Improving theory and reviewing applications. *Reliability Engineering and System Safety*, 144:265–284, 2015. ISSN 09518320. doi: 10.1016/j.ress.2015.07.027. URL `http://dx.doi.org/10.1016/j.ress.2015.07.027`.

A. M. Hanea, D. Kurowicka, R. M. Cooke, and D. A. Ababei. Mining and visualising ordinal data with non-parametric continuous BBNs. *Computational Statistics and Data Analysis*, 54(3):668–687, 2010. ISSN 01679473. doi: 10.1016/j.csda.2008.09.032. URL dx.doi.org/10.1016/j.csda.2008.09.032.

D. T. Hristopulos. *Random fields for spatial data modeling*. Springer, 2020.

Z. Hu, P. W. Willemsen, B. W. Borsje, C. Wang, H. Wang, D. Van Der Wal, Z. Zhu, B. Oteman, V. Vuik, B. Evans, et al. Synchronized high-resolution bed-level change and biophysical data from 10 marsh–mudflat sites in northwestern europe. *Earth System Science Data*, 13(2):405–416, 2021.

IPCC. Climate Change 2014 Part A: Global and Sectoral Aspects. Technical report, IPCC, 2014. URL papers2://publication/uuid/B8BF5043-C873-4AFD-97F9-A630782E590D.

U. Kjærulff. *A computational scheme for dynamic Bayesian networks*. PhD thesis, Aalbor University Denmark, 1993. URL http://citeseerx.ist.psu.edu/viewdoc/summary?doi=10.1.1.54.9016.

N. Kobayashi. WAVE ATTENUATION BY VEGETATION. *J. Waterway, Port, Coastal, Ocean Eng*, 119(1):30–48, 1993.

E. W. Koch, E. B. Barbier, B. R. Silliman, D. J. Reed, G. M. Perillo, S. D. Hacker, E. F. Granek, J. H. Primavera, N. Muthiga, S. Polasky, B. S. Halpern, C. J. Kennedy, C. V. Kappel, and E. Wolanski. Non-linearity in ecosystem services: Temporal and spatial variability in coastal protection. *Frontiers in Ecology and the Environment*, 7(1):29–37, 2009. ISSN 15409295. doi: 10.1890/080126.

F. J. Méndez, I. J. Losada, and M. A. Losada. Hydrodynamics induced by wind waves in a vegetation field. *Journal of Geophysical Research: Oceans*, 104(C8):18383–18396, 1999. ISSN 2169-9291. doi: 10.1029/1999jc900119.

P. Menéndez, I. J. Losada, M. W. Beck, S. Torres-Ortega, A. Espejo, S. Narayan, P. Díaz-Simal, and G. M. Lange. Valuing the protection services of mangroves at national scale: The Philippines. *Ecosystem Services*, 34(October):24–36, 2018. ISSN 22120416. doi: 10.1016/j.ecoser.2018.09.005. URL https://doi.org/10.1016/j.ecoser.2018.09.005.

P. Menéndez, I. J. Losada, S. Torres-Ortega, S. Narayan, and M. W. Beck. The Global Flood Protection Benefits of Mangroves. *Scientific Reports*, 10(1), 2020. ISSN 20452322. doi: 10.1038/s41598-020-61136-6. URL https://doi.org/10.1038/s41598-020-61136-6.

Ministerie van Infrastructuur en Milieu. Regeling veiligheid primaire waterkeringen 2017 Bijlage I. Technical Report 65697, Ministerie van Infrastructuur en Milieu, 2017a.

Ministerie van Infrastructuur en Milieu. Regeling veiligheid primaire waterkeringen 2017 Bijlage III Sterkte en veiligheid. Technical Report april 2016, Ministerie van Infrastructuur en Milieu, 2017b.

F. Mink and P. Sansoglou. NATUREEBASED SOLUTIONS: CHALLENGE OR OPPORTUNITY? Technical report, Terra et Aqua, 2020. URL https://platform.think-nature.eu.

I. Möller, T. Spencer, J. R. French, D. J. Leggett, and M. Dixon. Wave transformation over salt marshes: A field and numerical modelling study from north Norfolk, England. *Estuarine, Coastal and Shelf Science*, 49(3):411–426, 1999. ISSN 02727714. doi: 10.1006/ecss.1999.0509.

I. Möller, M. Kudella, F. Rupprecht, T. Spencer, M. Paul, B. K. Van Wesenbeeck, G. Wolters, K. Jensen, T. J. Bouma, M. Miranda-Lange, and S. Schimmels. Wave attenuation over coastal salt marshes under storm surge conditions. *Nature Geoscience*, 7(10):727–731, 2014. ISSN 17520908. doi: 10.1038/NGEO2251.

G. Mourik. Prediction of the erosion velocity of a slope of clay due to wave attack. Technical report, Deltares, 2020.

S. Muis, M. Irazoqui Apecechea, J. Dullaart, J. de Lima Rego, K. Skovgaard Madsen, J. Su, K. Yan, and M. Verlaan. A global high-resolution dataset of extreme sea level, including future projections. *Frontiers of Marine Sciences, under review*, 7(April):1–15, 2020. doi: 10.3389/fmars.2020.00263.

O. M. Nápoles, D. Worm, and P. van den Haak. Reader for course: Introduction to Bayesian Networks. Technical report, TNO, 2013.

U. Neumeier. Quantification of vertical density variations of salt-marsh vegetation. *Estuarine, Coastal and Shelf Science*, 63(4):489–496, 2005. ISSN 02727714. doi: 10.1016/j.ecss.2004.12.009.

M. H. K. Niazi. Flood Risk Prediction under Global Vegetated Hydrodynamics: A Bayesian Network, 2019.

M. H. K. Niazi, O. Morales Nápoles, and B. K. van Wesenbeeck. Probabilistic characterization of the vegetated hydrodynamic system using non-parametric bayesian networks. *Water*, 13(4), 2021. ISSN 2073-4441. doi: 10.3390/w13040398. URL `https://www.mdpi.com/2073-4441/13/4/398`.

D. Paprotny, O. Morales-nápoles, D. T. H. Worm, and E. Ragno. SoftwareX BANSHEE – A MATLAB toolbox for Non-Parametric Bayesian Networks. *SoftwareX*, 12:100588, 2020. ISSN 2352-7110. doi: 10.1016/j.softx.2020.100588. URL `https://doi.org/10.1016/j.softx.2020.100588`.

Rijkswaterstaat. WBI2017 Handboek voor de toezichthouder. Technical report, Ministerie van Infrastructuur en Waterstaat, Utrecht, 2017.

Rijkswaterstaat. Rijkswaterstaat waterinfo. `https://waterinfo.rws.nl/`, 6 2020.

D. Roelvink, A. van Dongeren, R. Mccall, B. Hoonhout, A. van Rooijen, P. van Geer, L. de Vet, and K. Nederhoff. Xbeach Manual. Technical report, Deltares, 2015.

M. Sadegh, E. Ragno, and A. Aghakouchak. Water Resources Research. *Journal of the American Water Resources Association*, 5(3):2–2, 1969. ISSN 1093-474X. doi: 10.1111/j.1752-1688.1969.tb04897.x.

M. Sklar. Fonctions de repartition an dimensions et leurs marges. *Publ. inst. statist. univ. Paris*, 8: 229–231, 1959.

S. Temmerman, P. Meire, T. J. Bouma, P. M. Herman, T. Ysebaert, and H. J. De Vriend. Ecosystem-based coastal defence in the face of global change. *Nature*, 504(7478):79–83, 2013. ISSN 00280836. doi: 10.1038/nature12859.

P. R. Thompson, C. G. Piecuch, M. A. Merrifield, J. P. McCreary, and E. Firing. Journal of Geophysical Research : Oceans. *Journal of Geophysical Research: Oceans*, 121(9):6762–6778, 2016. doi: 10.1002/2016JC012132.Received.

N. Trifonova, M. Karnauskas, and C. Kelble. Predicting ecosystem components in the Gulf of Mexico and their responses to climate variability with a dynamic Bayesian network model. *PLOS ONE*, 14(1): 1–23, 2019. ISSN 19326203. doi: 10.1371/journal.pone.0209257.

L. Uusitalo, M. T. Tomczak, B. Müller-Karulis, I. Putnis, N. Trifonova, and A. Tucker. Hidden variables in a Dynamic Bayesian Network identify ecosystem level change. *Ecological Informatics*, 45(March): 9–15, 2018. ISSN 15749541. doi: 10.1016/j.ecoinf.2018.03.003. URL `https://doi.org/10.1016/j.ecoinf.2018.03.003`.

J. W. van der Meer, N. Allsop, T. Bruce, J. De Rouck, A. Kortenhaus, T. Pullen, H. Schüttrumpf, P. Troch, and B. Zanuttigh. Manual on wave overtopping of sea defences and related structures. Technical report, EurOtop, 2018.

B. K. Van Wesenbeeck, J. P. Mulder, M. Marchand, D. J. Reed, M. B. De Vries, H. J. De Vriend, and P. M. Herman. Damming deltas: A practice of the past? Towards nature-based flood defenses. *Estuarine, Coastal and Shelf Science*, 140:1–6, 2014. ISSN 02727714. doi: 10.1016/j.ecss.2013.12.031. URL `http://dx.doi.org/10.1016/j.ecss.2013.12.031`.

V. Van Zelst. *Flood hazard reduction by foreshore vegetation.* PhD thesis, TU Delft, 2018.

V. Vuik, S. N. Jonkman, B. W. Borsje, and T. Suzuki. Nature-based flood protection: The efficiency of vegetated foreshores for reducing wave loads on coastal dikes. *Coastal Engineering*, 116:42–56, 2016. ISSN 03783839. doi: 10.1016/j.coastaleng.2016.06.001. URL http://dx.doi.org/10.1016/j.coastaleng.2016.06.001.

V. Vuik, H. Y. Suh Heo, Z. Zhu, B. W. Borsje, and S. N. Jonkman. Stem breakage of salt marsh vegetation under wave forcing: A field and model study. *Estuarine, Coastal and Shelf Science*, 200:41–58, 2018a. ISSN 02727714. doi: 10.1016/j.ecss.2017.09.028. URL https://doi.org/10.1016/j.ecss.2017.09.028.

V. Vuik, S. van Vuren, B. W. Borsje, B. K. van Wesenbeeck, and S. N. Jonkman. Assessing safety of nature-based flood defenses: Dealing with extremes and uncertainties. *Coastal Engineering*, 139 (December 2017):47–64, 2018b. ISSN 03783839. doi: 10.1016/j.coastaleng.2018.05.002. URL https://doi.org/10.1016/j.coastaleng.2018.05.002.

V. Vuik, B. W. Borsje, P. W. Willemsen, and S. N. Jonkman. Salt marshes for flood risk reduction: Quantifying long-term effectiveness and life-cycle costs. *Ocean and Coastal Management*, 171(January): 96–110, 2019. ISSN 09645691. doi: 10.1016/j.ocecoaman.2019.01.010. URL https://doi.org/10.1016/j.ocecoaman.2019.01.010.

P. W. Willemsen, B. W. Borsje, V. Vuik, T. J. Bouma, and S. J. Hulscher. Field-based decadal wave attenuating capacity of combined tidal flats and salt marshes. *Coastal Engineering*, 156(January): 103628, 2020. ISSN 03783839. doi: 10.1016/j.coastaleng.2019.103628. URL https://doi.org/10.1016/j.coastaleng.2019.103628.

X. Wu, H. Liu, L. Zhang, M. J. Skibniewski, Q. Deng, and J. Teng. A dynamic Bayesian network based approach to safety decision support in tunnel construction. *Reliability Engineering and System Safety*, 134:157–168, 2015. ISSN 09518320. doi: 10.1016/j.ress.2014.10.021. URL http://dx.doi.org/10.1016/j.ress.2014.10.021.

A

Vegetation Drag Coefficient

Various studies define the bulk drag coefficient to relate wave attenuation and vegetation parameters with one another. Defining energy dissipation as the product of the drag force and the horizontal wave motion velocity. By subsequently integrating over the vegetation height and multiplying with the total number of plants per unit area was derived. As can be seen in Equation A.1, the drag coefficient is included in this equation.

$$\epsilon_D = \overline{\int_{-h}^{s-h} \frac{1}{2} \cdot \rho \cdot C_D \cdot A \cdot u|u| \cdot u \, dz} \cdot N_v \tag{A.1}$$

Where:

h	=	Water depth
s	=	Elevation of the top of the plant
ρ	=	Fluid density
C_D	=	Drag coefficient
A	=	Drag area
u	=	Horizontal velocity
N_v	=	Plants per unit area

Various empirical studies defined the drag in terms of the Reynolds number (Méndez et al., 1999; Möller et al., 2014). Möller et al. (2014) defined the drag coefficient as shown in Equation A.2.

$$\widetilde{C_D} = (227/Re)^{1.62} + 0.16 \tag{A.2}$$

In turn, the Reynolds number is related to both vegetation and hydraulic parameters. Möller et al. (2014) performed large scale wave attenuation analysis and defined the Reynolds number for marshes as formulated in Equation A.3.

$$Re_v = U_{max} \frac{b_v}{v_k} \tag{A.3}$$

Where:

Re_v	=	Reynolds number for a single vegetation stem
b_v	=	Stem diameter
U_{max}	=	Orbital velocity in front of the vegetation at the bottom $f(H_s, T_p)$
v_k	=	Kinematic viscosity ($1 \cdot 10^{-6}$ m^2 s^{-1})

The orbital velocity in front of the vegetation is determined using Equation A.4 from linear wave theory.

$$u(z) = \omega\alpha\frac{cosh(k(h+z))}{sinh(kh)} \tag{A.4}$$

Where:

$u(z)$	=	Amplitude of orbital velocity at depth z
ω	=	Angular velocity $\frac{2\pi}{T_p}$
α	=	Wave amplitude
k	=	Wave number
h	=	Water depth

B

XBeach Processes Theory

The main XBeach processes used in are discussed below and based on the Deltares user manual (Roelvink et al., 2015).

B.1. Non-linear Shallow Water Equations

Combining the momentum balance equation with the continuity equation, results in the non-linear shallow water equations. When accounting for the wave induced mass-flux and return flows by transforming them to Lagrangian velocity, the Generalized Lagrangian Mean (GLM) formulation is defined. Lagrangian L velocities are the instantaneous velocities of a particle. They can be related to Eulerian E velocities by including stoke S drift:

$$u^L = u^E + u^S \tag{B.1}$$

In which stokes drift u^S can be represented as:

$$u^S = \frac{E_w}{\rho h c} \tag{B.2}$$

Using the Lagrangian velocity, the continuity equation is given by:

$$\frac{\delta \eta}{\delta t} + \frac{\delta h u^L}{\delta x} = 0 \tag{B.3}$$

The simplified momentum balance can be defined as:

$$\frac{\delta u^L}{\delta t} + u^L \frac{\delta u^L}{\delta x} - v_h \frac{\delta^2 u^L}{\delta x^2} = \frac{\tau_{bx}^E}{\rho h} - g \frac{\delta \eta}{\delta x} + \frac{F_x}{\rho h} + \frac{F_{v,x}}{\rho h} \tag{B.4}$$

Where:

u	=	Velocity
E_w	=	Wave energy
ρ	=	Water density
h	=	Water depth
c	=	Velocity
η	=	Water level
v_h	=	Horizontal viscosity
τ_{bx}^E	=	Bed shear
F	=	External forces

Combined Equations B.3 and B.4 form the GLM equations.

B.2. Wave Action Balance

The simplified wave action balance that is applied within the XBeach model is given by:

$$\frac{\delta A}{\delta t} + \frac{\delta c_g A}{\delta x} = -\frac{D_w + D_f + Dv}{\sigma} \tag{B.5}$$

In which the wave action A is equated as:

$$A = \frac{S_w}{\sigma} \tag{B.6}$$

Where:

A	=	Wave action
S_w	=	Wave energy density
σ	=	Wave frequency
c_g	=	Wave group velocity
D	=	Dissipation term

B.3. Dissipation

The three dissipation terms included in the short wave action balance include dissipation due to bottom friction, wave breaking and vegetation.

Bottom friction

Dissipation due to bottom friction is based on bottom dissipation which is represented using the Johnson friction factor f_w:

$$D_f = \frac{1}{2}\rho f_w |\widetilde{u}|^3 \tag{B.7}$$

In which the third even velocity moment $\widetilde{u}|^3$ can be defined as:

$$|\widetilde{u}|^3 = 0.42 u_{orb}^3 \tag{B.8}$$

Wave breaking

Wave dissipation is defined using:

$$D_w = \frac{S_w}{E_w}\overline{D}_w \tag{B.9}$$

In which the wave dissipation factor D_w is formulated as:

$$\overline{D}_w = 2\frac{\alpha}{T_{rep}} Q_b E_w \tag{B.10}$$

While Q_b is subsequently defined as:

$$Q_b = 1 - exp\left(-\left(\frac{H_{rms}}{H_{max}}\right)^2\right) \tag{B.11}$$

Where:

α = Wave dissipation coefficient
T_{rep} = Representative wave period
H_{rms} = Root mean square wave height
H_{max} = Maximum wave height

Vegetation
Dissipation due to vegetation is included through dissipation of short waves that interact with vertical elements that dampen the wave. Dissipation is then defined as:

$$D_v = A_v \frac{\rho \widetilde{C}_D b_v N_v}{2\sqrt{\pi}} \left(\frac{kg}{2\sigma}\right)^3 H_{rms}^3 \tag{B.12}$$

With:

$$A_v = \frac{(sinh^3 k\alpha h - sinh^3 k\alpha h) + 3(sinhk\alpha h - sinhk\alpha h)}{3kcosh^3 kh} \tag{B.13}$$

Where:

k = Wave number
α = Relative vegetation height (h_v/h)
$\widetilde{C}_D$ = Drag coefficient
b_v = Vegetation width
N_v = Vegetation density

B.4. Sediment Transportation

Sediment transport is modeled using an advection-diffusion equation that uses the depth averaged sediment concentration and the equilibrium sediment concentration:

$$\frac{\delta hC}{\delta t} + \frac{\delta hCu^E}{\delta x} + \frac{\delta}{\delta x}\left[D_h h \frac{\delta C}{\delta x}\right] = \frac{hC_{eq} - hC}{T_s} \tag{B.14}$$

Where:

C = Depth averaged sediment concentration
C_{eq} = Equilibrium sediment concentration
D_h = Sediment diffusion coefficient
T_s = Entrainment adaptation time

B.5. Bottom Updating

Bottom updating occurs when morphological effects are taken into account in the model. If so the updating is completed using sediment fluxes. These are in turn related to the sediment transport, and so the bed level changes according to:

$$\frac{\delta z_b}{\delta t} + \frac{f_{mor}}{(1-p)} \frac{\delta q_x}{\delta x} = 0 \tag{B.15}$$

Where:

z_b = Bed level
f_{mor} = Morphological acceleration factor (0-10)
p = Porosity
q_x = Sediment transport rates

C

Goodness of Fit Tests

The goodness of fit tests used throughout this thesis are presented below:

- Sum of squared differences (SSD);
- Akaike information criterion (AIC);
- Semi correlations;
- Cramér von Mises (CVM);
- d-calibration statistic.

Sum of Squared Differences
Comparing the cdf of the empirical data $F_e(X)$ to that of the theoretical distributions $F(X)$, enables the determination of the best 'fit'. The sum of squared differences (SSD) method defines the deviation between the value of the empirical distribution and the theoretical distribution as

$$SSD = \sum_{n=1}^{N} (F_e(n)\text{-}F(n))^2 \tag{C.1}$$

where $F_e(n)$ represents the empirical distribution and $F(n)$ corresponds with the theoretical distribution for $n \in N$. Small SSD values correspond with theoretical distributions that well represent the empirical data. Thus, enabling the derivation of the best fit by determining the smallest SSD value.

Akaike Information Criterion
Another comparative method used to assess statistical fits is the Akaike information criterion (AIC). A low AIC value implies a better fit to the data and so goodness of fit values can be compared to determine the best fit. In the formulation of the AIC, the goodness of fit and model simplicity are examined. This is achieved by including the number of parameters ($length(\theta)$) and the likelihood of the distribution fit (L), as shown in Equation C.2.

$$AIC = 2length(\theta) - 2log(L(\theta, X)) \tag{C.2}$$

Semi Correlations
This analysis is used to assess data obtained from the copulas by first creating an empirical normalized scatter-plot of R_i and S_i and calculating the correlation of each of the four quadrants. The four quadrants are defined by the four possible combinations of a positive value in either x or y direction. With the four empirical quadrant correlations Q_e, the theoretical copula can be sampled to obtain N correlated random samples. Subsequently, the theoretical sample can be normalized in a scatter plot and analysed in terms of theoretical quadrant correlations Q_t. Finally, the empirical Q_e and theoretical Q_e quadrants can be compared using a sum of square differences method. Again, a low SSD value corresponds to a 'good fit'.

Cramér von Mises
The Cramér von Mises (CVM) statistic provides both a statistic for the goodness of fit as a graphical interpretation of the difference between the empirical copula and the theoretical copula. Numerically, the CVM statistic compares the absolute difference between the empirical- and theoretical-copula for every pair $u, v \in [0, 1]$. Thus, the CVM statistic depends on the step size of u, v, the step size has been taken as 60 in this thesis. Moreover, the CVM statistic is comparable to a SSD method as can be seen in CVM Equation C.3.

$$CM_n = \sum_{i=1}^{N} \left(C_n\left(R_i, S_i\right) \text{-} C_{\theta n}\left(R_i, S_i\right)\right)^2 \tag{C.3}$$

d-calibration statistic
The determinant of the correlation matrix is introduced to present such a measure of dependence (Hanea et al., 2010). In a correlation matrix that is completely independent, only the diagonals will be equal to one, as the diagonal represents the correlation of a variable with itself. Therefore, the determinant of an independent correlation matrix is equal to 1. In case of complete dependence, the determinant equals 0. This property can be applied in the validation of the normal copula as the determinant of the empirical rank is compared with N samples of the determinant of the normal rank. The hypothesis that the empirical copula can be represented by the normal copula is accepted if it lies within the 90% central confidence interval (Hanea et al., 2010).

D

Synthetic Vegetation Data

Table D.1, presents the data obtained from literature to statistically create synthetic monthly vegetation. A number of statistical techniques were applied to develop a dataset for each vegetation parameter that well resembles physical evolution of the parameters. The objective in this section was to develop a monthly dataset containing vegetation height, diameter and density for multiple years of data that respects the inherent temporal dependence of the variable.

Table D.1: Vegetation parameters retrieved from field measurement studies for *Spartina angelica* marshes.

Study	**Month**	**Height [m]**	**Width [m]**	**Density [n/m^2]**
Vuik et al. (2016)	November	0.61	0.003	944
Vuik et al. (2016)	November	0.78	0.0034	1136
Vuik et al. (2016)	November	0.84	0.0027	1520
Rupprecht et al. (2015)	July	0.2787	0.003867	-
Vuik et al. (2018a)	December	0.327	0.0031	-
Vuik et al. (2018a)	April	0.285	0.0033	-
Vuik et al. (2018a)	September	0.544	0.0041	930
Vuik et al. (2018a)	November	0.608	0.0037	-
Neumeier (2005)	March	0.417	-	-
Neumeier (2005)	May	0.359	-	-
Neumeier (2005)	June	0.317	-	-
Neumeier (2005)	October	0.462	-	-
Neumeier (2005)	January	0.4	-	-

D.1. Vegetation Height

The vegetation height varies over time as expected due to seasonality (Neumeier, 2005) and the corresponding metocean conditions. Using the field data for vegetation height in Table D.1, the objective was to develop a yearly time series that well represents the variability in vegetation height. To do so an autocorrelation copula function was developed to ensure time dependence was present in the synthetic time series. Three approaches were executed and subsequently compared. The first utilized all data to develop a single marginal distribution used for inverse sampling in the autocorrelation copula. The second divides the variables into the four marginal distributions (i.e. clustered per quarters of the year). The third allocates marginal distributions to every month in the year.

In all approaches, the autocorrelation was determined for a monthly shift in the monthly averages for vegetation height. In doing so the data that was included in the determination of monthly averages consists of both the data belonging to the month being analysed as the data for the surrounding months (i.e. in the month of January, the data for December, January and February are included in the analysis). The expanded monthly data set is depicted in Figure D.1.

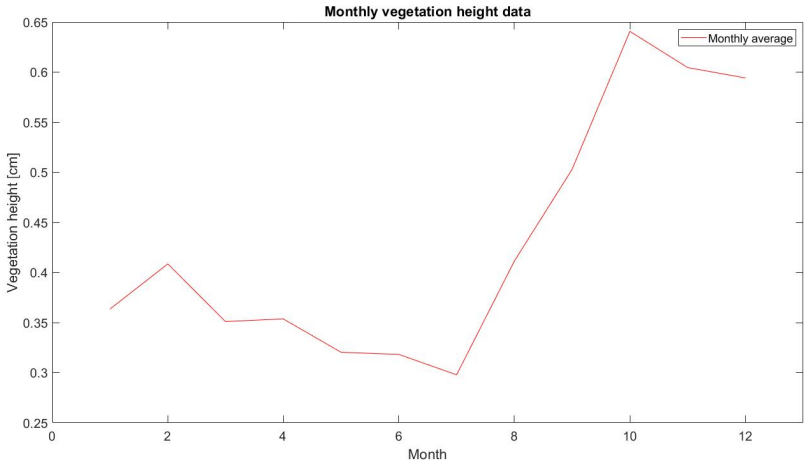

Figure D.1: Monthly average of the combined monthly vegetation data

The autocorrelation ρ_s for a monthly shift was found to be equal to 0.736 and declines rapidly per time step, which was expected as the monthly dependence bound to decrease with an increasing shift in months (i.e. comparing winter with summer). The autocorrelation array is shown in Figure D.2.

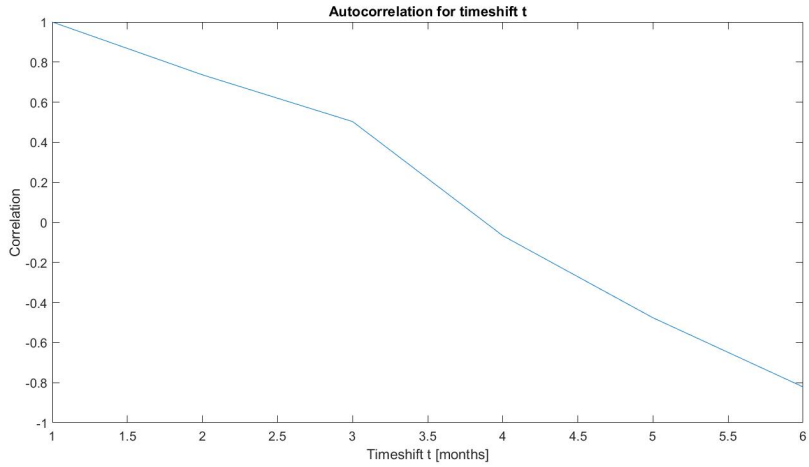

Figure D.2: Autocorrelation per monthly time shift for vegetation data

An autocorrelation script was defined in MATLAB to consecutively execute the following steps to obtain synthetic, temporally correlated (i.e. each sample is related to the previous sample) time series:

1. Create an array of 10 random uniform samples X_t;
2. Use X_t and ρ_s to create an array X_{t+1} containing 10 samples $\in$ [0 1] that are correlated to X_t;
3. Continue 2^{nd} step for all time steps N;
4. Average every array containing 10 values to obtain a single value $u_t \in$ [0 1] per time step t;
5. Use specified marginal distribution to convert u_n to corresponding variable values.

D.1.1. Single marginal distribution

In the single data set approach, all the vegetation height data was used to fit a marginal distribution. The reason for doing so was the fact that more data would be included in the marginal distribution fit. Multiple distributions were analysed and the best fit was determined to be a Log normal distribution, shown in Figure D.3 below.

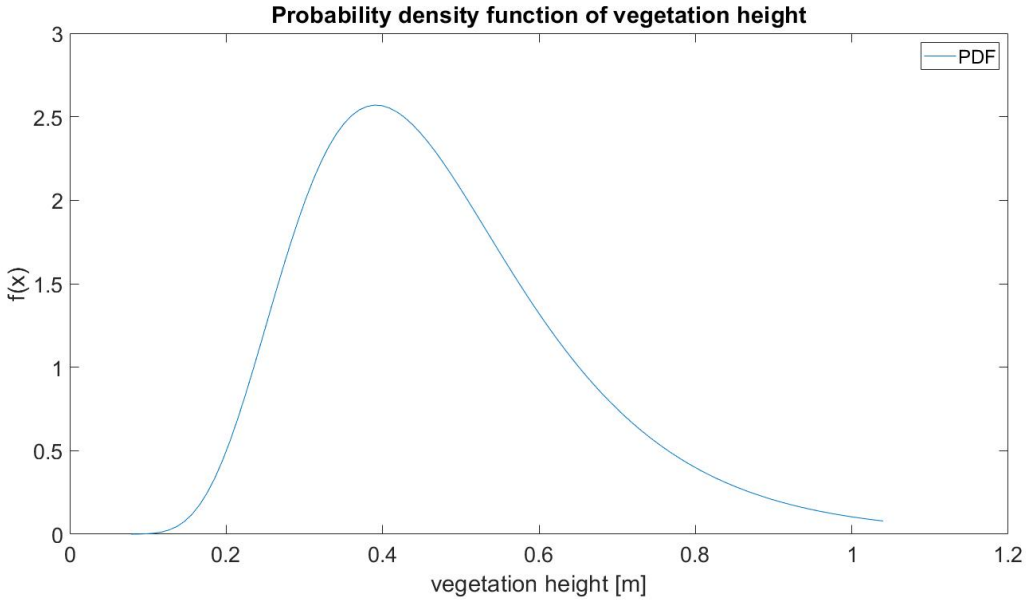

Figure D.3: Probability density functions of vegetation height

Using the autocorrelation script defined above, an array of uniform correlated samples was obtained. Using the marginal distribution Fig. D.3) to convert all uniform samples to vegetation heights, a synthetic dataset for monthly vegetation heights was obtained. These values are shown as blue markers in Figure D.4 for a total of 10 years. The red line defines the monthly average as shown in Figure D.1.

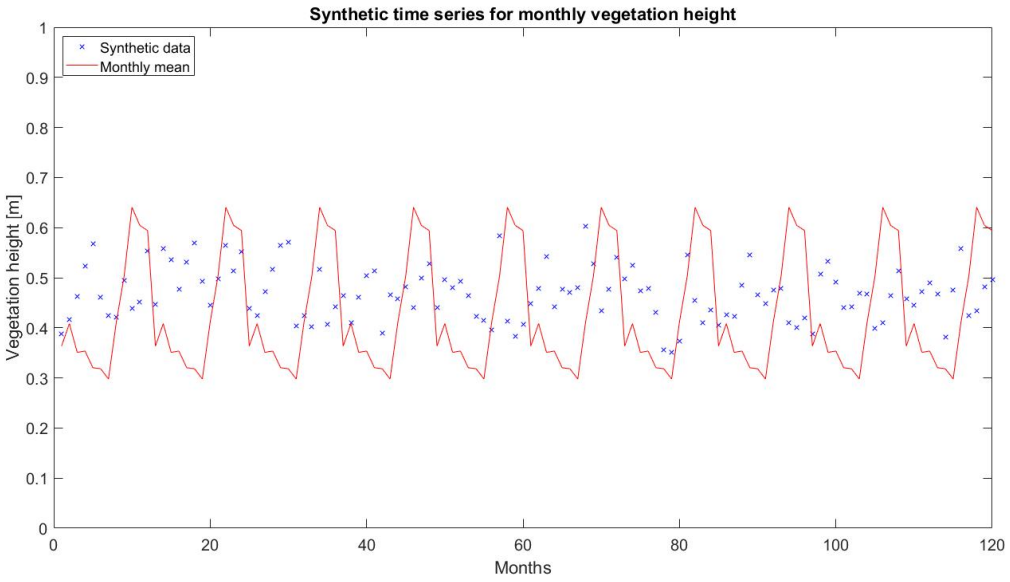

Figure D.4: Synthetic data for monthly vegetation height for a single pdf

To be able to determine the best approach, a sum of squared differences calculation was applied to assess the difference between the average discrepancy between the synthetic and average data. For a total of 1000 samples the average SSD value is determined to be 2.203. This value seems representative as the synthetic values do not seem to accurately follow the monthly average.

D.1.2. Quarterly marginal distribution

In the quarterly datasets approach four marginal distributions were obtained, one for each quarter. Subsequently, the most frequently occurring distribution type was chosen to represent each quarter individually. From the initial analysis the distribution that best represented vegetation height was found to be a Gamma distribution. Using the quarterly determined Gamma distribution parameters, the pdf's for each quarter were determined Fig. D.5).

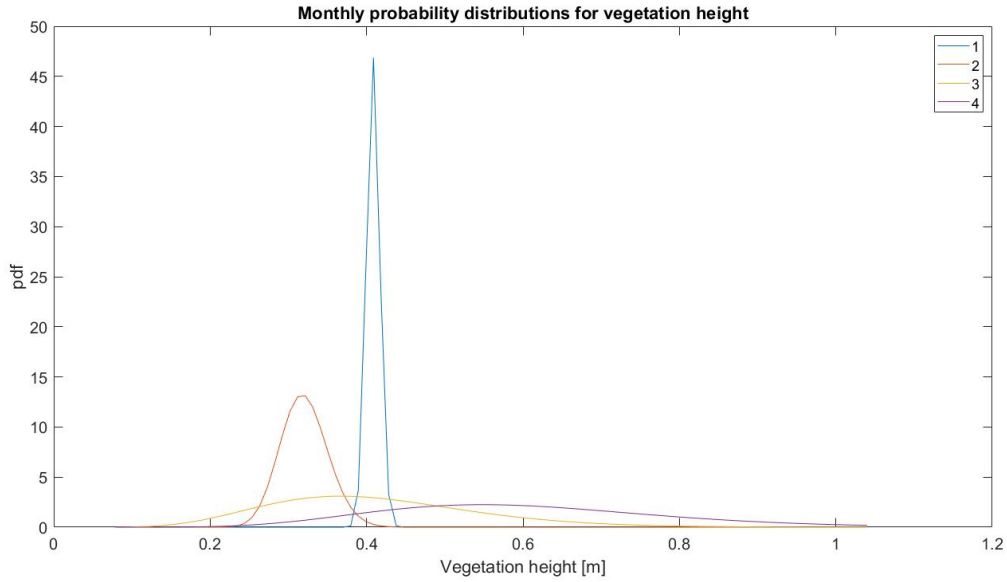

Figure D.5: Probability density functions of quarterly vegetation height

Using the autocorrelation script defined above, an array of uniform correlated samples was obtained. Combining the marginal distribution for each quarter to the corresponding uniform value, the monthly vegetation heights were obtained. In Figure D.6 the synthetic values for vegetation height are depicted as blue markers. Moreover, the red line represents the monthly average for each month as defined in Figure D.1. The figure represents a total of 10 years. Using the sum of squared differences test, an average SSD value of 0.675 has been determined for 1000 samples.

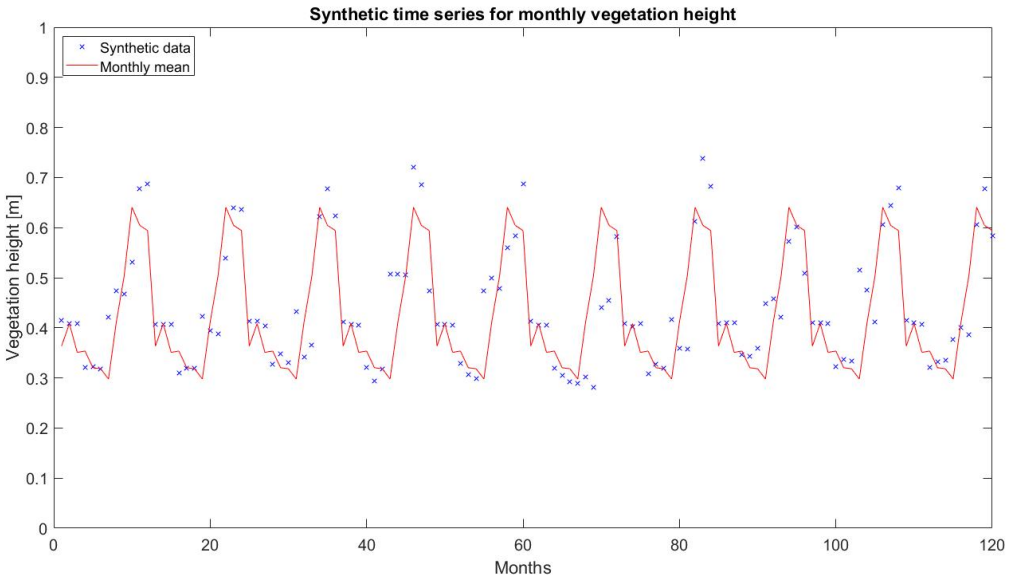

Figure D.6: Synthetic data for quarterly vegetation height

D.1.3. Monthly marginal distributions

In the multiple marginal distribution approach 12 theoretical distributions are determined, one for each month. Subsequently, the most frequently occurring distribution type was chosen to represent each month individually. From the initial analysis the distribution that best represents vegetation height was found to be a Gamma distribution. Using the monthly determined Gamma distribution parameters, the pdf's for each month were determined Fig. D.7).

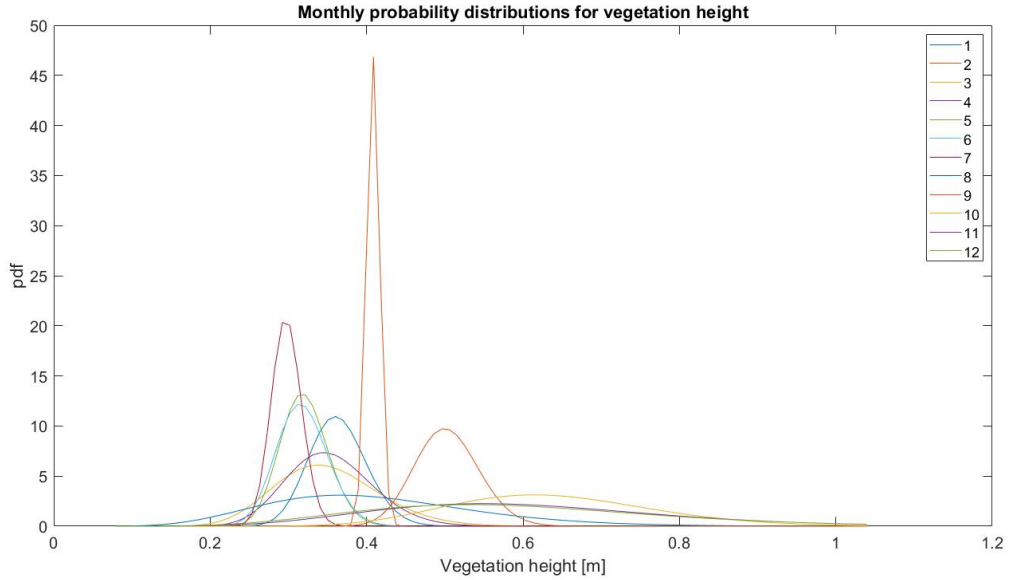

Figure D.7: Probability density functions of monthly vegetation height.

Using the autocorrelation script defined above, an array of uniform correlated samples was obtained. Combining the marginal distribution for each month to the corresponding uniform value, the monthly vegetation heights were obtained. In Figure D.8 the synthetic values for vegetation height are depicted as

blue markers. Moreover, the red line represents the monthly average for each month as defined in Figure D.1. The figure represents a total of 10 years.

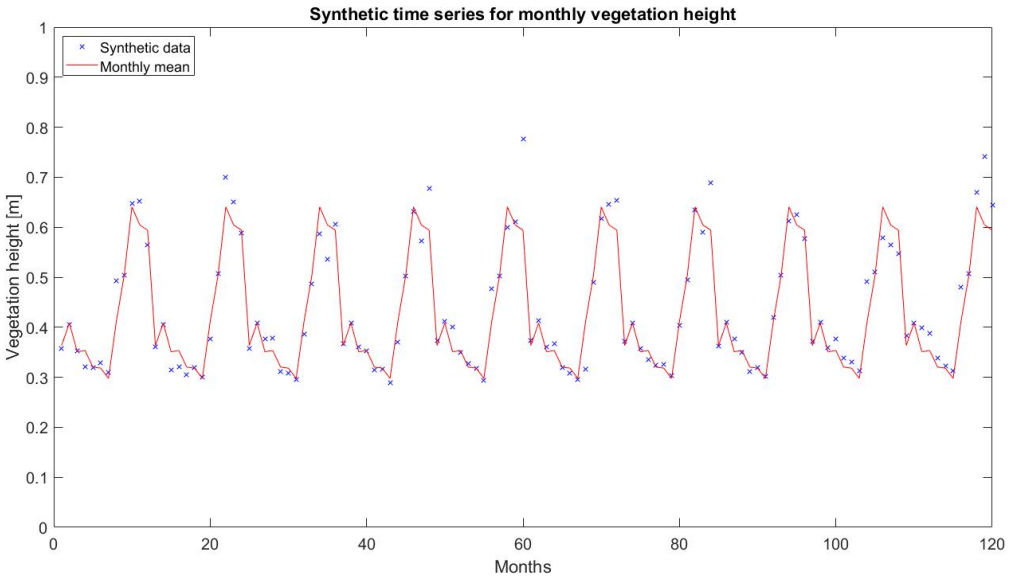

Figure D.8: Synthetic data for monthly vegetation height

Using the sum of squared differences test, an average SSD value of 0.157 has been determined for 1000 samples.

D.1.4. Discussion

The resulting sum of squared differences (SSD) values are presented in Table D.2. Based on visual analysis of the synthetic time series in the figures, combined with the SSD values, the quarterly probability distribution variant was deemed the best fit. Accuracy was not the only factor to keep in mind when developing a synthetic dataset. A dataset which is too accurate, will leave out room for randomness. Therefore, the option for quarterly data was chosen as it well follows the trend line of the seasons, yet also leaves room for random variations. The final result is shown in Figure D.9.

Table D.2: Resulting SSD values per synthetic vegetation sampling variant.

Index	Variant	SSD
i	Yearly Probability Distribution	2.203
ii	Quarterly Probability Distribution	0.675
iii	Monthly Probability Distribution	0.157

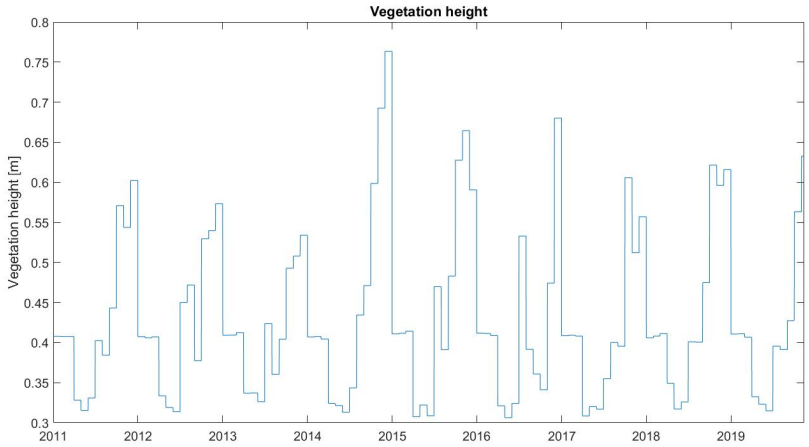

Figure D.9: Monthly vegetation height for the complete dataset at Hellegat between 2011 and 2020.

D.2. Vegetation Width & Density

For both the vegetation width and density the collected dataset in Table D.1 was used to obtain a minimum and maximum value. Subsequently, a MATLAB script was applied to create a synthetic time series for the data using a sine function and a coefficient of variation, Table D.3. The vegetation width used in the dataset for Hellegatpolder was provided in Figure D.10. Similarly, the vegetation density can be found in Figure D.11.

Table D.3: The mean and coefficient of variation for the vegetation width and density.

Variable	Mean	Coefficient of Variation
Width	3 mm	0.285 mm
Density	1200 n/m^2	433.33 n/m^2

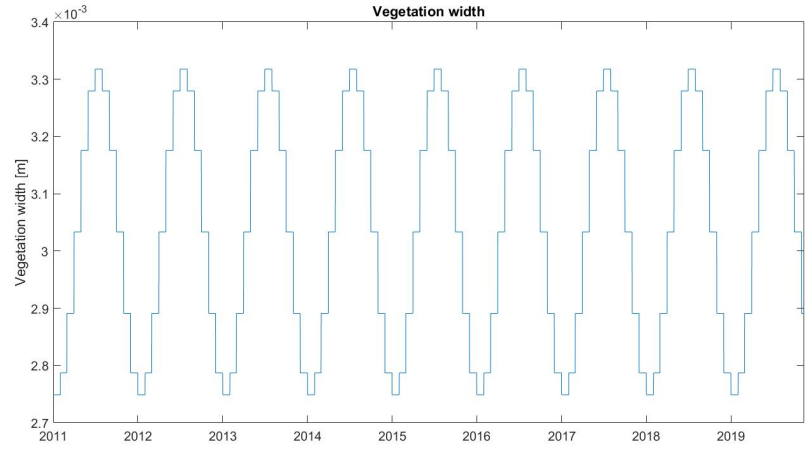

Figure D.10: Vegetation Width for the complete dataset at Hellegat

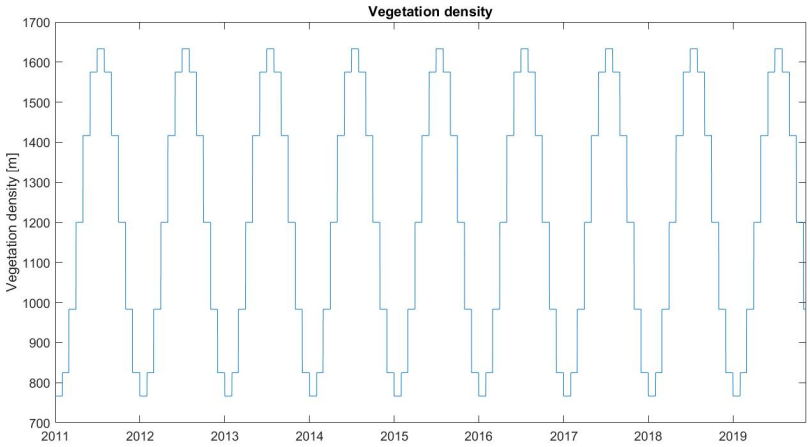

Figure D.11: Vegetation Density for the complete dataset at Hellegat

E

Numerical Model Outline

A numerical model is used to enrich the input dataset, based entirely on field data, with wave data on the nearshore side of the foreshore. To do so XBeach is chosen as the numerical model. Moreover, the XBeach toolbox in MATLAB is applied to exploit the freedom of coding with XBeach and the input dataset in MATLAB. The main outline of the MATLAB scripts is provided in Figure 4.7. In which the following steps are iterative while the run n is smaller than the total amount of runs N:

1. Preparing data;
2. Set-up of XBeach models;
3. Running of the XBeach model;
4. Processing of XBeach output for subsequent run.

Once the above steps have been completed, the total output is compressed and ready for analysis. Each of these steps reference a unique MATLAB script that ensures are discussed in more detail in the sections below.

E.1. Prepare Data

The first subscript ensures that a segment of input data is transformed into a MATLAB structure that contains information on hydraulic, vegetation and bathymetry parameters. Figure E.1 depicts this flow of data.

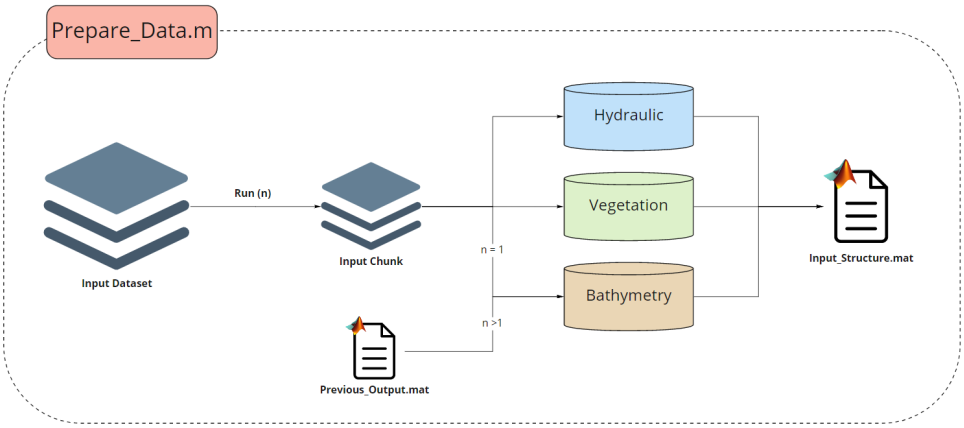

Figure E.1: Outline of MATLAB script 'prepare_data.m'

Important to note is the additional bathymetry input. After the first model run, the second model run is dependent on the previous output when morphology is included in the model settings.

E.2. Setup & Run Model

With the MATLAB structure containing a chunk of input data, the XBeach structures required to run the numerical model are set up as shown in Figure E.2. The various hydraulic settings, bathymetry settings, vegetation setting and general settings are included in this script. Ultimately the separate XBeach structures are combined into a single run folder where all files can be read by the executable.

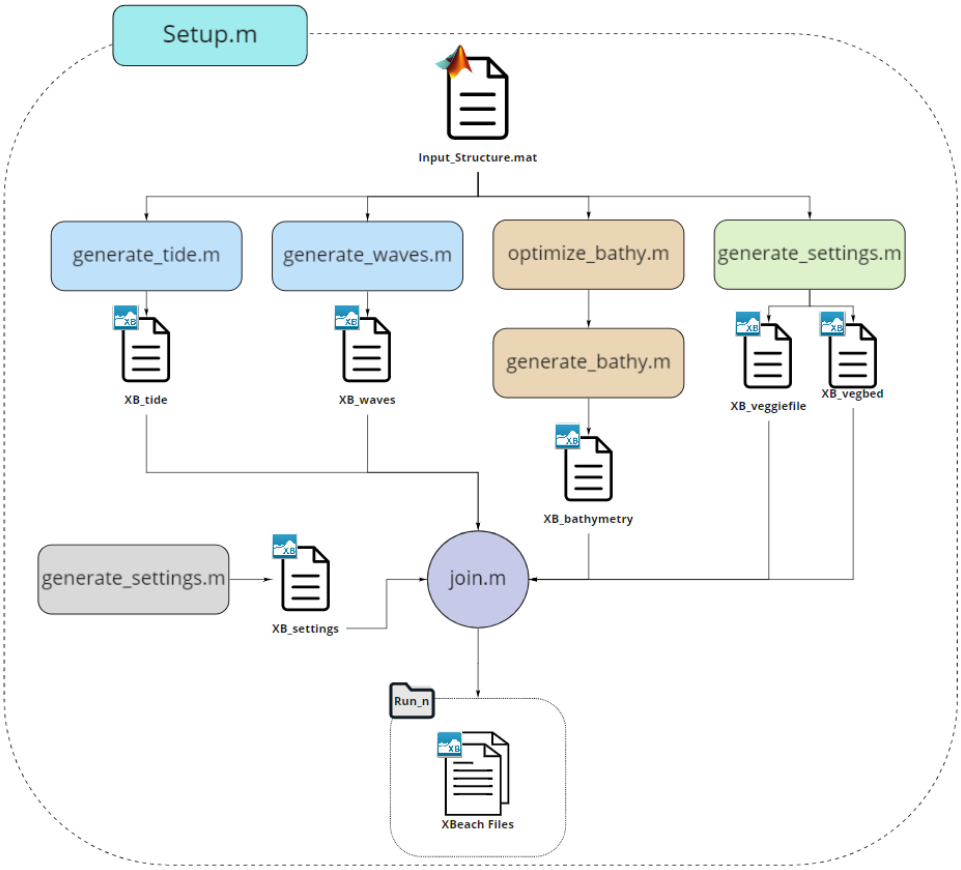

Figure E.2: Outline of MATLAB script 'setup.m'

The executable itself is run from the script shown in Figure E.3. This script subsequently waits for the numerical model to finish running before continuing. The output dataset is stored in the form of a .nc file which is saved in the run folder.

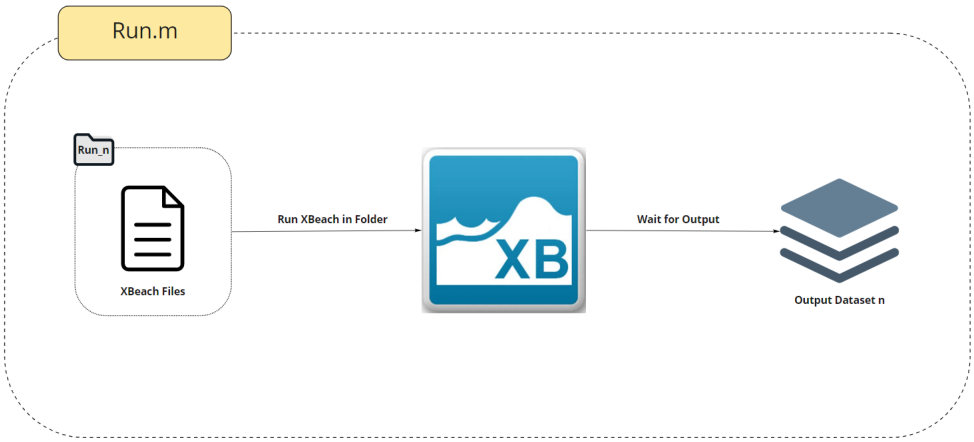

Figure E.3: Outline of MATLAB script 'run.m'

E.3. Process Output

Once the executable is finished running, the nc output file is read and segmented into multiple output parameters. The bathymetry output parameters are stored in a separate output structure as can be seen in Figure E.4. This structure is used in the following run as bathymetry input as defined in section E.1. All output parameters are simultaneously stored in a output dataset for later compression.

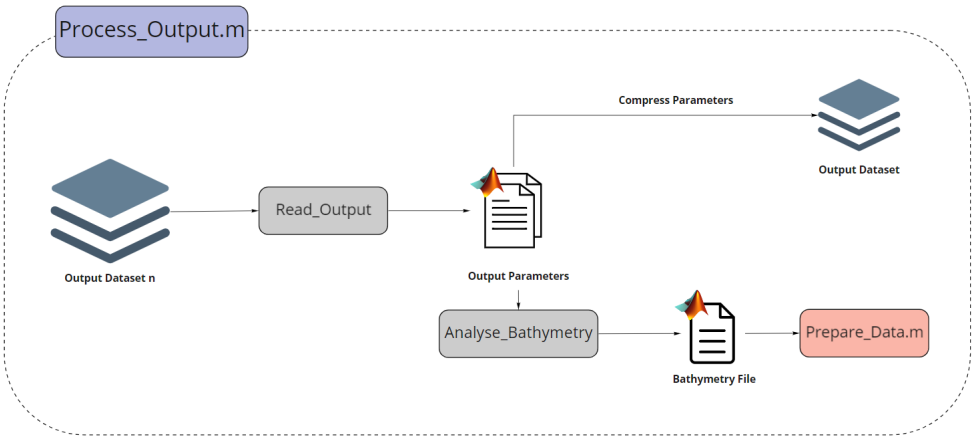

Figure E.4: Outline of MATLAB script 'process_output.m'

E.4. Compress Output

Once the model has finished running, all output datasets are compressed into a single dataset which analyses the input and output parameters, matches them on input date. There after the most important parameters are retrieved from the output datasets and inserted into the input table. Thereby creating the final synthetic dataset that included wave heights at the nearshore side of the foreshore.

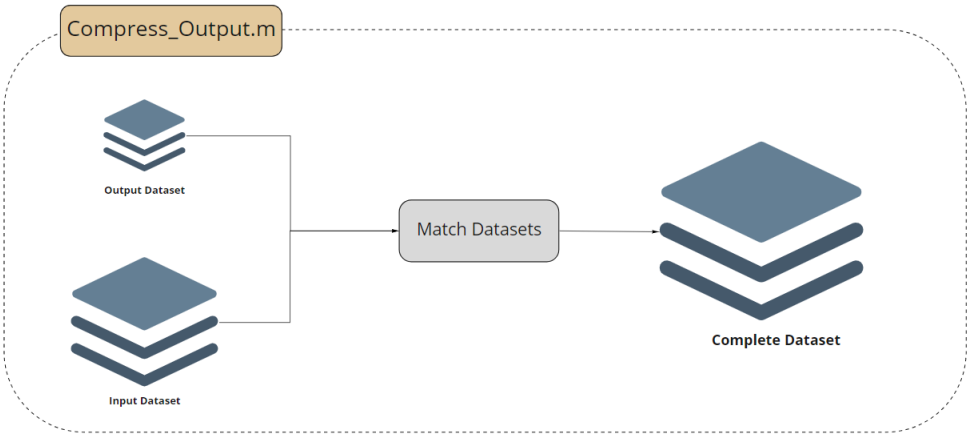

Figure E.5: Outline of MATLAB script 'compress_output.m'

F

XBeach Settings

The XBeach numerical model has an extensive library of model settings that can be applied to adjust the model to fit various hydraulic or morphodynamic scenarios defined by the user. In this thesis model settings are used to obtain accurate wave transformation over a vegetated foreshore. As this is done for a high temporal resolution combined with an extensive dataset, the model settings focus on including vegetation and optimizing computational time. The settings discussed include:

- XBeach grid size optimization;
- Morphology settings including the morphological acceleration factor;
- Wave settings that neglect currents, wind and incidence angle;
- Model run time that includes spin-up time;
- An output write interval of 30 seconds for all output types;
- Vegetation grid that defines the location of vegetation in the model; and
- Generation of a time-varying tide throughout the run.

F.1. Morphology

Morphology and sediment transportation was applied in a subset of model runs to analyse their effects on wave attenuation. In the model runs where morphology was included, a morphological acceleration factor was included. The morphological acceleration factor improves model run time by multiplying morphological processes by a factor α. A related setting, the morphological adaptation factor (morfacopt), was applied to maintain model output times when using the morphological acceleration factor. The combination of the two ensures increased model run time while maintaining a constant model output.

Sedimentation and erosion processes were included in the numerical model settings. To define the locations where these processes could occur a non-erodible file is defined in the bathymetry settings that defines the location of erodible sections. The dike was constantly specified as a non-erodible layer, while the rest of the profile was specified as non-erodible in runs where morphology was not to be included. Runs including morphology contained a non-erodible file where only the dike was specified. In doing so the benefits of morphological acceleration in the file were maintained while erosion was included and excluded using non-erodible layers.

F.2. Hydraulic

The hydraulic model settings include both waves and tides. In defining wave settings, a series of jonswap spectra files were created using the XBeach MATLAB toolbox. All spectra included the wave height and wave period defined in the input dataset. Moreover, their shore incidence was always assumed shore-normal. Additionally, hydraulic influence due to currents and wind were removed from the equations. This ultimately created a time-varying offshore boundary condition in which the waves were specified.

Similar to wave settings, tide settings were specified at the offshore boundary. The tide was included as a time varying boundary, with tidal levels specified every half hour. The tides reduce gradually between the specified time segments. These settings are believed to reproduce natural processes sufficiently.

F.3. Grid- & Output-Resolution

The numerical grid and output interval were adjusted in the model settings with the primary reason of improving computational time. The numerical grid is optimized in XBeach to ensure sufficient grid resolution at nearshore boundaries where complex hydraulic interactions are found and thus require an optimized grid resolution. The settings controlling the optimization are most greatly affected by the minimum nearshore grid size and the point per wave length. These settings are adjusted to ensure that the number of grid points does not exceed 500 in horizontal direction, for this is found to lead to an acceptable balance between computational time and model accuracy.

Model output resolution can be specified for a number of variables. As each variable is written to an output file during numerical execution. The output write interval greatly effects computation time. Again the optimal balance between time and accuracy was determined at 30 seconds and applied throughout all model runs.

G

XBeach Calibration

The XBeach numerical model is calibrated to ensure that model accuracy is maintained while optimizing computational time. Multiple calibration scenarios are assessed to experiment with a set of XBeach functions. The model functions calibrated are: the model grid resolution, morphology, run time and output interval.

All calibration scenarios are assessed using the same transect, shown in Figure G.1, to reduce external influence. Moreover, a subset of 33 records from the input dataset with wave heights larger than 110 cm were applied to obtain numerical results as these were expected to induce the most visible response in the model. Each scenario is judged on wave height accuracy compared to the reference scenario as well as computational time.

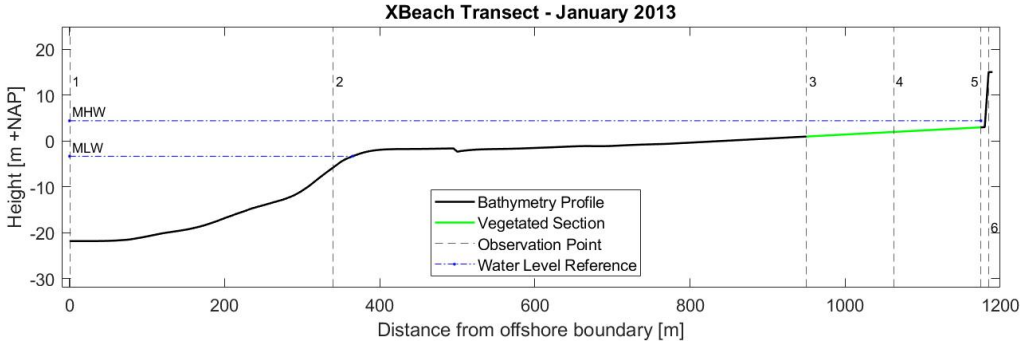

Figure G.1: XBeach bathymetry transect used as the initial bathymetry in the calibration models. The dashed lines represent observation points while the green line defines the vegetated section in the transect.

Table G.1: Calibration scenario results for computational time, relative temporal improvement (RTI) in comparison to the reference scenario and the accuracy of each scenario compared to the reference scenario through relative correlation (RC) and wave height comparison.

Scenario	**Time [min]**	**RTI [X]**	**RC**	**Accuracy [%]**
Reference	20	-	1	100
Optimized grid resolution	3	6.7	0.99	98
Previous + Decreased run time	0.68	29.4	0.98	95
Previous + Excluding morphology	0.63	31.7	0.98	95
Previous + Reduced output interval	0.57	35	0.98	95

G.1. Reference

As to compare the subsequent model runs, a reference scenario was created using 'optimal' model settings. With optimal being a numerical model setup that is expected to generate the most accurate results; an

extensive grid with morphology settings switched on and a complete run time of 1800 seconds (i.e. the hydraulic temporal resolution) per input segment.

In this scenario the variables worth mentioning regarding grid optimization, morphology and output interval are provided in Table G.2.

Table G.2: Numerical model settings for the reference scenario

Setting Definition	Value
Number of grid points	2290
Model run time percentage	100 %
Morphology settings	On
Output interval	1 s^{-1}

With the settings defined above, the computational time required to simulate a single record of data was clocked at 19 minutes. The wave height transformation over the foreshore is shown for one of the 30 minute model runs in Figure G.2. As one would expect, the wave height initially decreases due to bottom friction, increases at the height of the foreshore due to a decrease in wave celerity and subsequently decreases due to both bottom friction and wave dissipation due to vegetation.

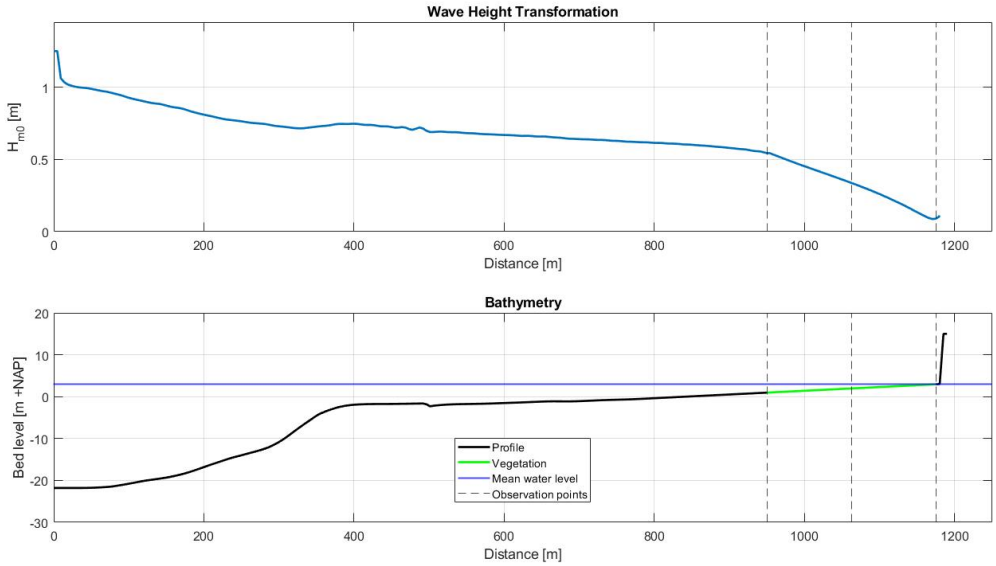

Figure G.2: Wave transformation over the foreshore during storm conditions

The observed wave heights at observation points 3 and 5 are depicted in Figure G.3 where the wave height was plotted for each water level. This forms the foundation of the calibration method as the water levels remained constant for each run, as this variables was forced, while wave heights varied per calibration scenario. Figure G.4 shows the reduction in relation to the offshore wave height at observation points 3 located before the marsh edge and observation point 5 at the toe of the dike.

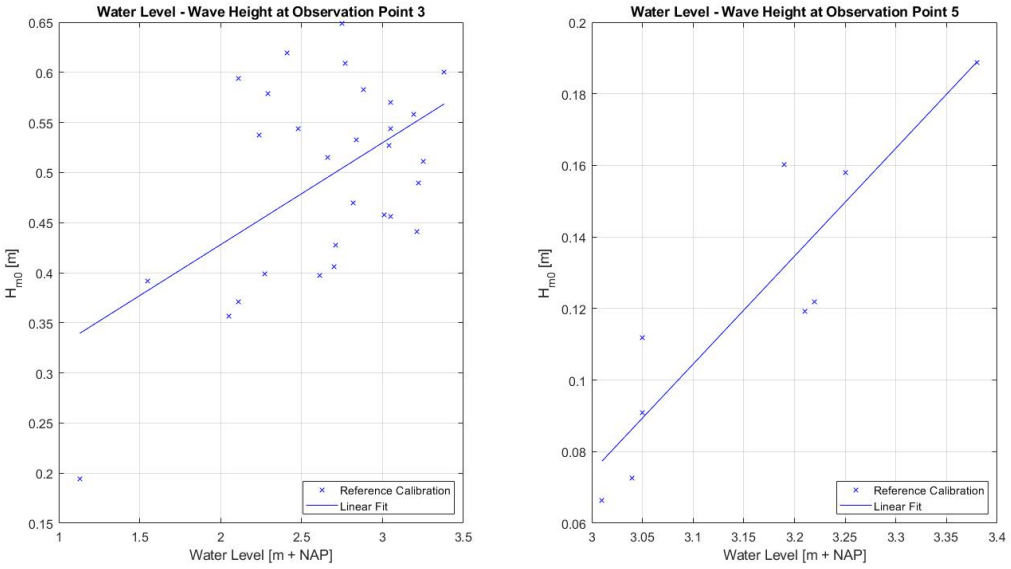

Figure G.3: Wave heights at observation points 3 and 5 plotted against the water level in the model run.

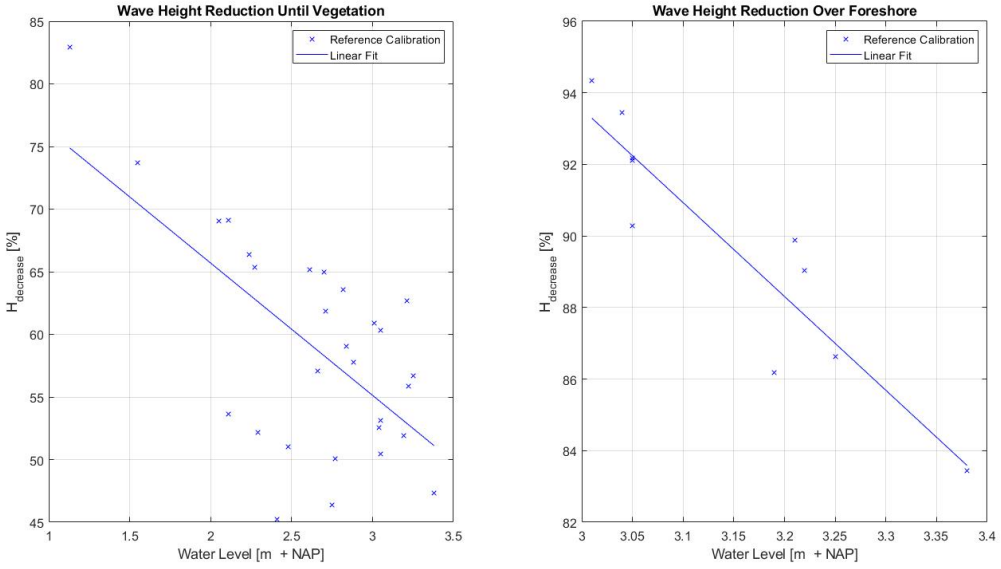

Figure G.4: Wave height reduction in relation to the offshore wave height at observation points 3 and 5 plotted against the water level in the model run.

G.2. Grid Size Optimization

One of the XBeach Toolbox functionalities optimizes the grid domain. This function ensures sufficiently small grid steps are present at locations where complex processes occur, nearshore for instance where wave breaking requires a finer domain to resolve all of the process present. The function automatically scales with the minimal wave period present in the model to ensure that all wave lengths are resolved.

Therefore the grid resolution remains variable, nevertheless, the order of magnitude of the domain can be controlled using minimum and maximum grid size settings.

By manipulating only these values, the adjusted settings for this model run are provided in Table G.3. All other settings are maintained, only the grid resolution is reduced by a factor four.

Table G.3: Numerical settings for the optimized grid resolution scenario

Setting Definition	**Value**
Number of grid points	560
Model run time percentage	100 %
Morphology settings	On
Output interval	1 s^{-1}

With the settings defined above, the computational time required to simulate a record of data was timed at 3 minutes. Thus, as one would expect the reduction in grid cells significantly decreases the computational time required. Moreover, the wave heights at observation points 3 and 5 are shown in Figure G.5, where the blue and red markers represent the reference and optimized scenarios respectively. Figure G.6 depicts the wave height reduction between offshore and observation points 3 and 5.

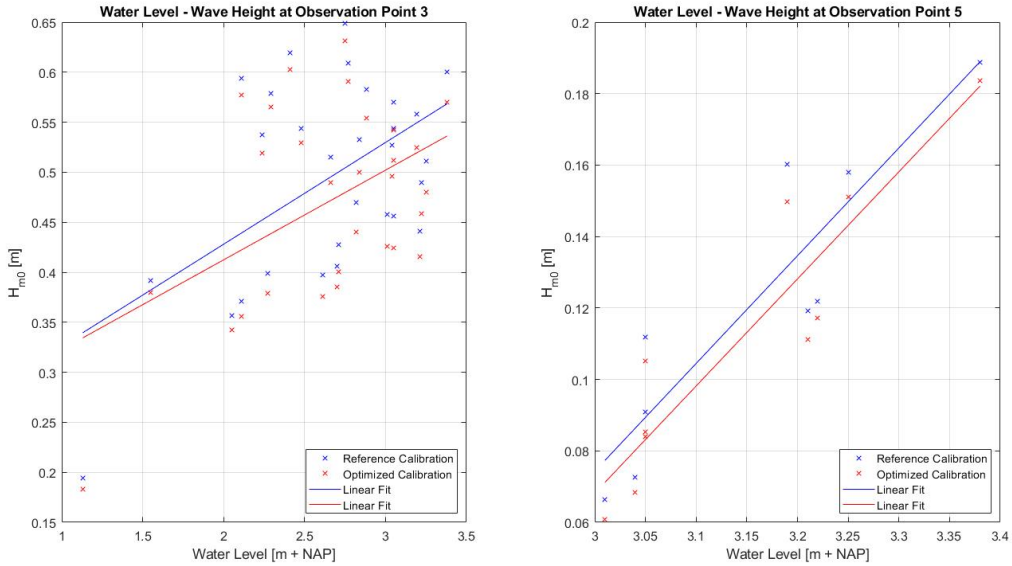

Figure G.5: Wave heights at observation points 3 and 5 plotted against the water level in the model run. Both the reference and optimized scenario are shown for comparison.

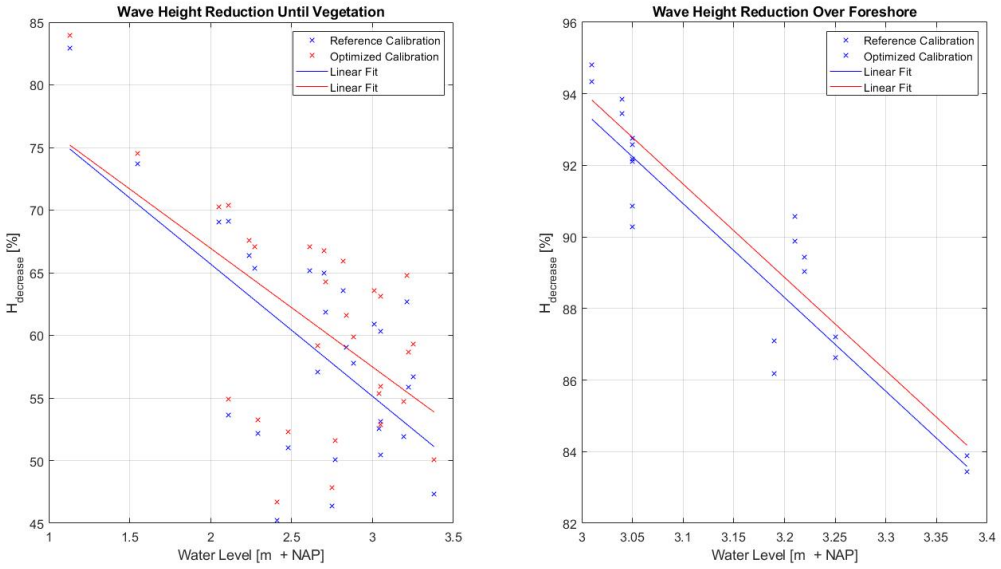

Figure G.6: Wave height reduction in relation to the offshore wave height at observation points 3 and 5 plotted against the water level in the model run. Both the reference and optimized scenario are shown for comparison.

A finer grid (i.e. the reference scenario) clearly produces an incremental increase in wave heights. This can be explained by the averaging that occurs in a coarse grid. In terms of accuracy, the wave heights for the reference and optimized scenarios were plotted against each other to determine their relative correlation, Figure G.7. With correlations of 0.995 and 0.975, sufficient accuracy is assumed present in the optimized scenario for the purpose of this thesis.

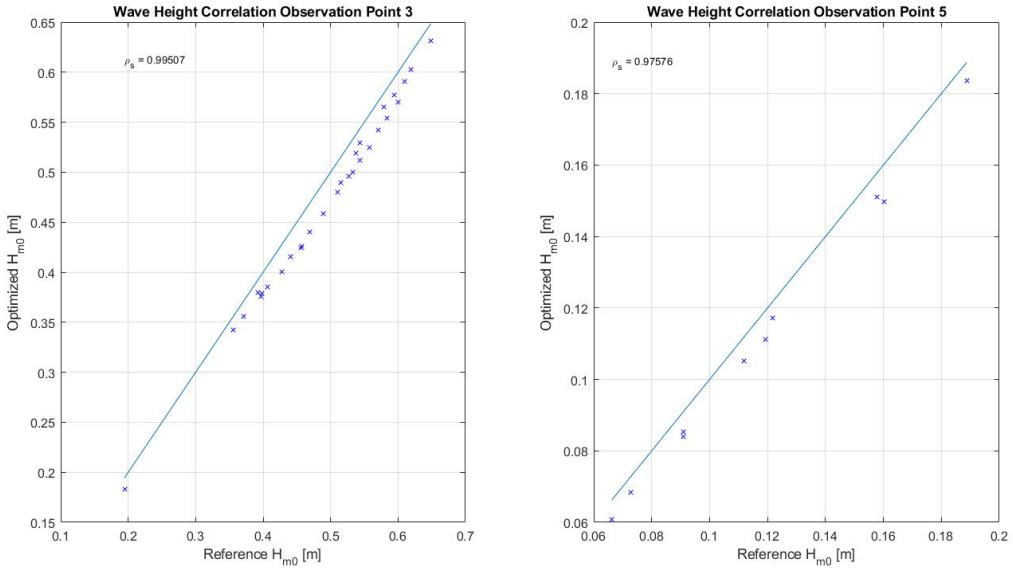

Figure G.7: Scatter plots for wave heights at observation points 3 and 5. The scatter plots compare the reference and optimized wave heights and also show the correlation between the two.

G.3. Run Time

The input dataset for all hydraulic variables are specified with a temporal resolution of 30 minutes. This time is referred to as the hydraulic time, which was decreased to reduce computational time. This has implications on the morphological time which is affected through reducing hydraulic time. Therefore, a morphological acceleration factor was included to multiply the morphological effects by the same factor that the hydraulic time was reduced by.

By manipulating only these values, the adjusted settings for this model run are provided in Table G.4. All other settings are maintained, only the grid resolution is reduced by a factor four.

Table G.4: Numerical settings for the optimized run time scenario

Setting Definition	Value
Number of grid points	560
Model run time percentage	25 %
Morphology settings	On
Output interval	1 s^{-1}

With the settings defined above, the computational time required to simulate a record of data was found to equal 41 seconds. The model run time was reduced by a factor 4, similar to the run time decrease factor. Again, the wave heights at observation points 3 and 5 are shown in Figure G.8, where the blue and red markers represent the reference and optimized scenarios respectively. Figure G.9 depicts the wave height reduction between offshore and observation points 3 and 5.

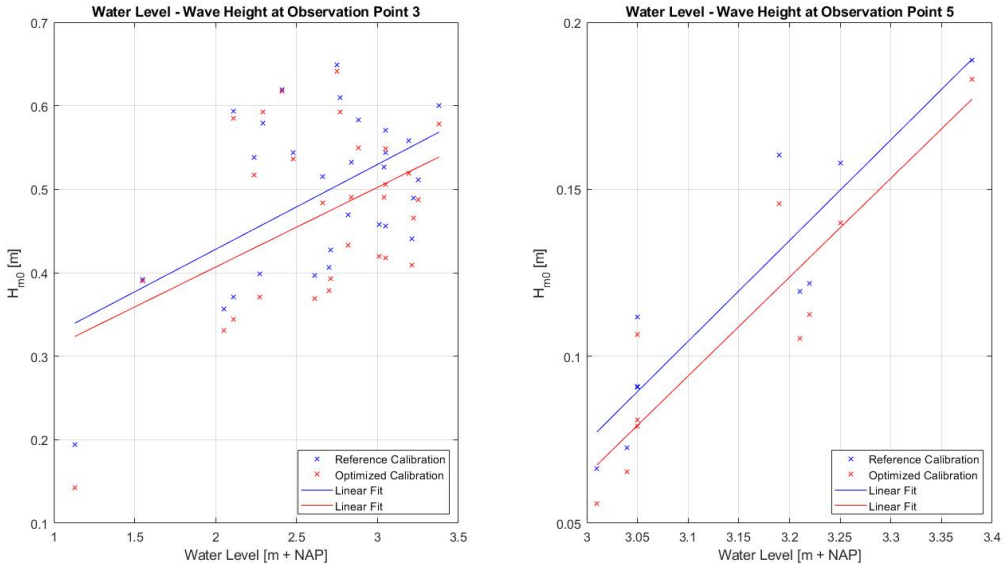

Figure G.8: Wave heights at observation points 3 and 5 plotted against the water level in the model run. Both the reference and optimized scenario are shown for comparison.

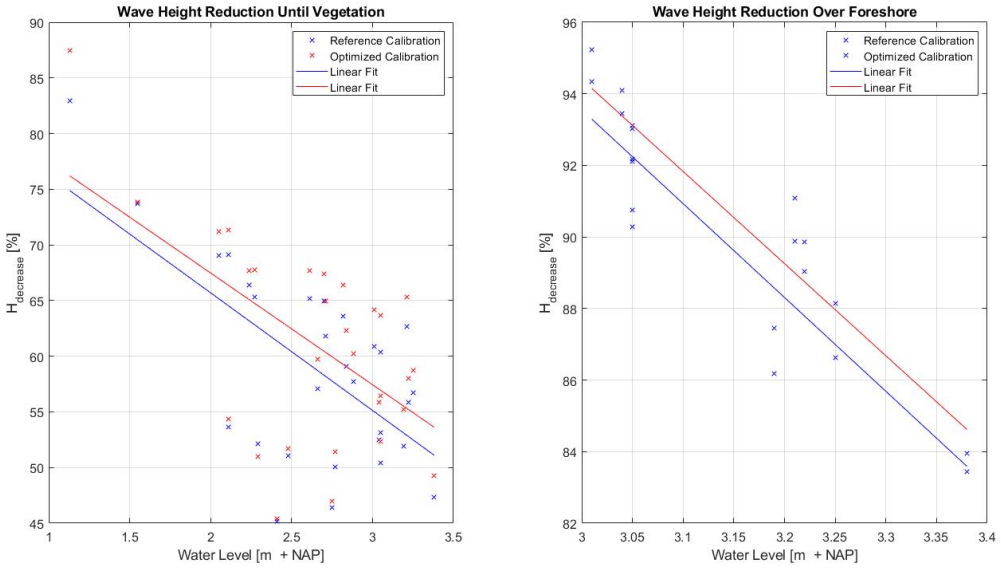

Figure G.9: Wave height reduction in relation to the offshore wave height at observation points 3 and 5 plotted against the water level in the model run. Both the reference and optimized scenario are shown for comparison.

Little effect was observed between the calibrated and reference scenario due to the adjustment in run time. In terms of accuracy, the wave heights for the reference and optimized scenarios were plotted against each other to determine their relative correlation, Figure G.8. With correlations of 0.995 and 0.988 between the wave heights of the calibrated and reference scenario, the scenario is assumed sufficiently accurate.

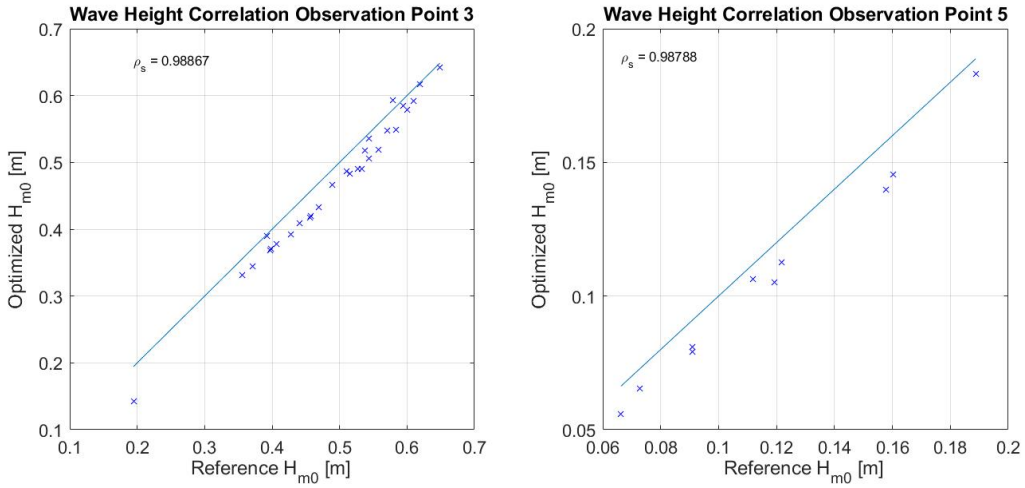

Figure G.10: Scatter plots for wave heights at observation points 3 and 5. The scatter plots compare the reference and optimized wave heights and also show the correlation between the two.

G.4. Morphology

Including morphology in the numerical settings affects the model run time as it requires additional processes to be calculated. The effect of removing morphology was assessed by turning off both sediment transport as morphology. Furthermore, the model run time decrease was maintained by decreasing the hydraulic time in the preparation of data.

By manipulating only the values related to morphology and the run time, the adjusted settings for this model run are provided in Table G.5. All other settings are maintained, only the grid resolution is reduced by a factor four.

Table G.5: Numerical settings for the optimized morphology scenario

Setting Definition	**Value**
Number of grid points	560
Model run time percentage	25 %
Morphology settings	Off
Output interval	1 s^{-1}

Model execution required 38 seconds to simulate an input record. The model output was identical to the previous output. Therefore no plots are provided and the reader is referenced to the figures in the previous calibration, figures G.8 - G.10.

G.5. Output Interval

In the general XBeach model settings, the output interval was specified for all model variables. The writing of variables to the output file influences the computational time while simultaneously affecting the amount of output used to assess wave height. The model output interval was increased from one every second to one output every 5 seconds. Resulting are the model settings shown in Table G.6.

Table G.6: Numerical settings for the optimized output interval scenario

Setting Definition	**Value**
Number of grid points	560
Model run time percentage	25 %
Morphology settings	Off
Output interval	5 s^{-1}

The computational time required for a single run was clocked at 0.34 seconds, an incremental computational improvement. Again, the model accuracy was identical to the output obtained in the run time improvement scenario.

H

Statistical Analysis of Synthetic Database

As a basis for the dynamic statistical model, a number of statistical analyses are required. Marginal distributions and correlation analysis assess the individual variables while

H.1. Marginal Analysis

All variables are analysed in terms of their theoretical distribution. Assessing the best fit has been completed using both the NLog method and the AIC method.

Table H.1: Best theoretical distributions for all variables that represent the HFD system.

Variable	**Probability Distribution Function**
H	Generalized extreme value
T	t Location-scale
W	Gaussian mixture
N_v	Weibull
b_v	Normal
h_v	Generalized Pareto
Cd	Generalized Pareto
H_{ns}	Gamma

H.1.1. Wave Height

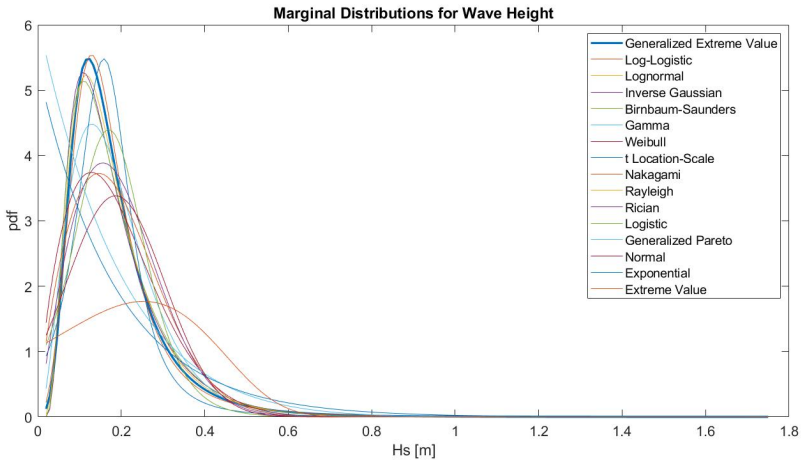

Figure H.1: All marginal distributions probability density functions with the best fit presented as a thicker line in the graph.

H.1.2. Wave Period

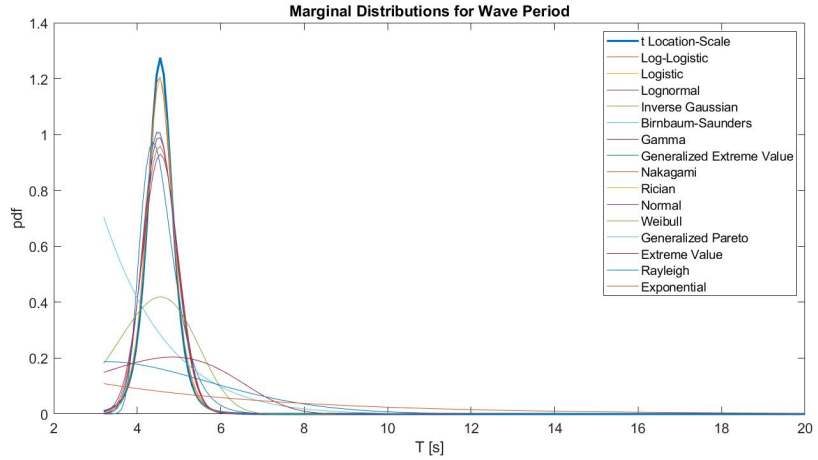

Figure H.2: All marginal distributions probability density functions with the best fit presented as a thicker line in the graph.

H.1.3. Water Level

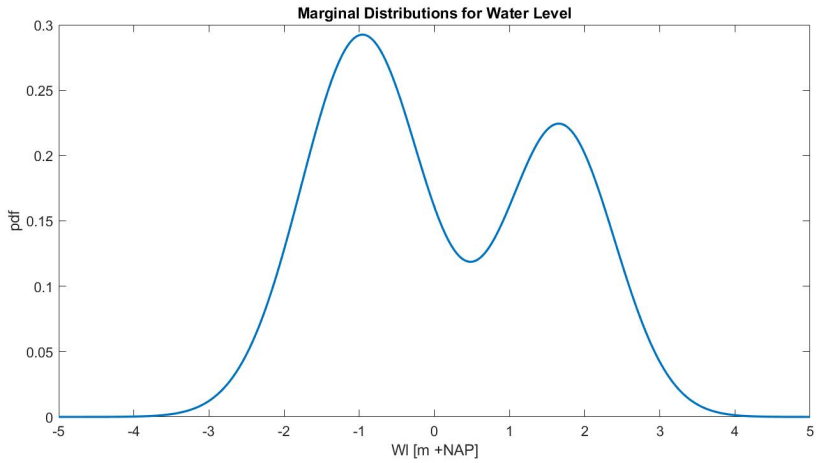

Figure H.3: All marginal distributions probability density functions with the best fit presented as a thicker line in the graph.

H.1.4. Vegetation Density

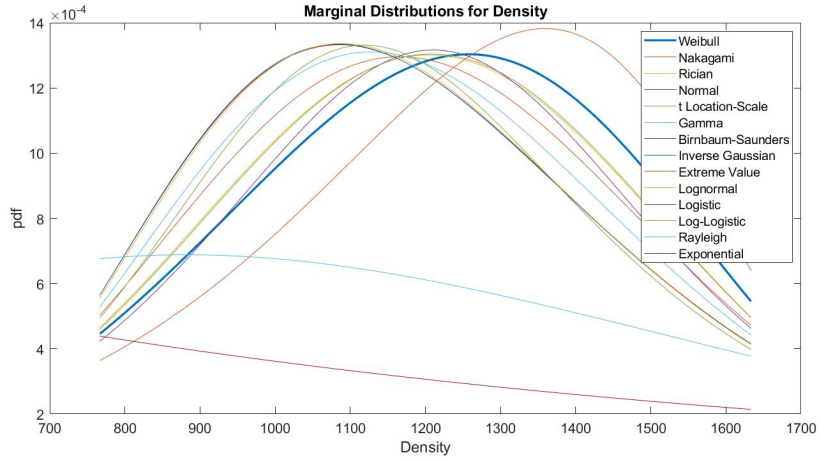

Figure H.4: All marginal distributions probability density functions with the best fit presented as a thicker line in the graph.

H.1.5. Vegetation Width

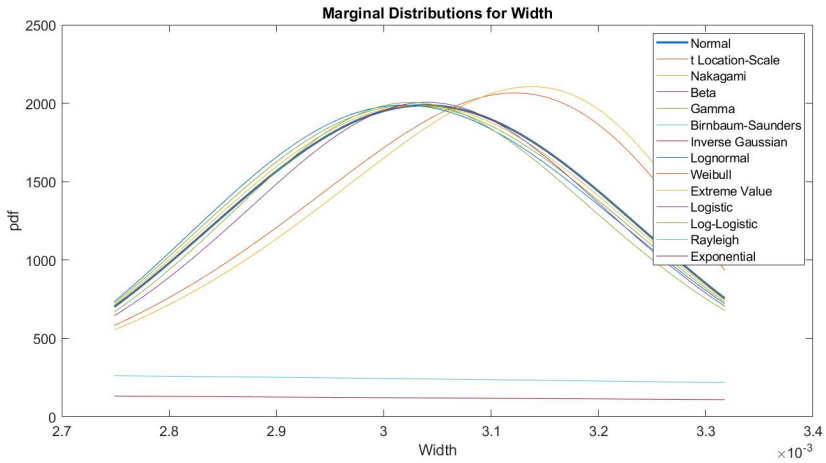

Figure H.5: All marginal distributions probability density functions with the best fit presented as a thicker line in the graph.

H.1.6. Vegetation Height

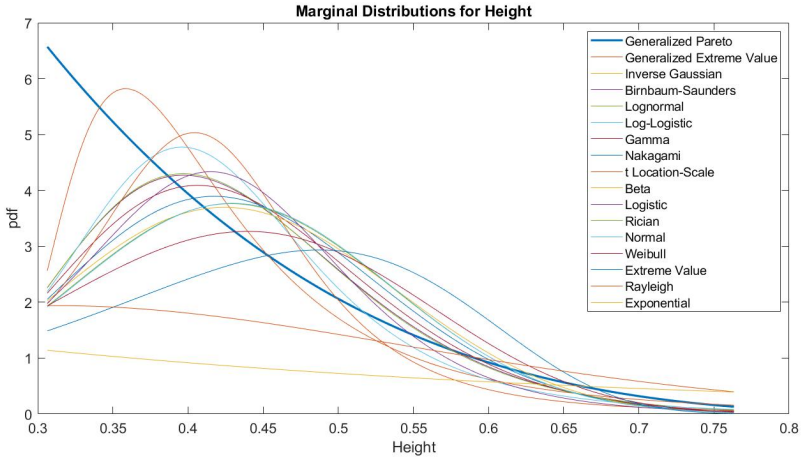

Figure H.6: All marginal distributions probability density functions with the best fit presented as a thicker line in the graph.

H.1.7. Drag Coefficient

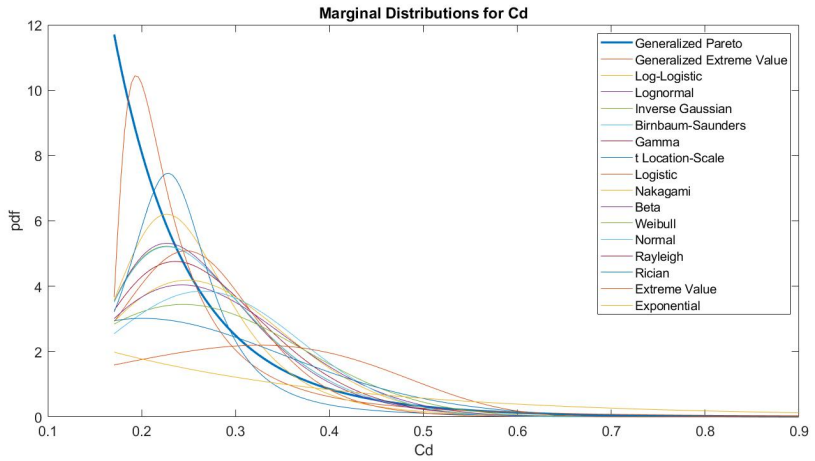

Figure H.7: All marginal distributions probability density functions with the best fit presented as a thicker line in the graph.

H.1.8. Nearshore Wave Height

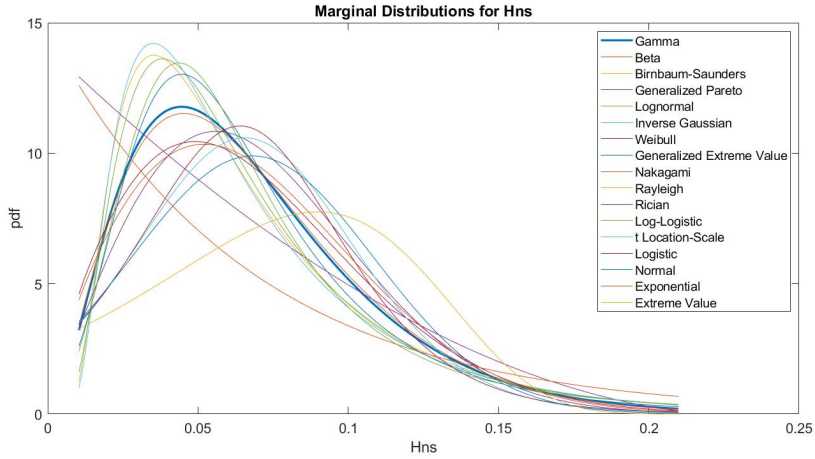

Figure H.8: All marginal distributions probability density functions with the best fit presented as a thicker line in the graph.

H.2. Correlation Analysis

For the variable groups: offshore hydraulics and foreshore vegetation, the (auto-) correlation structures were assessed. Correlations between variable pares define their mutual dependence and were required for the modelling of bivariate copulas. Auto-correlation arrays were used to examine the temporal character of each variable.

H.2.1. Correlation

Table H.2: Spearman's Correlation coefficients for each offshore hydraulic variable pair.

Variable	Wave Height	Wave Period	Water Level
Wave Height	1	-0.25	0.30
Wave Period	-0.25	1	-0.10
Water Level	0.30	-0.10	1

Table H.3: Spearman's Correlation coefficients for each vegetation variable pair.

Variable	Density	Width	Height
Density	1	0.99	-0.33
Width	0.99	1	-0.39
Height	-0.33	-0.39	1

H.2.2. Auto-Correlation

As to determine which variable is optimal in the statistical modelling of temporal dependence, an autocorrelation analysis is required. The offshore hydraulic variables are analysed as a group, while the vegetation parameters are also assessed as a segment. The auto-correlations were obtained by time-shifting the dataset. Following each time-shift, a correlation was determined between the original dataset and the time-shifted set. The resulting autocorrelation plots are shown in figure H.9.

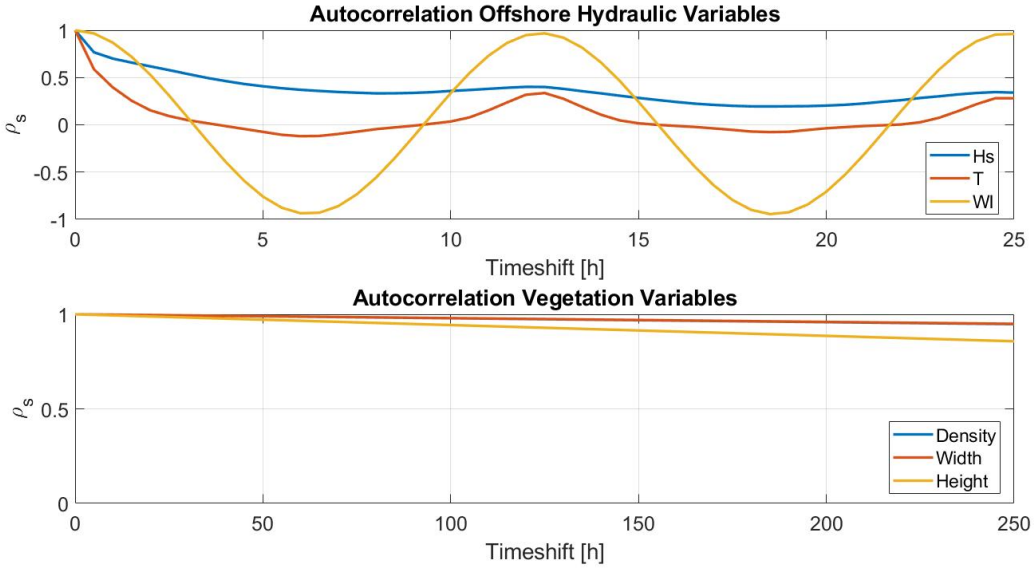

Figure H.9: Autocorrelation plot for all offshore and vegetation parameters shifted through time and assessed in terms of Spearmans correlation coefficient. Note the difference in time shift between the two plots.

Clearly there is a strong autocorrelation between water levels at short time-shifts. Moreover, the almost complete negative autocorrelation after a shift of 6 hours is also logical as the water level is forced by the tides. Vegetation parameters are highly correlated to itself, as supported by the correlation coefficient larger than 0.85 after a 250 hour time-shift. Again this is logical as the vegetated processes physically do not change significantly over the course of hours.

Based on the autocorrelation structures, offshore water level is assumed the best fit for modelling temporal

dependence as there is a strong continuing autocorrelation structure which can be captured within a short time period (i.e. 12 time shifts).

H.3. Copula Analysis

Bi-variate Copula analyses were completed for both the standard copula structures (i.e. in the same time step) and for the autocorrelation structures between water levels. Variable pairs that are physically related to one another, for instance the hydraulic parameters, were analysed. Relations between vegetation and hydraulic parameters are neglected due to lack of physical relation. Each pair was tested for five copula types:

(i) Gaussian

(ii) t

(iii) Gumbel

(iv) Clayton

(v) Frank

H.3.1. Standard Copula Analysis

For each copula sample a semi-correlation analysis determined the best copula fit to the empirical data. The best fit copula PDF and CDF are provided for each variable pair. The variable pairs that were analysed are presented in table H.4 where all best fits are included in the overview.

Table H.4: Overview of all bi-variate pairs that were analysed in terms of best copula fit using semi-correlations.

Variable Pairs	**Pair Notation**	ρ_s	**Best Fit Copula**
Wave Height & Wave Period	(H_s & T)	-0.25	t (6 degrees of freedom)
Wave Height & Water Level	(H_s & Wl)	0.3	Gaussian
Water Level & Wave Period	(Wl & T)	-0.1	Gaussian
Wave Height & Nearshore Wave Height	(H_s & H_{ns})	0.55	Gaussian
Wave Period & Nearshore Wave Height	(Wl & H_{ns})	-0.24	Clayton
Water Level & Nearshore Wave Height	(Wl & H_{ns})	0.76	Frank
Vegetation Density & Vegetation Width	(N_v & b_v)	0.99	Gumbel
Vegetation Density & Vegetation Height	(N_v & h_v)	-0.33	Gumbel
Vegetation Width & Vegetation Height	(b_v & h_v)	-0.39	Gaussian
Vegetation Density & Nearshore Wave Height	(N_v & H_{ns})	-0.21	t (3 degrees of freedom)
Vegetation Width & Nearshore Wave Height	(b_v & H_{ns})	-0.21	t (3 degrees of freedom)
Vegetation Height & Nearshore Wave Height	(h_v & H_{ns})	0.13	Gaussian
Drag Coefficient & Nearshore Wave Height	(C_d & H_{ns})	-0.41	Gaussian

For each pair the best fit copula and the semi correlation normalized scatter plot is presented in the sections below.

H.3.2. Wave Height & Wave Period

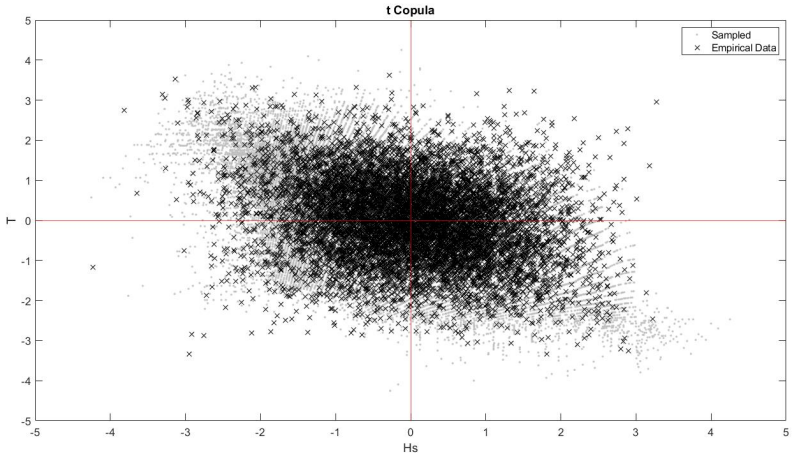

Figure H.10: Normalized scatter plot for the empirical data and 10.000 copula samples.

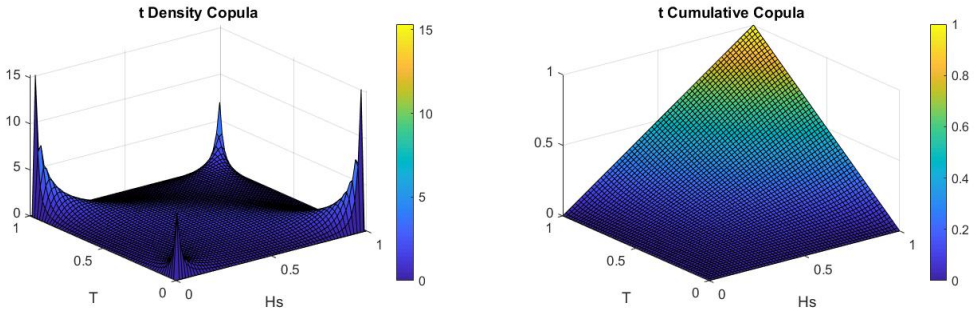

Figure H.11: Bi-variate density and cumulative copulas.

H.3.2.1 Wave Height & Water Level

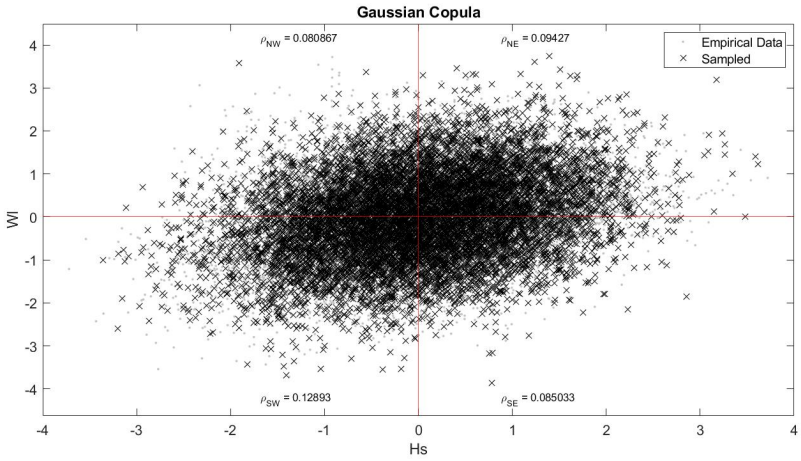

Figure H.12: Normalized scatter plot for the empirical data and 10.000 copula samples.

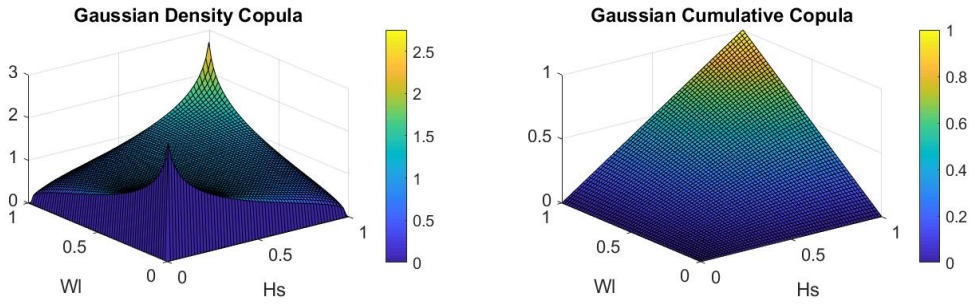

Figure H.13: Bi-variate density and cumulative copulas.

H.3.2.2 Water Level & Wave Period

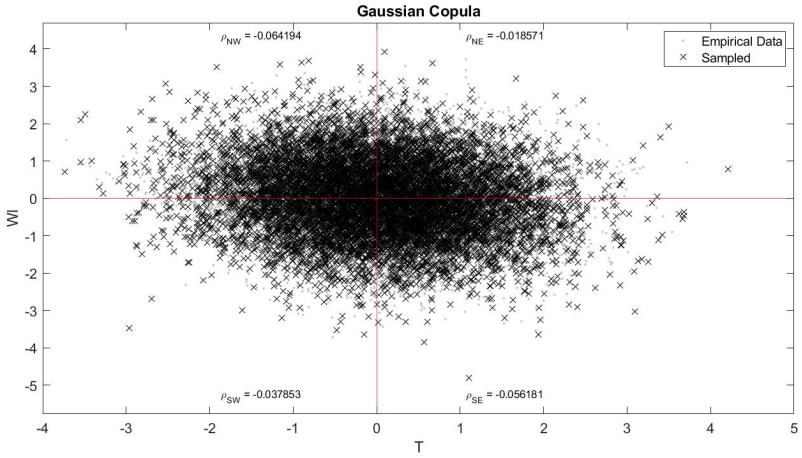

Figure H.14: Normalized scatter plot for the empirical data and 10.000 copula samples.

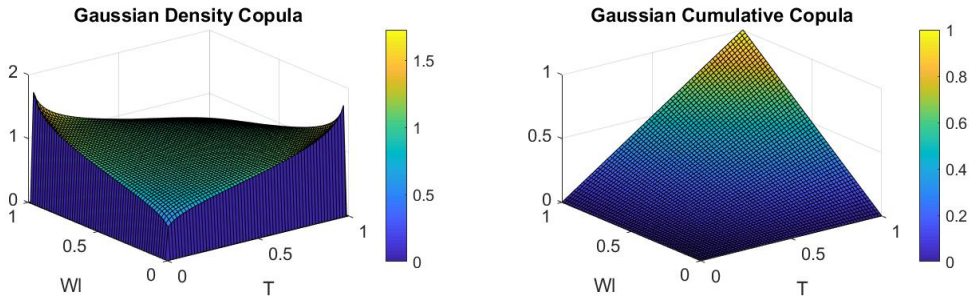

Figure H.15: Bi-variate density and cumulative copulas.

H.3.2.3 Wave Height & Nearshore Wave Height

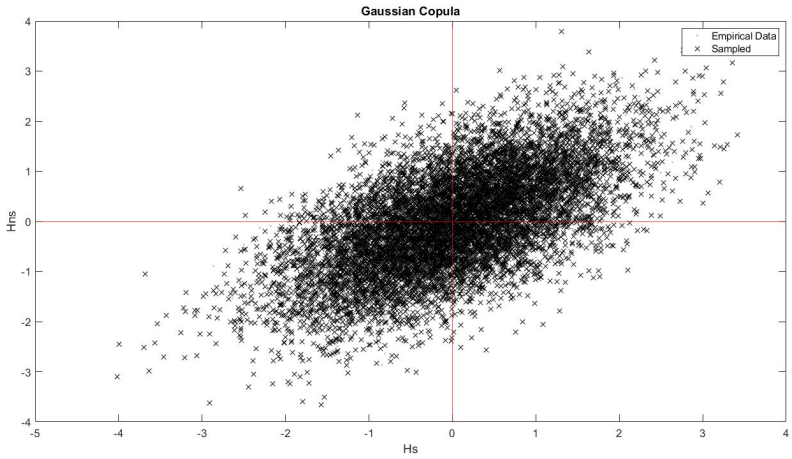

Figure H.16: Normalized scatter plot for the empirical data and 10.000 copula samples.

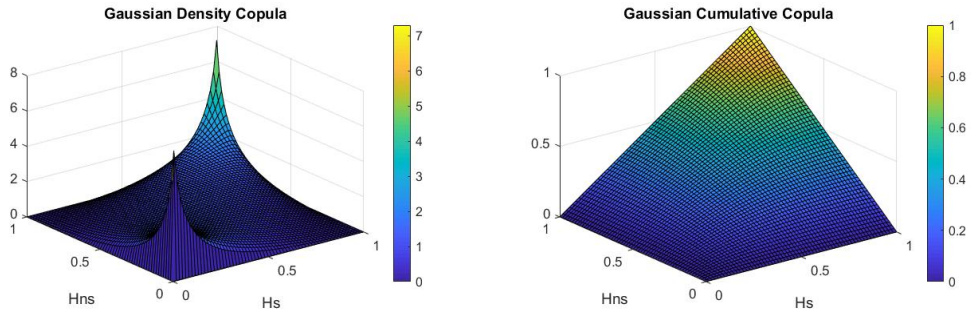

Figure H.17: Bi-variate density and cumulative copulas.

H.3.2.4 Wave Period & Nearshore Wave Height

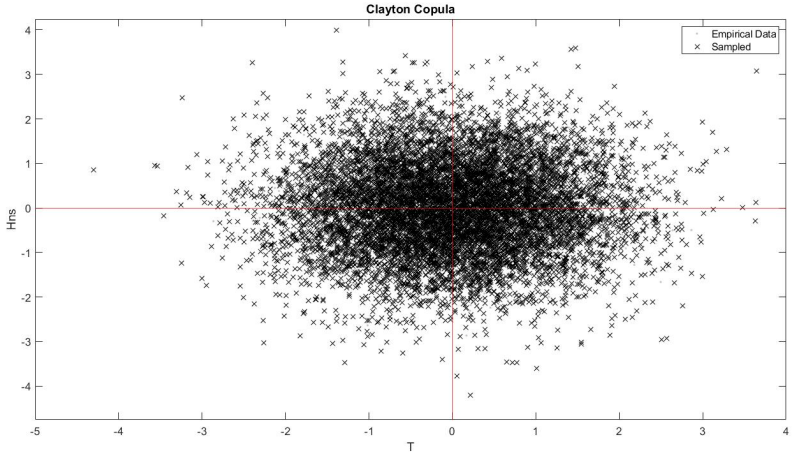

Figure H.18: Normalized scatter plot for the empirical data and 10.000 copula samples.

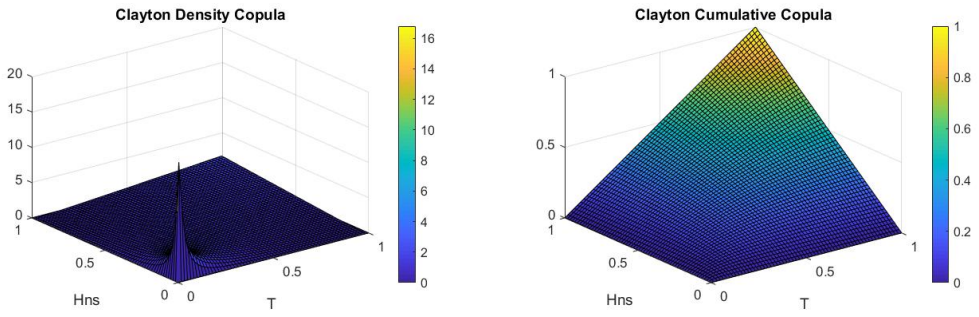

Figure H.19: Bi-variate density and cumulative copulas.

H.3.2.5 Water Level & Nearshore Wave Height

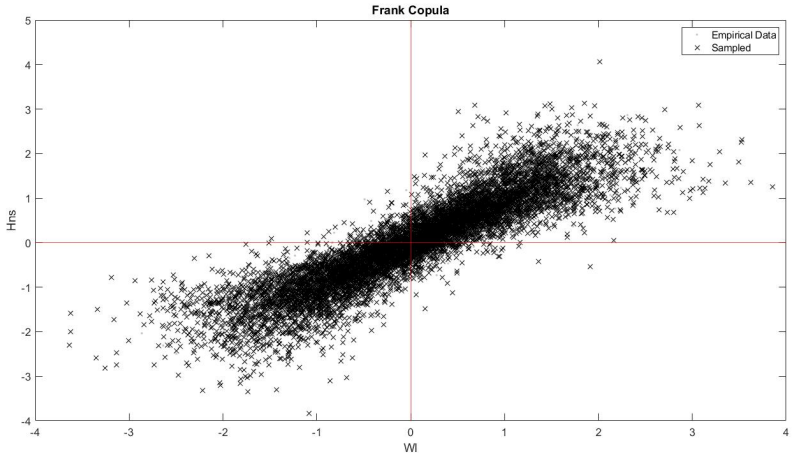

Figure H.20: Normalized scatter plot for the empirical data and 10.000 copula samples.

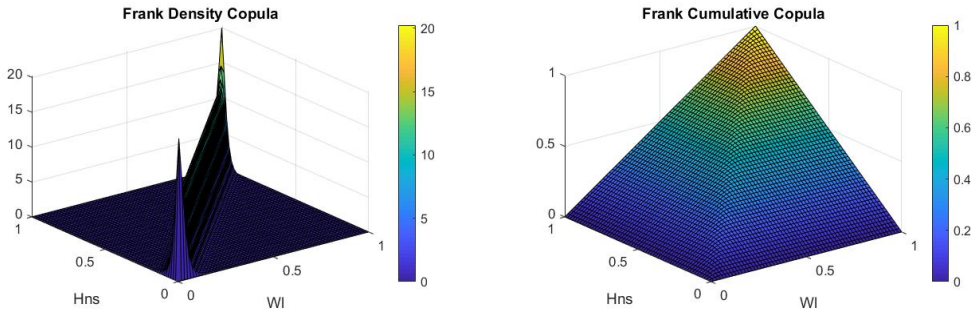

Figure H.21: Bi-variate density and cumulative copulas.

H.3.2.6 Vegetation Density & Vegetation Width

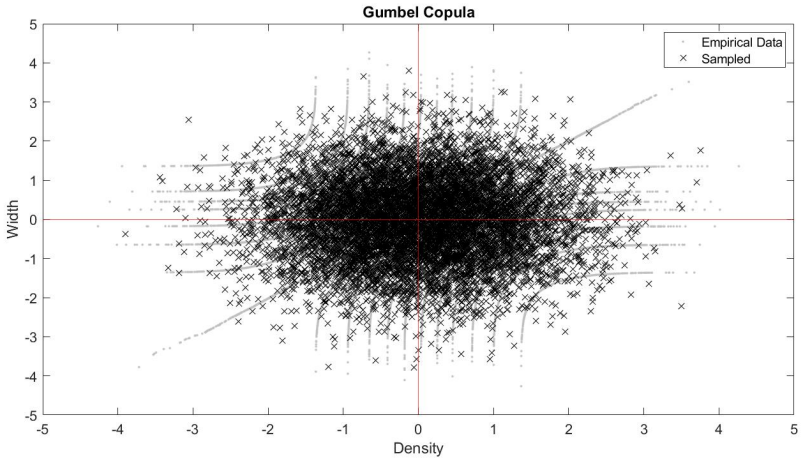

Figure H.22: Normalized scatter plot for the empirical data and 10.000 copula samples.

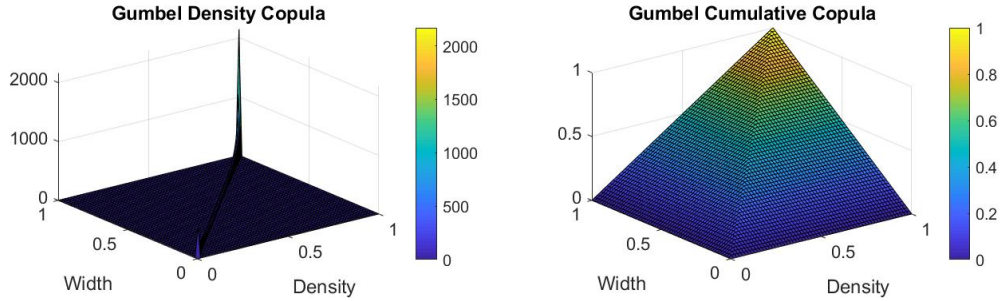

Figure H.23: Bi-variate density and cumulative copulas.

H.3.2.7 Vegetation Density & Vegetation Height

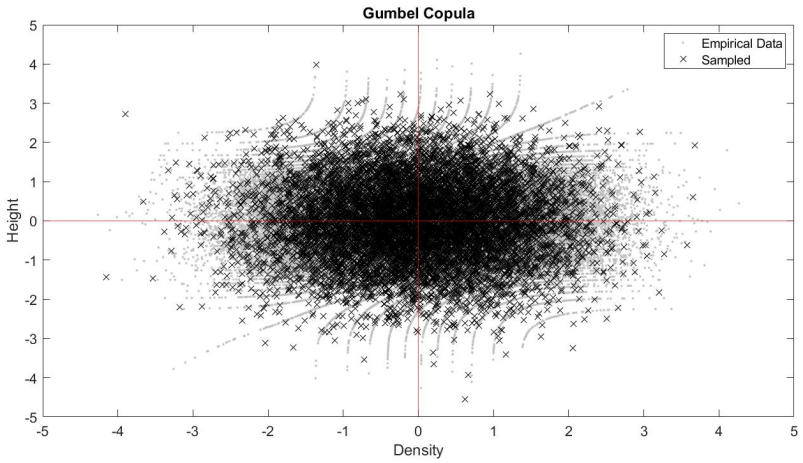

Figure H.24: Normalized scatter plot for the empirical data and 10.000 copula samples.

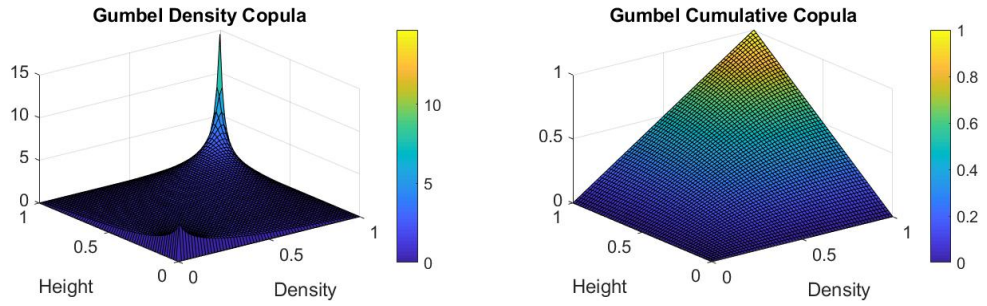

Figure H.25: Bi-variate density and cumulative copulas.

H.3.2.8 Vegetation Width & Vegetation Height

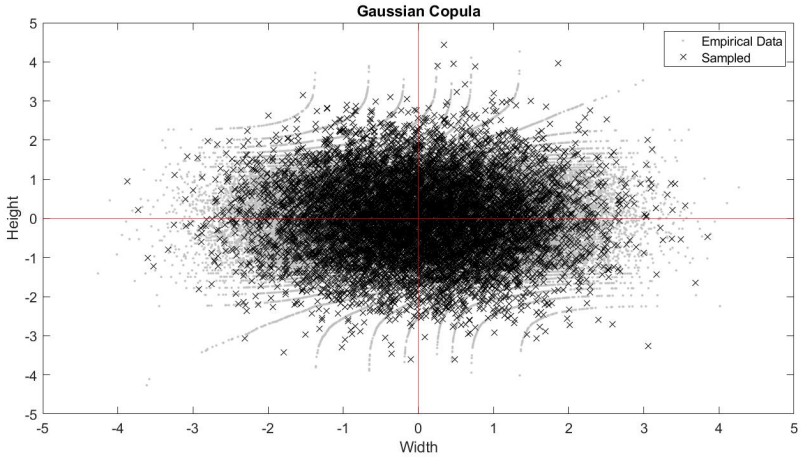

Figure H.26: Normalized scatter plot for the empirical data and 10.000 copula samples.

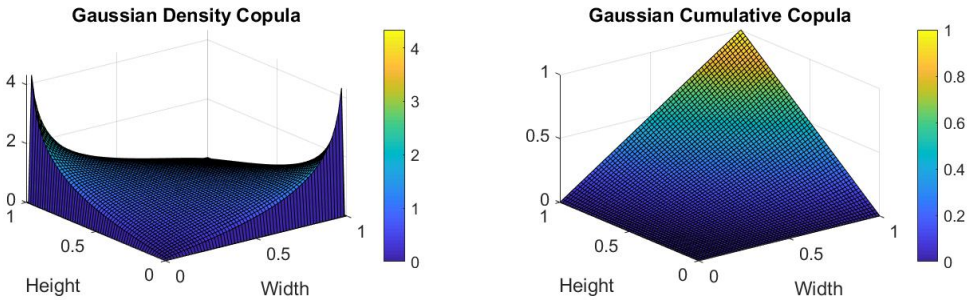

Figure H.27: Bi-variate density and cumulative copulas.

H.3.2.9 Vegetation Density & Nearshore Wave Height

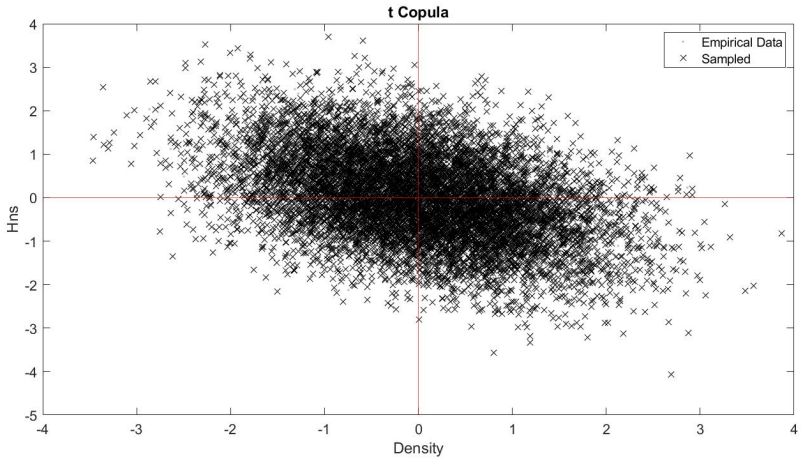

Figure H.28: Normalized scatter plot for the empirical data and 10.000 copula samples.

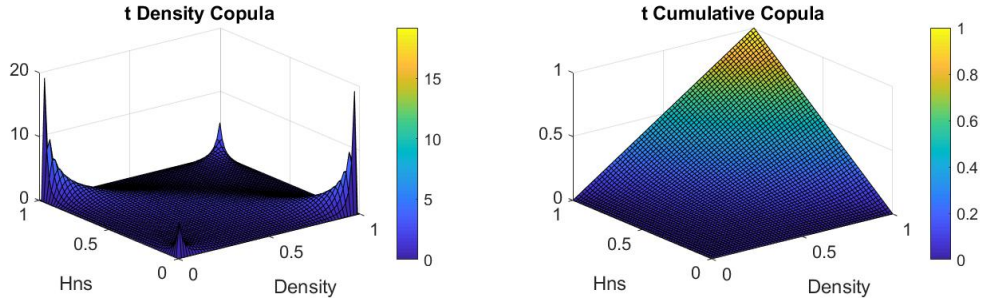

Figure H.29: Bi-variate density and cumulative copulas.

H.3.2.10 Vegetation Width & Nearshore Wave Height

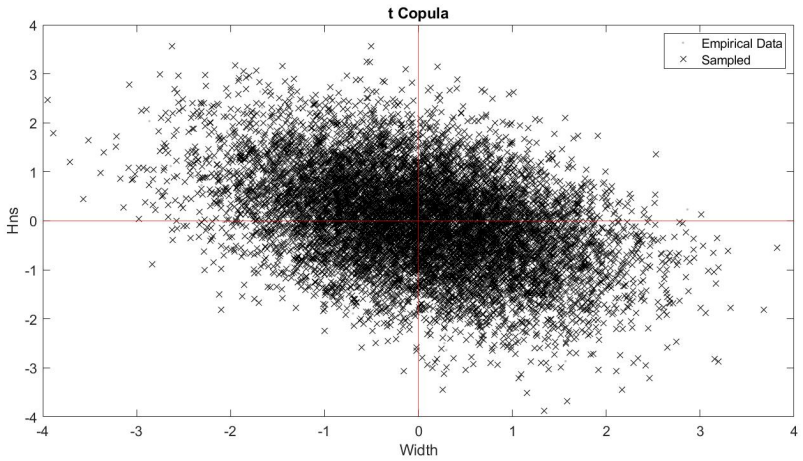

Figure H.30: Normalized scatter plot for the empirical data and 10.000 copula samples.

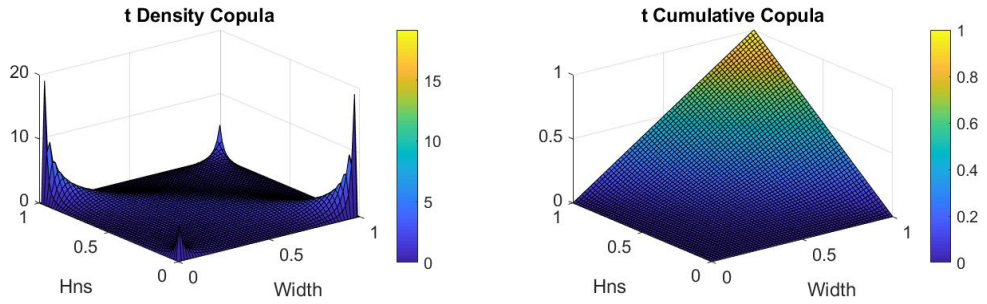

Figure H.31: Bi-variate density and cumulative copulas.

H.3.2.11 Vegetation Height & Nearshore Wave Height

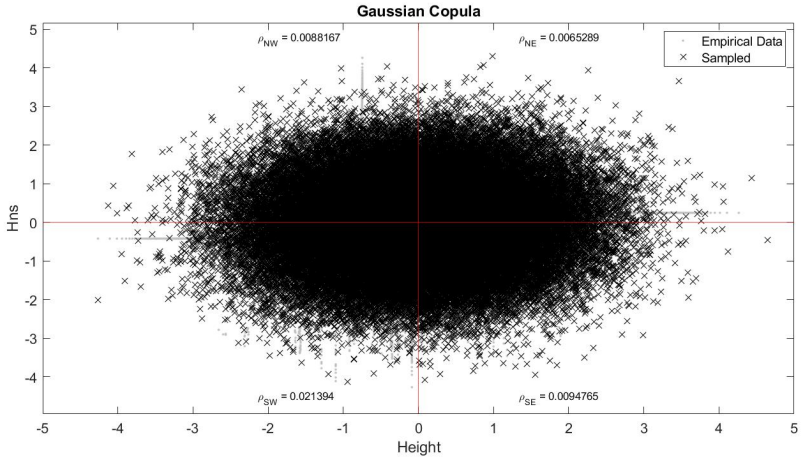

Figure H.32: Normalized scatter plot for the empirical data and 10.000 copula samples.

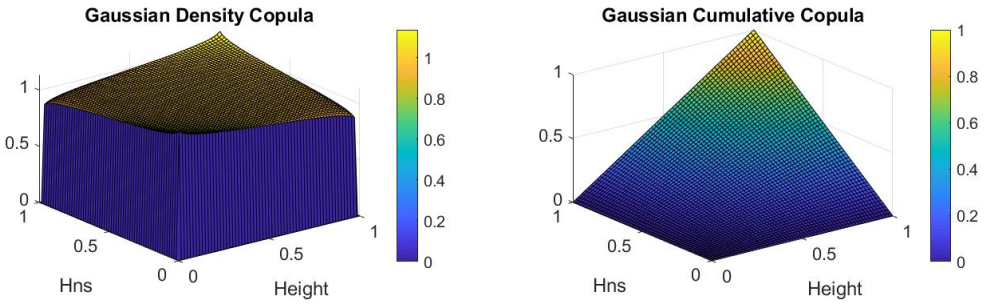

Figure H.33: Bi-variate density and cumulative copulas.

H.3.2.12 Drag Coefficient & Nearshore Wave Height

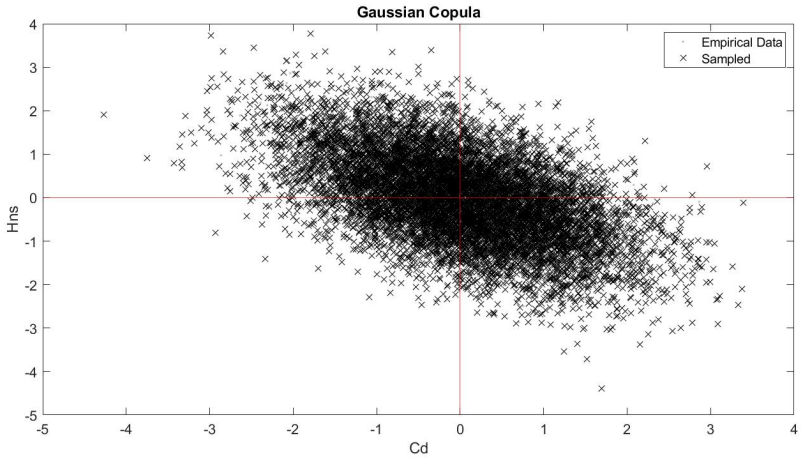

Figure H.34: Normalized scatter plot for the empirical data and 10.000 copula samples.

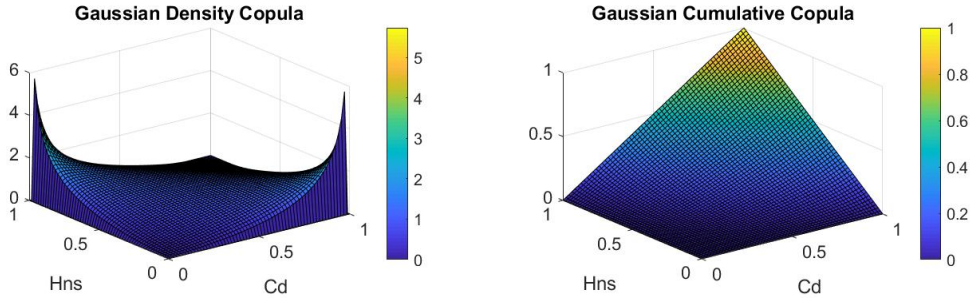

Figure H.35: Bi-variate density and cumulative copulas.

H.3.3. Autocorrelation Copula Analysis

Assessment of the autocorrelation copulas was conducted using a semi-correlation analysis to determine the best copula fits. Again the PDF and CDF copulas are presented in the sections below. The variable pairs and their best fit copulas are presented in table H.5.

Table H.5: Overview of best autocorrelation copula fits for various time shifts.

	Time Shift						
Variable	**.5 hour**	**1 hour**	**1.5 hours**	**2 hours**	**2.5 hours**	**3 hours**	**6 hours**
Water Level	Gaussian	Gaussian	Gaussian	Gaussian	Gaussian	Gaussian	t (4° freedom)
Wave Height	Clayton	Clayton	Clayton	-	-	-	-
Wave Period	Gumbel	Gumbel	Gumbel	-	-	-	-

H.3.3.1 Water Level - 0.5 Hour Time Shift

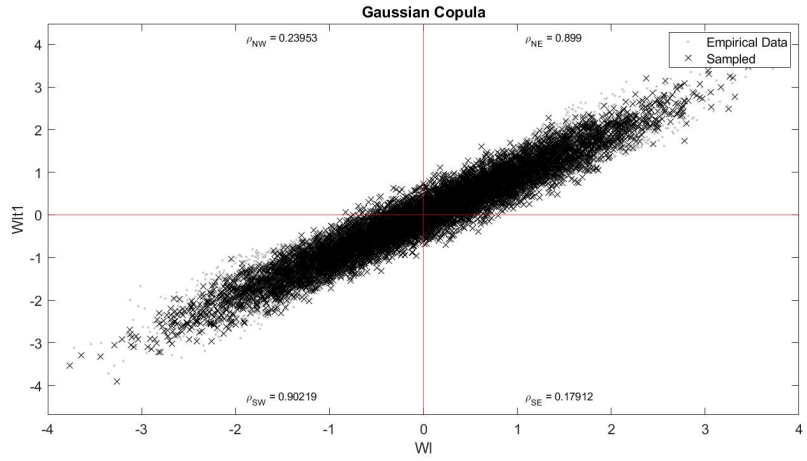

Figure H.36: Normalized scatter plot for the empirical data and 10.000 copula samples.

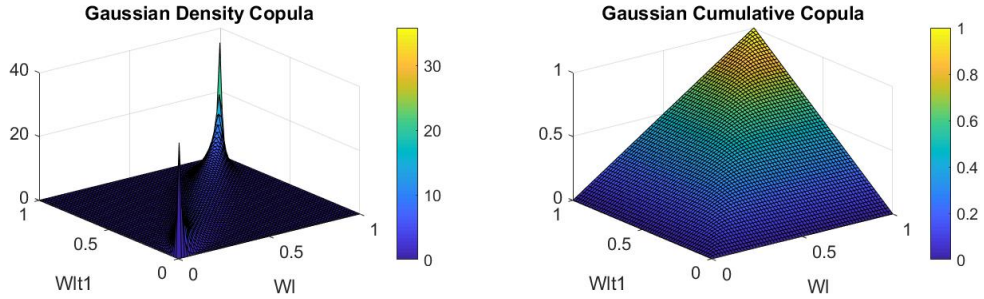

Figure H.37: Bi-variate density and cumulative copulas.

H.3.3.2 Water Level - 1 Hour Time Shift

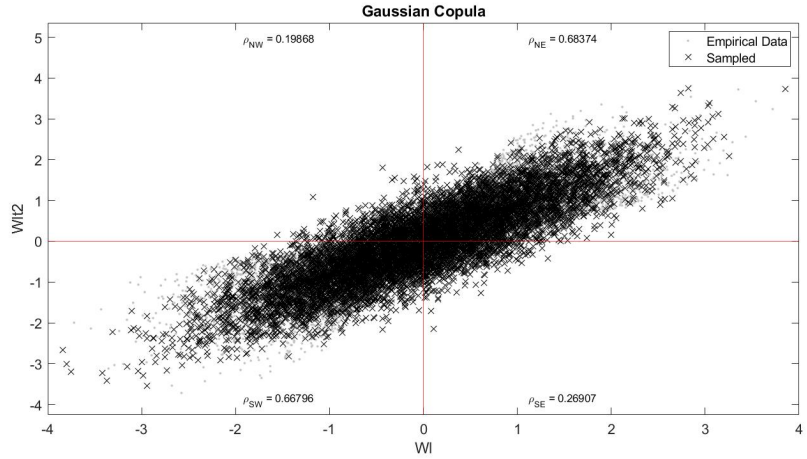

Figure H.38: Normalized scatter plot for the empirical data and 10.000 copula samples.

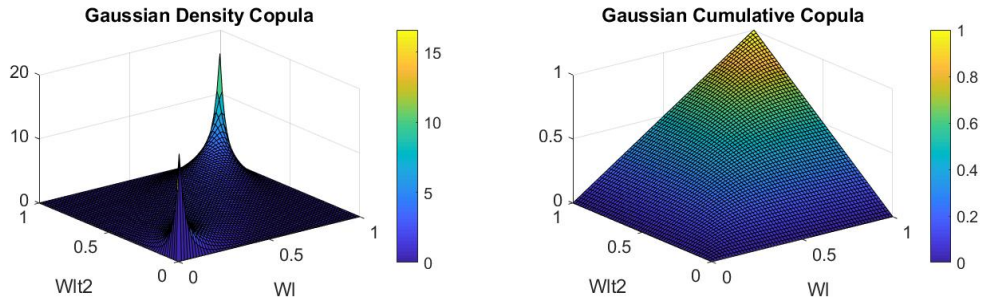

Figure H.39: Bi-variate density and cumulative copulas.

H.3.3.3 Water Level - 1.5 Hours Time Shift

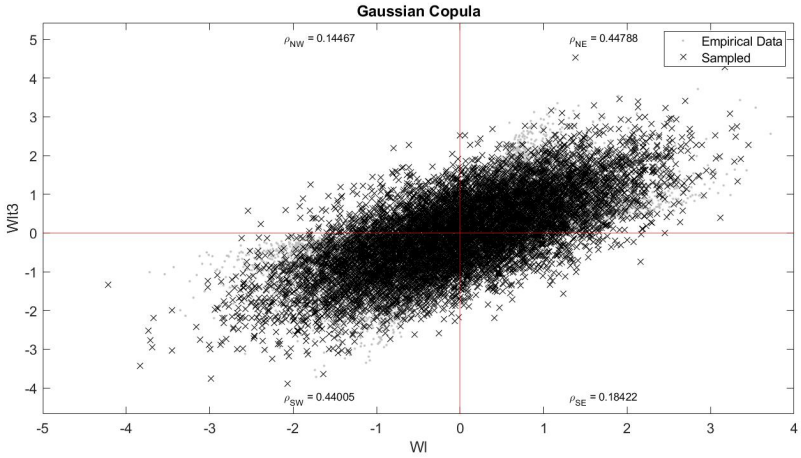

Figure H.40: Normalized scatter plot for the empirical data and 10.000 copula samples.

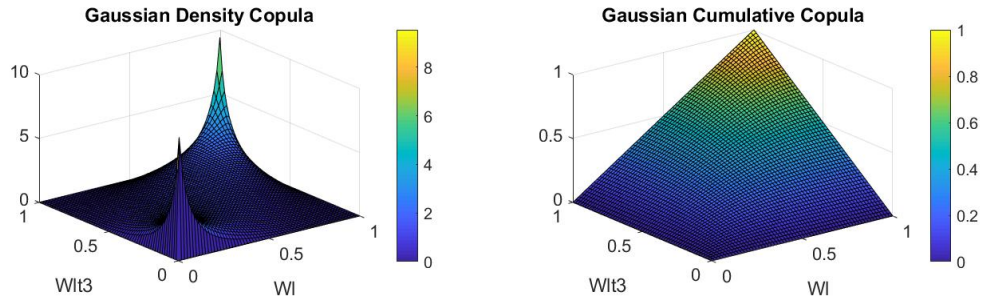

Figure H.41: Bi-variate density and cumulative copulas.

H.3.3.4 Water Level - 2 Hours Time Shift

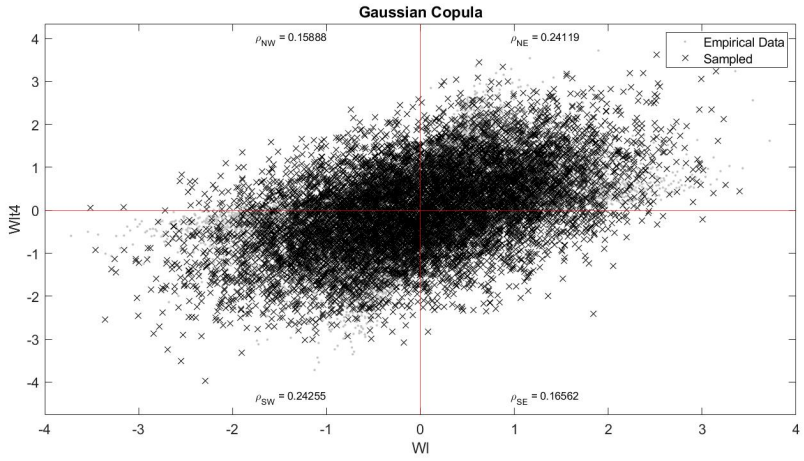

Figure H.42: Normalized scatter plot for the empirical data and 10.000 copula samples.

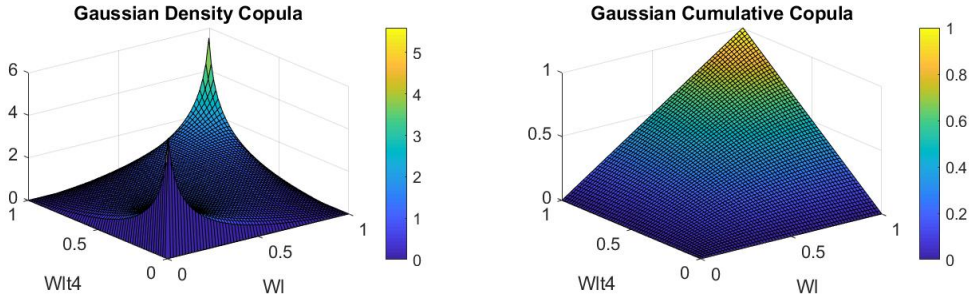

Figure H.43: Bi-variate density and cumulative copulas.

H.3.3.5 Water Level - 2.5 Hours Time Shift

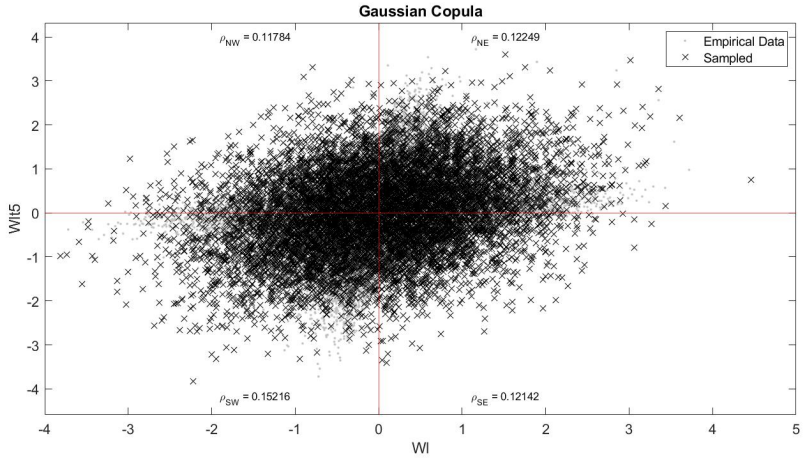

Figure H.44: Normalized scatter plot for the empirical data and 10.000 copula samples.

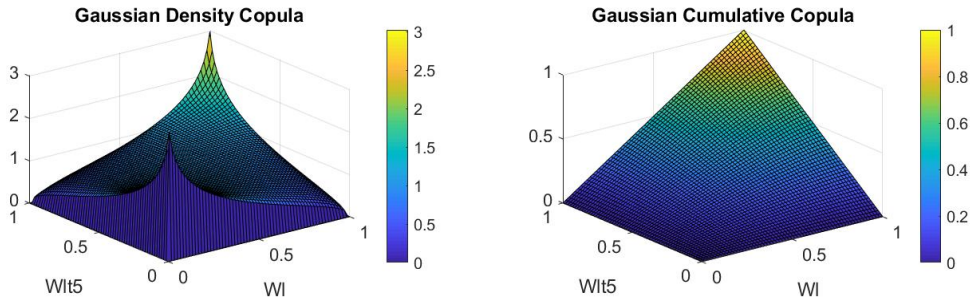

Figure H.45: Bi-variate density and cumulative copulas.

H.3.3.6 Water Level - 3 Hours Time Shift

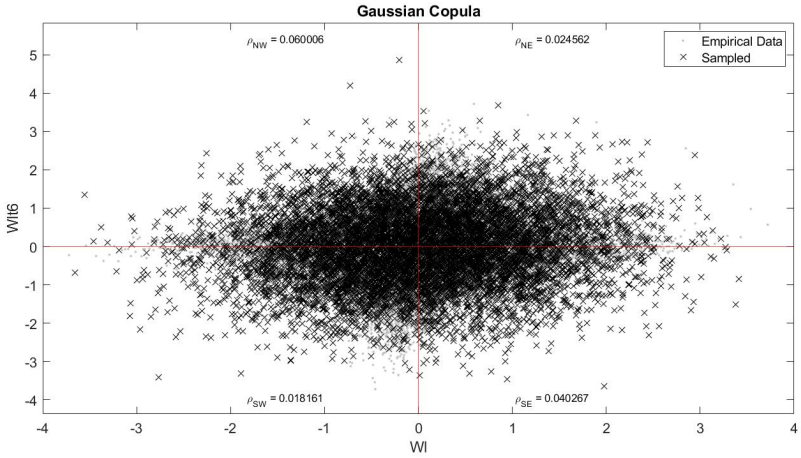

Figure H.46: Normalized scatter plot for the empirical data and 10.000 copula samples.

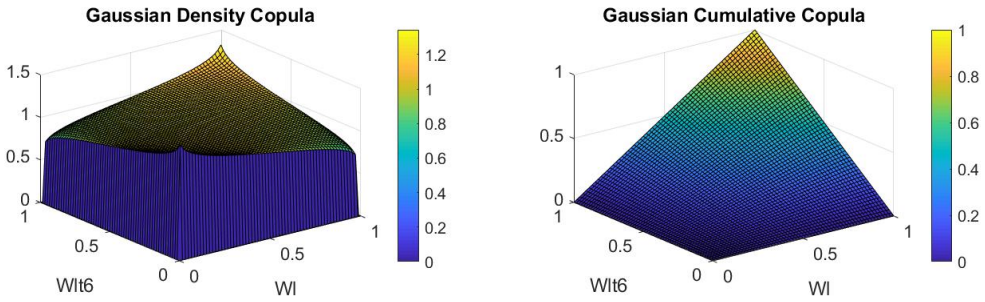

Figure H.47: Bi-variate density and cumulative copulas.

H.3.3.7 Water Level - 6 Hours Time Shift

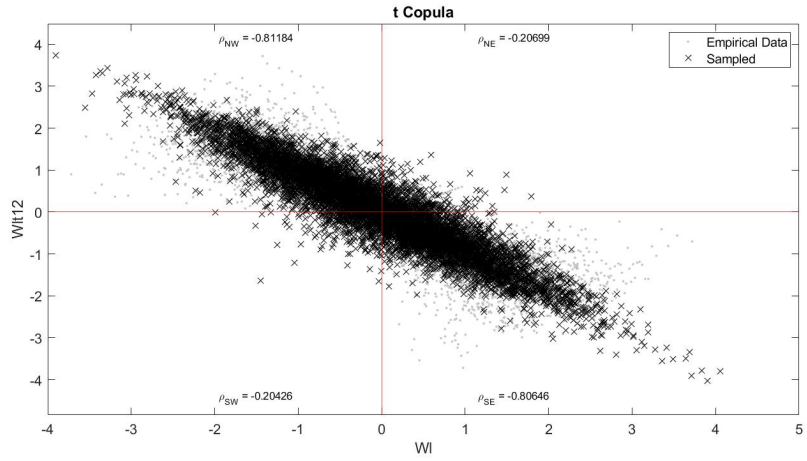

Figure H.48: Normalized scatter plot for the empirical data and 10.000 copula samples.

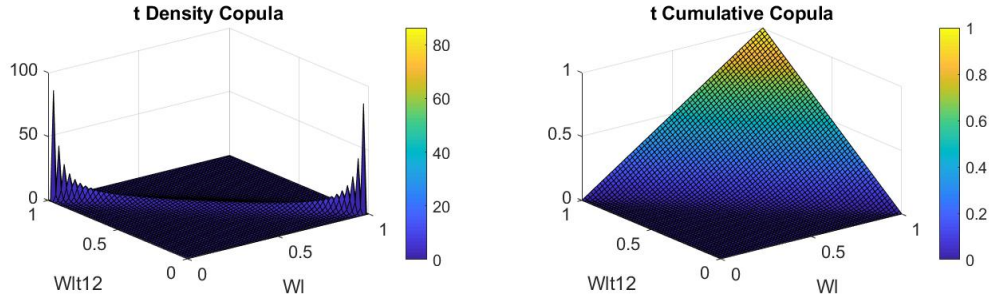

Figure H.49: Bi-variate density and cumulative copulas.

H.3.3.8 Wave Height - 0.5 Hour Time Shift

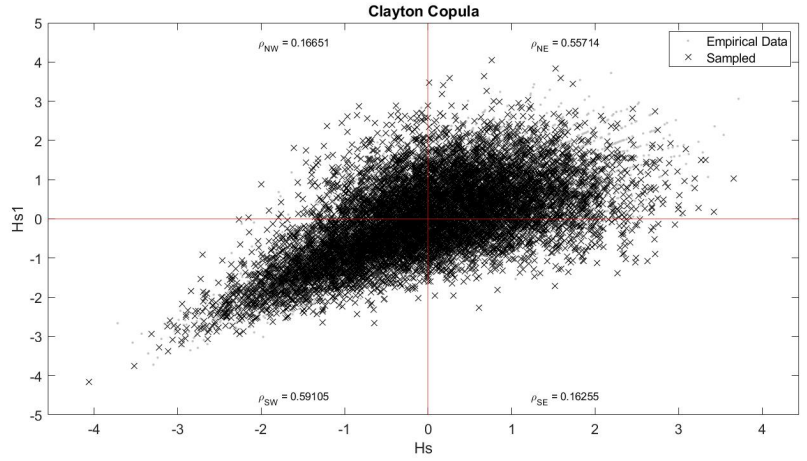

Figure H.50: Normalized scatter plot for the empirical data and 10.000 copula samples.

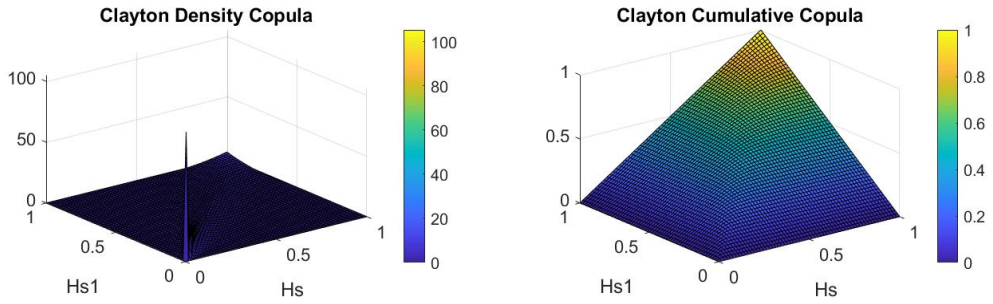

Figure H.51: Bi-variate density and cumulative copulas.

H.3.3.9 Wave Height - 1 Hour Time Shift

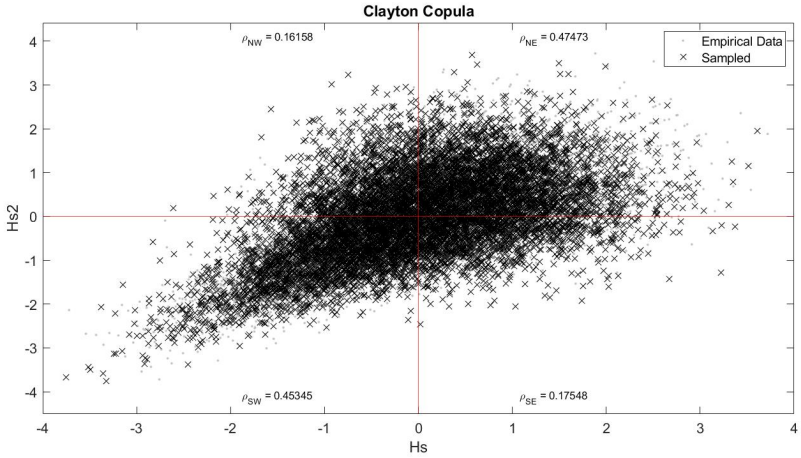

Figure H.52: Normalized scatter plot for the empirical data and 10.000 copula samples.

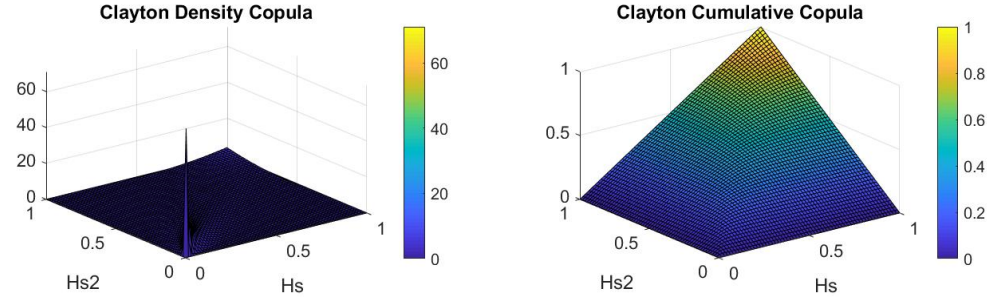

Figure H.53: Bi-variate density and cumulative copulas.

H.3.3.10 Wave Height - 1.5 Hours Time Shift

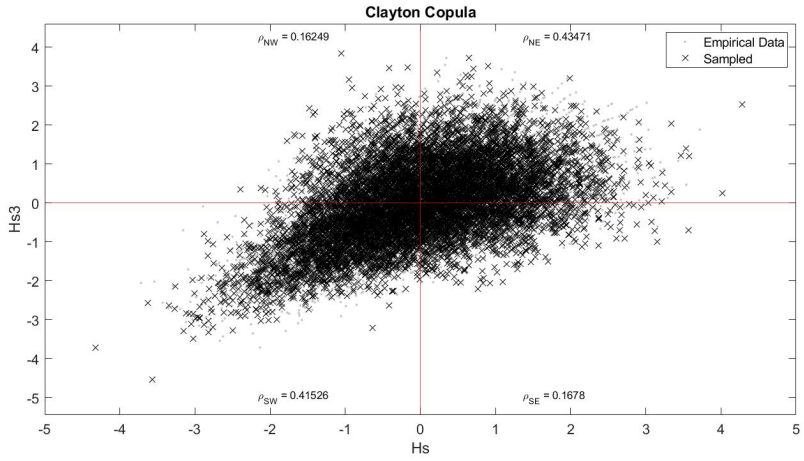

Figure H.54: Normalized scatter plot for the empirical data and 10.000 copula samples.

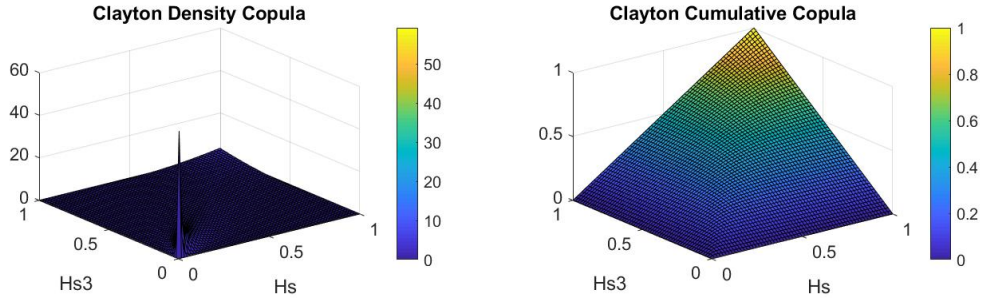

Figure H.55: Bi-variate density and cumulative copulas.

H.3.3.11 Wave Period - 0.5 Hour Time Shift

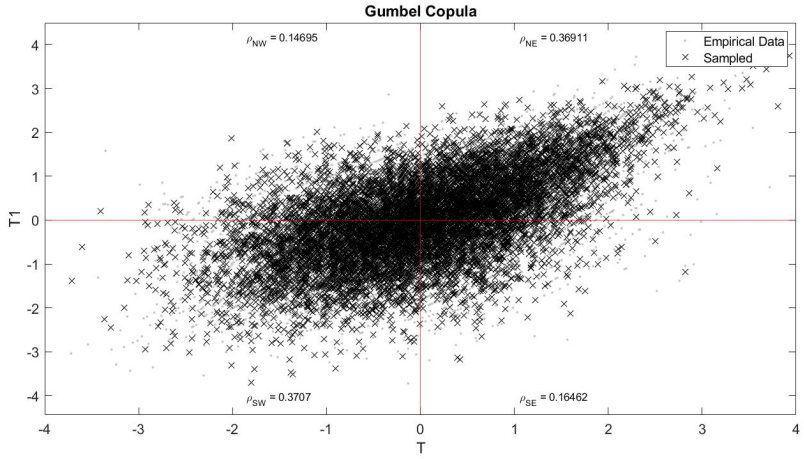

Figure H.56: Normalized scatter plot for the empirical data and 10.000 copula samples.

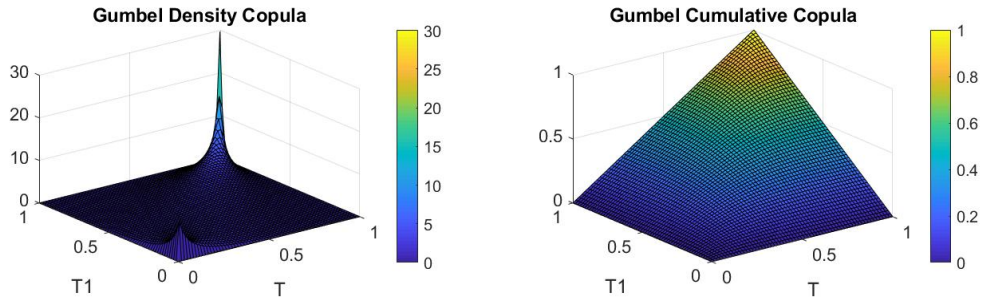

Figure H.57: Bi-variate density and cumulative copulas.

H.3.3.12 Wave Period - 1 Hour Time Shift

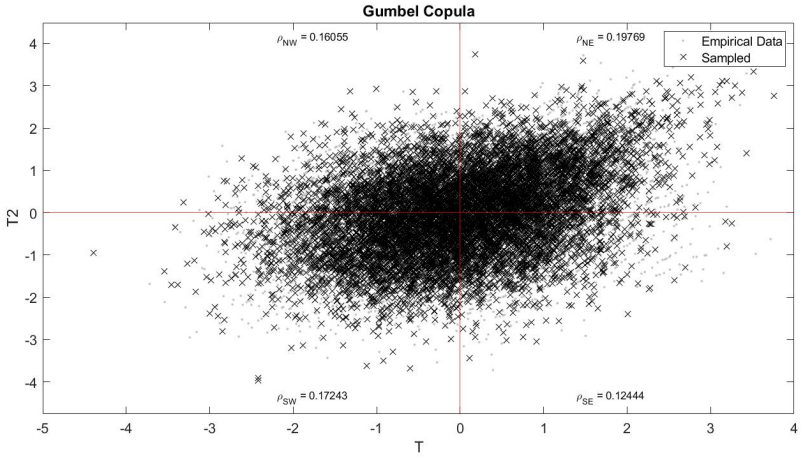

Figure H.58: Normalized scatter plot for the empirical data and 10.000 copula samples.

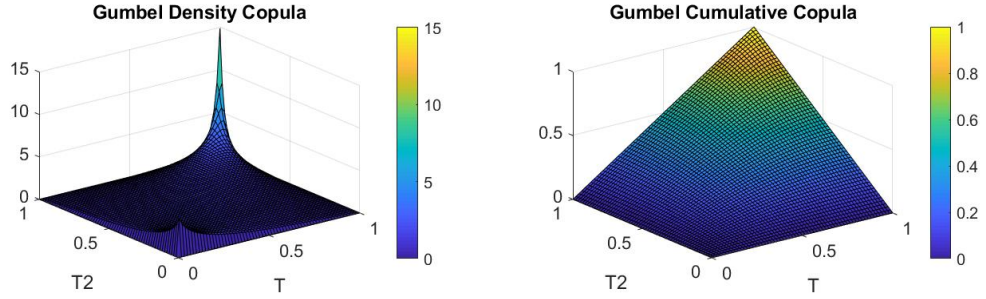

Figure H.59: Bi-variate density and cumulative copulas.

H.3.3.13 Wave Period - 1.5 Hours Time Shift

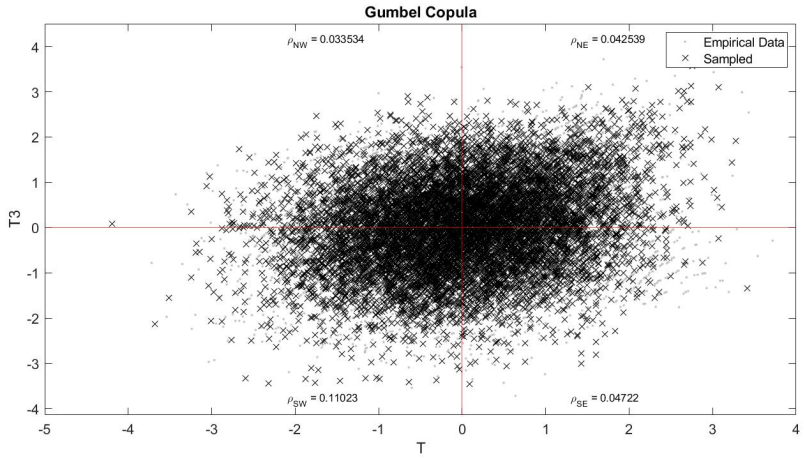

Figure H.60: Normalized scatter plot for the empirical data and 10.000 copula samples.

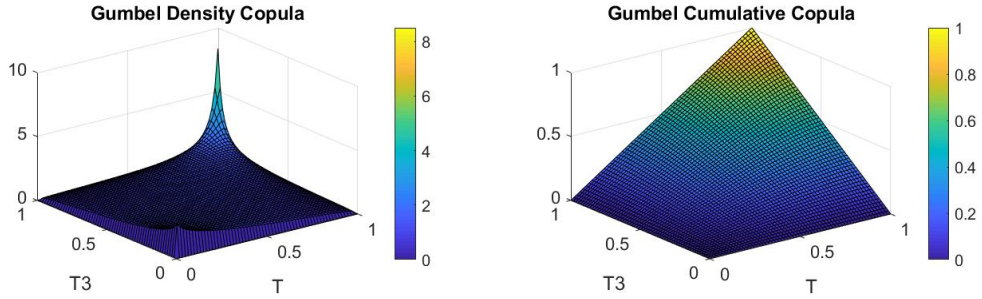

Figure H.61: Bi-variate density and cumulative copulas.

I

Calibration Probabilistic Models

Both the static and the dynamic Bayesian network are calibrated to ensure simplicity of the model. The process of calibration is conducted using a series of node and arc constructions to represent the system. Ultimately all possible variants are compared in terms of accuracy to the empirical data to determine which option was best fit to model the system.

I.1. Static Bayesian Network

Calibration of the static Bayesian network (SBN) was conducted using only the SBN created in MATLAB using the BANSHEE toolbox (Paprotny et al., 2020). Ultimately the application of the BN should provide accurate nearshore wave height values. Therefore, the various DAG scenarios were assessed in terms of nearshore wave height accuracy (compared to empirical values) and in terms of model simplicity (i.e. number of arcs and nodes). The full synthetic dataset was compressed to include only values for which their were nearshore wave height measurements.

I.1.1. Fully Saturated

A Bayesian network that is fully saturated has arcs between all nodes. Assessment of the parameter groups naturally removes many of the arcs (i.e. between vegetation and hydraulic). This results in the graph and rank correlation structure shown in Figure I.1.

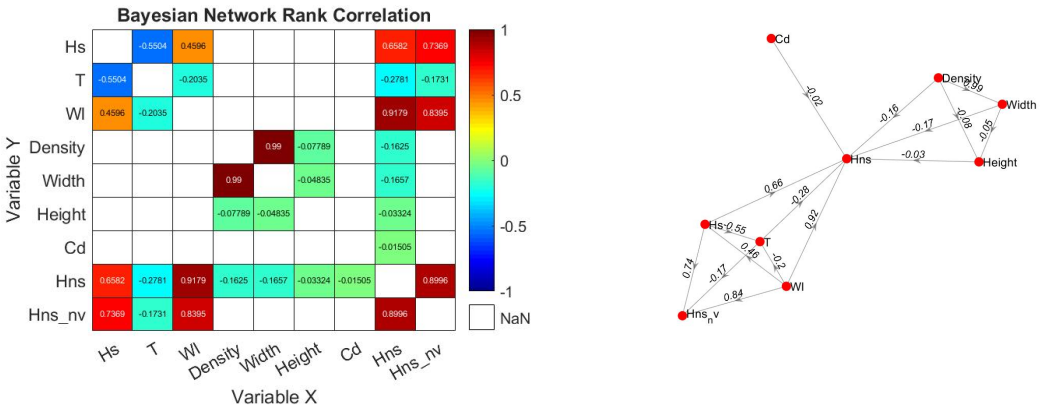

Figure I.1: Rank correlation matrix for semi-saturated static BN (left) and visualized BN structure (right)

Using inference through the BN, the nearshore wave height with and without vegetation was determined as depicted in Figure I.2. As 10000 samples were drawn for each distribution, the confidence bounds (dashed lines) show the range of outcomes. Using the 90% confidence bounds and comparing the empirical value with these bounds the accuracy of the model was determined to be 93% for the nearshore wave height with vegetation included and 84% for the nearshore wave height with vegetation excluded.

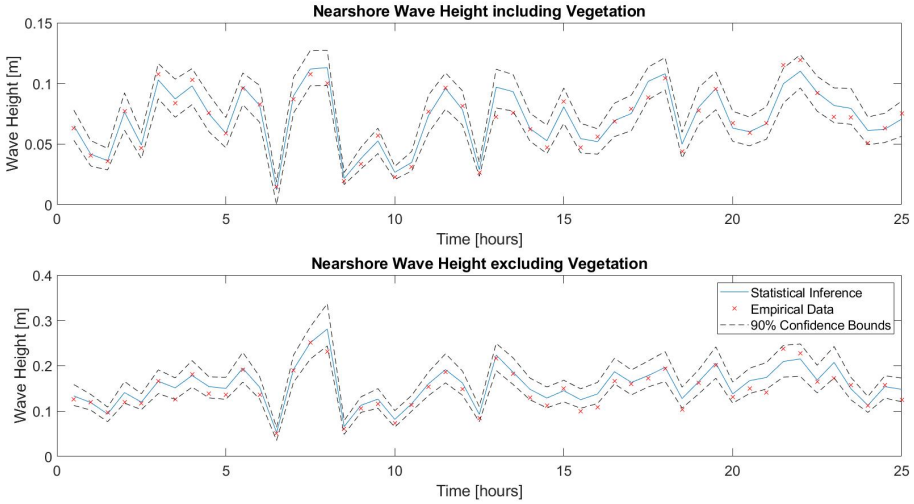

Figure I.2: Inference through the SBN for nearshore wave height without vegetation (top) and with vegetation (bottom)

I.1.2. Vegetation Independence

The notion of vegetation independence is not physically grounded as there is naturally inter dependence between these parameters. Nevertheless, these variables were synthetically developed in this thesis and therefore the actual dependence between these variables is unknown. Both the rank correlation matrix and the BN structure are presented in Figure I.3.

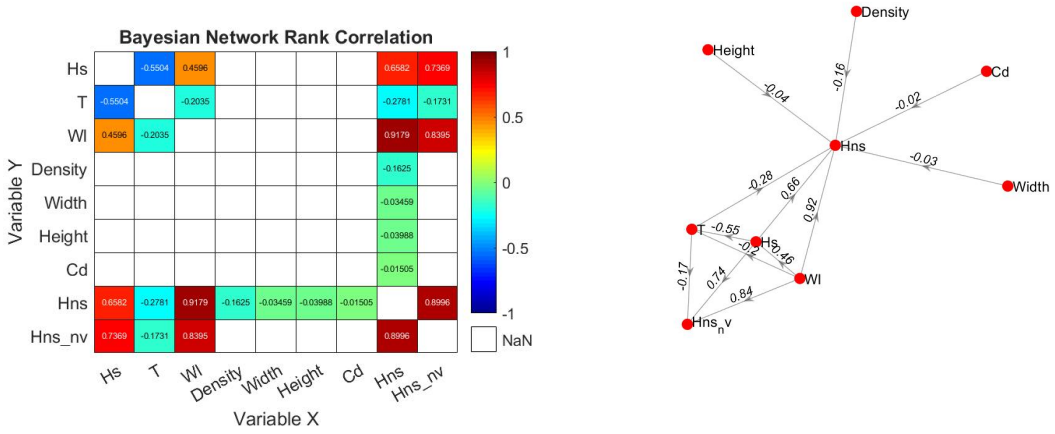

Figure I.3: Rank correlation matrix for the static BN (left) and visualized BN structure (right)

Using inference through the BN, the nearshore wave height with and without vegetation was determined as depicted in Figure I.4. As 10000 samples were drawn for each distribution, the confidence bounds (dashed lines) show the range of outcomes. Using the 90% confidence bounds and comparing the empirical value with these bounds the accuracy of the model was determined to be 95,9% for the nearshore wave height with vegetation included and 84% for the nearshore wave height with vegetation excluded.

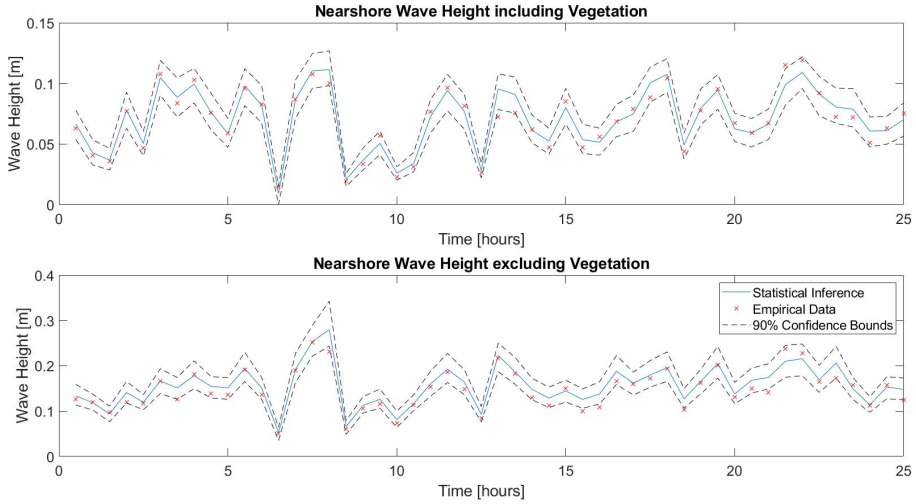

Figure I.4: Inference through the SBN for nearshore wave height without vegetation (top) and with vegetation (bottom)

I.1.3. Hydraulic Independence

Another DAG variant in which all hydraulic variables are assumed independent while maintaining full saturation for the vegetation parameters. Both the rank correlation matrix and the BN structure are presented in Figure I.5.

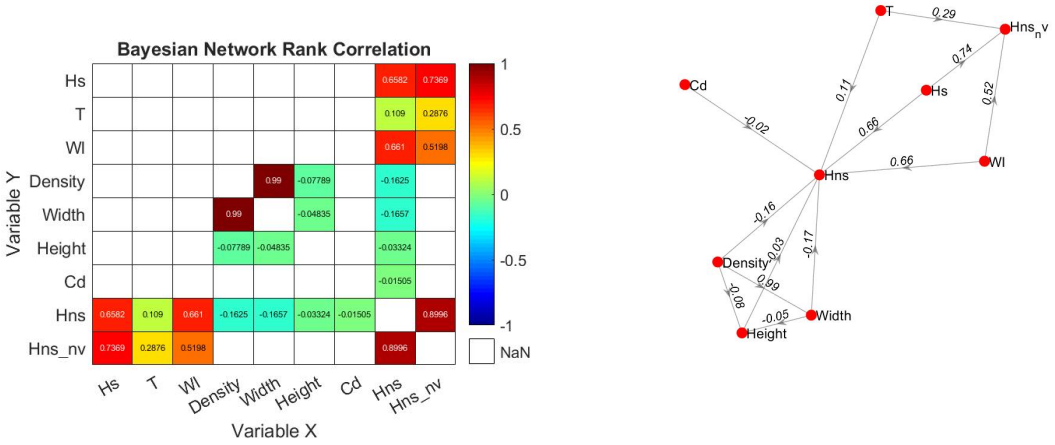

Figure I.5: Rank correlation matrix for the static BN (left) and visualized BN structure (right)

Using inference through the BN, the nearshore wave height with and without vegetation was determined as depicted in Figure I.6. As 10000 samples were drawn for each distribution, the confidence bounds (dashed lines) show the range of outcomes. Using the 90% confidence bounds and comparing the empirical value with these bounds the accuracy of the model was determined to be 76% for the nearshore wave height with vegetation included and 83.5% for the nearshore wave height with vegetation excluded.

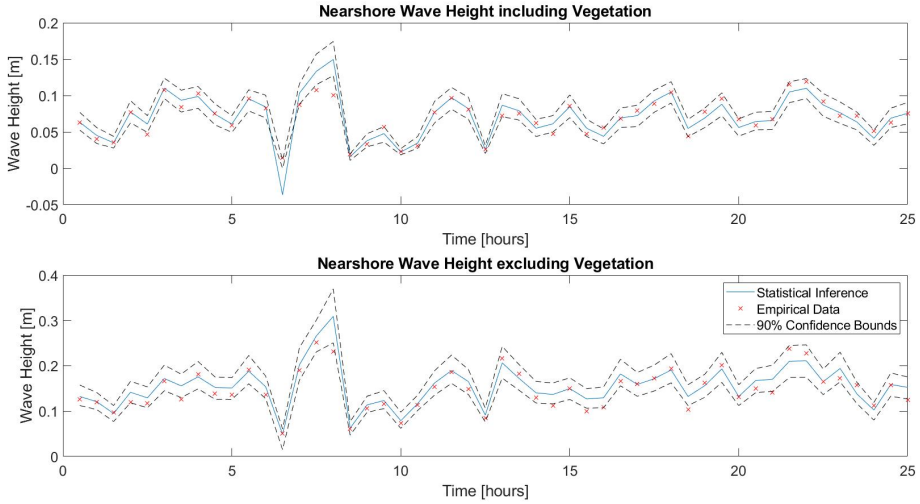

Figure I.6: Inference through the SBN for nearshore wave height without vegetation (top) and with vegetation (bottom)

I.1.4. Hydraulic Simplification

The dependence between water level and wave period was below 0.4 and was thus removed. This variant only assesses stronger correlation structures in the BN. Both the rank correlation matrix and the BN structure are presented in Figure I.7.

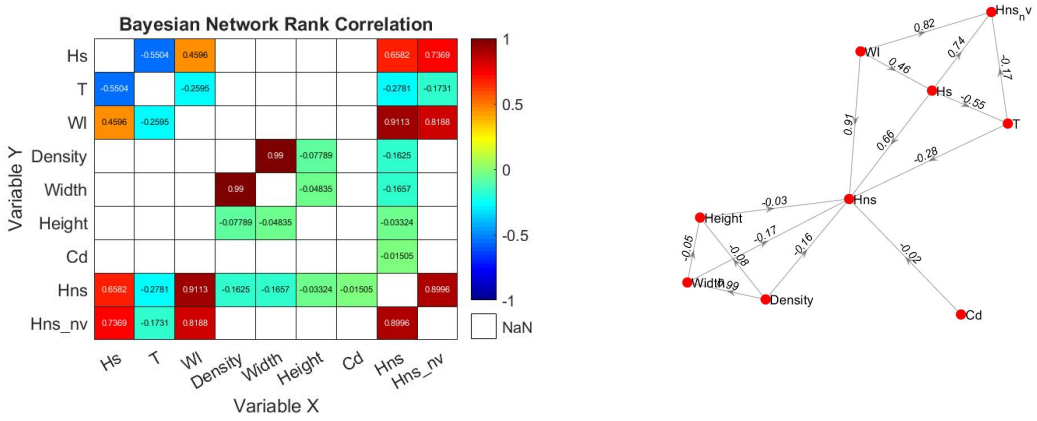

Figure I.7: Rank correlation matrix for the static BN (left) and visualized BN structure (right)

Using inference through the BN, the nearshore wave height with and without vegetation was determined as depicted in Figure I.8. As 10000 samples were drawn for each distribution, the confidence bounds (dashed lines) show the range of outcomes. Using the 90% confidence bounds and comparing the empirical value with these bounds the accuracy of the model was determined to be 91.5% for the nearshore wave height with vegetation included and 85% for the nearshore wave height with vegetation excluded.

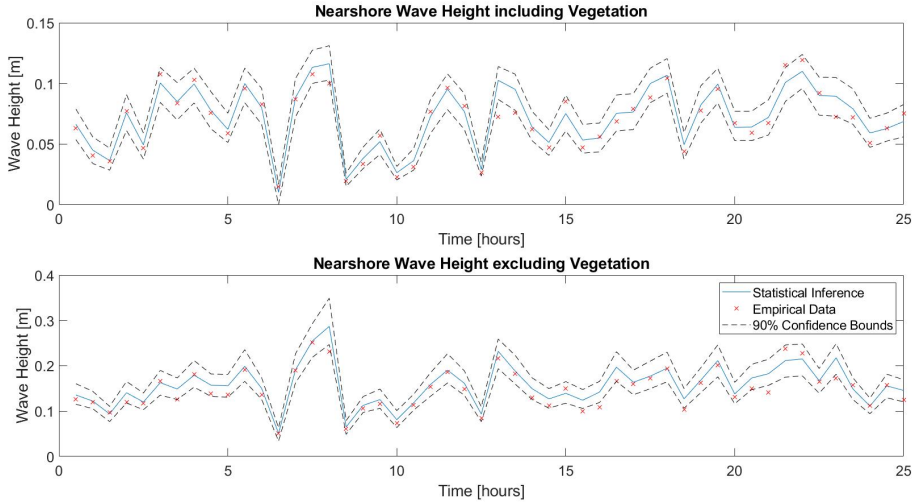

Figure I.8: Inference through the SBN for nearshore wave height without vegetation (top) and with vegetation (bottom)

I.1.5. Hydraulic & Vegetation Simplification

Combining the simplification of the vegetation dependence structure and combining it with the reduced dependence structure for hydraulic variables results in the final SBN variant. Both the rank correlation matrix and the BN structure are presented in Figure I.9.

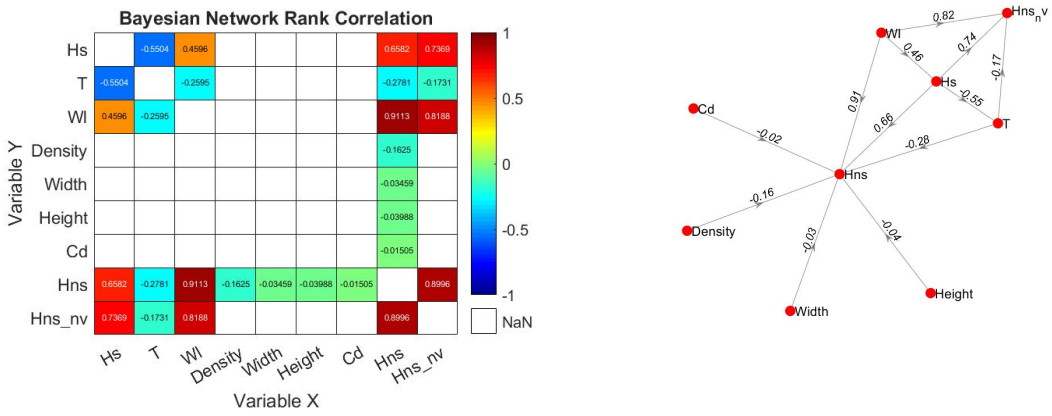

Figure I.9: Rank correlation matrix for the static BN (left) and visualized BN structure (right)

Using inference through the BN, the nearshore wave height with and without vegetation was determined as depicted in Figure I.10. As 10000 samples were drawn for each distribution, the confidence bounds (dashed lines) show the range of outcomes. Using the 90% confidence bounds and comparing the empirical value with these bounds the accuracy of the model was determined to be 93% for the nearshore wave height with vegetation included and 85% for the nearshore wave height with vegetation excluded.

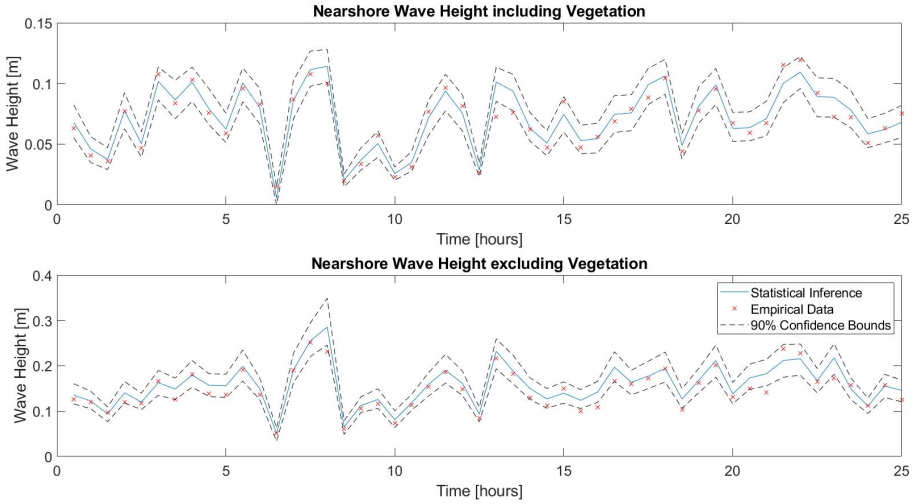

Figure I.10: Inference through the SBN for nearshore wave height without vegetation (top) and with vegetation (bottom)

I.1.6. Overview

For all DAG variants the accuracy for nearshore wave height with and without vegetation on the foreshore is determined by comparison with the 90% confidence bounds of the sampled values. These results are presented together with the amount of arcs in each DAG in Table I.1.

Table I.1: Summary of all static Bayesian network results in terms of accuracy and simplicity

DAG Variant	**Accuracy $\mathbf{H}_{ns}$ [%]**	**Accuracy $\mathbf{H}_{ns,nv}$ [%]**	**Arcs**
Saturation	92	84	16
Vegetation Independence	93	84	13
Hydraulic Independence	76	83	13
Hydraulic Simplification	91	85	15
Hydraulic & Vegetation Simplification	93	85	12

Based on both accuracy and simplicity the final variant is chosen as the representative DAG.

I.2. Dynamic Bayesian Network

The approach for developing a DBN was related to the autocorrelation values for the offshore hydraulic variables. As the autocorrelation decreases so does the relation between those time states. While the wave height and wave period decrease to 0 over time, which instinctively makes sense from a physical point of view, thew water level auto correlation oscillates. This periodic movement of the autocorrelation is physically related tot the tidal motion. The corresponding autocorrelation plots are shown in Figure I.11.

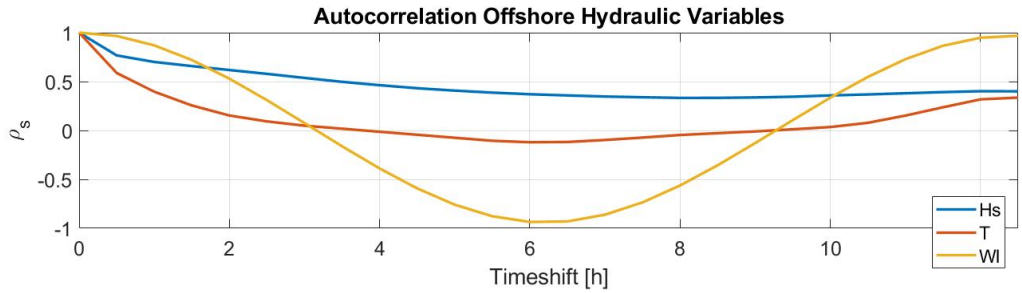

Figure I.11: Autocorrelation plot for offshore water level that is shifted through time and assessed in terms of Spearmans correlation coefficient.

The objective in developing a DBN that accurately models variables in the current time step based on its previous time states, the autocorrelation plays an important role. Namely, it represents dependence between the variables that can be used to relate the states to one another. Therefore, various combinations of time states were chosen to be included in the DAG structure of the DBN to assess their ability to model both the periodic movement (i.e. most notable in the tides) and their general accuracy of modelling the offshore variables within their 90% confidence bounds. Moreover, simplicity waas assessed through the amount of arcs and nodes present in the DBN. The variants and their accuracy are presented in Table I.2.

Table I.2: Summary of all DAG variant results in terms of accuracy and simplicity. Where the accuracy of the period is defined on a scale from able (++) to unable (–).

	Accuracy [%]				**Simplicity**	
Variant	**Wl**	**Hs**	**Tp**	**Period**	**Arcs**	**Nodes**
1	23	65	53	- -	5	6
2	16	63	44	- -	8	9
3	13	67	64	+	11	9
4	16	16	36	- -	11	12
5	17	66	57	-	20	12
6	11	66	66	+	24	13
7	28	70	71	++	25	11

I.2.1. Variant 1: 0.5 Hour Time-shift

In this variant all offshore variables were included as well as their 0.5 hour time shifted components. The corresponding rank correlation matrix and network structure are provided in Figure I.12.

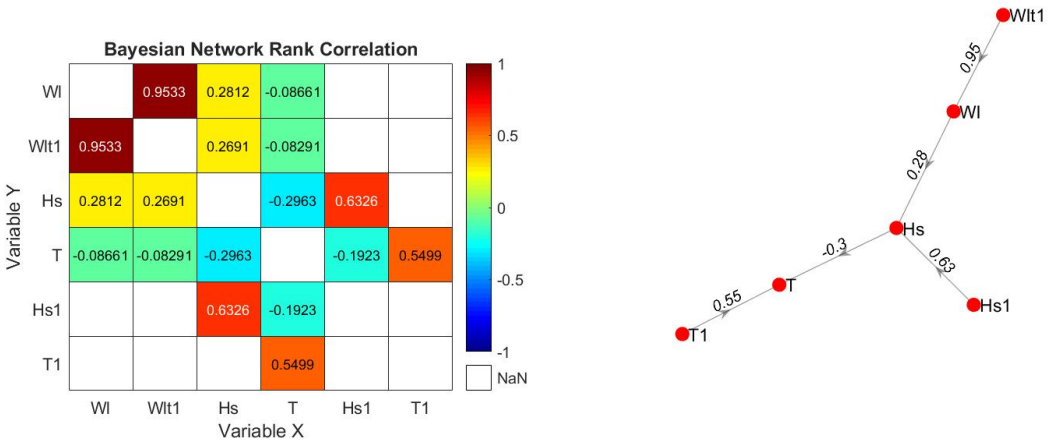

Figure I.12: Rank correlation matrix for the dynamic BN (left) and visualized dynamic BN structure (right)

Using the previous three determined water levels, the water level in the current time step was determined through inference. 1000 samples were drawn to determine the offshore water level time series in each time step. Using the mean and 90% confidence bounds(dashed lines) of the sample the accuracy was determined as shown in Figure I.13. The graph clearly shows the trend of the DBN towards the mean, and the inability to model the periodic character of the water level. For water level, wave height and wave period, the accuracy was determined to be 23%, 65% and 53% respectively for a period of 50 hours. Moreover, it is not able to represent the periodic motion of the variables.

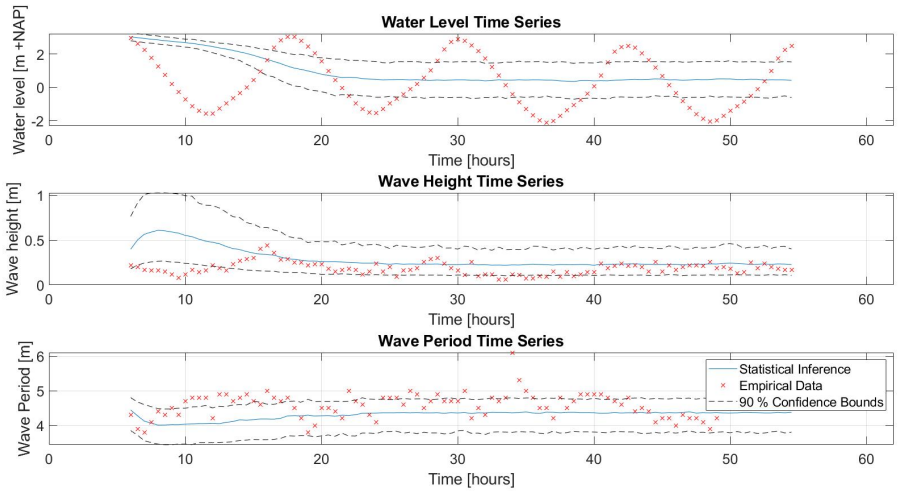

Figure I.13: Inference through the DBN for offshore water level.

I.2.2. Variant 2: 1 Hour Time-shift Low Saturation

In this variant all offshore variables were included as well as their 0.5 and 1 hour time shifted components. The corresponding rank correlation matrix and network structure are provided in Figure I.14.

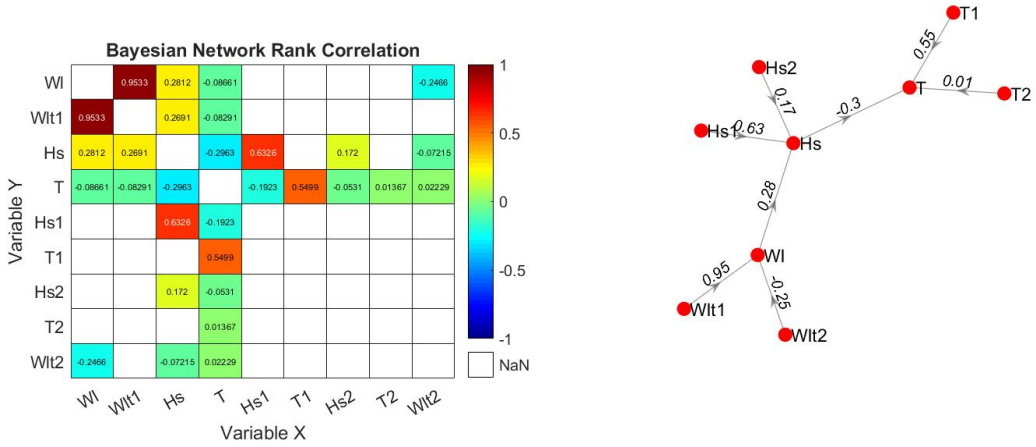

Figure I.14: Rank correlation matrix for the dynamic BN (left) and visualized dynamic BN structure (right)

Using the previous three determined water levels, the water level in the current time step was determined through inference. 1000 samples were drawn to determine the offshore water level time series in each time step. Using the mean and 90% confidence bounds(dashed lines) of the sample the accuracy was determined as shown in Figure I.15. The graph clearly shows the trend of the DBN towards the mean, and the inability to model the periodic character of the water level. For water level, wave height and wave period, the accuracy was determined to be 16%, 63% and 44% respectively for a period of 50 hours. Moreover, this variant was not able to represent the periodic motion of the variables.

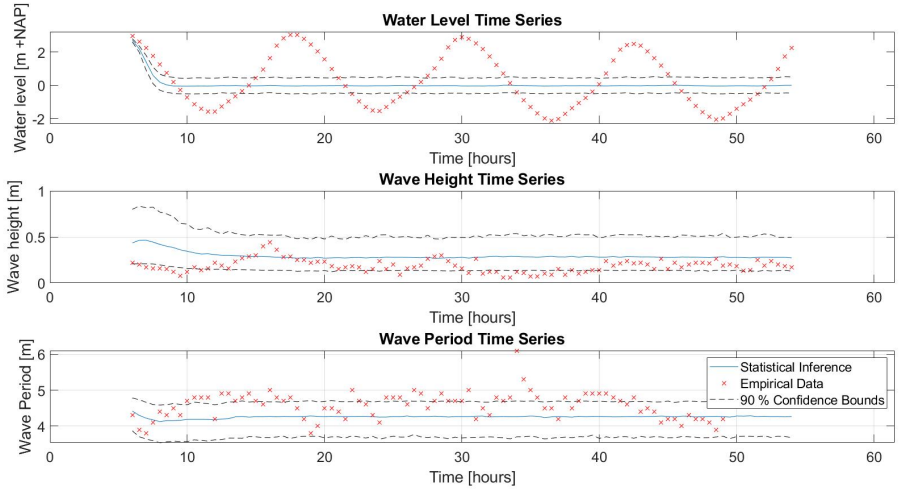

Figure I.15: Inference through the DBN for offshore water level.

I.2.3. Variant 3: 1 Hour Time-shift Full Temporal Saturation

In this variant all offshore variables were included as well as their 0.5 and 1 hour time shifted components. The corresponding rank correlation matrix and network structure are provided in Figure I.16.

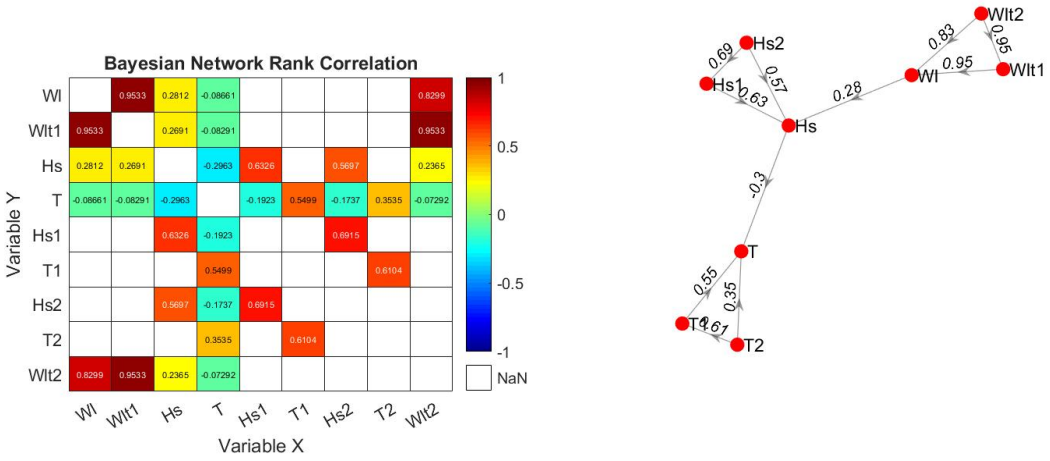

Figure I.16: Rank correlation matrix for the dynamic BN (left) and visualized dynamic BN structure (right)

Using the previous three determined water levels, the water level in the current time step was determined through inference. 1000 samples were drawn to determine the offshore water level time series in each time step. Using the mean and 90% confidence bounds(dashed lines) of the sample the accuracy was determined as shown in Figure I.17. The graph clearly shows the trend of the DBN towards the mean, and the inability to model the periodic character of the water level. For water level, wave height and wave period, the accuracy was determined to be 13%, 67% and 64% respectively for a period of 50 hours. Moreover, this variant was not able to represent the periodic motion of the variables.

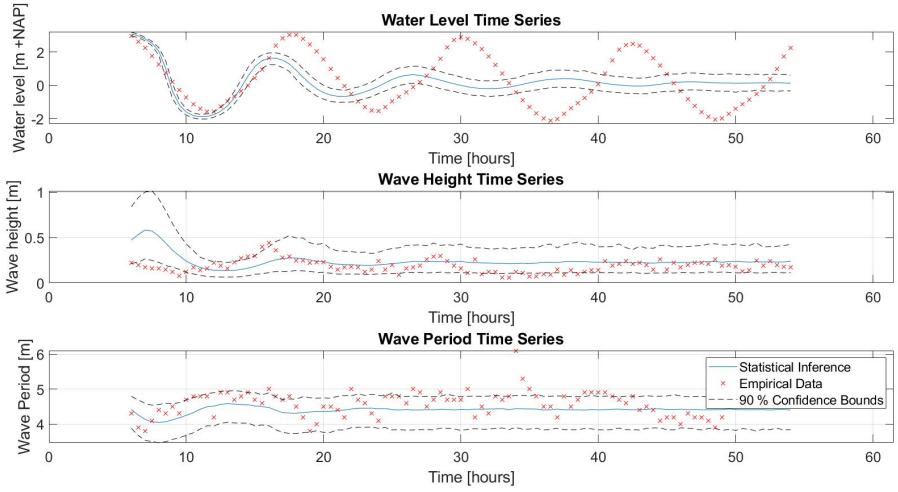

Figure I.17: Inference through the DBN for offshore water level.

I.2.4. Variant 4: 1.5 Hour Time-shift Simple Saturation

In this variant all offshore variables were included as well as their 0.5, 1 and 1.5 hour time shifted components. The corresponding rank correlation matrix and network structure are provided in Figure I.18.

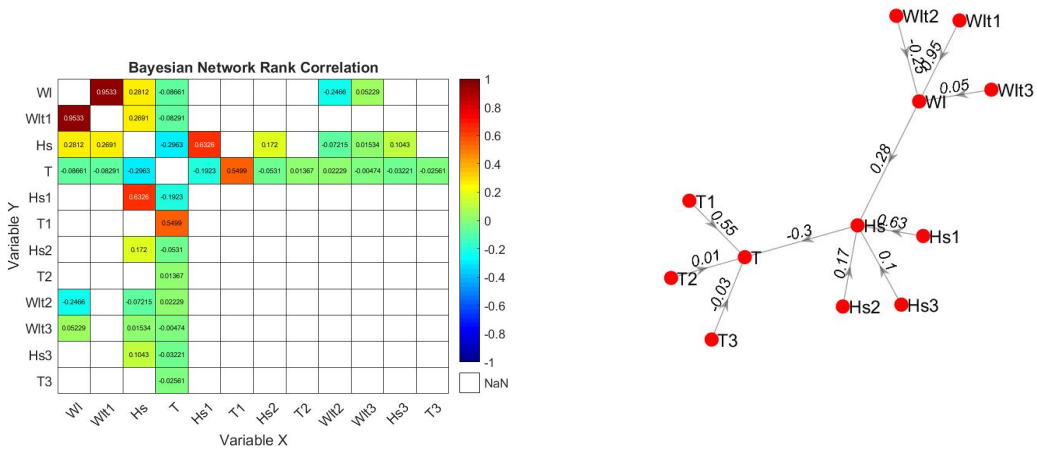

Figure I.18: Rank correlation matrix for the dynamic BN (left) and visualized dynamic BN structure (right)

Using the previous three determined water levels, the water level in the current time step was determined through inference. 1000 samples were drawn to determine the offshore water level time series in each time step. Using the mean and 90% confidence bounds(dashed lines) of the sample the accuracy was determined as shown in Figure I.19. The graph clearly shows the trend of the DBN towards the mean, and the inability to model the periodic character of the water level. For water level, wave height and wave period, the accuracy was determined to be 16%, 16% and 36% respectively for a period of 50 hours. Moreover, this variant was not able to represent the periodic motion of the variables.

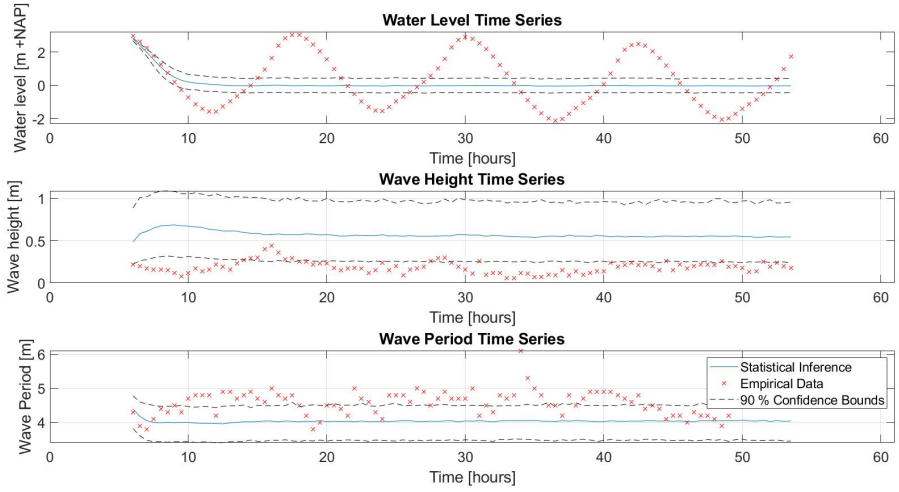

Figure I.19: Inference through the DBN for offshore water level.

I.2.5. Variant 5: 1.5 Hour Time-shift Full Saturation

In this variant all offshore variables were included as well as their 0.5, 1 and 1.5 hour time shifted components. The corresponding rank correlation matrix and network structure are provided in Figure I.20.

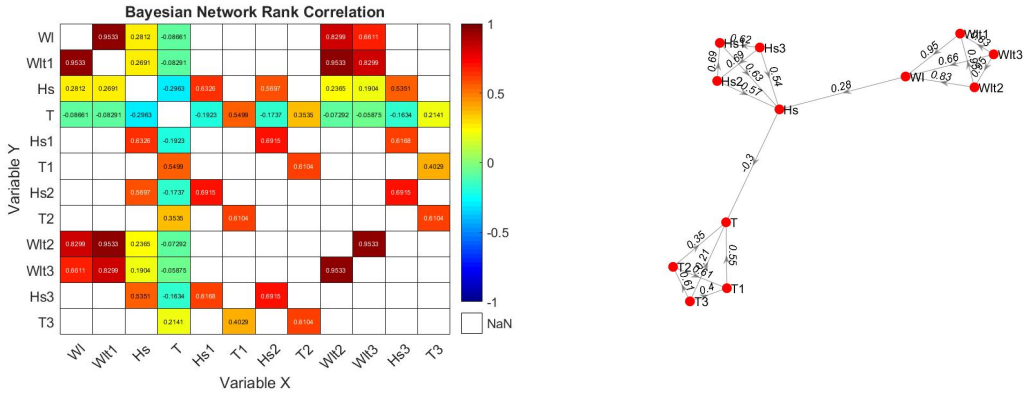

Figure I.20: Rank correlation matrix for the dynamic BN (left) and visualized dynamic BN structure (right)

Using the previous three determined water levels, the water level in the current time step was determined through inference. 1000 samples were drawn to determine the offshore water level time series in each time step. Using the mean and 90% confidence bounds(dashed lines) of the sample the accuracy was determined as shown in Figure I.21. The graph clearly shows the trend of the DBN towards the mean, and the inability to model the periodic character of the water level. For water level, wave height and wave period, the accuracy was determined to be 17%, 66% and 57% respectively for a period of 50 hours. Moreover, this variant was not able to represent the periodic motion of the variables.

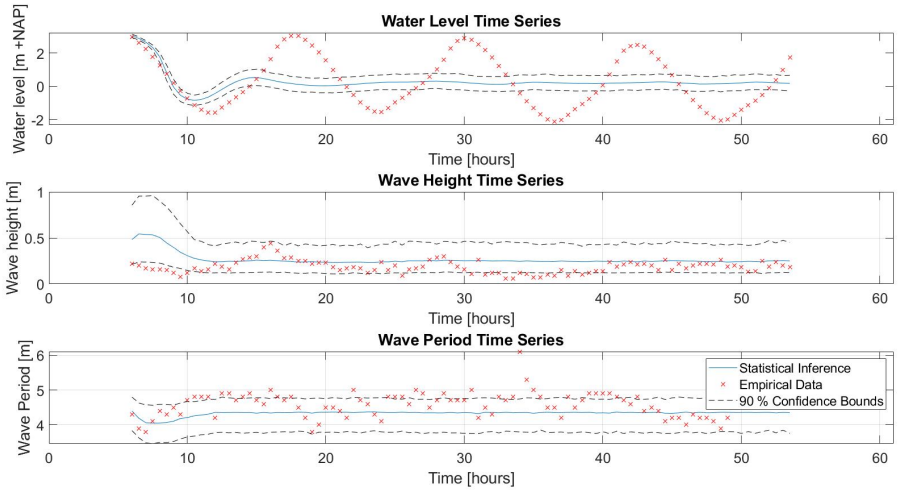

Figure I.21: Inference through the DBN for offshore water level.

I.2.6. Variant 6: 3 Hour Time-shift Full Saturation

In this variant all offshore variables were included as well as their 0.5, 1, 1.5 hour time shifted components. For the water level its 3 hour timeshifted component was included. The corresponding rank correlation matrix and network structure are provided in Figure I.22.

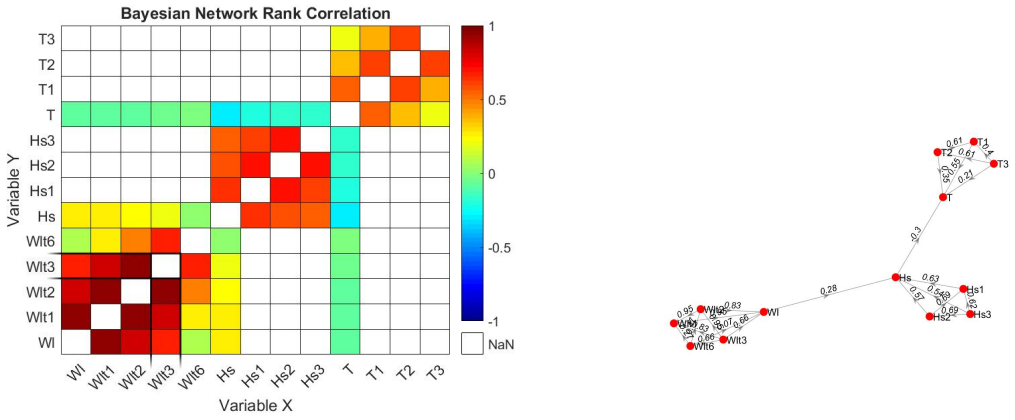

Figure I.22: Rank correlation matrix for the dynamic BN (left) and visualized dynamic BN structure (right)

Using the previous three determined water levels, the water level in the current time step was determined through inference. 1000 samples were drawn to determine the offshore water level time series in each time step. Using the mean and 90% confidence bounds(dashed lines) of the sample the accuracy was determined as shown in Figure I.23. The graph clearly shows the trend of the DBN towards the mean, and the inability to model the periodic character of the water level. For water level, wave height and wave period, the accuracy was determined to be 11%, 66% and 66% respectively for a period of 50 hours. Moreover, this variant was not able to represent the periodic motion of the variables.

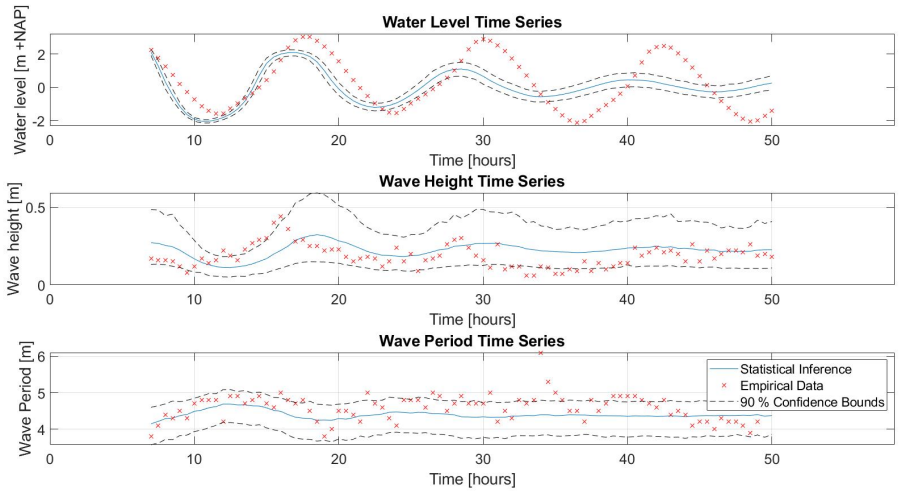

Figure I.23: Inference through the DBN for offshore water level.

I.2.7. Variant 7: 6 Hour Time-shift Full Saturation

In this variant all offshore variables were included as well as their 0.5 hour time shifted components. For the water level its 1, 1.5, 3, 5.5 and 6 hour time shifted components were included. The corresponding rank correlation matrix and network structure are provided in Figure I.24.

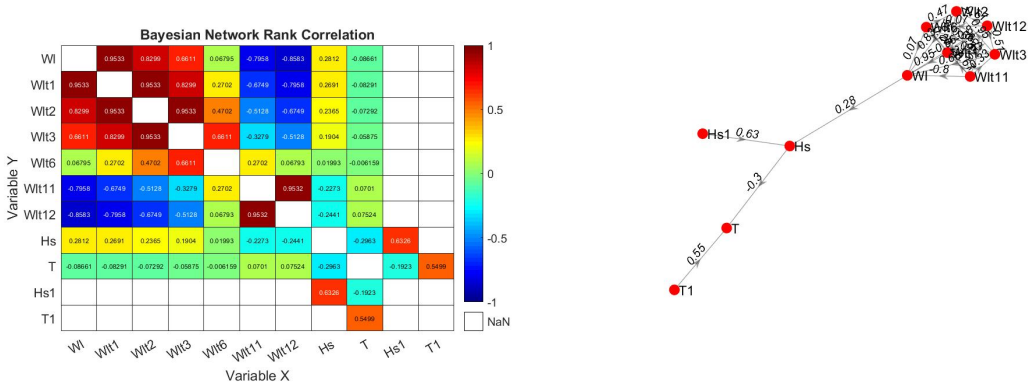

Figure I.24: Rank correlation matrix for the dynamic BN (left) and visualized dynamic BN structure (right)

Using the previous three determined water levels, the water level in the current time step was determined through inference. 1000 samples were drawn to determine the offshore water level time series in each time step. Using the mean and 90% confidence bounds(dashed lines) of the sample the accuracy was determined as shown in Figure I.25. The graph clearly shows the trend of the DBN towards the mean, and the inability to model the periodic character of the water level. For water level, wave height and wave period, the accuracy was determined to be 28%, 70% and 71% respectively for a period of 50 hours. Moreover, this variant was able to represent the periodic motion of the variables.

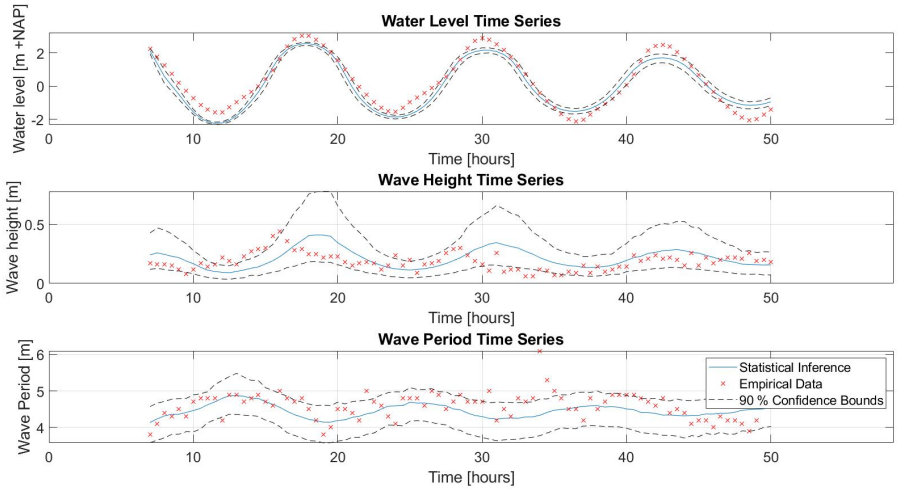

Figure I.25: Inference through the DBN for offshore water level.

J

Validation Probabilistic Models

Validation of both Bayesian networks was conducted to ensure that the model used was valid in a statistical and physical sense. The validation approach was segmented per BN (i.e. static and dynamic). Statistical validation was conducted by partly using the copula analysis available in the statistical analysis (appendix H) and complemented with a Cramer von Mises (CVM) statistic to assess the copula structures of the BN. Additionally the d-calibration score of the empirical rank correlation matrix was examined for the sake of completeness. The combination was used to assess the statistical validity of the BN.

Two sided sampling was used to assess the physical accuracy of the model. Splitting the dataset created two halves. The first was used to obtain the rank correlation matrix and marginal distributions for the BN. The other half was applied to conditionalize the BN and to compare the sampled output with. This method ensures independence between the training dataset and the validation dataset.

J.1. Static Bayesian Network

The SBN structure consists of multiple parameters that are represented by a single Bayesian network. Representing the model using a Bayesian network was assessed in terms of statistical and physical validity.

J.1.1. Statistical Validity

The validity of applying a BN depends on the underlying copula structures as a BN uses a Gaussian copula to represent the multivariate dependence structure. The statistical analysis in appendix H provided insight into the limitation of a Bayesian network as all main copula families (i.e. Gaussian, Clayton, Frank, Gumbel and t) represented the underlying bi-variate dependence structures (Table 5.10.

Determining the best copula fits described above was based on the semi-correlations method. Additionally the Cramer von Mises statistic was determined for all underlying variable pairs to complete the statistical bi-variate analysis of the underlying parameters in the BN. The copula families analysed were Gumbel, Gaussian, Clayton and Frank. The resulting test values are provided in Figure J.1.

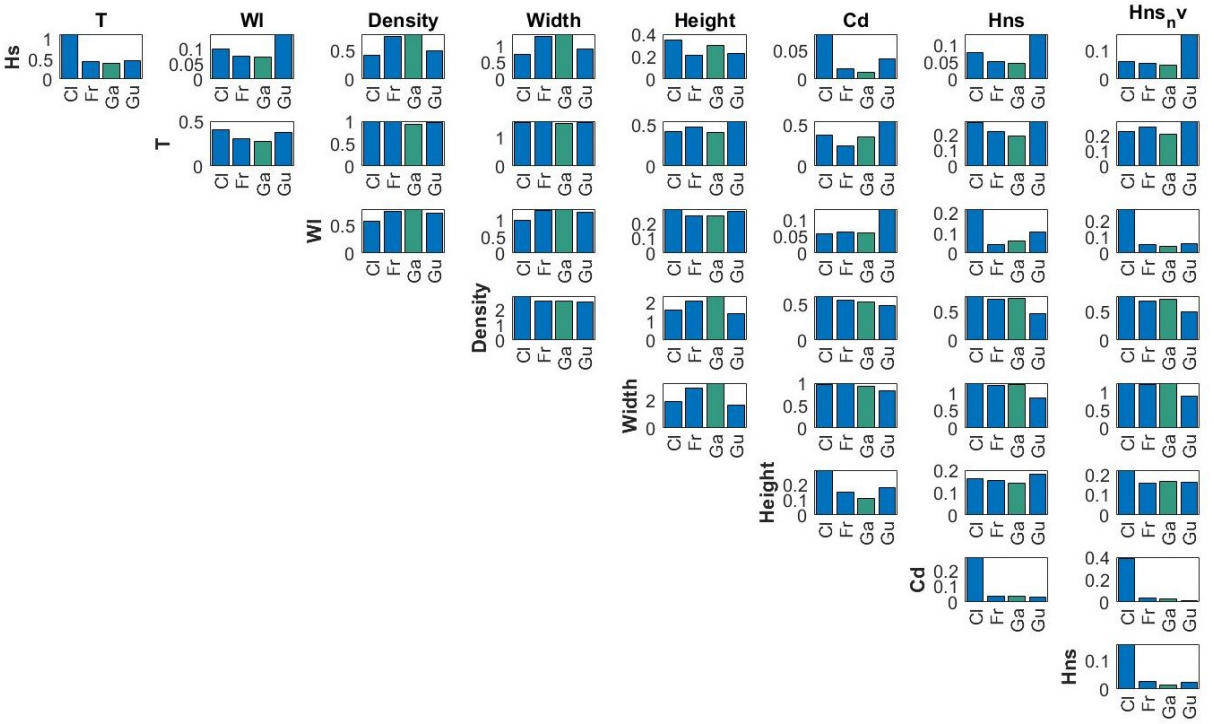

Figure J.1: Resulting Cramer von Mises statistics for all variable pairs included in the static Bayesian network. The Gaussian CVM statistic bar is highlighted in light green.

Out of the 36 variable pairs only six pairs were best represented by a Gaussian copula according to the Cramer van Mises statistic. The resulting accuracy of the Gaussian copula is thus 17% of the variable pairs. This highlights the limitation of the Bayesian network.

The d-calibration score was used to assess the determinant of the empirical rank correlation (ERC) in comparison to the normal rank correlation (NRC) matrix. Two sample sizes were drawn to determine the sample size for which the d-calibration score would lie inside and outside of the 90% confidence bounds of the normal rank correlation matrix. The resulting figures are shown below in Figure J.2.

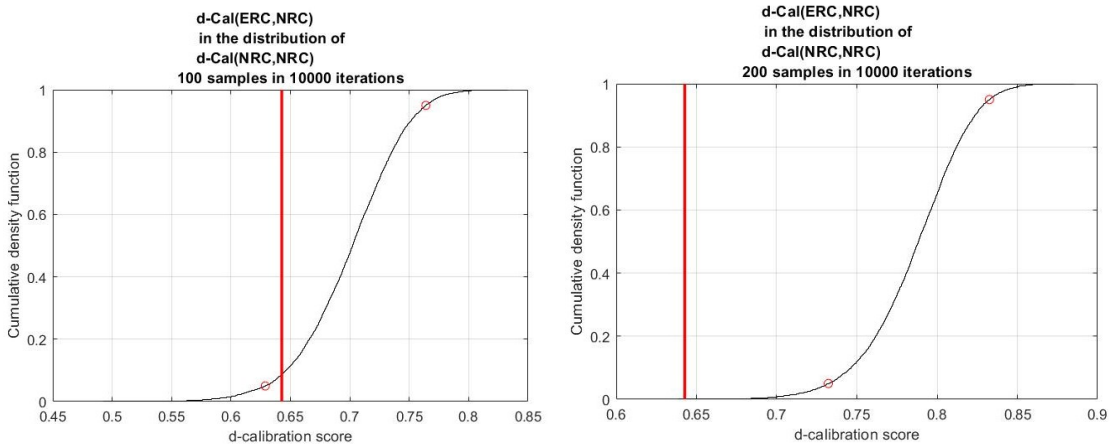

Figure J.2: d-calibration score (red line) for the empirical rank correlation (ERC) matrix in the distribution of the normal rank correlation (NRC) matrix for 100 samples (left) and 200 samples (right).

The resulting d-calibration scores provides another example of the limitation of the Bayesian network.

Drawing more than 100 samples results in the d-calibration score falling outside of the 90% confidence bounds. This is not uncommon as the d-calibration statistic is rather severe for larger datasets Hanea et al. (2015) as a larger set of variables leads to a lower determinant, thus making comparison more difficult.

Although acceptance of the d-calibration score for 100 samples is not unacceptable in terms of statistical validity, it underlines the limitations of the Gaussian copula structure that is forced upon the bi-variate dependence structures that are naturally not normal. Given the fact that the model is based on a large dataset with many variables and non-Gaussian bi-variate copula structures the current model is acceptable within its current application and can be improved in further research.

J.1.2. Physical Validity

Applying a two sided sampling method provided an initial application of the SBN using actual data. Conditionalizing all parameters except the nearshore wave heights and subsequently drawing 10000 samples from the corresponding conditionalized distributions resulted in a mean output value including the 90% confidence bounds of the sample. The accuracy of the sampled nearshore wave heights was again conducted through comparison of the sampled confidence bounds with the validation dataset. The resulting sampled nearshore wave height graphs for 50 hours of simulations are shown in Figure J.3 for which the accuracy was found to be 89% and 91% respectively for including and excluding vegetation on the foreshore.

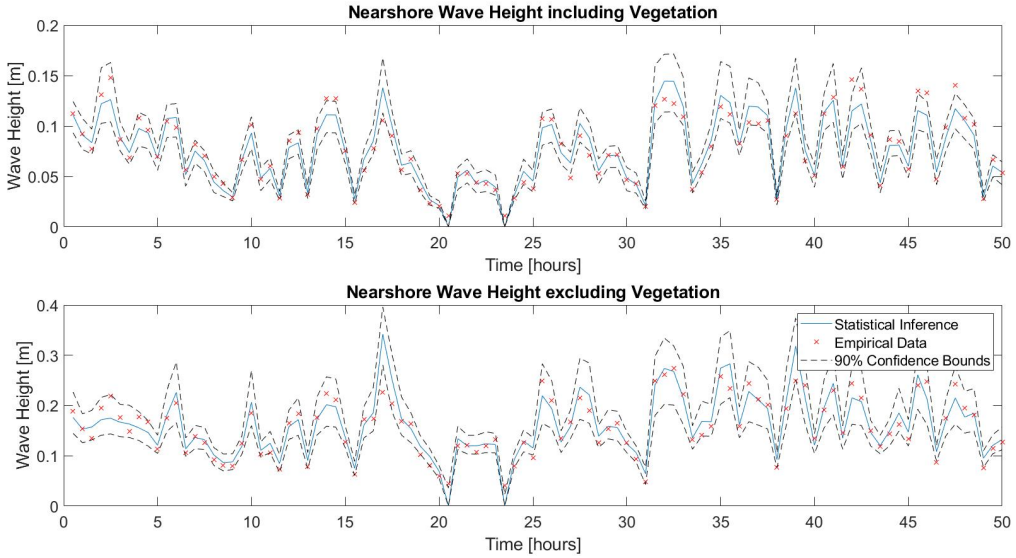

Figure J.3: Comparison of the sampled results of the split test with the validation dataset for nearshore wave heights including vegetation on the foreshore (top) and excluding vegetation on the foreshore (bottom).

J.2. Dynamic Bayesian Network

The DBN structure used to model temporal dependence for the water level was best represented by a network structure containing 7 water level shifted variables. This network, modelled by a dynamic Bayesian network was assessed in terms of statistical and physical validity.

J.2.1. Statistical Validity

Initial statistical validity was assessed in the autocorrelation copula analysis conducted in appendix H. Here semi correlations were used to assess best fit bi-variate copula structures. Gaussian copulas were found to well represent the dependence structure. Complementing the semi correlation validation method,

the CVM statistic was assessed for all variables. The copula families assessed were: Gaussian, Clayton, Gumbel and Frank. Figure J.4 presents the resulting statistics for all variable pairs.

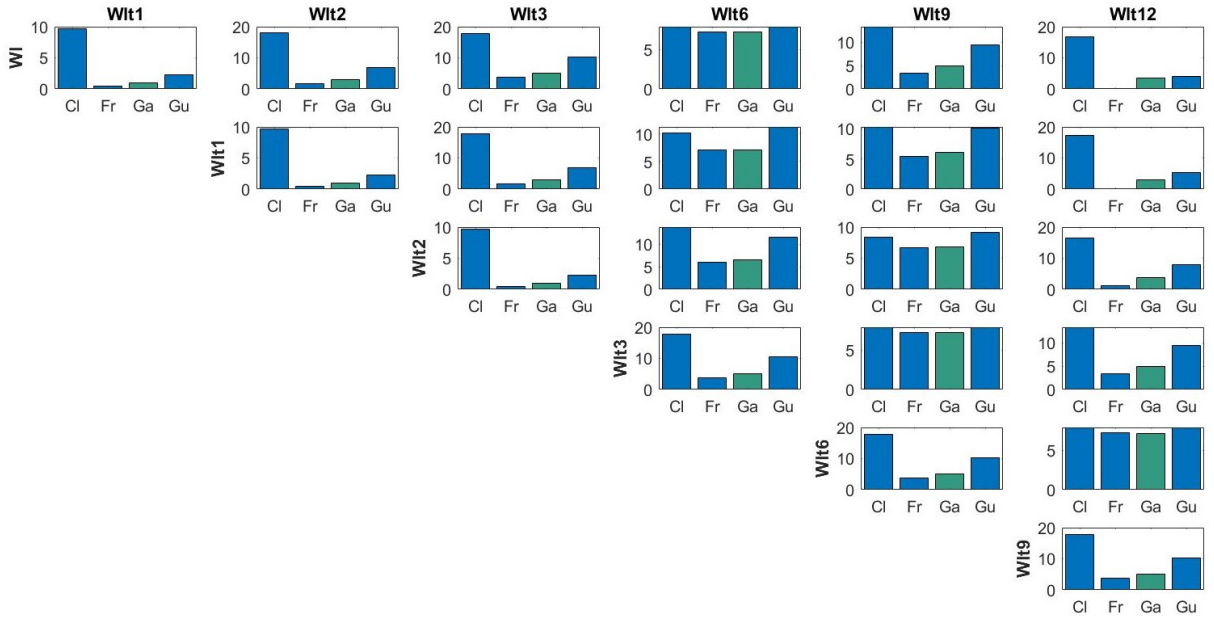

Figure J.4: Resulting Cramer von Mises statistics for all variable pairs included in the static Bayesian network. The Gaussian CVM statistic bar is highlighted in light green.

The CVM statistics contradict the findings in the semi correlation analysis. The Gaussian copula was never found to be the best fit according to the CVM analysis. Instead the Clayton copula best represents almost all variable pairs. This implies that the current Gaussian copula that is forced on the network does not resemble the empirical dependence structure. Naturally this leads to inaccuracies in model application.

The d-calibration score was used to assess the determinant of the empirical rank correlation (ERC) in comparison to the normal rank correlation (NRC) matrix. Two sample sizes were drawn to determine the sample size for which the d-calibration score lies inside and outside of the 90% confidence bounds of the normal rank correlation matrix. The resulting figures are shown below in Figure J.5.

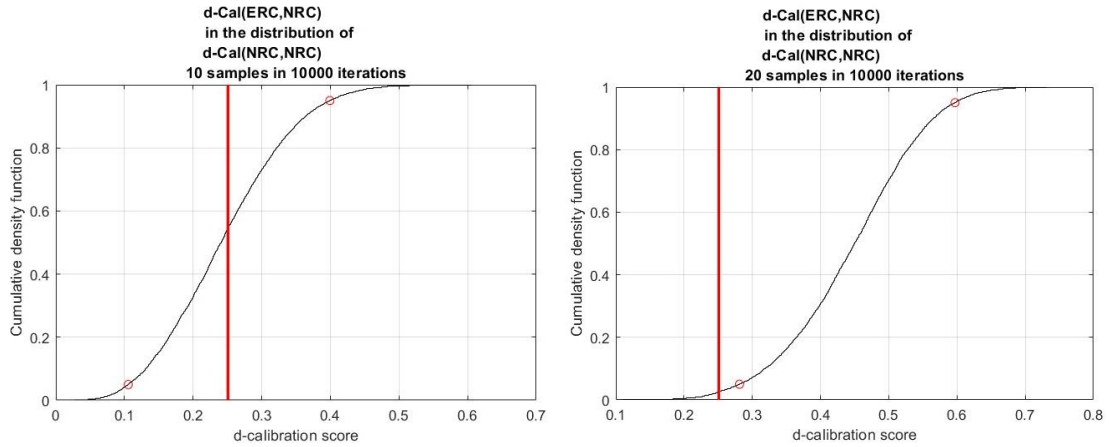

Figure J.5: d-calibration score (red line) for the empirical rank correlation (ERC) matrix in the distribution of the normal rank correlation (NRC) matrix for 10 samples (left) and 20 samples (right).

Complementing the CVM statistic, the d-calibration score underlines the limitation of representing the water level parameters with a Bayesian network. The d-calibration hypothesis was passed only when 10 samples were drawn. A sample size this small will almost always pass the d-calibration hypothesis and it was therefore concluded that the hypothesis was not passed. To ensure statistical validity of the DBN, other methods require analysis to assess better compatibility of the parameter network with the dependence structure.

J.2.2. Physical Validity

A two sided sampling method gave initial insight into actual application results of the DBN. The validation dataset was used to initialize the DBN for the previous 12 time steps for the water levels, whereafter the DBN sampled the water levels, offshore wave periods and offshore wave heights for the subsequent time steps through inference. For all three offshore parameters, 1000 samples were drawn, thus enabling the validation data to be compared with the 90% confidence bounds of the drawn samples. The resulting sampled nearshore wave height graphs for 50 hours of simulations are shown in Figure J.6. The first 6 hours are removed as these resemple the 12 time steps that were used to initiate the water level DBN. The accuracy for the offshore water level, wave height and wave period was found to be 10%, 88% and 85% respectively.

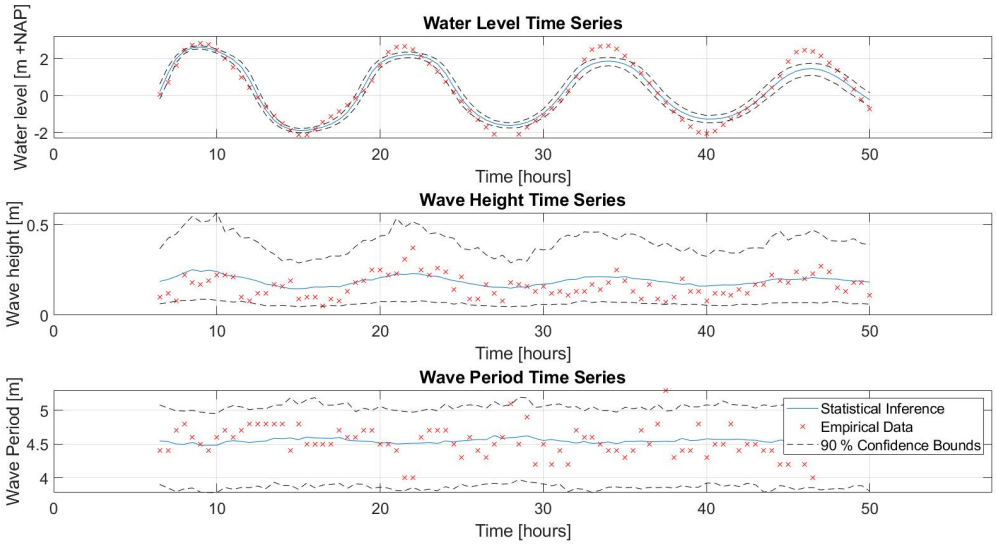

Figure J.6: Comparison of the sampled results of the split test with the validation dataset for offshore variables through time for water level (top), wave height (middle) and wave period (bottom).

K

Bathymetry Parameters Simplification Algorithm

The objective in this appendix was to develop a script that can analyse all bathymetry profiles and return a set of simplified values required for probabilistic modelling. A primary analysis of the output was obtained visually to provide insight into the function of the script. Moreover a statistical analysis of each parameter is performed for each transect.

K.1. Probabilistic Bathymetry Parameters

Due to the spatial and temporal variability of bathymetric profiles, it was simplified by the light brown line shown in figure K.1 to enable probabilistic modelling. The simplification resulted in a set of five parameters that were used to represent the system. At the offshore boundary, a constant offshore slope (S_0) was defined towards the foreshore edge. Thereafter, a foreshore of length (L_f), with a slope (S_f) leads to the toe of the dike. There, a dike with slope (S_d) and crest height (h_c) leads to the nearshore boundary and concludes the profile.

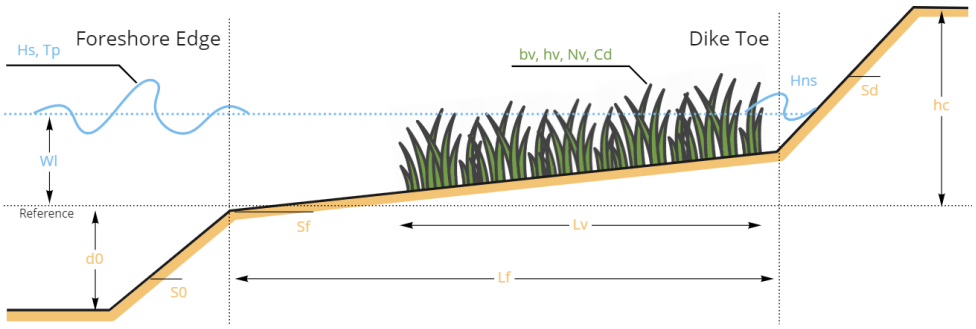

Figure K.1: HFD system with simplified bathymetry parameters usable in probabilistic modelling.

K.2. Simplification Approach

The approach in analysing the existing bathymetry and converting each transect to the simplified parameters defined to represent the bathymetry: offshore depth, offshore slope, vegetation length and vegetation slope. Subsequently, a visual comparison of the actual and simplified data provides insight into the limitations of the simplification. Once completed, the parameters can be analysed over time to give insight into the current temporal variability.

The first step in analysing the transect is loading the original bathymetry data (x,z). Subsequently, the bend points of the bathymetry profile are determined using the second derivative of the (x,z) data using the *deriv* function shown in the MATLAB script provided below. By running this script, the derivative is determined at every grid point in X, the output provides an array with the length of the grid points with the derivative of the input values (X,Z) at every location.

Deriv Function

```
function dx = deriv(X,Z)
for j = 2:length(X)
    dx(j-1) = (Z(j)-Z(j-1))/(X(j)-X(j-1));
end
dx(j) = 0;
end
```

Having obtained an array with second derivatives, the following step was to analyse this array to determine the bend points. This was done using the MATLAB function *Bendpoints*, which splits the array of second derivatives into sections which were analysed individually for the maximum and minimum value. If the value exceeds the minimum threshold, both the value and the index are concatenated to the bend points arrays.

Bendpoints Function

```
function [bend_val, bend_ind] = Bendpoints(X)
thresh = 0.001;
stepsize = 50;

% Split array into segments with size 'stepsize'
nrsteps = length(X)/stepsize;

bend_val = [];
bend_ind = [];

for i = 1:nrsteps-5
    % reset values
    Min = 0;
    Min_i = 0;
    Max = 0;
    Max_i = 0;

    % Determine max and min bending points per stepsize
    segment = X(((i-1)*stepsize)+1:i*stepsize);
    [min_val,min_ind] = min(segment);
    [max_val,max_ind] = max(segment);

    % Determine if min & max exceed minimal threshold
    if abs(min_val) > thresh
        Min = min_val;
        Min_i = min_ind+((i-1)*stepsize)+1;
    end

    if max_val > thresh
        Max = max_val;
        Max_i = max_ind + ((i-1)*stepsize)+1;
    end

    % Add bendpoints and indices to array

    if Min ~=0 && Max ~= 0
        if min_ind < max_ind
            bend_val  = [bend_val Min Max];
            bend_ind  = [bend_ind Min_i Max_i];
        else
            bend_val  = [bend_val Max Min];
            bend_ind  = [bend_ind Max_i Min_i];
        end
    elseif Min ~=0 && Max == 0
        bend_val  = [bend_val Min];
        bend_ind  = [bend_ind Min_i];
    elseif Min ==0 && Max ~= 0
        bend_val = [bend_val Max];
        bend_ind  = [bend_ind Max_i];
    end
end
end
```

With the indices of the bend points available, the function *analyseBendpoints* was developed in MATLAB to determine the index of the first negative derivative which represents the point between the vegetation slope and the offshore slope. Subsequently, the index of the derivative which represents the point between the offshore slope and the offshore depth is determined. With this information available the important indices are known and can be used to create a simplified bathymetry profile.

analyseBendpoints Function

```
function [index] = analyseBendpoints(b_ind,X)
index = [1];
thresh_down = 0.05;

% Return if there are not enough bend points to analyse
if length(b_ind)<3
    return
end

% Correct for the shift in indice location for the first three bendpoints
b_ind(1:3)=[b_ind(1:3)]+1;

% Create an array with all derivatives (X_t)
X_t = X;

% Create an array with the derivatives corresponding with the bendpoints
X = X([b_ind]);

try
    % Analyse derivatives at bend points to determine first negative bend
    % point
    for i = 1:length(X)

        % Check if the derivative is negative and larger than the minimal
        % threshold
        if X(i) < 0 && abs(X(i)) > thresh_down
            index = [index b_ind(i)]; % Add to index if true
            break;
        end
    end

    % Analyse all subsequent derivatives (>i) to determine first positive
    % derivative
    for j = b_ind(i):length(X_t)
        if X_t(j) > 0
            index = [index j];
            break;
        end
    end
% Catch possible errors and ensure continuation of the script
catch ME
    if (strcmp(ME.identifier,'MATLAB:catenate:dimensionMismatch'))
        msg = ['Could not find derivative in vaklodingen above set threshold'];
        causeException = MException('MATLAB:analysingVaklodingen',msg);
        ME = addCause(ME,causeException);
    end
    rethrow(ME)
end
```

Using the indices and the original bathymetry data, three simplified lines are drawn to represent the original dataset. The first line represents the foreshore where the vegetated section spans from the most

landward location of the transect to the marsh edge (located at +1 NAP at Hellegatpolder (Vuik et al., 2018a)). The green line in the plot represents this section. Moreover, the dashed blue line represents the MHW at Hellegatpolder (Vuik et al., 2018a). In the situations where the bathymetry did not contain enough information, the script does not have enough information to determine a simplified profile and thus skips the bathymetry analysis. Two examples are provided below in figures K.2 and K.3.

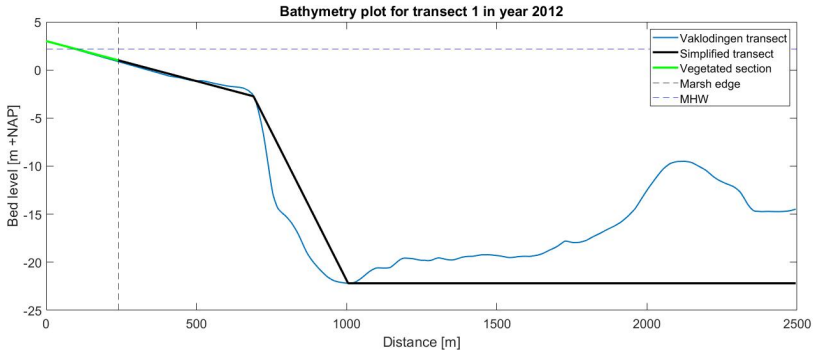

Figure K.2: A bathymetry plot with successful simplification

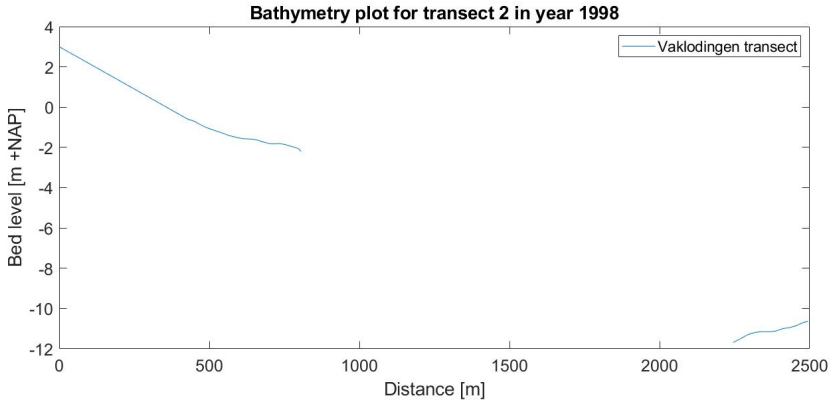

Figure K.3: A bathymetry plot with missing information and no simplification

L

Wave Parameter Correlation Analysis

The unexpected negative correlation between wave height and wave period was further assessed in this appendix. The data in the time series provided in Figure 4.6, can be analysed using correlations as all timestamps that do not contain data for all parameters are removed. The parameters of interest in the correlation analysis are wave height and wave period as these are related physically. Examining the correlation between water level and the other parameters does not add to this thesis as no conclusions can be drawn from the results.

As extensive data is available a two methods have been applied to reduce the total data to be analysed. The first analyses the correlation between wave height and wave period above a given threshold. The second analyses the correlation per month. In doing so information is gathered Spearman's correlation coefficient, equation 2.11. Assessing the results a number of conclusions can be made.

In the threshold analysis the correlation is determined between wave height and wave period. Two threshold analyses are performed, one for each parameter. Additionally the confidence bounds for the correlations are determined using equation 2.12. Figures L.1 andL.2 show the threshold correlations graphically. Figures L.3 and L.4 provide scatter plots for H_s and T_p respectively, to illustrate the relation between the variables above a threshold.

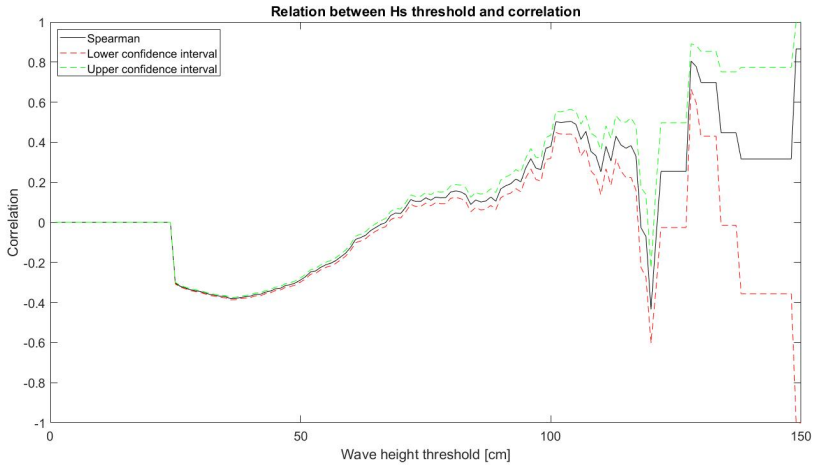

Figure L.1: Spearman's correlation analysis for various H_s thresholds

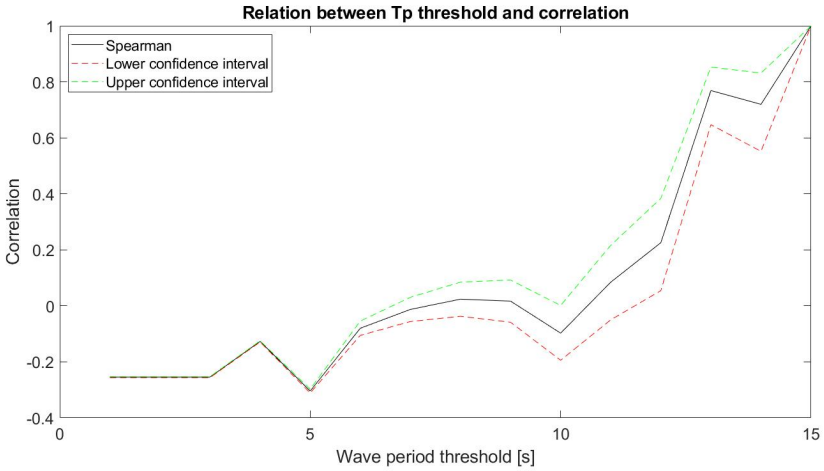

Figure L.2: Spearman's correlation analysis for various T_p thresholds

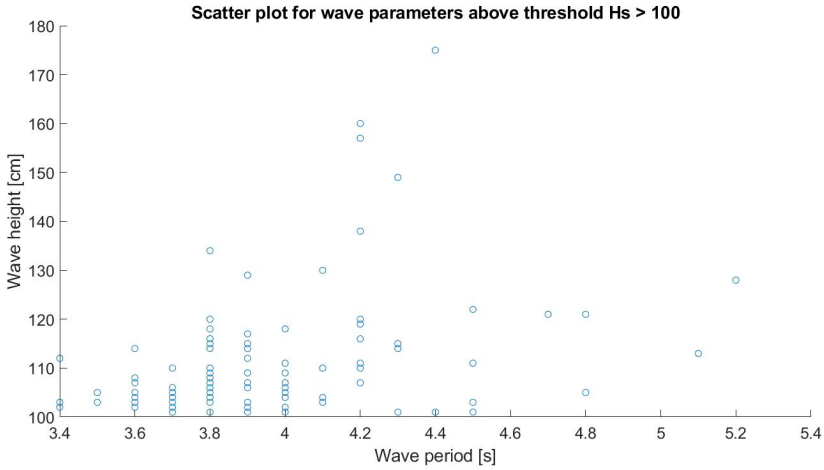

Figure L.3: Scatter plot for H_s above the threshold of 100 cm

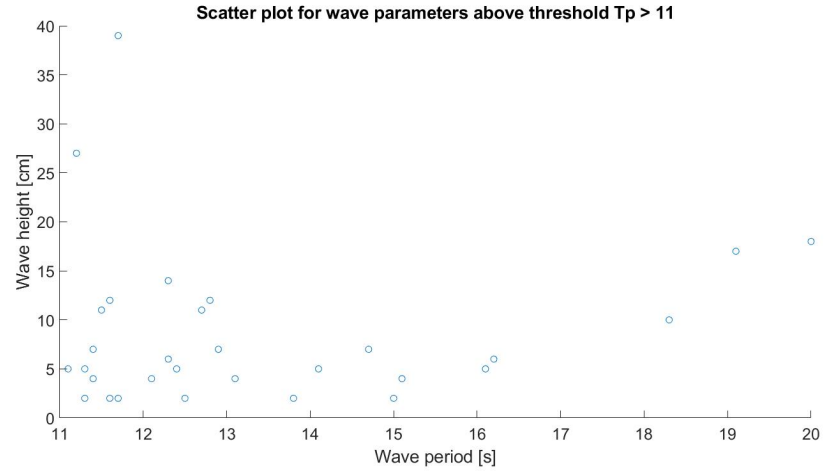

Figure L.4: Scatter plot for T_p above the threshold of 11 seconds

On top of the threshold analysis, a monthly correlation analysis of the data is also completed. Figures L.5 and L.6 present the correlation coefficients separated monthly.

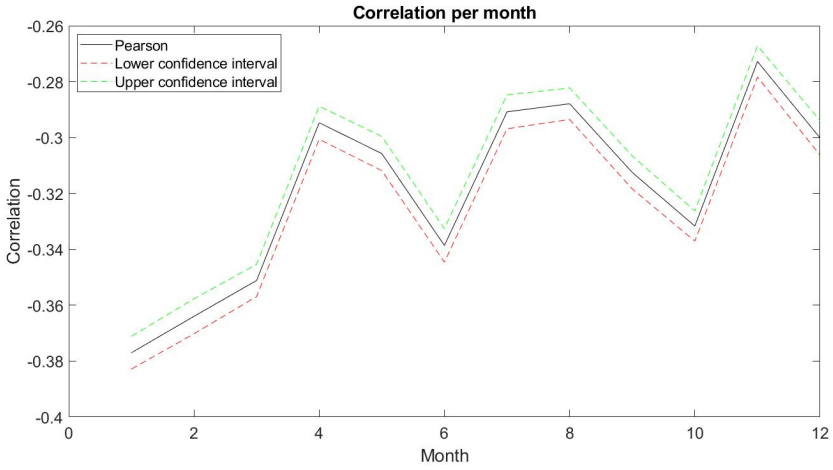

Figure L.5: Monthly Pearson correlation coefficient between wave parameters

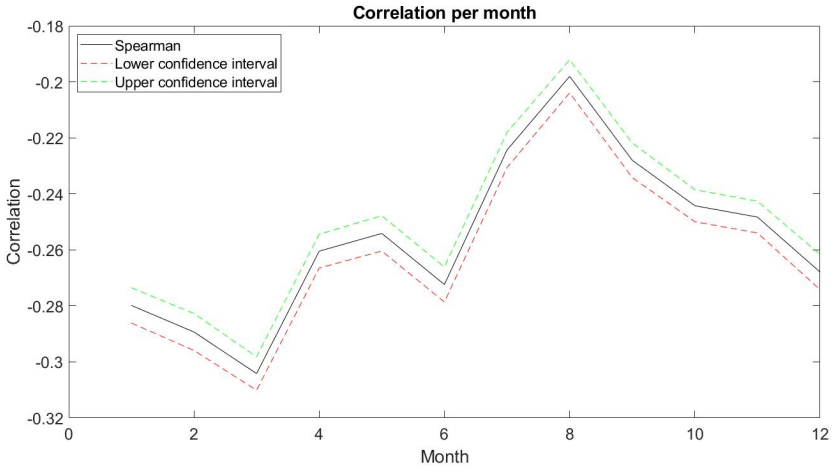

Figure L.6: Monthly Spearman's correlation coefficient between wave parameters

M

Alternative Applications

The current dynamic probabilistic tool is limited in its application possibilities. This is mainly due to the lack of available data collected and synthetically expanded in this thesis. Moreover, the statistical prediction modules (i.e. the Bayesian networks) were tuned to function using only the available parameters. Therefore, adjusting the various 'modules' belonging to each main DPT element (i.e. the database, model settings and the statistical prediction modules) will alter the realm of application possibilities.

Multiple alternative applications were defined and presented in Table M.1. Here the type of application was defined as well as the limitations currently present in the model and finally complemented with the current challenges that need to be overcome. Each of the applications are discussed in more detail in the subsequent sections below. It should be noted that each alternative application will require the development of an alternative module. Many of the alternative applications are also dependent on modules discussed in other applications areas (e.g. assessment of sea level rise will require the module developed in the application of assessing foreshore morphology).

Table M.1: Overview of the alternative applications and the main limitations in the current DPT.

Application	**Current Limitations**
Foreshore Morphology	Temporal / Spatial Bathymetry Data & Long Term Statistical Method
Vegetation Morphology	Temporal Vegetation Data & Long Term Statistical Method
Sea Level Rise	Hydraulic Data for SLR Scenarios & Long Term Statistical Method
Monitoring	Real Time Connection to Hydraulic Database
Human Intervention	Dredging Parameters & Corresponding Data

M.1. Foreshore Morphology

Depth induced wave breaking is one of the main wave attenuating elements in regard to HFD. Therefore, the morphology of the foreshore is an important element in terms of assessing HFD. Two main reasons of importance can be discerned. The first is the importance of foreshore stability during extreme forcing. Such a failure is included in the scope of failure possibilities in the Dutch design codes and is thus an important mechanism to assess. Second is the long term response of foreshore morphology. As flood defenses are designed for multiple years the response of the foreshore over longer time periods can affect the system as a whole. The strengthening or weakening of the system due to foreshore morphology is thus important to monitor.

M.1.1. DPT Applications

Given the importance of bathymetry within the HFD system, the interest of DPT application to assess the morphology is self explanatory. Both a long term application analysis and short term, during extreme conditions, are of interest in regard to flood defence analysis. A long term examination could shed light on expansion or retreat of the foreshore. The resulting effects would naturally influence the nearshore wave height and could lead to strengthening or weakening of the system. A short term response analysis

strengthens the understanding of the system under extreme conditions, which is often used in the design of the system.

While the short term analysis can be used as a parametric design tool, the analysis through time can be used by engineers to support the design choices based on the expected response through it's lifetime. For instance, if the lifetime analysis provided insight into erosion of the system, a maintenance plan of the foreshore could be developed, complementing the initial design. Or in contrast, if accretion is forecasted, a milder flood defense could initially suffice, due to the expected strengthening of the system, leading to a reduction in construction costs due to expected building with nature approach of the system.

M.1.2. Additional Model Requirements

If one was to use a DPT to assess foreshore morphology, two additional modules would have to be obtained. The first module belongs to the database, which naturally needs to be expanded to include bathymetric parameters (defined in Appendix K; foreshore slope, offshore slope, offshore depth and foreshore length) and corresponding temporal data. The data should correspond with various forcing conditions that well resemble common day to day forcing conditions for long term application. As well as bathymetric response data during extreme conditions to assess the effects of storms.

Aside from the underlying dataset, the statistic module needs to be expanded to include a dynamic static model (e.g. Bayesian network or vine-copula model) which can be used to model bathymetric response through time. A statistical analysis of the underlying dataset would be required to assess the dependence structures in relation to the bathymetry. As an initial hypothesis, Figure M.1 was developed which uses a physical foundation as a basis of the dependence structure. One should note that this is a simplified model used only as an indication with no statistical basis. The bathymetry (B) in the current time step (t1) is related to the bathymetry (B), hydraulic (H) and vegetation (V) parameters in the previous time step (t).

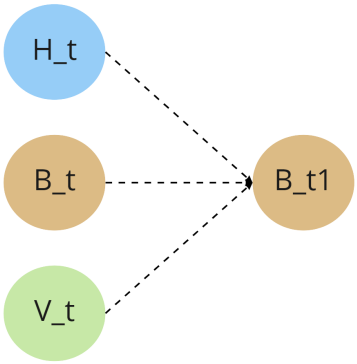

Figure M.1: Example of DBN which relates bathymetry in the current time step (t1) to the variables in the previous time step (t).

M.2. Vegetation Morphology & Secondary Effects

The HFD would not be complete without vegetation present on the foreshore. The numerous beneficial effects are of interest to decision makers due to the increasing interest in building with nature solutions. Therefore, both the evolution of the biological system as the secondary effects it has on soil structure, ecology and wave attenuation are of great interest as information regarding these parameters can help determine the actual value of a HFD system.

M.2.1. DPT Applications

The effects of vegetation morphology can be related to many dependent elements such as strengthening the subsoil. The transformation of the vegetation through time can thus be defined as a parameter that

influences the foreshore stability and thus the strength of the flood defence. Aside from the relation to bathymetric stability, vegetation also shapes the response of wave progression over the foreshore. In even more depth the vegetation itself is also influenced by the hydraulic conditions (i.e. stem breakage models use hydraulic conditions to determine breaking of stems (Vuik et al., 2018a)), leading to a complex dependence structure that can greatly effect the safety of the flood defense and is thus of interest for engineers in the design of HFD systems.

Expansion and retreat of the vegetation edge is additionally an effect which can greatly affect hydraulic conditions as the overall vegetation area is affected by the progression of the edge. Similar to the evolution of the foreshore, predicting the evolution of the marsh edge using a DPT, can provide engineers with the knowledge required to improve a dike design.

M.2.2. Additional Model Requirements

Due to the strong relation of vegetation to bathymetry, the previous module defined in section M.1 is required for the applications defined in the assessment of vegetation morphology. Furthermore, additional data is required for the assessment of vegetation processes. This poses one of the largest challenges as there is little data available, especially on shorter time scales. In order to analyse the effects of storms, vegetation evolution throughout such an extreme event also requires to be captured within the dataset.

Additionally, data needs to be collected concerning the relation between vegetation and its secondary effects such as strengthening the subsoil, capture of sediment and even effects on water quality. In doing so the model application can be expanded significantly to provide long term insights into the effects on flood protection as well as secondary important effects.

Again the statistical methods will have to be expanded to be able to include the secondary effects as well as include the complex dependence structures related to stem breakage and subsoil strengthening.

M.3. Sea Level Rise

As discussed in the introduction of this thesis, the importance of flood defences are increasing due to the effects of sea level rise. The implications of an increasing mean water level large within the context of HFD systems. The vegetation submergence increases and depth induced breaking over the foreshore is affected by the change in water depth. While research into HFD systems have shown promising effects in terms of sediment capture (i.e. leading to accretion of the foreshore and possibly equal expansion in the vertical direction), the prediction of the actual response is dependent on many factors and is thus an interesting knowledge gap for engineers and decision makers in the application of HFD systems.

M.3.1. DPT Applications

A DPT that combines the previous modules, concerning bathymetry and vegetation response, with a module that predicts sea level rise (SLR) has a variety of application possibilities. Using the combined DPT, the varying hydraulic load can be assessed to determine failure of the defense throughout its lifetime. Moreover, the building with nature character of the HFD can be assessed.

For instance, an analysis of the hydraulic conditions with SLR could lead to more extreme conditions being present over the course of 10 - 20 years. The additional bathymetry and vegetation morphology analysis could provide insight into their evolution (i.e. equal accretion compared to SLR for instance) during the same period. The combined effects provide the insight required for an engineer to either assess the HFD or develop a maintenance plan to mitigate the liabilities imposed by SLR.

M.3.2. Additional Model Requirements

The complexity of SLR is the inherent uncertainty of the scenarios. Therefore, an analysis of the effects of SLR will require an extensive dataset with varying hydraulic conditions that capture these scenarios and their corresponding effect on parameters such as wave attenuation, bathymetry morphology and vegetation evolution. Again a long term analysis module will be required as a statistic method to analyse the effects of SLR.

M.4. Effect of Human Intervention

Artificial strengthening of foreshores through dredging is a common method applied regularly in the Western Scheldt. Dredging influences the bathymetry and thus indirectly the hydraulic loads. Various dredging strategies lead to different responses of the system. For instance sediment deposition in the channels to be forced through the tides has a different effect in comparison with sediment placement on the foreshore. Moreover, there are many secondary effects related to dredging. Especially in relation to vegetation and ecology. Therefore, an analysis tool that provides insight into the effects of dredging in relation to HFD systems is of interest to engineers.

M.4.1. DPT Applications

Applications of this module are instinctively related to bathymetry morphology as dredging has a direct influence of the bathymetry. The combined modules could be applied to assess maintenance strategies of HFD systems due to climate change or for other assessment reasons. Furthermore, assessment of dredging could be a necessity for locations such as the Western Scheldt where it is applied on a regular basis for shipping channel maintenance. The direct effects on the bathymetry and thus wave attenuation as well as secondary effects on the vegetation evolution can support design conditions in the process of HFD development.

M.4.2. Additional Model Requirements

The additional requirements in terms of statistical model development are more complex as additional research into the parameters that are of influence require further analysis. Again a corresponding database for those parameters requires collection as to form the basis for the statistical modules. Those modules are related to the previously determined bathymetry and vegetation morphology models. Moreover, the model settings will have to be adjusted significantly to include the systematic implementation of dredging processes during specific time periods.